UNIVERSIDADE DE SANTIAGO DE COMPOSTELA

DEPARTAMENTO DE ELECTRÓNICA E COMPUTACIÓN

TESIS DOCTORAL

FORENSIC IDENTIFICATION BY CRANIOFACIAL SUPERIMPOSITION USING SOFT COMPUTING

Presentada por:
Óscar Ibáñez Panizo

Dirigida por:
Óscar Cordón García
Sergio Damas Arroyo

Santiago de Compostela, Mayo de 2010

Dr. **Óscar Cordón García**,
Investigador principal del
European Center for Soft
Computing

Dr. **Sergio Damas Arroyo**,
Investigador asociado del
European Center for Soft
Computing

Dr.**Manuel Mucientes**
Investigador Ramón y Cajal
Departamento de Electrónica e
Computación de la Universidad
de Santiago de Compostela

HACEN CONSTAR:

Que la memoria titulada **Forensic identification by Craniofacial Superimposition using Soft Computing** ha sido realizada por D. **Óscar Ibáñez Panizo** dentro del *programa de doctorado Interuniversitario en Tecnologías de la Información* del Departamento de Electrónica e Computación de la Universidad de Santiago de Compostela bajo la dirección de los Doctores D. Óscar Cordón García y D. Sergio Damas Arroyo, y constituye la Tesis que presenta para optar al grado de Doctor en Informática.

Santiago de Compostela, Mayo de 2010

Asdo: **Óscar Cordón García**
Codirector da tese

Asdo: **Sergio Damas Arroyo**
Codirector da tese

Asdo: **Manuel Mucientes**
Titor da tese

Asdo: **Javier Díaz Bruguera**
Director del Departamento de Electrónica e Computación

Asdo: **Óscar Ibáñez Panizo**
Autor de la Tesis

Agradecimientos

En primer lugar quiero agradecer a mis directores, Óscar y Sergio, todo lo que han hecho por mí y por esta tésis desde el día que empecé a trabajar en ella hasta el día en que terminé. Durante este largo viaje, me han motivado, me han enseñado, me han iluminado, me han guiado y me han ayudado. Ellos han hecho de mí lo que yo buscaba en ellos, ser un investigador.

Esta tésis lo es también gracias a muchas otras personas: Jose Santamaría, sin él esta tésis no habría sido posible. Inma y Fernando, su ayuda, además de necesaria, siempre ha sido muy fácil de encontrar. Mis compañeros del Soft Computing, con su apoyo no sólo he escrito una tesis, sino que también he pasado felizmente una gran parte de los dos últimos años de mi vida.

También tengo mucho que agradecerle al European Centre for Soft Computing, mucho de lo que aquí dentro he aprendido ha hecho posible este documento. A mis antiguos jefes, compañeros y amigos del laboratorio RNASA/IMEDIR de la Universidad de la Coruña, de donde no sólo me llevé muchas lecciones aprendidas sino que también *moi bos amigos*. También en Coruña, no puedo olvidarme de la gente del VARPA, ellos fueron los culpables de que empezará en todo esto.

Muchas gracias también al Dpto. de Electrónica e Computación de la Universidad de Santiago de Compostela y en especial a Manuel Mucientes y a Alberto Bugarín por prestarme su ayuda desinteresada.

Por último, quiero darle las gracias a mis padres y amigos, todo lo que soy se lo debo a ellos.

Acknowledgements

This work was partially supported by the Spain's Ministerio de Educación y Ciencia (ref. TIN2006-00829 and ref. TIN2009-07727) and by the Andalusian Dpt. of Innovación, Ciencia y Empresa (ref. TIC-1619).

We would like to acknowledge all the team of the Physical Anthropology lab at the University of Granada (headed by Dr. Botella and Dr. Alemán) for their support during the data acquisition and validation processes.

Part of the experiments related to this work was supported by the computing resources at the Supercomputing Center of Galicia (CESGA), Spain.

A mis Padres, porque me habeis dado más de lo que yo nunca podré daros en toda mi vida

A mi hermano Alberto y a mi abuelo Alberto, por lo orgullosos que debeis sentiros

Contents

List of Figures

List of Tables

Resumen

En materia de amor y desamor somos
como recién nacidos toda la vida.

Eduard Punset

A. Introducción

La Antropología Forense estudia las cuestiones médico-legales relacionadas con una persona fallecida mediante el examen de sus restos óseos (Burns 2007). Entre otros objetivos, trata de determinar su identidad y la forma y causa de la muerte. Una de sus aplicaciones más importantes es la identificación de seres humanos a partir de su esqueleto, normalmente en casos de personas desaparecidas, así como en circunstancias de guerra y desastres de masas. Este trabajo requiere la comparación de datos ante-mortem (los cuales pueden obtenerse de material visual y de entrevistas con parientes y testigos) y post-mortem. Por ejemplo, puede implicar la comparación de datos relacionados con parámetros como el sexo, la altura, la estatura, la constitución física o la dentadura (Rathburn 1984). El estudio del esqueleto se aplica normalmente como primer paso del proceso de identificación forense, previo a cualquier otra técnica. También se considera cuando las demás formas de identificación han demostrado ser dudosas o no aplicables (Krogman and Iscan 1986).

Para ponerla en práctica, el antropólogo mide y compara los datos del esqueleto para determinar los citados parámetros. Si este estudio es positivo, se aplican técnicas más específicas como autopsia interna y externa o técnicas de ADN. Sin embargo, estos métodos de identificación pueden dar problemas ya que en ocasiones no hay información (ante- o post-mortem) suficiente para poder aplicarlos. En esas circunstancias, la identificación antropológica basada únicamente en el estudio de los restos óseos puede considerarse como la última oportunidad para la identificación forense. En dichos casos, se aplican como alternativa técnicas más específicas basadas en el estudio de restos óseos, como es el caso de la **superposición craneofacial** (Rathburn 1984; Iscan 1993; Taylor and Brown 1998; Stephan 2009b), en la que se comparan fotografías o fotogramas de video de la "persona desaparecida" con el cráneo encontrado. Proyectando ambas fotografías una sobre otra (o, mejor, emparejando la foto con un modelo tridimensional del cráneo) se puede tratar de determinar si pertenecen a la misma persona de acuerdo al emparejamiento de algunos puntos característicos (puntos antropométricos). En consecuencia, hay que tener en cuenta que dichos puntos característicos se localizan en dos objetos diferentes (el cráneo encontrado y la cara mostrada en la fotografía). Este hecho representa una fuente de incertidumbre a considerar durante todo el proceso de superposición craneofacial, incluyendo la decisión final de la identificación.

Uno de los inconvenientes más importantes de la identificación por superposición craneofacial es que no existe una metodología sistemática para el análisis por superposición de imágenes, sino que cada investigador aplica la suya propia. Sin embargo, hay dos factores comunes a cualquier investigación (Donsgsheng and Yuwen

1993):

- la determinación del tamaño real de las figuras (escalado), puesto que sería imposible superponer imágenes con un tamaño distinto. La distancia focal de la foto de la cara es determinante para esta tarea; y
- el método de orientación del cráneo, para hacerlo corresponder con la posición de la cara en la foto. Hay tres movimientos posibles: inclinación, extensión y rotación.

Es importante reseñar que "el proceso de orientación dinámica es una parte de la técnica de superposición craneofacial muy exigente y tediosa. Ajustar correctamente el tamaño y orientar las imágenes puede suponer varias horas de trabajo" (Fenton et al. 2008). Por lo tanto, parece clara la necesidad de un método sistemático y automático de superposición craneofacial para la comunidad de antropólogos forenses.

Como puede verse, este proceso tiene una clara relación con el problema del registrado de imágenes. El **registrado de imágenes** (Zitová and Flusser 2003) es una tarea fundamental en visión por computador empleada para hallar la transformación (rotación, traslación...) que solapa dos o más imágenes obtenidas en condiciones distintas, acercando los puntos tanto como sea posible mediante la minimización del error dado por una métrica de similitud. Durante años, el registrado de imágenes se ha aplicado a un conjunto amplio de situaciones desde teledetección a imagen médica o visión artificial y se han propuesto distintas técnicas, originando un área de investigación importante (Goshtasby 2005).

Resolver el problema de superposición craneofacial siguiendo una aproximación de registrado de imágenes para el solapamiento de un modelo 3D del cráneo sobre una fotografía de la cara conlleva una tarea de optimización realmente compleja. El correspondiente espacio de búsqueda es enorme y presenta muchos mínimos locales, por lo que los métodos de búsqueda exhaustivos no resultan útiles. Además, los antropólogos forenses exigen una gran robustez y precisión en los resultados. Los enfoques de registrado de imágenes basados en algoritmos evolutivos (Bäck et al. 1997; Eiben and Smith 2003) son una solución prometedora para abordar este exigente problema de optimización. Gracias a su naturaleza de optimizadores globales, los algoritmos evolutivos tiene la capacidad de realizar búsquedas robustas en problemas complejos vagamente definidos como es el caso del registrado de imágenes (Cordón et al. 2007; Santamaría et al. 2010).

La superposición craneofacial no sólo conlleva un problema de optimización complejo, sino también la necesidad de abordar la incertidumbre subyacente al uso de

dos objetos diferentes (un cráneo y una cara). La correspondencia entre los puntos antropométricos no es siempre simétrica y perpendicular, algunos están localizados en una posición más alta en la cara de la persona viva que en el cráneo y otros no tienen un punto directamente relacionado en el otro conjunto. Como consecuencia, tenemos una situación clara de emparejamiento parcial. Además, la decisión final de la identificación se expresa de acuerdo a varios niveles de confianza, dependiendo del grado de conservación de la muestra y del proceso analítico realizado: "coincidencia absoluta", "no coincidencia absoluta", "coincidencia relativa", "no coincidencia relativa" y "falta de información". Así, de nuevo encontramos la presencia de la incertidumbre y la verdad parcial en el proceso de identificación.

El objetivo de la presente tesis es proponer un marco metodológico basado en el uso del ordenador para asistir al antropólogo forense en la identificación mediante la técnica de superposición craneofacial. En concreto, este trabajo se centrará en el diseño de un método automático para el solapamiento de un modelo 3D del cráneo sobre una fotografía 2D de la cara, explotando para ello las capacidades del **soft computing** de dos maneras. Por un lado, se usarán algoritmos evolutivos para obtener el mejor ajuste entre el cráneo encontrado y la fotografía de la cara de forma automática. Por otro lado, se pretende modelar las diferentes fuentes de incertidumbre presentes en el proceso mediante el uso de conjuntos difusos (Zadeh 1965).

B. Objetivos

Como ya se ha mencionado, uno de los principales inconvenientes de la identificación forense por superposición craneofacial es la ausencia de un método sistemático para su aplicación. Por contra, cada investigador aplica su propia metodología basada en su experiencia y habilidad. Además, la superposición craneofacial es un procedimiento exigente y tedioso. El principal objetivo de la presente tesis se centra en proponer una metodología sistemática y automática para la identificación forense por superposición craneofacial, explotando las capacidades del soft computing para la tarea de solapamiento cráneo-cara. Este objetivo global se divide en una serie de objetivos más concretos:

- *Estudiar el estado del arte en identificación forense mediante superposición craneofacial*. Tenemos el propósito de estudiar el campo de la superposición craneofacial, prestando especial atención a los métodos basados en el uso del ordenador. También queremos esclarecer el verdadero rol que juegan los ordenadores en los

métodos considerados y analizar las ventajas y desventajas de las aproximaciones existentes, con especial interés en las automáticas.

- *Proponer un marco metodológico para la superposición craneofacial basada en el uso de ordenadores*. Pretendemos o bien escoger una metodología de entre las existentes o bien proponer un nuevo marco metodológico que identifique claramente las diferentes etapas implicadas en el proceso de superposición craneofacial basada en el uso del ordenador.

- *Proponer una formulación matemática para el problema del solapamiento cráneo-cara*. Nos planteamos formular la superposición cráneo-cara como un problema de optimización numérica. Dicha formulación se basará en el problema de registrado 3D-2D.

- *Proponer un método automático para el solapamiento cráneo-cara basado en algoritmos evolutivos*. Pretendemos proponer diferentes diseños de algoritmos evolutivos capaces de resolver el problema de optimización formulado anteriormente de manera automática, rápida y precisa.

- *Estudiar los fuentes de incertidumbre presentes en el solapamiento cráneo-cara*. Aspiramos a identificar y estudiar las diferentes fuentes de incertidumbre relacionadas tanto con la tarea de solapamiento cráneo-cara como con el procedimiento evolutivo de registrado de imágenes 3D-2D propuesto.

- *Modelar las fuentes de incertidumbre anteriores*. Tenemos como objetivo modelar las fuentes de incertidumbre identificadas considerando conjuntos difusos para mejorar el rendimiento de las técnicas evolutivas consideradas para resolver el problema.

- *Analizar el rendimiento de los métodos propuestos*. Pretendemos validar los métodos evolutivos de solapamiento cráneo-cara diseñados sobre casos de identificación reales resueltos previamente por el personal del laboratorio de Antropología Física de la Universidad de Granada en colaboración con la policía científica española. También nos planteamos evaluar los mejores resultados obtenidos de manera automática para los diferentes casos de identificación reales con respecto a los solapamientos efectuados por los antropólogos forenses.

C. Trabajo realizado y conclusiones

En esta tesis hemos propuesto varios métodos automáticos, basados en técnicas de soft computing, para resolver el problema del solapamiento cráneo-cara en superposición craneofacial. En concreto, hemos aplicado algoritmos evolutivos y teoría de conjuntos difusos para resolver este problema tan complejo y con tanta incertudimbre. Los resultados obtenidos han sido prometedores, como han confirmado los antropólogos forenses del laboratorio de Antropología Física de la Universidad de Granada, con lo que se demuestra la idoneidad de nuestra propuesta. Estos expertos forenses han remarcado el corto periodo de tiempo necesario para obtener solapamientos de manera automática así como la precisión de los mismos. De hecho, han usado recientemente nuestro método para la resolución de un problema real de identificación, dependiente de la policía científica española, de una persona cuyos restos aparecieron en los alrededores de la Alhambra.

En los apartados siguientes analizaremos los resultados obtenidos en esta memoria, así como el grado de satisfacción conseguido para cada uno de los objetivos planteados al principio de la misma:

- *Estudiar el estado del arte en identificación forense mediante superposición craneofacial*. Después de raelizar un amplio estudio del campo de superposición craneofacial, profundizando en sus fundamentos y en las principales contribuciones del área, podemos concluir que la técnica ha demostrado ser un método de identificación sólido. Sin embargo, todavía no se han establecido unos criterios metodológicos que aseguren su fiabilidad. Por contra, en lugar de seguir una metodología uniforme, cada forense suele aplicar su propio enfoque al problema según la tecnología disponible y su profundo conocimiento de la anatomía humana refente al cráneo, al tejido blando y a la relación entre ambos.

- *Proponer un marco metodológico para la superposición craneofacial basada en el uso de ordenadores*. Hemos propuesto un nuevo marco genérico para la superposición craneofacial basada en el uso del ordenador con el objetivo de paliar la ausencia de una metodología uniforme asociada a esta técnica de identificación forense. Dicho marco metodológico divide el proceso en tres etapas: mejora facial y modelado del cráneo, solapamiento cráneo-cara y toma de decisiones. Tomando este marco genérico como referente, hemos revisado y analizado los trabajos existentes en el área de superposición craneofacial basada en el uso del ordenador, clasificándolos de acuerdo a la etapa del proceso abordada mediante el uso de este dispositivo.

El trabajo llevado a cabo para satisfacer los anteriores objetivos ha resultado en la escritura de un artículo que describe el marco metodológico propuesto para la superposición craneofacial basada en el uso del ordenador, así como la revisión completa del estado del arte de dicha técnica. Este trabajo ha sido aceptado para su publicación en la revista con mayor índice de impacto en el área de Informática. Además, cuestiones relacionadas con el marco metodólógico propuesto y la aplicación de técnicas de soft computing en sus diferentes etapas han sido publicadas también en una revista de edición digital:

  - S. Damas, O. Cordón, O. Ibáñez, J. Santamaría, I. Alemán, MC. Botella, F. Navarro. Forensic identification by computer-aided craniofacial superimposition: A survey. ACM Journal on Computing (2010), en prensa. Factor de impacto 2008: 9.920. Categoría: Computer Science, Theory & Methods. Orden: $1/84$.
  - O. Cordón, S. Damas, R. del Coso, O. Ibáñez, C. Peña. Soft Computing Developments of the Applications of Fuzzy Logic and Evolutionary Algorithms Research. eNewsletter: Systems, Man and Cybernetics Society (2009). Vol. 19. Disponible *on-line* en $http://www.my-smc.org/main\_article1.html$.

- *Proponer una formulación matemática para el problema del solapamiento cráneo-cara*. Hemos formulado la tarea de solapamiento cráneo-cara como un problema de optimización numérica, lo que nos permite resolver el problema de registrado 3D-2D subyacente siguiendo un enfoque basado en parámetros. La transformación de registrado a estimar incluye una rotación, un escalado, una traslación y una proyección. Se ha especificado un conjunto de ocho ecuaciones con doce incógnitas.

- *Proponer un método automático para el solapamiento cráneo-cara basado en algoritmos evolutivos*. Hemos propuesto y validado el uso de algoritmos evolutivos con codificación real para el problema del solapamiento cráneo-cara de un modelo de cráneo 3D y una fotografía 2D de la cara de la persona desaparecida. En concreto, hemos propuesto el uso de dos diseños diferentes de un algoritmo genético con codificación real, así como de la estrategia evolutiva CMA-ES y del método evolutivo SS. Estos dos últimos han demostrado un mejor rendimiento, logrando resultados de alta calidad para todos los casos tratados a la vez que se han comportado de manera muy robusta. Además, SS ha presentado una mayor velocidad de convergencia que CMA-ES.

La formulación matemática desarrollada para el problema de solapamiento cráneo-cara así como los diferentes algoritmos evolutivos propuestos para su resolución nos han permitido desarrollar de diferentes contribuciones incluyendo artículos internacionales, capítulos de libro y conferencias internacionales:

- O. Ibáñez, L. Ballerini, O. Cordón, S. Damas, and J. Santamaría (2009). An experimental study on the applicability of evolutionary algorithms to craniofacial superimposition in forensic identification. Information Sciences 179, 3998–4028. Factor de impacto 2008: 3.095. Categoría: Computer Science, Information Systems. Orden: $8/99$.
- O. Ibáñez, O. Cordón, S. Damas, and J. Santamaría (2009). Multimodal genetic algorithms for craniofacial superimposition. In R. Chiong (Ed.), Nature-Inspired Informatics for Intelligent Applications and Knowledge Discovery: Implications in Business, Science and Engineering, pp. $119-142$. IGI Global.
- J. Santamaría, O. Cordón, S. Damas, and O. Ibáñez (2009). 3D–2D image registration in medical forensic identification using covariance matrix adaptation evolution strategy. In 9th International Conference on Information Technology and Applications in Biomedicine, Larnaca, Cyprus.
- O. Ibáñez, O. Cordón, S. Damas, J. Santamaría. An advanced scatter search design for skull-face overlay in craniofacial superimposition. ECSC Research Report: AFE 2010-01, Mieres. Submitted to Applied Soft Computing. Feb 2010. Factor de impacto 2008: 1.909. Categoría: Computer Science, Artificial Intelligence. Orden: $30/94$. Categoría: Computer Science, Interdisciplinary Applications. Orden: $23/94$.

- *Estudiar las fuentes de incertidumbre presentes en el solapamiento cráneo-cara*. Hemos identificado y estudiado las fuentes de incertidumbre relacionadas tanto con el método como con la técnica propuesta para el solapamiento cráneo-cara. En dicho estudio distinguimos entre la incertidumbre asociada con los objetos considerados y la incertidumbre inherente al proceso de solapamiento. Además, hemos analizado como la coplanaridad de los conjuntos de puntos cefalométricos afecta al resultado final de la técnica de solapamiento cráneo-cara propuesta.

- *Modelar las fuentes de incertidumbre anteriores*. Hemos propuesto dos enfoques diferentes para tratar de manera conjunta la localización imprecisa de los puntos cefalométricos y el problema de coplanaridad. Comparando los dos enfoques, marcadores difusos y marcadores ponderados, el primero ha demostrado

ser la mejor opción para modelar la localización imprecisa a la vista de los resultados mostrados en esta memoria. La principal ventaja de esta propuesta es la posibilidad de localización de un mayor número de puntos cefalométricos que proporciona los antropólogos forenses. Esto conlleva la obtención de mejores resultados finales en el solapamiento cráneo-cara.

Hemos desarrollado diferentes contribuciones describiendo el estudio de las fuentes de incertidumbre, los dos enfoques de localización propuestos y el estudio de coplanaridad. Estos trabajos se han publicado tanto en congresos nacionales como internacionales, entre los que cabe destacar el 3DIM, uno de los congresos más importantes en el área de visión por computador:

- O. Ibáñez, O. Cordón, S. Damas, and J. Santamaría (2008). Craniofacial superimposition based on genetic algorithms and fuzzy location of cephalometric landmarks. In Hybrid artificial intelligence systems, Number 5271 in LNAI, pp. 599–607.
- O. Ibáñez, O. Cordón, S. Damas, and J. Santamaría (2008). Superposición craneofacial basada en algoritmos genéticos y localización difusa de puntos de referencia cefalométricos. In Actas del XIV Congreso Español sobre Tecnologías y Lógica Fuzzy, pp. 323–329.
- O. Ibáñez, O. Cordón, S. Damas, and J. Santamaría (2009). A new approach to fuzzy location of cephalometric landmarks in craniofacial superimposition. In International Fuzzy Systems Association − European Society for Fuzzy Logic and Technologies (IFSA-EUSFLAT) World Congress, Lisbon, Portugal, pp. 195–200.
- J. Santamaría, O. Cordón, S. Damas, and O. Ibáñez (2009). Tackling the coplanarity problem in 3D camera calibration by means of fuzzy landmarks: a performance study in forensic craniofacial superimposition. In 3DIM Workshop, IEEE International Conference on Computer Vision, Kyoto, Japan, pp. 1686–1693.
- O. Ibáñez, O. Cordón, S. Damas, and J. Santamaría (2010). Uso de marcadores difusos para solucionar el problema de la coplanaridad en la calibración de la cámara en 3D. Aplicación en identificación forense por superposición craneofacial. In Actas del XV Congreso Español sobre Tecnologías y Lógica Fuzzy, pp. 501–506.

- *Analizar el rendimiento de los métodos propuestos*. Hemos realizado una comparativa entre los solapamientos cráneo-cara que nos han proporcionado los

antropólogos del laboratorio de Antropología Forense de la Universidad de Granada y aquellos obtenidos mediante nuestro enfoque basado en el algoritmo SS y el uso de puntos cefalométricos difusos. Tras una evaluación visual hemos concluido que los solapamientos obtenidos siguiendo nuestro enfoque son competitivos con los logrados por los antropologos forenses y, en algunas ocasiones, incluso son mejores. De todas formas, comparando el tiempo requerido por nuestra técnica evolutiva (entre 10 y 20 segundos usando marcadores precisos y de 2 a 4 minutos usando marcadores difusos) con el que los antropólogos forenses necesitan para llevar a cabo un solapamiento cráneo-cara de forma manual –varias horas por cada caso– los enfoques evolutivos son siempre mucho mejores, necesitando un tiempo varias órdenes de magnitud menor.

Debido a esto, aparte de la ventaja en la calidad mencionada, se abren nuevas perspectivas a partir de los trabajos realizados en la presente tesis. Por un lado, nuestra propuesta podría ser considerada como una inicialización rápida de gran calidad con la que el antropólogo forense empezaría a trabajar, de manera que solo necesitaría refinarla ligeramente para obtener un solapamiento de gran precisión. Por otro lado, surge la posibilidad de comparar un modelo 3D de cráneo con una base de datos de personas desaparecidas, donde el tiempo requerido para una comparación masiva puede ser equivalente al tiempo que un antropólogo forense invierte en un solo caso de identificación por superposición craneofacial.

Por último, nos gustaría destacar que a partir de los planteamientos y resultados obtenidos en la presente tesis hemos desarrollado una patente, “Método y sistema de identificación forense por superposición craneofacial”, la cual ha sido sometida a la agencia nacional de patentes el pasado mes de Julio de 2009.

- Inventores (p.o. de firma): O. Cordón, S. Damas, O. Ibáñez, J. Santamaría, I. Alemán, M. Botella, Título: Método y sistema de identificación forense por superposición craneofacial. N. de solicitud: P200901732/3. País de prioridad: España. Fecha de prioridad: 2009-07-30. Entidad titular: Fundación para el progreso del Soft Computing y Universidad de Granada.

D. Trabajos futuros

A continuación, discutiremos varias líneas abiertas de investigación en relación a los temas tratados en esta tesis. Además, consideramos diferentes extensiones de nuestras propuestas que serán desarrolladas en futuros trabajos.

- *Incrementar el número de casos reales considerados*. Pretendemos abordar un mayor número de casos reales de identificación ya resueltos por el laboratorio de Antropología Forense de la Universidad de Granada. De esta manera, una vez solventados los problemas legales que nos permitan usar un mayor número de casos, nuestros resultados se validarían sobre un estudio más extenso y por lo tanto más significativo.

- *Realizar una encuesta entre diferentes antropólogos forenses expertos*. Pretendemos realizar una encuesta *on-line* entre diferentes antropólogos forenses que consistirá en localizar los puntos cefalométricos sobre un conjunto de fotografías. Planeamos estudiar aspectos como la variación en la localización de los puntos, cómo se ve afectado el proceso de localización por la calidad de la imagen, qué puntos cefalométricos son más difíciles de localizar y cómo se ve influenciado el proceso de localización por la pose de la cara en la fotografía. Esta encuesta servirá también para definir la forma y el tamaño más adecuados para los marcadores cefalométricos difusos correspondientes a varios casos reales de identificación ya resueltos.

- *Conseguir una solución ground-truth para el solapamiento cráneo-cara*. Es necesario conseguir una solución *ground-truth* para poder hacer comparaciones justas y objetivas entre los diferentes solapamientos cráneo-cara resultantes. Las tomografías computerizadas de la cabeza pueden ser una opción intersante a estudiar para tal fin.

- *Estudiar nuevas definiciones de distancias difusas*. Planeamos el estudio de distancias punto *crisp*-conjunto difuso alternativas, a partir del cuál seleccionar la más adecuada, con el objetivo de mejorar el rendimiento de nuestro método basado en algoritmos evolutivos y conjuntos difusos.

- *Abordar la incertidumbre en el emparejamiento*. Pretendemos abordar la incertidumbre inherente al emparejamiento de cada par de puntos cefalométrico-craneométrico. Tomando como punto de partida los trabajos de Stephan y Simpson (2008a, 2008b) y con el asesoramiento de los antropólogos forenses del laboratorio de Antropología Forense de la Universidad de Granada, pretendemos modelar la situación de emparejamiento parcial mediante el uso de conjuntos difusos y medidas de distancia difusas.

- *Estudiar la influencia de la pose de la cara sobre la incertidumbre en el emparejamiento*. Planeamos estudiar la variación de las distancias de emparejamiento

entre pares de puntos cefalométrico-craneométrico con respecto a los cambios en la pose de la cara.

- *Extraer la pose 3D a partir de una fotografía 2D*. Tenemos como objetivo aproximar la orientación 3D de la cabeza a partir de una fotografía 2D de la cara. Esta información será de gran ayuda para reducir el espacio de búsqueda sobre el que actuan los métodos evolutivos propuestos. También será útil para modificar la incertidumbre asociada al emparejamiento de pares de puntos antropométricos.

- *Abordar la fase de toma de decisiones*. Planeamos abordar la última etapa de la identificación por superposición craneofacial, es decir la toma de decisiones, mediante el uso de lógica difusa. Con la automatización de esta etapa se pretende asistir al antropólogo forense en la toma de decisiones final.

- *Estudiar nuevas formulaciones para el problema*. Una línea de investigación futura muy prometedora es la relativa al estudio de nuevas formulaciones posibles para la transformación geométrica que conlleva el problema de solapamiento cráneo-cara. En concreto, nos gustaría encontrar una manera de incluir los parámetros internos de la cámara en el modelo de manera que también puedan ser tenidos en cuenta por el método evolutivo propuesto. Estos nuevos modelos pueden ser especialmente útiles en aquellos casos en los que las fotografías disponibles hubieran sido tomadas con cámaras muy antiguas.

Statement

A friend is someone who gives you,
total freedom to be yourself.

Jim Morrison (1943-1971)

A. Introduction

Forensic anthropology studies medico-legal questions related to a deceased person through the examination of his or her skeletal remains (Burns 2007). Among other objectives, it aims to determine the person's identity and the manner and cause of death. One of its most important applications is the identification of human beings from their skeletal remains, usually in the case of missing people, as well as under circumstances of war and mass disasters (Iscan 1981b). That work involves comparing ante-mortem data (which can be retraced on the basis of visual material and interviews with relatives or witnesses) to the available post-mortem data. This may require a comparison of data pertaining to sex, age, stature, build and teeth (Rathburn 1984). Hence, the study of the skeleton is usually applied as the first step of the identification process, previous to the application of any other technique. Besides, the skeletal specialist takes over after the most established means of identification have become doubtful or impossible (Krogman and Iscan 1986).

In order to develop the forensic identification process, the anthropologist measures and compares the skeleton data to determine the said parameters. If this study shows positive results, more specific techniques are applied such as: comparison of fingerprints, foot and hand prints; comparison of data on the jaw and teeth (dental information); external and internal autopsy; or DNA techniques, which have demonstrated a blood relation with known family members. Nevertheless, there could be a problem with the latter identification methods as sometimes there is not enough (ante- or post-mortem) information available to apply them. Hence, anthropological identification based only on the skeleton information can also be considered as the last chance for forensic identification when none of the previous methods can be applied.

If the latter is the case, more specific skeleton-based identification techniques are alternatively applied such as **craniofacial superimposition** (Rathburn 1984; Iscan 1993; Taylor and Brown 1998; Stephan 2009b). This method aims to compare either photographs or video shots of the "disappeared person" with the skull that is found. By projecting photographs of the skull and of the disappeared person on top of each other (or, even better, matching a scanned three-dimensional skull model against the face photo/series of video shots), the forensic anthropologist can try to establish whether that is the same person as regards the matching of some characteristic points (anthropological landmarks). Notice that, those landmarks are located in two different objects (the skull found and the face photograph). That fact represents a source of uncertainty to deal with during the whole craniofacial superimposition process, including the final identification decision.

One of the most important drawbacks of craniofacial superimposition identification is that there is no systematic method for the analysis by image superposition, but every researcher applies his own methodology. However, there are two common factors to every research (Donsgsheng and Yuwen 1993):

- the determination of the real size of the figures (scaling), since it would be impossible to overlay images with a different relative size. The focal distance of the face picture is determinant for this issue; and
- the orientation method for the skull, to make it correspond to the face position in the photograph. There are three possible moves: inclination, extension and rotation.

It is important to note that "the dynamic orientation process is a very challenging and time-consuming part of the skull-photo superimposition technique. Correctly adjusting the size and orienting the images can take several hours to complete" (Fenton et al. 2008). Hence, a systematic and automatic method for craniofacial superimposition is a real need in forensic anthropology.

There is a clear relation between the desired procedure and the **image registration** problem. Image registration (Zitová and Flusser 2003) is a fundamental task in computer vision used for finding the transformation (rotation, translation, etc.), that overlays two or more pictures taken under different conditions, bringing the points as close together as possible by minimizing the error of a given similarity metric. Over the years, image registration has been applied to a broad range of situations from remote sensing to medical images or artificial vision, and different techniques have been independently studied resulting in a large body of research (Goshtasby 2005).

Solving craniofacial superimposition following an image registration approach to overlay the skull 3D model over the face photograph involves a really complex optimization task. The corresponding search space is huge and presents many local minima. Hence, exhaustive search methods are not useful. Furthermore, forensic experts demand highly robust and accurate results. Image registration approaches based on evolutionary algorithms (Bäck et al. 1997; Eiben and Smith 2003) are a promising solution for facing this challenging optimization problem. Thanks to their global optimization nature evolutionary algorithms own the capability to perform robust search in complex and ill-defined problems as image registration (Cordón et al. 2007; Santamaría et al. 2010).

Craniofacial superimposition not only involves a complex optimization problem but also the need of dealing with the underlying uncertainty since two different objects

are implicated in the process (a skull and a face). The correspondence between the anthropometric landmarks is not always symmetrical and perpendicular, some landmarks are located in a higher position in the alive person face than in the skull, and some others have not got a directly related landmark in the other set. So, we found a clear partial matching situation. Moreover, as final result, the identification decision can be expressed according to several confidence levels, depending on the degree of conservation of the sample and of the analytical process put into effect: "absolute matching", "absolute mismatching", "relative matching", "relative mismatching", and "lack of information". Hence, we again find the uncertainty and partial truth involved in the identification process.

The aim of the current dissertation is to propose a computer-based methodological framework to assist the forensic anthropologist in the human identification by means of the craniofacial superimposition technique. In particular, the current work will be focused on the design of an automatic method to overlay a 3D skull model and a face 2D photograph, exploiting the capabilities of **soft computing** in a two-fold manner. On the one hand, evolutionary algorithms will be used to automatically find the best fit between the the skull found and the face photograph. On the other hand, fuzzy sets (Zadeh 1965) will be considered in order to manage the different sources of uncertainty involved in the process.

B. Objectives

As said, one of the most important drawbacks of forensic identification by craniofacial superimposition is the absence of a systematic method. Instead, every researcher applies his/her own methodology based on his/her expertise and experience. Besides, craniofacial superimposition is a very challenging and time-consuming procedure. The main objective of the current dissertation focuses on proposing a systematic and automatic methodology for forensic identification by craniofacial superimposition, exploiting the capabilities of soft computing for the skull-face overlay task. Specifically, this objective is divided into the following ones:

- *Study the state of the art in forensic identification by craniofacial superimposition*. We aim to study the craniofacial superimposition field, paying a special attention to computer-based methods. We also aim to clarify the actual role played by computers in the considered methods and analyze advantages and drawbacks of the existing approaches, with an emphasis on the automatic ones.

- *Propose a methodological framework for computer-based craniofacial superimposition*. We aim to either choose a methodology from the existing ones or propose a new methodological framework which clearly identifies the different stages involved in the computer-based craniofacial superimposition process.

- *Propose a mathematical formulation for the skull-face overlay problem*. We aim to formulate skull-face superimposition as a numerical optimization problem. Such formulation will be based on the 3D-2D image registration problem.

- *Propose an automatic method for skull-face overlay based on evolutionary algorithms*. We aim to introduce different evolutionary algorithms designs in order to solve the formulated optimization problem in an automatic, fast, robust, and accurate way.

- *Study the sources of uncertainty present in skull-face overlay*. We aim to identify and study the different sources of uncertainty related to the skull-face overlay task and with the automatic evolutionary 3D-2D image registration procedure proposed.

- *Model the latter sources of uncertainty*. We aim to model the identified sources of uncertainty considering fuzzy sets in order to improve the performance of the evolutionary techniques considered to solve the problem.

- *Analyze the performance of the proposed methods*. We aim to validate the different evolutionary skull-face overlay method designed over several real-world identification cases previously addressed by the staff of the Physical Anthropology lab at the University of Granada in collaboration with the Spanish Scientific police. We also aim to evaluate the best results automatically derived when tackling those real-world identification cases in comparison to the overlays obtained by the forensic anthropologists.

C. Structure

In order to achieve the previous objectives, the current dissertation is organized in seven chapters. The structure of each of them is briefly introduced as follows.

In Chapter 1 we introduce the area of forensic identification by craniofacial superimposition, analyzing its fundamentals, evolution and the shortcomings of current

techniques. We also present image registration and evolutionary algorithms. In particular, the basis of covariance matrix adaption-evolutionary strategy and scatter search are reviewed, as these two algorithms will become the base of our proposal.

Chapter 2 provides a deep description of the field of computer-aided craniofacial superimposition, updating previous reviews existing in the literature by both adding recent works and considering a new computing-based classification criterion. We study advantages and disadvantages of different approaches and propose a new general framework for computer-based craniofacial superimposition.

In Chapter 3 we propose a novel formulation for the skull-face overlay task as a numerical optimization problem. Different designs of real-coded evolutionary algorithms to tackle this problem are introduced and tested on some real-world identification cases previously addressed by the staff of the Physical Anthropology lab at the University of Granada. In addition, an analysis on the performance of the algorithms depending on the selected parameter values is accomplished.

Chapter 4 introduces a scatter search-based approach to tackle skull-face overlay with the aim of providing a faster and more robust algorithm than those in the literature and in our previous proposal. The new method is also validated on some real-world identification cases.

In Chapter 5 we study the sources of uncertainty associated with the skull-face overlay and the objects involved there in (a skull and a face). In order to overcome most of the shortcomings related to the different sources of uncertainty, two different approaches to handle the imprecision in landmark location are proposed. Again, we validate these proposals considering real-world identification cases.

Chapter 6 is devoted to evaluate the actual performance of the proposed skull-face overlay methodology based on evolutionary algorithms and fuzzy sets theory. To do so, the overlays achieved by our automatic method when tackling the real-world forensic identification cases presented in this dissertation are compared to the manual skull-face overlays attained by the forensic experts.

Finally, the results achieved in this dissertation are summarized in Chapter 7, which also includes some conclusions and future works. The most relevant achievements extracted from the experimentation carried out in the different chapters composing this dissertation are reported. Besides, some new research lines for further improvements of automatic methods to develop forensic identification by craniofacial superimposition using soft computing are proposed.

Chapter 1

Introduction

Live as if you were to die tomorrow.
Learn as if you were to live forever.

Mahatma Gandhi (1869-1948)

1.1 Introduction

This chapter is devoted to introduce the reader to those research fields where the current dissertation is focused on. On the one hand, the basis of the forensic identification by craniofacial superimposition technique will be reviewed, since the main goal of the dissertation lies in the development of new approaches to automatically tackle this task with the help of the computer. On the other hand, the remainder of the chapter refers to image registration and advanced evolutionary algorithms, as the proposed approaches to deal with the craniofacial superimposition task will be based on those computer science techniques, as well as on other soft computing methods.

1.2 Craniofacial superimposition

In this Section we first introduce forensic medicine and human identification, focusing on forensic anthropology procedures. Then, forensic identification by craniofacial superimposition is described. After reviewing the fundamentals of craniofacial superimposition, its evolution concerning the devices used is given. Finally, drawbacks of current craniofacial superimposition techniques are presented.

1.2.1 Introduction to human identification and Forensic Medicine

Forensic medicine is the discipline that deals with the identification of alive and dead human beings. Within forensic medicine, we can find three different specialties: forensic anthropology, forensic odontology, and forensic pathology. The former discipline is “best conceptualized more broadly as a field of forensic assessment of human skele-

tonized remains and their environments" (Iscan 1981a; Iscan 1981b). This assessment includes both the identification of the victim's physical characteristics and cause and manner of death from the skeleton (Krogman and Iscan 1986). This way, the most important application of forensic anthropology is to determine the identity of a person from the study of some skeletal remains, usually in the case of missing people, as well as under circumstances of war and mass disasters (Burns 2007).

Before making a decision on the identification, anthropologists follow different processes to assign sex, age, human group, and height to the human remains from the study of ante-mortem data (which can be retraced on the basis of visual material and interviews with relatives or witnesses) and the post-mortem data (the skeletal remains found, i.e. bones). For these purposes, different methodologies have been proposed, according to the features of the different human groups of each region (Alemán et al. 1997; Iscan 2005; Urquiza et al. 2005; González-Colmenares et al. 2007; Landa et al. 2009). These anthropological studies are usually taken as the first step of the identification process, previous to the application of any other technique, since the determination of the main parameters (sex, age, stature, build, teeth, possible pathologies, etc.) allows the set of people to compare with to be delimited.

Nevertheless, there are several other identification procedures which can be applied either after the forensic anthropology study or without it, being more reliable than skeleton-based identification, such as (Stratmann 1998):

1. Comparison of fingerprints, foot and hand prints.

2. Comparison of data on the jaw and teeth (dental information).

3. External and internal autopsy. In the former, the location, size and significance of scars, moles, tattoos and even callous spots on hands and feet are compared. Meanwhile, the internal autopsy looks for correspondence with regard to diseases and operations of the "disappeared person" which are retraceable in the body found.

4. DNA research demonstrating a blood relation with known family members.

The problem with the latter identification methods is that in some occasions there is not enough (ante- or post-mortem) information available to apply them. With regards to post-mortem data, the state of preservation of a corpse can considerably vary as a result of several chemical and mechanical factors. While the skeleton usually survives to both natural and non natural decomposition processes (fire, salt, water, . . .),

the soft tissues (skin, muscles, hair, etc.) progressively vanish. The disadvantage of the DNA test is concretely the required availability of a relatively large amount of high-quality tissue material, which is not so usual in remains that were buried since long time ago. On the other hand, as regards the ante-mortem information, the first method needs of a print database, the second of dental records (although teeth are more resistant -in comparison with bones and skin- against the effects of fire and salt water), the third of previous X-ray images (among other information), and the last one of a DNA sample of the same person or of a relative.

Hence, anthropological identification based only on the skeleton information can be considered as the last chance for forensic identification when none of the previous methods can be applied. If the previous skeleton study shows positive results and none of those methods can be applied, more specific skeleton-based identification techniques are alternatively applied such as *craniofacial superimposition* (CS) (Rathburn 1984; Iscan 1993; Taylor and Brown 1998), where photographs or video shots of the "disappeared person" are compared with the skull that is found. This technique is deeply described in the following section since it is the core of all the approaches proposed in this dissertation.

1.2.2 Fundamentals of the craniofacial superimposition identification method

As said, CS (Iscan 1993) is a forensic process where photographs or video shots of a missing person are compared with the skull that is found. By projecting both photographs on top of each other, the forensic anthropologist can try to establish whether that is the same person (Krogman and Iscan 1986).

Successful comparison of human skeletal remains with artistic or photographic replicas has been achieved many times using the CS technique, ranging from the studies of the skeletal remains of the poet Dante Alighieri in the nineteenth century (Welcker 1867) to the identification of victims of the recent Indian Ocean tsunami (Al-Amad et al. 2006). Among the huge number of case studies where CS has been applied[1], it is worth noting it was helpful in the identification of well-known criminals as John Demanjuk (known to Nazi concentration camp survivors as "Ivan the Terrible") and Adolf Hitler's chief medical officer Dr. Josef Mengele at Sao Paulo, Brazil in 1985 (Helmer

[1] Although there is not a register to evaluate the exact number of cases in which CS has been used and/or resulted in positive results, it would appear to be in the hundreds only in Australia (Stephan et al. 2008). Besides, Lan et. al reported in 1992 that their system had been used to identify more than 300 cases in China by that time (Lan 1992).

Figure 1.1: From left to right, principal craniometric landmarks: lateral and frontal views

1986). Furthermore, it is currently used in the identification of terrorists (Indriati 2009).

Important contributions during the first period of CS are those devoted to study the correspondence of the cranial structures with the soft tissue covering them (Broca 1875). Bertillon (1896) introduced the basis to collect physiognomic data of the accused of a crime at the end of the nineteenth century. Such data is still used nowadays.

Beyond that information, the drawback of CS identification is that there is not still a systematic method for the forensic analysis by image superimposition, but every researcher applies his own methodology. However, there are of course common factors to every research. Indeed, in every system for skull identification by CS two objects are involved: the skull found and the image of the face of the candidate subject. The latter is typically a photograph although it can be sometimes replaced by a series of video shots or, in few cases, a portrait of the missing person. The final goal, common to every system, is to assess the anatomical consistency between the skull and the face.

This process is guided by a number of anthropometrical landmarks located in both the skull and the photograph of the missing person. The selected landmarks are located in those parts where the thickness of the soft tissue is low. The goal is to facilitate their location when the anthropologist must deal with changes in age, weight, and facial expressions. The typically used skull landmarks (George 1993) (see Figure 1.1) follows:

Craniometric landmarks:

Dacryon (Da): The point of junction of the frontal, maxillary, and lacrimal bones on the lateral wall of the orbit.

Frontomalar temporal (Fmt): The most lateral point of junction of the frontal and zigomatic bones.

Glabella (G): The most prominent point between the supraorbital ridges in the midsagittal plane.

Gnathion (Gn): A constructed point midway between the most anterior (Pog) and most inferior (Me) points on the chin.

Gonion (Go): A constructed point, the intersection of the lines tangent to the posterior margin of the ascending ramus and the mandibular base, or the most lateral point at the mandibular angle.

Nasion (N): The midpoint of the suture between the frontal and the two nasal bones.

Nasospinale (Ns): The point where a line drawn between the lower margins of the right and left nasal apertures is intersected by the midsagittal plane (MSP).

Pogonion (Pog): The most anterior point in the midline on the mental protuberance.

Prosthion (Pr): The apex of the alveolus in the midline between the maxillary central incisor.

Zygion (Zy): The most lateral point on the zygomatic arch.

Meanwhile, the most usual face landmarks (see Figure 1.2) are:

Cephalometric landmarks:

Alare (al): The most lateral point on the alar contour.

Ectocanthion (Ec): The point at the outer commissure (lateral canthus) of the palpebral fissure just medial to the malar tubercle (of Whitnall) to which the lateral palpebral ligaments are attached.

Endocanthion (En): The point at the inner commissure (medial canthus) of the palpebral fissure.

Glabella (g'): In the midline, the most prominent point between the eyebrows.

Gnathion (gn'): The point on the soft tissue chin midway between Pog and Me.

Gonion (go'): The most lateral point of the jawline at the mandibular angle.

Figure 1.2: From left to right, principal facial landmarks: lateral and frontal views

Menton (Me): The lowest point on the MSP of the soft tissue chin.

Nasion (n): In the midline, the point of maximum concavity between the nose and forehead. Frontally, this point is located at the midpoint of a tangent between the right and left superior palpebral folds.

Pogonion (pog'): The most anterior point of the soft tissue chin.

Labiale inferius (Li): The midpoint on the vermilion line of the lower lip.

Labiale superius (Ls): The midpoint on the vermilion line of the upper lip.

Subnasale (sn): The midpoint of the columella base at the angle where the lower border of the nasal septum meets the upper lip.

Tragion (t) Point in the notch just above the *tragus* of the ear; it lies 1 to 2 mm below the spine of the helix, which can be palpated.

Zygion (Zy'): The most lateral point of the check (zygomaticomalar) region.

Regarding the process to superimpose the skull and face images, there are two common operations that have to be done (Chandra Sekharan 1993; Donsgsheng and Yuwen 1993; Yuwen and Dongsheng 1993): i) the determination of the real size of the figures (scaling), since it would be impossible to overlay images with a different relative size; and ii) the orientation method for the skull, to make it correspond to the face position in the photograph. There are three possible moves: inclination, extension, and rotation. This way, the strong relation between the desired procedure and *the image registration* problem in computer vision (Brown 1992; Zitová and Flusser 2003) which will be described in Section 1.3, can be easily identified.

Besides, from the former we can draw the underlying uncertainty involved in the process. The correspondence between facial and cranial anthropometric landmarks

is not always symmetrical and perpendicular as some landmarks are located in a higher position in the face than in the skull, and some others have not got a directly related landmark in the opposite landmark set. The identification can be manually done by measuring the distances between the different pairs of points, although this procedure can be influenced by errors when resizing (scaling) the images. It should be kept in mind that in anthropometry the allowed error is of 1 millimeter in long bones and of 0.5 millimeters in face and small bones measurements. So, we found a clear partial matching situation.

As a final result, the identification decision is usually expressed according to several confidence levels, depending on the chances of the sample (degree of conservation) and of the analytical process put into effect:

- Positive identification.
- Negative identification.
- Highly likely positive identification.
- Lowly likely positive identification.
- No identification due to lack of evidence or insufficient material.

In other words, "absolute matching" "absolute mismatching", "relative matching", "relative mismatching", and "lack of information". Hence, we again find the uncertainty and partial truth involved in the identification process.

1.2.3 Historical evolution of craniofacial superimposition concerning the supporting technical devices

The advancement of the technological support from the initial identifications has leaded to a large number of very diverse CS approaches found in the literature.

Although the common foundations of those approaches were previously laid, the technical procedure evolved as new technology was becoming available. That could be one of the reasons for the current diversity of CS methods and terms. Instead of following a uniform methodology, every expert tends to apply his own approach to the problem based on the available technology and on his deep knowledge on human craniofacial anatomy, soft tissues, and their relationships.

Some of these approaches were classified in a review by Aulsebrook et. al. (Aulsebrook et al. 1995) according to the technology used to acquire the data and to support the skull-face overlay and identification processes, i.e. static photographic transparency, video technology, and computer graphics. Similar classification schemes have been also reported by other authors (Nickerson et al. 1991; Yoshino and Seta 2000), which describe how CS has passed through three phases: photographic superimposition (developed in the mid 1930s), video superimposition (widely used since the second half of the 1970s), and computer-aided superimposition (introduced in the second half of the 1980s).

Following, the more representative works along the historical development of this process are presented. Important contributions during the first epoch of CS are those devoted to study the correspondence of the cranial structures with the soft tissue covering them (Broca 1875). Bertillon (1896) introduced the basis to collect physiognomic data of the accused of a crime at the end of the nineteenth century. As said, such data is still used nowadays. Much later, Martin and Saller (1966) proposed all the anthropological measurements, indices, and features which are the base of the anthropological studies presently. Following those premises, the usual procedure of the first identifications by means of CS consisted of obtaining the negative of the original face photograph and marking the cephalometric landmarks on it. The same task was to be done with a skull photograph. Then, both negatives were overlapped and the positive was developed. This procedure was specifically named *photographic superimposition*.

When the rapid development of video technology arised in the late eighties, forensic anthropologists exploited the benefits of those devices for *video superimposition* (Seta and Yoshino 1993; Shahrom et al. 1996; Yoshino et al. 1997). Video superimposition has been preferred to photographic superimposition since the former is simpler and quicker (Jayaprakash et al. 2001). It overcomes the protracted time involved with photographic superimposition, where many photographs of the skull must be taken in varying orientations (Nickerson et al. 1991). However, it has been indicated that CS based on the use of photographs is better than using video in terms of resolutions of details (Yoshino et al. 1995a).

The use of computers to assist the anthropologists in the identification process involved the next generation of CS systems (Yoshino et al. 1997). Attempts to achieve high identification accuracy through the utilization of advanced computer technology (*computer-aided CS*) has been a monumental task for experts in the field in the last two decades (Lan 1992). Without a doubt, the next challenge for CS is the ability to seize the opportunity provided by computer science in general, and computer graphics, computer vision, and artificial intelligence disciplines in particular. Beyond those

works using computers just as storage devices or simple visualization tools, there are different proposals exploiting the real advantages of both digital devices and computer science (Nickerson et al. 1991; Ghosh and Sinha 2001). Moreover, the use of 3D models and advanced computer-assisted techniques has recently demonstrated to be helpful in closely related forensic fields as personal identification (De Angelis et al. 2009) and facial approximation (Benazzi et al. 2009).

1.2.4 Discussion on the craniofacial superimposition reliability

CS itself is a really solid identification method. As said, the basis of this technique were introduced by Bertillon in (1896). Thus, it has been used for more than one hundred years, helping to solve hundreds of identification cases. It peaked in the 1990-1994 period and subsequently declined. According to Ubelaker (Ubelaker 2000), these frequencies appear to reflect the availability of the necessary equipment and expertise in 1990, coupled with awareness of the value of this approach in the forensic science and law enforcement communities. The decline in use likely reflects both the increased awareness of the limitations of this technique and the greater availability of more precise methods of identification, especially the molecular approaches.

In fact, basic methodological criteria that ensure the reliability of the technique have not been established yet. Whatever the nature of the approach to tackle CS, some authors (Shahrom et al. 1996; Jayaprakash et al. 2001; Cattaneo 2007) agree that this technique should be used only for excluding identity, rather than for positive identification. Seta and Yoshino (1993) state the general rule that superimposition is of greater value in ruling out a match, because it can be definitely stated that the skull and photograph are not those of the same person. If they do align, it can only be stated that the skull might possibly be that of the person in the photograph. Nevertheless, a research carried out on a very large number of comparisons indicates that there is a 9% chance of misidentification if just one photograph is used for the comparison, and this probability of false identification diminishes to less than 1% if multiple photographs from widely different angles to the camera are used (Austin-Smith and Maples 1994). Unfortunately, these successful identification rates have not been accepted by judges as a fully reliable identification technique. In particular, Spanish courts only accept CS results as an excluding evidence.

In a similar way, Yoshino et al. (1995b) study the anatomical consistency of CS images for evaluating the validity in personal identification by the superimposition method. They concluded that the CS method is reliable for individualization when two or more facial photographs taken from different angles are used in the examination.

However, according to (Albert et al. 2007) it is recommended to use recent photographs or not to consider age-related features, otherwise algorithms for predicting what an adult head and face at one point in time might look like several years later will be necessary.

1.3 Image Registration

Image registration (IR) (Brown 1992; Zitová and Flusser 2003; Goshtasby 2005) is a fundamental task in computer vision and computer graphics used to finding either a spatial *transformation* (e.g, rotation, translation, etc.) or a correspondence (matching of similar image features) among two or more images acquired under different conditions: at different times, using different sensors, from different viewpoints, or a combination of them. IR aims to achieve the best possible overlapping transforming those independent images into a common one. Over the years, IR has been applied to a broad range of practical environments ranging from remote sensing to medical imaging, artificial vision, and computer-aided design (CAD). Likewise, different techniques facing the IR problem have been studied resulting in a large body of research.

As said, IR is the process of finding the optimal *transformation* achieving the best fitting between typically two images, usually called *scene* and *model*. They both are related by the said transformation and the degree of resemblance between them is measured by a *Similarity metric*. Such transformation estimation is interpreted into an iterative *optimization procedure* in order to properly explore the search space.

Several works reviewing the state of the art on IR methods have been contributed in the last few years (Brown 1992; Maintz and Viergever 1998; Zitová and Flusser 2003; Goshtasby 2005; Salvi et al. 2007). Despite an extensive survey on every aspect related to the IR framework is out of the aim of this work, we would like to briefly describe the key concepts concerning the IR methodology in order to achieve a better understanding of our work.

There is not a universal design for a hypothetical IR method that could be applied to all registration tasks, since various considerations on the particular application must be taken into account. Nevertheless, IR methods usually require the four following components (see Figure 1.3): two input **Images** (see Section 1.3.1) named scene $I_s = \{\vec{p}_1, \vec{p}_2, \ldots, \vec{p}_n\}$ and model $I_m = \{\vec{p}_1{}', \vec{p}_2{}', \ldots, \vec{p}_m{}'\}$, with $\vec{p}_i$ and $\vec{p}_j{}'$ being image points; a **Registration transformation** f (see Section 1.3.2), being a parametric function relating the two images; a **Similarity metric** F (see Section 1.3.3), in order to measure a qualitative value of closeness or degree of fitting between the transformed

scene image, noted $f'(I_s)$, and the model image; and an **Optimizer** which looks for the optimal transformation f inside the defined solution search space (see Section 1.3.4). Next, each of the four IR components are described. Besides, a brief overview of the state-of-the-art in evolutionary IR is given in Section 1.3.5 since these concepts are required for a good understanding of this dissertation.

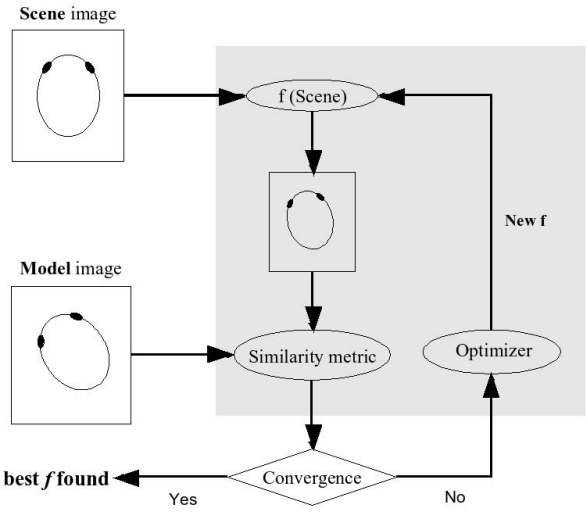

Figure 1.3: The IR optimization process

1.3.1 Nature of the images

IR methods proposed in the literature have addressed problems in different 2D and 3D image modalities. The former is commonly addressed in aerial and satellite applications, while the later is present in more challenging real-world problems such a medical applications (Goshtasby 2005; Zitová and Flusser 2003).

Medical image is an extensive application field for IR dealing with 2D and 3D images acquired by well-known medical image devices such as the magnetic resonance images (MRIs), computer tomography (CT) images, and single-photon emission computerized tomography (SPECT) images. In addition, other acquisition devices as laser range scanners are also extensively used in the area for other IR domains as 3D object recognition, 3D object modeling/reconstruction, and a wide variety of computer vision and computer graphics-related fields (Bernardini and Rushmeier 2002).

Laser range scanners use the optical principle of triangulation to obtain a dense point set of surface data. In order to achieve a complete 3D model, they acquire multiple 3D images (named range images) of the object from different viewpoints. Every range image partially recovers the complete geometry of the sensed object and it is placed in a different coordinate system (see Figure 1.4). Then, to achieve a complete and reliable model of the physical object it is mandatory to consider a reconstruction technique to perform the accurate integration of the images. This framework is usually called *3D model reconstruction* and is based on applying *range IR* (RIR) techniques (Blais and Levine 1995; Campbell and Flynn 2001; Ikeuchi and Sato 2001; Salvi et al. 2007; Ikeuchi and Miyazaki 2008). There are two RIR approaches to integrate multiple range images. The *accumulative* approach accomplishes successive applications of a pair-wise RIR method[2]. Once an accumulative RIR process is carried out the *multiview* approach takes into account all the range images at the same time to perform a final global RIR step.

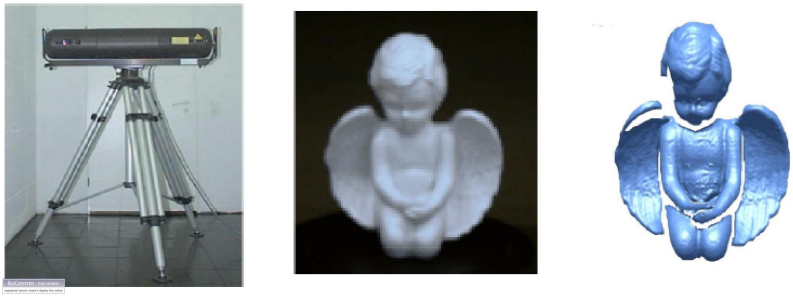

Figure 1.4: From left to right: laser range scanner, photograph of the object scanned, and range image acquired from that viewpoint

Regardless the acquisition device, IR methods can be classified as *voxel*-based (or *intensity/surface*-based) and *feature*-based according to the nature of the images they must deal with (Brown 1992; Zitová and Flusser 2003). While the former approaches directly operate with the images raw data, the latter ones introduce a pre-processing step of the images (before the application of the IR method) in order to extract a reduced subset with the most relevant features. Since voxel-based methods can deal with a larger amount of data, they are often considered as *fine-tuning* registration processes. On the other hand, feature-based methods typically achieve a *coarser* approximation to the global solution due to the reduced set of characteristics they take

[2]The use of the term *pair-wise* is commonly accepted to refer to the registration of pairs of adjacent range images.

into account. Thus, the latter approach is usually followed by a final refinement stage to achieve accurate IR results.

Most of the voxel-based approaches tackle the IR problem looking for corresponding patterns in the scene and the model images. There is a need to delimit the region where the search is accomplished because of the large datasets under study. Therefore, voxel-based IR methods usually rely on a rectangular window that constrains the search of correspondences between scene and model images. That is an important drawback when the images are deformed by complex transformations. In those cases, this type of window will not be able to cover the same parts of the transformed scene and model images. Moreover, if the window contains a smooth image region without any prominent detail, it will be likely incorrectly matched to other smooth image region in the model image by mistake. Nevertheless, the principal shortcoming of voxel-based methods appear when there are changes in the illumination conditions during the acquisition of the scene and the model images. In that case, the similarity metric offers unreliable measurements and it induces the optimization process to be trapped in local minima.

In order to avoid many of the drawbacks related to voxel-based methods, the second IR approach is based on the extraction of prominent geometric primitives (*features*) from the images (Brown 1992; Zitová and Flusser 2003). The proper comparison of feature sets will be possible using a reliable feature detector that accomplishes the accurate extraction of invariant features. Those are features which are not affected by changes in the geometry of the images, radiometric conditions, and appearance of noise. There are many different kinds of features that can be considered, e.g., *region features*, *line features*, and *point features*. Among them, corners are widely used due to their invariance to the image geometry.

1.3.2 Registration transformations

We can classify IR methods according to the registration transformation model used to relate both the scene and the model images. The first category of transformations includes *linear transformations*, which preserve the operations of vector addition and scalar multiplication, being a combination of translation, rotation, scaling, and shear components. Among the most common linear transformations in IR we found rigid, similarity, affine, projective, and curved.

Linear transformations are global in nature, thus not being able to model local deformations. The second category of transformation models includes *"elastic"* or *"non-rigid"* transformations. These transformations allow local warping of image

features, thus allowing local deformations.

The transformation to be considered will depend on the application addressed and the nature of the images involved in IR.

1.3.3 Similarity metric

One of the most important components of any IR method is the similarity metric (Svedlow et al. 1976). It is considered as a function F that measures the goodness of the IR problem solution given by a registration transformation f. The final performance of any IR method will rely on the accurate estimation of F.

Each solution is evaluated by F as follows. First, f is applied to one of the two input images, usually the scene image ($f(I_s)$). Next, the degree of closeness or fitting between the transformed scene and the model images, $\Psi()$, must be determined:

$$F(I_s, I_m, f) = \Psi(f(I_s), I_m). \tag{1.1}$$

There are different definitions of $\Psi()$ depending on the dimensionality (2D or 3D) and the nature of the considered images:

- Voxel-based approaches: sum of squared differences (Barnea and Silverman 1972), normalized cross-correlation (i.e., correlation coefficient (Svedlow et al. 1976) or phase correlation (De Castro and Morandi 1987)), and mutual information (Viola and Wells 1997).
- Feature-based approaches: metrics based on feature values and distance between corresponding geometric primitives (Audette et al. 2000; Muratore et al. 2002; Allen et al. 2003; Chao and Stamos 2005).

As the previous IR components, the F function is also affected by both the discretization of images and the presence of noise, causing worse estimations and favoring the IR method to get trapped in local minima.

Notice that, the huge amount of data often required makes the problem solving very complex and the IR procedure very time-consuming. Therefore, most of the IR contributions use any *spatial indexing* data structure in order to speed up the similarity metric computation. It aims to improve the efficiency of the considered optimization method, each time the closest point assignment computation between the transformed scene and model images must be computed. Likewise, that data structure is computed

only once at the beginning of the IR method. Two main variants of spatial indexes can be found in the IR literature:

- *Kd-tree,* it is based on a generalization of bisection in one dimension to k dimensions (k=2 in 2D and k=3 in 3D). It consists of a binary tree that successively splits the whole space into two rectangular parallelepipeds such that there is an approximately equal number of points on both sides of the cutting plane, for the xy, xz, and yz planes. The first proposal applying kd-trees to the IR problem is to be found in (Zhang 1994).

- *Distance map,* according to either a 3D or 2D image modalities, a discretized volume or plane is built, respectively. Every cell of this data structure usually stores the Euclidean distance to the closest point of the mapped image, commonly the model one. Distance maps have been widely used in image processing and they have been recently applied to solve IR problems with genetic algorithms (Rouet et al. 2000) (see next subsection and Section 1.3.5). Moreover, Yamany et al. (Yamany et al. 1999) considered a particular distance map, named *grid closest point* (GCP), which consists of two cubes splitting the 3D space. The first one divides it into a grid of $L \times W \times H$ cells and it wraps around scene and model images. The second one only covers the model image within a rectangular volume of double resolution ($2L \times 2W \times 2H$ cells). The goal of this second grid is to reduce the discretization error of the former in order to achieve more accurate outcomes in the final stages of the IR process.

1.3.4 Search strategies

As said, the key idea of the IR process is focused on determining the unknown parametric *transformation f* that relates two images by placing them in a common coordinate system, bringing corresponding points as close as possible. According to the search strategy component, we can distinguish two different IR approaches in the literature to determine that parametric transformation:

- *Matching*-based approach: it performs a search in the space of feature correspondences (typically, correspondences of image points). Once the matching of scene and model features is accomplished, the registration transformation is derived.

- *Parameter*-based approach: a direct search in the space of the f parameters is carried out.

Matching-based image registration approach This search space exploration strategy needs to develop the two following steps. First, a set of correspondences in both the scene and the model images must be established. Next, the transformation f is retrieved by numerical methods considering that matching (see Figure 1.5). *Least squares* (LSq) estimators are the most commonly used numerical methods (Arun et al. 1987; Horn 1987; Faugeras 1996) within this approach, due to their special and interesting properties, e.g., they only require means, variances and covariances (Luenberger 1997).

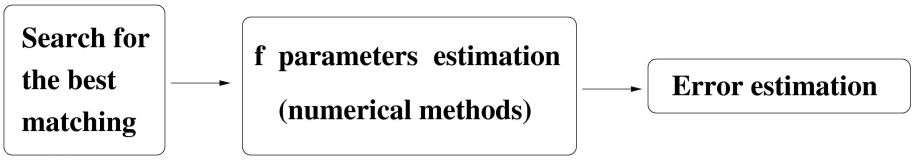

Figure 1.5: Matching-based IR approach

In the classical theory of estimation, the notion of outliers is vague. They can be interpreted as erroneous (noisy) observations which are well separated from the bulk of the data, thus demanding special attention. Besides, it is assumed that outliers will not provide any outstanding information about f parameters. On the contrary, they can severely damage its correct estimation.

LSq estimators assume that the observation of errors must be normally distributed to perform correctly. In the related literature, we can find some works proposing extensions of the LSq estimator based on the analysis of residuals of the *L2 norm* (least squares) to identify erroneous observations (El Hakim and Ziemann 1984; Förstner 1985). Since outliers have an unknown distribution of observations, these kinds of estimators cannot guarantee inferring the true transformation. Thus a robust estimator may be better suited. In particular, the well known *M-estimators* (Huber 1981) are based on a re-weighting scheme and they have been considered to tackle the IR problem (Arya et al. 2007).

Therefore, the complexity of both the matching step and the subsequent registration transformation estimation strongly depends on the method being considered. Likewise, an iterative process may be followed either for the estimation of the matching, or the registration, or both, until reaching convergence within a tolerance threshold of the concerned similarity metric. This is the case of the *Iterative Closest Point (ICP)* algorithm (Besl and McKay 1992), well-known in computer-aided design systems and originally proposed to recover the 3D transformation of pairs of range images. Next, we will briefly describe the structure of this local optimizer in order to get a better understanding of the strategy. The method proceeds as follows:

- A point set P with N_p points $\vec{p}_i$ (cloud of points) from the data shape (scene) and the model image X —with N_x supporting geometric primitives: points, lines, or triangles— is given. The original paper dealt with 3D rigid transformations stored in the solution vector

$$\vec{q} = [q_1, q_2, q_3, q_4, t_1, t_2, t_3]^t$$

  where the first four parameters corresponded to the four components of a quaternion determining the 3D rotation, and the last three parameters stored the translation vector.

- The procedure is initialized by setting $P_0 = P$, the initial registration transformation to $\vec{q}_0 = [1,0,0,0,0,0,0]^t$, and the iteration counter $k = 0$. The next four steps are applied until convergence within a tolerance $\tau > 0$:

  1. Compute the matching between the data (scene) and model points by the closest assignment rule: $Y_k = C(P_k, X)$
  2. Estimate the registration by least squares: $f_k = \rho(P_0, Y_k)$
  3. Apply the registration transformation to the scene image: $P_{k+1} = f_k(P_0)$
  4. Terminate iteration if the change in *Mean Square Error* (MSE) falls below τ. Otherwise, $k = k+1$. Go to 1.

Notice that ICP is not directly guided by the similarity metric but by the computed matching, as the remaining matching-based IR methods. In this strategy, the function F (typically the Mean Square Error, MSE) only plays the role of the stopping criterion. Moreover, the transformation estimator (numerical method) is dependent on the good outcomes of the matching step. Thus, the better the choice of the correspondences that is performed, the more precise the estimation of the transformation f. Consequently, the value of the similarity metric will be more accurate leading to a proper convergence.

The original ICP proposal has three main drawbacks: i) the algorithm is very dependent on the initial guess and it likely gets trapped in local optima solutions, which forces the user to manually assist the IR procedure in order to overcome these undesirable situations; ii) one of the two images (typically the scene one) should be contained in the other, e.g., in feature-based IR problems, the geometric primitives of one

image should be a subset of those in its counterpart image; and iii) as previously mentioned, it can only handle normally distributed observations. Since that original proposal, many contributions have been presented extending and partially solving the latter shortcomings (Zhang 1994; Feldmar and Ayache 1996; Rusinkiewicz and Levoy 2001; Liu 2004).

On the other hand, additional matching-based IR methods based on evolutionary algorithms and metaheuristics can be found in (Cordón and Damas 2006; Cordón et al. 2008)

Parameter-based image registration approach Opposite to the previous approach, this second one involves directly searching for the solution in the space of parameters of the transformation f (see Figure 1.6). In order to perform that search, the registration transformation f is parameterized and each solution to the IR problem is encoded as a vector composed of each one of the values for the parameters of f.

Figure 1.6: Parameter-based IR approach

Thus, the IR method generates possible vectors of parameter values, that is, candidate registration transformation definitions. Unlike ICP-based strategies, the search space exploration is directly guided by the similarity metric F. Each solution vector is evaluated by such metric, thus clearly stating the IR task as a numerical optimization problem involving the search for the best values defining f that minimize F.

Notice that, orders of magnitude in the scale of f parameters are crucial for IR methods dealing with this search space strategy. Unit changes in angle have much greater impact on an image than unit changes in translation. Indeed, when applying a rotation, the further a given point on the image from its center of mass (origin of rotation), the greater the displacement. Meanwhile, the distance between the transformed scene and the model images is kept constant in case of translations. This difference in the scale appears as elongated valleys in the parameter search space, causing difficulties for the traditional gradient-based local optimizers (Besl and McKay 1992; He and Narayana 2002). Therefore, if the considered IR method is not robust tackling these scenarios, the theoretical convergence of the procedure is not guaranteed and it will get

trapped in local minima in most cases.

Together with the commonly used local optimizers (Maes et al. 1999), evolutionary algorithms are the most used optimization procedure for IR when this search space strategy is considered. That is shown by the large number of evolutionary IR contributions proposed so far (Simunic and Loncaric 1998; Yamany et al. 1999; Matsopoulos et al. 1999; Rouet et al. 2000; Yuen et al. 2001; Chalermwat et al. 2001; Chow et al. 2001; He and Narayana 2002; Chow et al. 2004; Silva et al. 2005; Cordón et al. 2006; Cordón et al. 2006; Lomonosov et al. 2006) (see Section 1.3.5). Unlike IR methods based on local optimizers, the main advantage of using evolutionary IR methods is that they do not require a solution near to the optimal one to achieve high quality registration results.

1.3.5 Evolutionary image registration

Solving CS following an IR approach involves a really complex optimization task. The corresponding search space is huge and it presents many local minima. Hence, exhaustive search methods are not useful. Furthermore, forensic experts demand highly robust and accurate results. IR approaches based on evolutionary algorithms are a promising solution for facing this complex optimization problem. Due to the global optimization nature of evolutionary techniques, they own the capability to perform robust search in complex and ill-defined problems as IR. Taking the latter as a base, we have considered the use of genetic algorithms and two advanced evolutionary algorithms, Covariance Matrix Adaption Evolutionary Strategy (CMA-ES) (Hansen and Ostermeier 2001) and Scatter Search (SS) (Glover et al. 2003). The fundations of these evolutionary methods will be described in Section 1.4 while the reminder of the current section will be devoted to briefly review the evolutionary IR field.

The application of evolutionary algorithms to the IR optimization process has caused an outstanding interest in the last few decades. Unlike traditional ICP-based IR approaches, evolutionary ones need neither rough nor near-optimal prealignment of the images to proceed. Thus, they have become a more robust alternative to tackle complex IR problems. Indeed, thanks to the global optimization nature of evolutionary algorithms, they aim to solve the drawbacks described by the ICP-based schemes (see Section 1.3.4). Figure 1.7 depicts the evolution of the interest of the scientific community in this sort of approaches[3].

[3]The graph in Figure 1.7 was directly obtained from Thomson Reuter's Web of Science using the query (Title OR Topic) ="image AND (registration OR alignment OR matching) AND (evolution* OR swarm OR chc OR neural OR scatter OR annealing OR tabu OR genetic)".

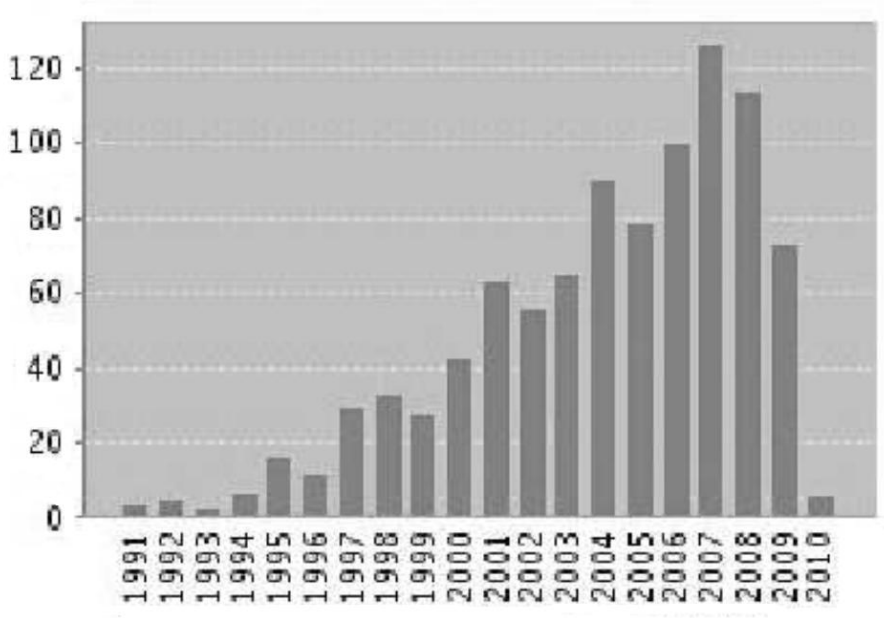

Figure 1.7: Scientific production in evolutionary IR

Regardless the IR approach to be followed, IR arises as a *non-linear optimization problem* that cannot be solved by a direct method (e.g. resolution of a simple system of linear equations) because of the uncertainty underlying the estimation of f. On the contrary, it must be tackled by means of an iterative procedure searching for the *optimal estimation* of f, following one of the said approaches. Classical numerical optimizers can be used. However they usually get trapped in a local minima solution. Hence, *the interest on the application of evolutionary algorithms to the IR optimization process has increased in the last decade due to their more suitable and improved global optimization behavior*.

The first attempts to solve IR using evolutionary computation approaches can be found in the early eighties. The size of data as well as the number of parameters that are looked for prevent from an exhaustive search of the solutions. An approach based on a genetic algorithm was proposed in 1984 for the 2D case and applied to angiographic images (Fitzpatrick et al. 1984). Later, in 1989, Mandava et al. (1989) used a 64-bit structure to represent a possible solution when trying to find the eight parameters of a bilinear transformation through a binary-coded genetic algorithm. Brunnström and Stoddart (1996) proposed a new method based on the manual pre-alignment of

range images followed by an automatic IR process using a novel genetic algorithm that searches for solutions following the matching-based approach. Tsang (1997) used 48-bit chromosomes to encode three test points as a base for the estimation of the 2D affine registration function by means of a binary-coded genetic algorithm. In the case of Yamany et al. (1999) and Chalermwat et al. (2001) proposals, the same binary coding is found when dealing with 3D and 2D rigid transformations, respectively. Yamany et al. enforced a range of $\pm 31^{\circ}$ over the angles of rotation and ± 127 units in displacement by defining a 42-bit chromosome with eight bits for each translation parameter and six bits for each rotation angle. Meanwhile, Chalermwat et al. used twelve bits for the coding of the 2D rotation parameter to get a search scope of $\pm 20.48^{\circ}$, therefore allowing the use of a precision factor for the discretization of the continuous rotation angle interval. Other ten bits stored each of the two translation parameters (± 512 pixels).

All the latter approaches showed several pitfalls from an evolutionary computation perspective. On the one hand, they make use of the basic binary coding to solve inherently real coded problems, when it is well known that binary coding suffers from discretization flaws (as problem solutions of search space never visited) and requires transformations to real values for each solution evaluation. Moreover, the kind of genetic algorithm considered is usually based on the old-fashioned original proposal by Holland (Holland 1975; Goldberg 1989). In this way, a selection strategy based on fitness-proportionate selection probability assignment and the stochastic sampling with replacement, as well as the classical one-point crossover and simple bit flipping mutation, are used. On the one hand, it is well known that such selection strategy causes a strong selective pressure, thus having a high risk of premature convergence of the algorithm. On the other hand, it has also been demonstrated that it is difficult for the single-point crossover to create useful descendants as it is excessively disruptive with respect to the building blocks (Goldberg 1989). Hence, the consideration of that old genetic framework is a clear pitfall affecting the latter group of proposals.

Summarizing, the application of several emerging EAs to IR has caused an outstanding interest to solve the problems of traditional local optimizer-based IR process. Since the first attempts to solve IR using EAs in 1984 (Fitzpatrick et al. 1984), a large amount of proposals has been carried out. Although many of them presented important limitations (Cordón, Damas, and Santamaría 2007), the topic has started to mature and some interesting proposals have solved many of the previous shortcomings.

1.4 Advanced Evolutionary Algorithms: CMA-ES and scatter search

An extensive survey on every aspect related to the evolutionary computation (EC) paradigm is out of the scope of this work. Interested readers can find a great amount of literature reviewing this field (Bäck et al. 1997; Eiben and Smith 2003; Fogel 2005). Nevertheless, we would like to briefly describe the key concepts of EC in order to achieve a better understanding of the basis of evolutionary IR.

In addition, we are particulary interested in two of the EAs considered as the current state-of-the-art in real coding optimization problems: Scatter Search (SS) (Glover et al. 2003) and Covariance Matrix Adaptation Evolution Strategy (CMA-ES) (Hansen and Ostermeier 2001; Hansen and Ostermeier 1996). Since they are the base of the proposed methods of this work, they will be described in Sections 1.4.2 and 1.4.3, respectively.

1.4.1 Evolutionary computation basics

Approximate or *heuristic* optimization methods (also named *metaheuristics* (Glover and Kochenberger 2003)) belonging to the field of EC (Bäck et al. 1997) use computational models of evolutionary processes for evolving population of solutions as key elements in the design and implementation of computer-based problem solving systems. EC approaches constitute a very interesting choice since they are able to achieve good quality outcomes when, for instance, global solutions of hard problems cannot be found with a reasonable amount of computational effort.

There is a variety of EC models that have been proposed and studied, which are referred as EAs (Bäck et al. 1997). Among them we refer to four well-defined EAs which have served as the basis for much of the activity in the field: genetic algorithms (GAs) (Goldberg 1989; Michalewicz 1996), evolution strategies (ES) (Schwefel 1993), genetic programming (GP) (Koza 1992), and evolutionary programming (EP) (Fogel 1991).

In particular, GAs are probably the most used EAs in the literature to face real-world optimization problems. GAs are theoretically and empirically found to provide global near-optimal solutions for various complex optimization problems. The search space represented in GAs is a collection of individuals (problem solutions) or chromosomes conforming a population, each of them simultaneously operating on several points of the search space. As depicted in Figure 1.8, an initial set/population of solu-

tions (noted as P) is randomly generated. Then, a pool of parents is randomly selected for reproduction on the basis of their *fitness function*, which measures how good is each candidate solution and guides the search space exploration strategy. The fitness or objective function is one of the most important components of heuristic methods whose design dramatically affects the performance of the method implemented. The reproduction procedure based on crossover and mutation operators is iteratively performed at every generation (iteration) in order to generate the offspring population. Crossover operators systematically/randomly mix parts (block of genes) of two individuals of the previous population, and additionally every new combined individual is subjected to random changes by using mutation operators. The next generation is produced using a replacement operator which selects individuals from the pool composed of the parents and the new offsprings generated.

Procedure Genetic Algorithm

```
begin
        t = 0;
        Initialize(P(t));
        Evaluate(P(t));
        While (Not termination-condition) do
        begin
                t = t + 1;
                P'(t) = Select(P(t − 1));
                P''(t) = Crossover(P'(t));
                P'''(t) = Mutate(P''(t));
                Evaluate(P'''(t));
                P(t) = Replace(P(t − 1), P'''(t));
        end
end
```

Figure 1.8: Pseudo-code of a basic GA

Some other EAs have been proposed in the last few years improving the state-of-the-art on this field by adopting more suitable optimization strategies: CHC algorithm[4] (Eshelman 1991; Eshelman and Schaffer 1991) and memetic algorithms (MAs) (Moscato 1989), among others (Bäck et al. 1997; Fogel 2005).

[4]The CHC acronym stands for: Cross generational elitist selection, Heterogeneous recombination, Cataclysmic mutation.

1.4.2 Covariance matrix adaption evolutionary strategy

Covariance Matrix Adaptation Evolution Strategy (CMA-ES) (Hansen and Ostermeier 2001; Hansen and Ostermeier 1996) is an evolutionary strategy for difficult non-linear non-convex optimization problems in continuous domains. More specifically, it is an advanced $(\mu - \lambda)$-evolution strategy that updates the covariance matrix (that is, on convex-quadratic functions, closely related to the inverse Hessian) of the multivariate normal mutation distribution. New candidate solutions are sampled according to the mutation distribution and the covariance matrix describes the pairwise dependencies between the variables in it. This makes the method feasible on non-separable and/or badly conditioned problems. In contrast to quasi-Newton methods the CMA-ES does not use or approximate gradients and does not even presume or require their existence. Hence, the method result to be feasible on non-smooth and even non-continuous problems, as well as on multimodal and/or noisy problems.

CMA-ES is considered as the state of the art in real-coded EAs. Its high performance was demonstrated in the IEEE CEC'2005 Competition on Real Parameter Optimization. For the given set of test functions (Suganthan et al. 2005), it had the lowest average error rate among all the participant EAs (Hansen 2005).

1.4.2.1 Fundamentals

The basic principle is to emulate classical methods of analytical optimization that use the Hessian matrix but with stochastic and evolutionary techniques for a very general family of functions with realistic behavior. The covariance matrix describes the pairwise dependencies between the variables in this distribution. Adaptation of the covariance matrix amounts to learning a second order model of the underlying objective function similar to the approximation of the inverse Hessian matrix in the Quasi-Newton method in classical optimization. In contrast to classical methods, only the ranking between candidate solutions is exploited during learning. A peculiarity of this method is that it does not requires derivatives nor even the function values.

Two principles for the adaptation of parameters of the mutation distribution are exploited in the CMA-ES algorithm. First, a maximum likelihood principle, based on the idea to increase the probability of a successful mutation step. The covariance matrix of the distribution is updated such that the likelihood of previously realized successful steps to appear again is increased. Consequently the CMA conducts an iterated principal components analysis of successful mutation steps while retaining all principle axis (see Figure 1.9. While estimation of distribution algorithms (Larrañaga and

Lozano 2002) are based on very similar ideas, they estimate the covariance matrix in maximizing the likelihood of successful solution points rather than successful mutation steps. Second, two paths of the time evolution of the distribution mean of the strategy are recorded, called evolution paths. Such paths contain significant information of the correlation between consecutive steps. Specifically, if consecutive steps are taken in a similar direction, the evolution path becomes longer. The evolution paths are exploited in two ways. One path is used for the covariance matrix adaptation procedure in place of single successful mutation steps and facilitates a possibly much faster variance increase of favored directions. The other path is used to conduct an additional step-size control. This step-size control aims to make consecutive movements of the distribution mean orthogonal in expectation. The step-size control effectively prevents premature convergence yet allowing fast convergence to an optimum.

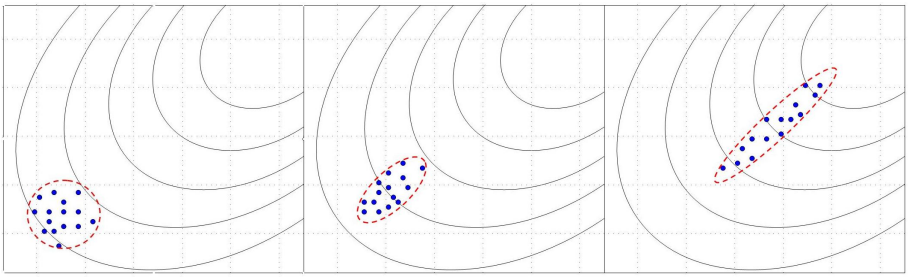

Figure 1.9: Concept behind the covariance matrix adaptation. As the generations develop, the distribution shape adapts to an ellipsoidal or ridge-like landscape.

1.4.2.2 General Flow

The most commonly used $(\mu/\mu_w, \lambda)$-CMA-ES design is outlined as follows, where in each iteration a weighted combination of the μ best out of λ new candidate solutions is taken in order to compute the distribution centre.

Given are the search space dimension n and, at iteration step g, the five state variables:

- $m_g \in \mathbb{R}^n$, the distribution mean and current best solution to the optimization problem,

- $\sigma_g > 0$, the step-size,
- C_g, a symmetric and positive definite $n \times n$ covariance matrix, and
- $p_\sigma \in \mathbb{R}^n, p_c \in \mathbb{R}^n$, two evolution paths.

The decision variable matrix distribution x is specified by:

- The distribution centre, which is defined by a point in the search space $\overrightarrow{m}$.
- An orientation in the coordinate axis, defined by the covariance matrix C.
- A variance, defined by the parameter σ^2.

In each iteration (g+1) the algorithm follows the next steps:

1. λ offsprings are independently created following a multi-variable normal distribution:

$$\overrightarrow{x}_k^{(g+1)} \sim N(\overrightarrow{m} =< \overrightarrow{x} >_w^t, \sigma^2 C^{(g)}) \tag{1.2}$$

for $k = 1, \ldots, \sigma$. Where $N(\overrightarrow{m}, C)$ noted a normally random vector distributed with mean $\overrightarrow{m}$ and covariance matrix C.

2. The λ created solutions are evaluated on the objective function $f : \mathbb{R}^n \to \mathbb{R}$ to be minimized and sorted depending on their fitness function value.

3. The μ best individuals are selected and the new mean value is computed:

$$m_{g+1} = \sum_{i=1}^{\mu} w_i x_{i:\lambda} \tag{1.3}$$

where $f(x_{1:\lambda}) \leq \cdots \leq f(x_{\mu:\lambda}) \leq f(x_{\mu+1:\lambda}) \ldots$, and the positive (recombination) weights $w_1 \geq w_2 \geq \cdots \geq w_\mu > 0$ sum to one.

Typically, $\mu \leq \lambda/2$ and the weights are chosen such that $\mu_w := 1/\sum_{i=1}^{\mu} w_i^2 \approx \lambda/4$. The only feedback used from the objective function here and in the following is an ordering of the sampled candidate solutions due to the indices $i : \lambda$.

4. Parameters $\overrightarrow{m}$, σ and C are updated only considering the μ best solutions, to focus the exploitation on the regions which contain these points.

   The updating process indicated in latter step is performed as follows:

$$\overrightarrow{m} =< \overrightarrow{x} >_w^{(g+1)} = \sum_{i=1}^{\mu} \omega_i \overrightarrow{x}_{i:\lambda}^{(g+1)} \tag{1.4}$$

   where $\omega_i \in \mathbb{R}$, $\omega_i \leq 0$ and $\sum_{i=1}^{\mu} \omega_i = 1$.

   The equations to update the rest of the parameters (size of the distribution σ and covariance matrix C) are described as follows:

   The step-size σ_g is updated using cumulative step-size adaptation, also known as path length control.

$$p_\sigma^{(g+1)} \leftarrow \underbrace{(1-c_\sigma)}_{\text{discount factor}} p_\sigma^{(g)} + \overbrace{\sqrt{c_\sigma(2-c_\sigma)\mu_{eff}}}^{\text{normalization constant for } p_c} \underbrace{C^{(g)\,-1/2}\ \frac{m^{(g+1)}-m^{(g)}}{\sigma^{(g)}}}_{\text{distributed as } \mathcal{N}(0,I) \text{ under neutral selection}}$$

$$\sigma^{(g+1)} = \sigma^{(g)} \exp\left(\frac{c_\sigma}{d_\sigma}\left(\frac{\|p_\sigma^{(g+1)}\|}{E\|\mathcal{N}(0,I)\|} - 1\right)\right) \tag{1.5}$$

   where:

   - $p_\sigma^{(g)} \in \mathbb{R}^n$ is the conjugate evolution path at generation g.

   - $c_\sigma < 1$, and, $1/c_\sigma$ is the backward time horizon of the evolution path. For small μ_{eff}, a time horizon between $\sqrt{n}$ and n is reasonable.

   - $\mu_{eff} = (\sum_{i=1}^{\mu} w_i^2)^{-1} = 1/\|w\|^2$, the variance effective selection mass

   Finally, the covariance matrix is updated, where again the respective evolution path is updated first.

$$p_c^{(g+1)} \leftarrow \underbrace{(1-c_c)}_{\text{discount factor}}\ p_c^{(g)} + \overbrace{\sqrt{c_\sigma(2-c_\sigma)\mu_{eff}}}^{\text{normalization constant for } p_c}\ \frac{m^{(g+1)}-m^{(g)}}{\sigma^{(g)}}$$

$$C^{g+1} = \underbrace{(1-c_1-c_\mu)}_{\text{discount factor}} C^g + c_1 \underbrace{p_c^{(g+1)} p_c^{(g+1)\,T}}_{\text{rank one updated}} + c_\mu \underbrace{\sum_{i=1}^{\mu} w_i \frac{x_{i:\lambda}^{(g+1)} - m^{(g)}}{\sigma^{(g)}} \left(\frac{x_{i:\lambda}^{(g+1)} - m^{(g)}}{\sigma^{(g)}} \right)^T}_{\text{rank-}\mu\text{ update}} \tag{1.6}$$

where:

- $c_1 \approx 2/n^2$
- $c_1 \approx min(\mu_{eff}/n^2, 1-c_1)$

In this way, in each iteration the set of variables is adapted. The distribution centre $\overrightarrow{m}$ moves to a weighted mean of the better solutions found. The covariance matrix C is adapted to the shape of the μ best solutions created. Besides, the step-size σ is adapted depending on the obtained improvement: its value grows up if the new solutions are better than the old ones and brings down otherwise. This iterative process continue until a prefixed number of evaluations is reached.

The method only needs two parameters to be specified since in (Hansen and Ostermeier 2001) the authors proposed the best values for the rest. These parameters are the initial distribution centre $\overrightarrow{m} =< \overrightarrow{x} >_{\omega}^{(0)}$ and the mutation normal distribution variance σ.

1.4.2.3 Properties

CMA-ES presents two interesting properties related with the design of the algorithm:

Invariance. Invariance properties of a search algorithm denote identical behavior on a set, or a class of objective functions. Invariance is an important property of the CMA-ES. Translation invariance should be taken for granted in continuous domain optimization. Translation invariance means that the search behavior on the function $x \mapsto f(x+a), x^{(0)} = b-a$, is independent of $a \in \mathbb{R}^n$. Further invariances, e.g. to certain linear transformations of the search space, are highly desirable: they imply uniform performance on classes of functions and therefore allow for generalization of empirical results. The CMA-ES exhibits the following invariances:

- Invariance to order preserving (i.e. strictly monotonic) transformations of the objective function value. The algorithm only depends on the ranking of function values.

- Invariance to angle preserving (rigid) transformations of the search space (rotation, reflection, and translation) if the initial search point is transformed accordingly.
- Scale invariance if the initial scaling, e.g. $\sigma^{(0)}$, and the initial search point, $m^{(0)}$, are chosen accordingly.
- Invariance to a scaling of variables if the initial diagonal covariance matrix $C^{(0)}$, and the initial search point, $m^{(0)}$, are chosen accordingly.
- Invariance to any invertible linear transformation of the search space, A, if the initial covariance matrix, $C^{(0)} = A^{-1}(A^{-1})^T$, and if the initial search point, $m^{(0)}$, are transformed accordingly.

Invariance should be a fundamental design criterion for any search algorithm. Together with the ability to efficiently adapt the invariance governing parameters, invariance is a key to competitive performance.

Stationarity. An important design criterion for a stochastic search procedure is *unbiasedness* of variations of object and strategy parameters (Hansen and Ostermeier 2001). Consider random selection, e.g. the objective function $f(x) = rand$ to be independent of x. The population mean is unbiased if its expected value remains unchanged in the next generation, that is $E[m^{(g+1)}|m^{(g)}] = m^{(g)}$. For the population mean, stationarity under random selection is a rather intuitive concept. In the CMA-ES, stationarity is respected for all parameters in the basic equation 1.2. The distribution mean m, the covariance matrix C, and $ln\,\sigma$ are unbiased.

For distribution variances (or step-sizes) a bias toward increase or decrease entails the danger of divergence or premature convergence, respectively, whenever the selection pressure is low. Nevertheless, on noisy problems a properly controlled bias towards increase might be appropriate even on the log scale.

Finally, due to all these characteristics, the CMA-ES overcomes typical problems that are often associated with evolutionary algorithms.

1. Poor performance on badly scaled and/or highly non-separable objective functions. Equation 1.6 adapts the search distribution to badly scaled and non-separable problems.
2. The inherent need to use large population sizes. A typical, however intricate to diagnose reason for the failure of population based search algorithms is the de-

generation of the population into a subspace. This is usually prevented by non-adaptive components in the algorithm and/or by a large population size (considerably larger than the problem dimension). In the CMA-ES, the population size can be freely chosen, because the learning rates c_1 and c_μ in Equation 1.6 prevent the degeneration even for small population sizes, e.g. $\lambda = 9$. Small population sizes usually lead to faster convergence, large population sizes help to avoid local optima.

3. Premature convergence of the population. Step-size control in Equation 1.6 prevents the population to converge prematurely. It does not prevent the search to end up in a local optimum.

1.4.3 Scatter search

SS fundamentals were originally proposed by Fred Glover (Glover 1977) and have been later developed in some texts like (Laguna and Martí 2003). The main idea of this technique is based on a systematic combination between solutions (instead of a randomized one like that usually done in GAs) taken from a considerably reduced evolved pool of solutions named Reference set (between five and ten times lower than usual GA population sizes) as well as on the typical use of a local optimizer. This way, an efficient and accurate search process is encouraged thanks to the latter and to other innovative components we will describe later.

1.4.3.1 General flow

In this section we give the basic flow of the SS based on the well-known "five methods" (Laguna and Martí 2003), while the specific designs are covered in Section 1.4.3.2. The advanced features of SS are related to the way these five methods are implemented. That is, the sophistication comes from the implementation of the SS methods instead of the decision to include or exclude some elements. The fact that the mechanisms within SS are not restricted to a single uniform design allows the exploration of strategic possibilities that may prove effective in a particular implementation. These observations and principles led the authors in (Laguna and Martí 2003) to propose the following template for implementing SS that consists of five methods.

1. A *diversification generation method* to generate a collection of diverse trial solutions, using an arbitrary trial solution (or seed solution) as an input.

2. An *improvement method* to transform a trial solution into one or more enhanced trial solutions. Neither the input nor the output solutions are required to be feasible, though the output solutions will more usually be expected to be so. If no improvement of the input trial solution results, the "enhanced" solution is considered to be the same as the input solution.

3. A *reference set update method* to build and maintain a reference set consisting of the b "best" solutions found (where the value of b is typically small, e.g., no more than 20), organized to provide efficient accessing by other parts of the method. Solutions gain membership to the reference set according to their quality or their diversity.

4. A *subset generation method* to operate on the reference set, to produce a subset of its solutions as a basis for creating combined solutions.

5. A solution combination method to transform a given subset of solutions produced by the subset generation method into one or more combined solution vectors.

This basic design starts with the creation of an initial set of solutions P and then extracts from it the reference set (*RefSet*) of solutions. The diversification generation method is used to build a large set P of diverse solutions. The size of P (*PSize*) is typically at least 10 times the size of *RefSet*. The reference set, *RefSet*, is a collection of both high quality solutions and diverse solutions that are used to generate new solutions by way of applying the combination method. In this basic design we can use a simple mechanism to construct an initial reference set and then update it during the search. The size of the reference set is denoted by $b = b_1 + b_2 =\mid RefSet \mid$. The construction of the initial reference set starts with the selection of the best b_1 solutions from P. These solutions are added to *RefSet* and deleted from P. For each solution in *P-RefSet*, the minimum of the distances to the solutions in *RefSet* is computed. Then, the solution with the maximum of these minimum distances is selected. This solution is added to *RefSet* and deleted from P and the minimum distances are updated[5].

The latter process is repeated b_2 times, where $b2 = b - b_1$. The resulting reference set has b_1 high quality solutions and b_2 diverse solutions. Regardless the rules used to select the reference solutions, the solutions in *RefSet* are ordered according to quality, where the best solution is the first one in the list. The simplest form of the subset generation method consists of generating all pairs of reference solutions. That

[5] In applying this maximum-minimum criterion, or any criterion based on distances, it can be important to scale the problem variables, to avoid a situation where a particular variable or subset of variables dominates the distance measure and distorts the appropriate contribution of the vector components.

is, the method would focus on subsets of size 2 resulting in $(b^2 - b)/2$ *NewSubsets*. The pairs in *NewSubsets* are selected one at a time in lexicographical order and the solution combination method is applied to generate one or more trial solutions. These trial solutions are subjected to the improvement method, if one is available. Then, the reference set update method is applied once again. The basic procedure terminates after all subsets in *NewSubsets* are subjected to the combination method and none of the improved trial solutions are admitted to *RefSet* under the rules of the reference set update method.

Figure 1.10 graphically shows the interaction among these five methods and puts in evidence the central role of the reference set. Of the five methods in the SS methodology, only four are strictly required. The improvement method is usually needed if high quality outcomes are desired, but a SS procedure can be implemented without it.

1.4.3.2 Component design

The SS framework is very flexible, since each of its elements can be implemented in a variety of ways and degrees of sophistication. Specific designs generally, but not always, translate into higher complexity and additional search parameters. There is no simple recipe that can be used to follow a predetermined order in which advanced strategies should be added to progressively improve the performance of a SS implementation. Therefore, the order in which these strategies are described in this section does not reflect their importance or ranking.

1.4.3.2.1 Subset generation method Solution combination methods in SS typically are not limited to combining just two solutions and therefore the subset generation method in its more general form consists of creating subsets of different sizes. The SS methodology assures that the set of combined solutions may be produced in its entirety at the point where the subsets of reference solutions are created. Therefore, once a given subset is created, there is no merit in creating it again. This creates a situation that differs noticeably from those considered in the context of GAs, where the combinations are typically determined by the spin of a roulette wheel. The procedure for generating subsets of reference solutions uses a strategy to expand pairs into subsets of larger size while controlling the total number of subsets to be generated. In other words, the mechanism avoids the extreme type of process that creates all the subsets of size 2, then all the subsets of size 3, and so on until reaching the subsets of size $b-1$ and finally the entire *RefSet*. This approach would clearly not be practical, considering

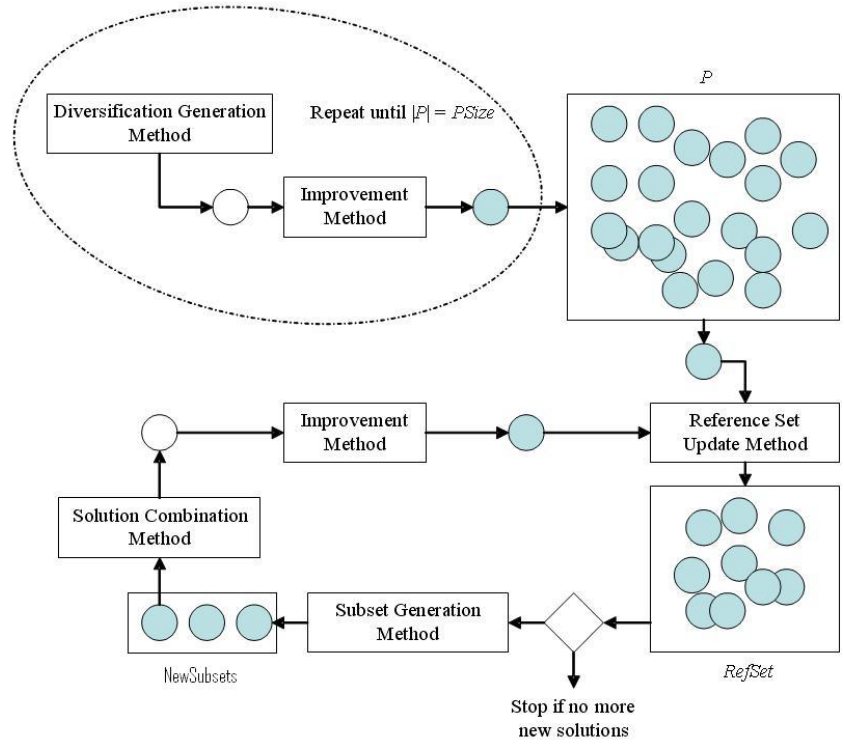

Figure 1.10: The control diagram of SS.

for example that there are 1013 subsets in a reference set of a typical size $b = 10$. Even for a smaller reference set, combining all possible subsets is not effective because many subsets will be almost identical. The following approach selects representative subsets of different sizes by creating subset types:

- Subset type 1: all 2-element subsets.
- Subset type 2: 3-element subsets derived from the 2-element subsets by augmenting each 2-element subset to include the best solution not in this subset.
- Subset type 3: 4-element subsets derived from the 3-element subsets by augmenting each 3-element subset to include the best solution not in this subset.

- Subset type 4: the subsets consisting of the best i elements, for $i = 5$ to b.

1.4.3.2.2 RefSet updating The reference set is the heart of a SS procedure. If at any given time during the search all the reference solutions are alike, as measured by an appropriate metric, the SS procedure will most likely be incapable of improving upon the best solution found even when employing a sophisticated procedure to perform combinations or improve new trial solutions. The combination method is limited by the reference solutions that it uses as input. Hence, having the most advanced combination method is of little advantage if the reference set is not carefully built and maintained during the search.

In the SS basic design, the ***static update*** of the reference set is used after the application of the combination method. Following a static update, trial solutions that are constructed as combination of reference solutions are placed in a solution pool, denoted by *Pool*. After the application of both the combination method and the improvement method, the *Pool* is full and the reference set is updated. The new reference set consists of the best b solutions from the solutions in the current reference set and the solutions in the pool, i.e., the update reference set contains the best b solutions in $RefSet \bigcup Pool$.

The alternative to the static update is the ***dynamic update*** strategy, which applies the combination method to new solutions in a manner that combines new solutions faster than in the basic design. That is, if a new solution is admitted to the reference set, the goal is to allow this new solution to be subjected to the combination method as quickly as possible. In other words, instead of waiting until all the combinations have been performed to update the reference set, if a new trial solution warrants admission in the reference set, the set is immediately updated before the next combination is performed. Therefore, there is no need for an intermediate pool in this design, since solutions are either discarded or become part of the *RefSet* as soon as they are generated.

The advantage of the dynamic update is that if the reference set contains solutions of inferior quality, these solutions are quickly replaced and future combinations are made with improved solutions. The disadvantage is that some potentially promising combinations are eliminated before they can be considered. The implementation of dynamic updating is more complex than its static counterpart. Also, in the static update the order in which the combinations are performed is not important because the *RefSet* is not updated until all combinations have been performed. In the dynamic updating, the order is quite important because it determines the elimination of some potential combinations. Hence, when implementing a dynamic update of the reference set, it may be necessary to experiment with different combination orders as part of the fine

tuning of the procedure.

1.4.3.2.3 RefSet rebuilding This is an updating procedure that is triggered when no new trial solutions are admitted to the reference set. This update adds a mechanism to partially rebuild the reference set when the combination and improvement methods do not provide solutions of sufficient quality to displace current reference solutions.

The *RefSet* is partially rebuilt with a diversification update that works as follows and assumes that the size of the reference set is $b = b_1 + b_2$. Solutions $x^{b_1+1}, \ldots, x^b$ are deleted from *RefSet*. The diversification generation method is reinitialized considering that the goal is to generate solutions that are diverse with respect to the reference solutions $x^1, \ldots, x^{b_1}$. Then, the diversification generation method is used to construct a set P of new solutions. The b_2 solutions $x^{b_1+1}, ..., x^b$ in *RefSet* are sequentially selected from P with the criterion of maximizing the diversity. It is usually implemented with a distance measure defined in the context of the problem being solved. Then, the maximization of diversity is achieved by maximizing the minimum distance. The maximum-minimum criterion, which is part of the reference set update method, is applied with respect to solutions $x^1, \ldots, x^{b_1}$ when selecting solution x^{b_1+1}, then it is applied with respect to solutions $x^1, \ldots, x^{b_1+1}$ when selecting solution x^{b_1+2}, and so on.

1.4.3.2.4 Diversity control SS does not allow duplications in the reference set and its combination methods are designed to take advantage of this lack of duplication. Hashing is often used to reduce the computational effort of checking for duplicated solutions. The following hash function, for instance, is an efficient way of comparing solutions and avoiding duplications when dealing with problems whose solutions can be represented with a permutations p of size m:

$$Hash(p) = \sum_{i=1}^{m} ip(i)^2 \tag{1.7}$$

Campos et al. (Campos et al. 2001) reported the benefits of this form of hashing in the context of the linear ordering problem. While the simpler SS implementations are designed to check that the reference set does not contain duplications, they generally do not monitor the diversity of the b_1 high quality solutions when creating the initial *RefSet*. On the other hand, recall that the b_2 diverse solutions are subjected to a strict diversity check with the maximum-minimum criterion. A minimum diversity test can be applied to the b_1 high quality solutions chosen as members of the initial *RefSet* as follows. After the P set has been created, the best solution according to the objective

function value is selected to become x^1 in the reference set. Then, x^1 is deleted from P and the next best solution x in P is chosen and added to *RefSet* only if $d_{min}(x) \geq th\_dist$. In other words, at each step we add the next best solution in P only if the minimum distance between the chosen solution x and the solutions currently in *RefSet* is at least as large as the threshold value *th_dist*.

1.5 Concluding remarks

On the one hand, we have introduced forensic medicine and human identification, focusing on forensic anthropology procedures. Then, we reviewed the fundamentals of forensic identification by CS since it is the core of all the approaches proposed in this dissertation. It has been demonstrated it is a really solid identification method. As said, the basis of this techniques were introduced by Bertillon more than a hundred years ago, helping to solve hundreds of identification case.

However, basic methodological criteria that ensure the reliability of the technique have not been established yet. Instead of following a uniform methodology, every expert tends to apply his own approach to the problem based on the available technology and on his deep knowledge on human craniofacial anatomy, soft tissues, and their relationships. In fact, the technical procedure evolved as new technology was available. That could be one of the reasons for the current diversity of CS methods and terms.

On the other hand, we have explained the IR as an important process in computer vision because of its applicability to the CS problem. Finally the foundations of EAs have been presented. In particular, CMA-ES and SS, have been also explained since these are basic principles to understand the forthcoming chapters.

Chapter 2

Computer-based Approaches for Craniofacial Superimposition

Getting older is no problem.
You just have to live long enough.

Groucho Marx (1890-1977)

2.1 Introduction

The aim of this chapter is to introduce the reader to the field of computer-aided CS. We will do so by updating previous reviews existing in the literature, both adding recent works and considering a new computing-based classification criterion. That criterion is more related to the use of computers in the different stages of the CS process itself. The different stages involved in the computer-aided CS process will be thus clearly defined. In our opinion, to properly characterize any CS system (and specifically computer-aided ones), the whole process should be considered as divided up into three consecutive stages, namely face enhancement and skull modeling, skull-face overlay, and decision making. We will point out advantages and disadvantages of different approaches, *with an emphasis on the computer-aided techniques that have been employed and on the tasks these techniques solve in a more automatic manner.* We are interested in the methods, not on the analysis of specific cases. Hence, papers reporting only case studies will be out of the scope of this study.

We should emphasize that we will not judge the effectiveness of the methods due to the unavailability of detailed information about the tackled cases and used equipments, and therefore the impossibility to reproduce the experimental setup and to perform comparative experiments. As stated by Carl N. Stephan, "presently, it is not possible to draw firm statements concerning the overarching performance of superimposition methods because formal published studies on the accuracy and reliability of the methods have been infrequent, have used small samples, and have often not been replicated" (Stephan 2009a).

The current chapter is organized as follows. In Section 2.2 a discussion about the different names used to refer the CS technique is presented. In Section 2.3 we will introduce our proposal of a general computer-aided CS framework based on three

stages, explaining the role performed by the computer to accomplish each of them. We will review and categorize the existing contributions in Section 2.4. Some works partially related to the CS process will be shortly reviewed in Section 2.5. Section 2.6 will be devoted to a discussion of solved and unsolved problems, trends, and challenges for future research. Finally, some concluding remarks are presented in Section 2.7.

2.2 Terminology

Different terms have been used to refer to the CS technique during its more than one century of development. This fact has been mainly due to the use of close synonyms and specially to the coining of new, more specific terms depending on the supporting technical devices considered through time. The following points justify our choice of "craniofacial superimposition" as the most general and currently extended name for this forensic identification method:

- Craniofacial superimposition is the most widely found term in the literature to refer to all the tasks related to this forensic identification technique (Ubelaker et al. 1992; Yoshino et al. 1995a; Cattaneo 2007). In particular, the most recent studies confirm the suitability of this terminology (Stephan 2009a; Stephan 2009b; Stephan et al. 2009; Ranson 2009; Pickering and Bachman 2009).

- The term arises as a mean to differentiate between the general forensic technique itself and the technical devices used to tackle the identification problem. Indeed, CS were initially conducted using tracings made from photographs (Webster 1955; Sen 1962) and authors referred to the procedure as "photographic superimposition" (Dorion 1983; Brocklebank and Holmgren 1989; Maat 1989). Because of the rapid developments in video technology, the term "video superimposition" was later used when this tool became common in forensic identification (Seta and Yoshino 1993; Pesce Delfino et al. 1993; Shahrom et al. 1996; Yoshino et al. 1997). Finally, the use of computers to assist the anthropologists in the identification process involved the next generation of craniofacial superimposition systems[1]. The latter approaches are usually referred to as "computer-aided" or "computer-assisted CS"[2] (Pesce Delfino et al. 1986; Ubelaker et al.

[1] Attempts to achieve high identification accuracy through the utilization of advanced computer technology has been a monumental task for experts in the field in the last two decades (Lan 1992).

[2] Notice that the terms "skull-face superimposition", "skull-photo superimposition", "photographic superimposition", or "video superimposition" have also been used in combination with the "computer-aided/assisted" adjective.

1992; Aulsebrook et al. 1995; Yoshino et al. 1997). The review developed in the current chapter will be devoted to these kinds of systems and specifically to the most advanced ones based on the use of computer vision, 3D modeling and machine learning-based automatic methods. These systems have not been carried a specific distinctive name till now despite the fact of being fundamental tools in current computer-aided procedures.

- Hence, when using the generic term "craniofacial superimposition" we are assuming neither a particular acquisition device nor a given data format as the inputs to our problem. We just consider that any CS method will deal with a 2D image of the disappeared person (typically a photograph) and the skull found (maybe as a part of other skeletal remains).

- There are some sources that use the term "photographic supraprojection" (Bronkhorst 2006; Stratmann 1998) instead. We avoid its use because it does not explicitly indicate that a matching of a skull with a face is specifically involved.

- Finally, CS should not be misled by craniofacial identification. Notice that, the latter term is used as an umbrella including both CS and facial approximation[3] (Clement and Ranson 1998; Stephan 2009b; Wilkinson 2009). Both methods are underpinned by knowledge of human craniofacial anatomy. It is this principle which ties these two techniques together despite the use of different technical protocols for each of them.

2.3 A new general framework for computer-based craniofacial superimposition

In our view, the whole computer-based CS process can be seen as composed of three stages (see Figure 2.1):

1. The first CS stage involves achieving a digital model of the skull and enhancing the face image. The subject of the identification process, i.e. the skull, is a 3D object. Hence, the use of a skull 3D model instead of a skull 2D image

[3] "In the past, facial approximation methods have been known by many other names. The most popular of these is *facial reconstruction*. This name is strongly misleading as it leaves the erroneous impression that the methods are exact, reliable and scientific" (Stephan 2009a).

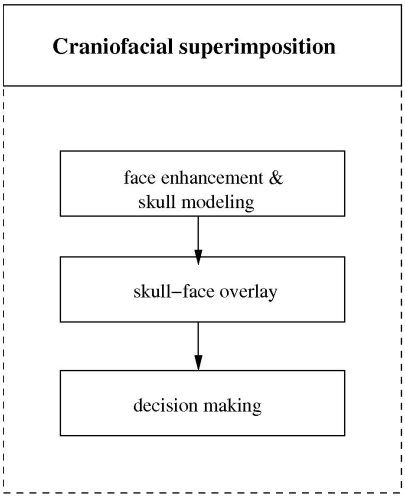

Figure 2.1: The three stages involved in any computer-based CS process

should be preferred because it is definitively a more accurate representation that avoids the usual distorsions of 2D cameras (Eliášová and Krsek 2007). It also overcomes some typical limitations of 2D approaches (De Angelis et al. 2009). Furthermore, the skull 3D model is more versatile because it can be more easily repositioned and reoriented to reach the most suitable superimposition.

As we will explain in Section 2.4.1, obtaining an accurate 3D cranial model has been considered a difficult task by forensic anthropologists in the past. However, it is nowadays an affordable and attainable activity using laser range scanners like the one used by our team (Figure 2.2), available in the Physical Anthropology Lab at the University of Granada (Spain). 3D skull modeling by means of laser range scanners is an active research field (Santamaría et al. 2007a; Santamaría et al. 2007b; Santamaría et al. 2009; Fantini et al. 2008). When available, other imaging modalities can be also considered for 3D skull modeling, as computed tomography (Benazzi et al. 2009).

Concerning the face image, the most recent systems use a 2D digital image. This stage aims to apply image processing techniques (Gonzalez and Woods 2008) in order to enhance the quality of the face image that was typically provided when the person disappeared. Such techniques depend on the available format (digital camera image or scanned photographic paper) and include frequency domain filters to fix artifacts due to aliasing and sampling problems present in scanned documents, as well as removal of non uniform illumination effects and

sharpening methods to deal with blurring and problems related to movements.

Figure 2.2: Acquisition of a skull 3D partial view using a Konica-Minolta^{TM} laser range scanner

2. The second stage is the *skull-face overlay*. It consists of searching for the best overlay of either the 2D images of the skull and face, or the 3D model of the skull and the 2D image of the face, achieved during the first stage. This is usually done by bringing to match some corresponding anthropometrical landmarks on the skull and the face.

3. Finally, the third stage of the CS process corresponds to the *decision making*. Based on the skull-face overlay achieved, the identification decision is made by either judging the matching between the corresponding landmarks in the skull and in the face, or by analyzing the respective profiles. Notice that, the use of computers in this stage aims to support the final identification decision that will be always made by the forensic anthropologist.

As said, the differentiation between methods that do not use computer technology and those that use it has already been proposed (Aulsebrook et al. 1995). In the literature, photographic and video superimposition have been considered to belong to the former category. Meanwhile, methods defined as digital or computer-aided CS techniques have been considered to belong to the latter. Thus, the distinction between computer-aided and non-computer-aided methods has been clearly guided by the use of computer-based technology along the CS process up to now. Nevertheless, the distinct roles the computer can play in the different stages of that process is really important nowadays and it was not considered in previous reviews. Moreover, the analysis of

previous contributions is especially difficult when some authors claim they propose a "computer-aided" or "computer-assisted" system (Ricci et al. 2006) and the computer mainly plays the role of a simple visualization tool.

Hence, to fill that gap, we will expand the computer-aided category defined in previous reviews by distinguishing between non-automatic and automatic methods. *Computer-aided non-automatic methods* use some kind of digital infrastructure to support the CS process, i.e. computers are used for storing and/or visualizing the data. However, they are characterized by the fact that their computational capacity to automate human tasks is not considered. On the other hand, *computer-aided automatic methods* use computer programs to accomplish an identification sub-task itself. There are some remarks that should be done concerning the three stages of the process:

1. Regarding the first stage, automatic methods may deal with either the 2D image of the face or the skull. On the one hand, when dealing with the 2D image of the face, automatic systems accomplish the restoration of the photograph by means of digital image processing techniques. On the other hand, the aim of automatic methods concerning the skull is the achievement of an accurate 3D model.

2. Concerning the second stage, we will point out a clear division between computer-aided non-automatic and automatic skull-face overlay methods. The former ones use computers to support the overlay procedure and/or to visualize the skull, the face, and the obtained superimposition. Nevertheless, the size and orientation of the skull are changed manually to correctly match that one of the head in the photograph. This is achieved by either physically moving the skull, while computers are simply used to visualize it on the monitor, or (with the help of some commercial software) by manually moving its digital image on the screen until a good match is found. On the opposite, the automatic skull-face overlay methods find the optimal superimposition between the 3D model or the 2D image of the skull and the 2D image of the face using computer programs.

3. Finally, regarding the decision making stage, automatic systems can assist the forensic expert by applying decision support systems (Keen 1978). Those computer programs must use objective and numerical data for evaluating the obtained matching between the skull and the face. Based on that evaluation, the system suggests an identification decision to the forensic expert. Thus, the decision support system is intended to help decision makers compile useful information from the analysis of the skull-face overlay outcomes. Of course, the final decision will be always made by the anthropologist according to both the support of the automatic system and his expertise. On the other hand, if the identification

decision only relies on the human expert who visually evaluates the skull-face overlay obtained in the previous stage, then the method will be considered as a non-automatic system, although it might use digital data as supporting means.

2.4 Classification and discussion of existing works

In this section we will review and categorize the existing contributions of computer-aided CS systems. They will be classified according to the stage of the process which is addressed using a computer-aided method. Information about the methods used for the remaining stages will be given shortly together with a brief discussion.

Unfortunately, these stages are not so clearly distinguished in some of the existing CS methods as we might expect. This fact causes some confusion as sometimes authors themselves define their own method as computer-aided CS when they refer only to the decision making stage and others refer to identification method when they tackle the skull-face overlay stage. That is one of the reasons why our categorization is different from the previous ones that can be found in the literature.

Table 2.1 gives an overview of the papers describing computer-aided systems examined in this chapter. Studies are listed in chronological order. Additional information about the input data needed and/or the "classic" superimposition method used are included, when available.

2.4.1 Face enhancement and skull modeling

Let us highlight the main differences between the image of the face and the model of the skull. The face image is typically a photograph. It was acquired under some conditions that are fixed and usually unknown at the moment of the forensic analysis. With a digital image, the only possibility is to attempt to enhance its quality. If it is not in digital format, it can be scanned and transformed into a 2D digital image. Then, it can be enhanced using digital image filters and/or processing algorithms. However, the skull is an available physical object and its model needs to be obtained to accomplish an automatic procedure.

We will detail both face enhancement and skull modeling procedures. Regarding the image of the face, good quality is needed (Nickerson et al. 1991). Therefore enhancement techniques could be could be applied (Gonzalez and Woods 2008). Such techniques depend on the available format (digital camera image or scanned photography). They include frequency domain filters to fix artifacts due to aliasing and sampling

Table 2.1: An overview of the literature on computer-aided forensic identification systems by CS. The stage of the process, i.e. skull modeling (SM), skull-face overlay (SF), and decision making (DM), that is addressed using a computer-aided method is labeled with CA (computer-aided automatic methods) or CN (computer-aided non-automatic methods). Notice that, particular stages not tackled using computers are noted by NC.

	SM	SF	DM	Remarks
(Lan and Cai 1985)		CN		uses "digital" superimposition
(Tao 1986), Lan et al. (1988, 1990, 1993)		CN	CA	uses "digital" superimposition
PesceDelfino et al. (1986, 1993)			CA	manual positioning of the skull
(Nickerson et al. 1991)	CA	CA		binary-coded genetic algorithm
(Ubelaker et al. 1992)		CN	CA	uses "digital" superimposition
(Bajnóczky and Királyfalvi 1995)			CA	based on video superimposition
Yoshino et al. (1995a, 1997)		CN	CA	photo-video superimposition
(Shahrom et al. 1996)	CN			3D model in facial approximation
Ghosh and Sinha (2001, 2005)		CA		works on 2D skull images
(Scully and Nambiar 2002)		CN		works on 2D skull images
(Bilge et al. 2003)		CN	NC	based on commercial software
(Biwasaka et al. 2005)	CA			based on optical techniques
(Al-Amad et al. 2006)		CN	NC	based on commercial software
(Galantucci et al. 2006)	CN			computed tomography vs. laser
(Ricci et al. 2006)		CN	CA	based on 2D skull radiographs
Santamaría et al. (2007a, 2007b, 2009)	CA			adjancent overlapping regions
(Fantini et al. 2008)	CN			based on commercial software
(Benazzi et al. 2009)	CN			based on commercial software
(Ballerini et al. 2009)	CA			use of heuristic features

problems present in scanned documents, as well as removal of non uniform illumination effects and sharpening methods to deal with blurring and problems related to movements. Notice that, the proper filter and its most suitable parameters are a choice that must be performed by the expert since they depend strongly on the acquisition conditions. According to Section 2.3, approaches that use human operated commercial software for the 2D face image enhancement will be considered non-automatic methods. Automatic methods perform such 2D image enhancement using computer programs with almost no human intervention.

Regarding the model of the skull, recent techniques for CS need an accurate 3D model. In the biomedical field computed tomography scanning images are the starting data to reconstruct the skull (Singare et al. 2009; Fantini et al. 2008). However, the possibilities of recording 3D forensic objects are not so many considering the available resources of a typical forensic anthropology lab. Indeed, many forensic labs are exploiting the capabilities of laser range scanners nowadays. That is due to the fact that these devices present a greater availability and a lower cost. Thus, we will focus our skull modeling study on the contributions that use laser range scanners instead of other devices that have also been considered to obtain a 3D model of the skull in other application domains (Nakasima et al. 2005; Enciso et al. 2003).

Laser range scanners are based on the optical principle of triangulation and acquire a dense set of three-dimensional point data in a very rapid, non-contact way (Bernardini and Rushmeier 2002). Some laser range scanners are also equipped with an additional positioning device named rotary table and an appropriate software that permits the 3D reconstruction. Nevertheless, there are situations where that software does not provide suitable 3D models. Moreover, there are scenarios where it is not even possible to use a rotary table.

Before going on with the 3D modeling process, every 3D view of the skull acquired by the laser range scanner must be preprocessed. This task involves the cleaning, smoothing, and filling of the view. Cleaning aims to remove those artifacts that were acquired by the scanner as part of the scene but which do not correspond to the skull. Meanwhile, smoothing is mainly concerned with the removal of some artificial vertices that could have been wrongly included by the scanner on the borders of the surface because of a perspective distortion. Fortunately, this task is not needed so often. Finally, filling is used to avoid small holes to appear in those parts of the skull that are not properly scanned because they are too dark for the scanner capabilities or because they are located in shadow regions.

In order to accomplish the 3D model some anthropologists are skilled enough to deal with the set of 3D views and they supervise the procedure with a commercial

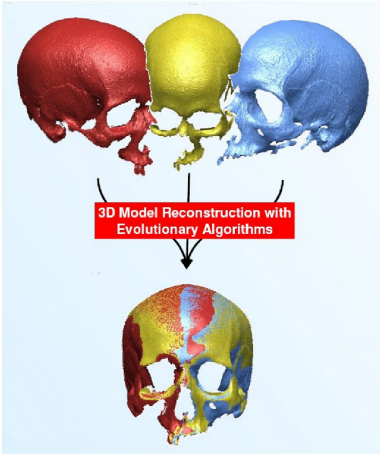

Figure 2.3: Three different views of a skull and the reconstructed 3D model

software like RapidForm^{TM}. Sometimes, this software does not provide the expected outcomes and the anthropologists even have to *stitch up* manually every couple of adjacent views. Hence, 3D image reconstruction software is a real need to construct the 3D model by aligning the views in a common coordinate frame. Such process is usually referred as RIR (Brown 1992; Ikeuchi and Sato 2001; Zitová and Flusser 2003) (see Section 1.3 in Chapter 1). It consists of finding the best 3D rigid transformation (composed of a rotation and a translation) to align the acquired views of the object. An example of three different views of a skull and the reconstructed 3D model is shown in Figure 2.3.

In this section we will mainly focus on contributions that include an automatic 3D modeling procedure because the other methods do not consider this stage and directly acquire a 2D projection of the skull (i.e., a skull photo). According to Section 2.3, all the approaches that use computers but do not consider the 3D skull model will be considered as non-automatic methods (Yoshino et al. 1995a; Ghosh and Sinha 2001; Pesce Delfino et al. 1986; Ricci et al. 2006).

Up to our knowledge, Nickerson et al. (1991) were the first researchers to propose the use of a 3D model to tackle the CS problem. In their work, a range scanner and a digital camera were used for 3D digitalization of the skull surface mesh and the 2D antemortem facial photograph, respectively. Well known image processing algorithms were used for image enhancement (median filtering, histogram equalization, Wiener filtering) (Gonzalez and Woods 2008). Rendering was done through computer graph-

ics techniques. A feature-based algorithm to reduce the computational and memory complexities inherent in solid modeling was also described.

Shahrom et al. (1996) followed a similar approach based on the use of a 3D laser range scanner. Authors used a skull holder, which could be slowly rotated through 360° in a horizontal plane under computer control. The 3D model was later used in facial approximation.

A completely different approach was presented in (Biwasaka et al. 2005) where the authors examined the applicability of holography in the 3D recording of forensic objects. Holography is an optical technique capable of recording the 3D data of an object. Two types of images, real and virtual, can be recorded in a holographically exposed film or hologram. Two superimposition systems using holographic images were examined in order to evaluate the potential use of this recording method. The authors claimed that the performance of holography is comparable to that of the computer graphics system, which consists of an image scanner, software, and a display unit. Moreover, they argued it can even be superior to the computer technique with respect to the 3D reconstruction of images. The suitability of this technique needs further studies. In particular, the use of an automatic superimposition method and a comparison with a reconstructed 3D range image could have objectively proved the actual utility of holography in this field.

Galantucci et al. (2006) compared two different acquisition techniques of images of a skull. In particular, computed tomography and laser range scanners performance were tested to ascertain which enabled more accurate reproductions of the original specimen. Comparison between the original forensic object and every model yielded satisfactory results for both techniques. However, computed tomography scanning demonstrated some advantages over the laser technique, as it provided a cleaner point cloud, enabling shorter pre-processing times, as well as data on the internal parts, which resulted in the reproduction of a more faithful model.

Santamaría et al (2007a, 2007b, 2009) proposed a method, based on EAs (Bäck et al. 1997), for the automatic alignment of skull range images. Different views of the skull to be modeled were acquired by using a laser range scanner. A two step pairwise RIR technique was successfully applied to such images. The method includes a pre-alignment stage that uses a SS based algorithm (Laguna and Martí 2003) and a refinement stage based on the classical iterative closest point algorithm (Besl and McKay 1992). The procedure is very robust since it reconstructs the 3D model of the skull even if there is no turn table and the views are wrongly scanned. In a later work, Ballerini et al. (2009), the same authors proposed the automatic reduction of the data provided by the laser range scanner used in the skull 3D model reconstruction task.

The dense point cloud corresponding to every skull view is synthesized by considering heuristic features that are based on the curvature values of the skull surface. Those features guide the automatic 3D skull model reconstruction by means of the SS-based RIR algorithm.

Fantini et al. (2008) used a laser range scanner to create a 3D model of a medieval damaged skull. The large missing part of the skull allowed scanning both outer and inner surfaces of the object. Thirty three partial views were needed to complete the acquisition of the whole surface by rotating the skull. Through post-processing of the data collected from the 3D scans, a triangular mesh was finally obtained. Those operations were performed by RapidForm 2006, RE^{TM} commercial software.

Finally, a similar approach was followed in (Benazzi et al. 2009) in order to tackle the 3D skull reconstruction of Dante Alighieri (1265-1321) as part of a project to achieve the facial approximation of the famous poet. Based on the data provided by a laser range scanner, the model of Dante's skull was constructed using the utilities provided by the Rapidform XOS2^{TM} commercial software. In particular, authors refer to operations as registration and merging of the point clouds, and simplification and editing of the digital model.

2.4.2 Skull-face overlay

The success of the superimposition technique requires positioning the skull in the same pose of the face as seen in the given photograph. The orientation process is a very challenging and time-consuming part of the CS technique (Fenton et al. 2008). Most of the existing CS methods are guided by a number of landmarks of the skull and the face (see Section 1.2.2 of Chapter 1). Once these landmarks are available, the skull-face overlay procedure is based on searching for the skull orientation leading to the best matching of the two sets of landmarks.

Scientific methods for positioning the skull had already been proposed before computers became largely available (Glaister and Brash 1937; Maat 1989; Kumari and Chandra Sekharan 1992; Chandra Sekharan 1993). These methods are not computer-aided but are somehow closer to them than to trial and error procedures. In these approaches the skull is manually placed on a tripod and its pose is estimated using a mathematical procedure, instead of a trial and error routine. The researchers applying these methods calculate the head size and orientation in the photograph, so they can position the skull in the same posture. We briefly summarize those contributions as follows:

- In very early approaches (Glaister and Brash 1937) the enlargement factor is calculated based on linear measurements of items within the antemortem photograph, such as fabric, button, tie, and other objects of known geometry (doors, chairs, etc.) (Chandra Sekharan 1993). Other scale correlation methodology has included measurement of the interpupillary distance and size of dentition (Austin-Smith and Maples 1994).

- Maat (1989) proposed to use a set of anthropometrical landmarks, along with relative reference lines, to calculate the three components of head rotation ("bending forward", "turning sideways", and "rolling sidewards") to position the skull. The principle of central projection and a minimum photographic distance of 1.5 *m* are important preconditions.

- Chandra Sekharan (1993) suggested using the vertical distance "d" between the *ectocanthions* and *tragion* as a measure for calculating the extent of flexion or extension of the head. The extent of the rotation of the face was calculated from the L/R ratio, where L and R denote the distances between the left and right *ectocanthion* from the midline of the face. Using these factors, the skull under examination was positioned on a tripod stand with the help of a remote control positioning device (Kumari and Chandra Sekharan 1992). A practical suggestion for the camera distance was also given.

However, these methods are out of the scope of this proposal that is focused on computer-aided skull-face overlay contributions. Within this group of approaches we will differentiate between non-automatic and automatic works as follows.

2.4.2.1 Non-automatic skull-face overlay methods

Below, we describe skull-face overlay methods known as computer-aided methods in the literature. Nevertheless, we prefer to refer to them as computer-aided non-automatic skull-face overlay methods. They are typical examples of the use of a digital infrastructure but without taking advantage of its potential utility as automatic support tools for the forensic anthropologists. Notice that, they depend on good visualization and overlay mechanisms to aid human operators. Hence, processes following this approach are prone to be time-consuming, hard to be reproduced, and subjective.

- Lan and Cai (1985) developed a CS apparatus called TLGA-1, based on the principles of dual projection. During the following years, these authors evolved this

system resulting in new subsequent versions, TLGA-2 and finally TLGA-213 (Tao 1986), Lan and Cai (1988, 1993), (Lan 1990). The TLGA-213 system was mainly composed of a TV camera, a computer, an A/D and D/A converter, a mouse, and the 213 system software library. The system calculated the pitch angle of the photograph of the face by measuring the ratio between the distances in the vertical line segments *glabella* to *nasion* and *gnathion* to *nasion*. The natural head size was calculated from the distance between the *ectocanthions* and the deflection angle in the photograph. The latter parameters were iteratively computed and considered as a guide for the manually performed skull-face overlay.

- Ubelaker et al. (1992) solved a huge number of cases submitted to the Smithsonian Institute by the FBI. Their software allows any desired combination of skeletal-photograph comparison, including the chance to remove the soft tissue to view the underlying skeletal structure. It works on digitalized images of both face and skull and offers the possibility to assess the consistency between them. The identification procedure usually requires less than one hour. It is not specified if this time includes the acquisition and skull-face overlay steps or only the decision making stage. However for the acquisition of the digital images, the authors visualize the facial photograph and trace anatomical landmarks on a plastic slide taped on the monitor. Then, they visualize the skull and manually manipulate it to match the marked landmarks. The quality of the photograph and the proper orientation of the skull are claimed to highly influence the success of the technique.

- Yoshino et al.'s skull identification system (1997) consists of two main units, namely a video skull-face overlay system and a computer-aided decision making system. In the former, the determination of the orientation and size of the skull to those of the facial photograph is done by a pulse motor-driven mechanism, through the help of the fade-out or wipe mode of the video image mixing device. Then, the skull and facial images are digitalized, stored in the computer, and superimposed on the monitor.

- Ricci et al. (2006) presented an algorithm to compare a facial image with a skull radiograph. Thus they work with pairs of 2D images and the overlay is done by the human operator that manually marks anatomical points and brings them to match. Their software seems to account only for translation and scaling, while the algorithm is able to compensate for up to 10^o of head rotation. However, the algorithm only calculates distances and thresholds in an automatic way, while the skull-face overlay is done manually.

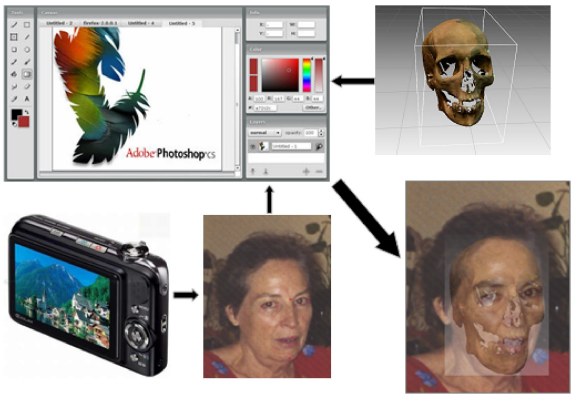

Figure 2.4: Non-automatic skull-face overlay based on Photoshop™

- The use of commercial software as Adobe Photoshop™ has been reported by Bilge et al. (2003) and Al-Amad et al. (2006). They use the "free transform" tool to adjust the scale of the photograph of the face, projected over the skull photo. The "semi-transparent" utility allows the operator to see both images while moving, rotating, and resizing the overlaid image (see Figure 2.4). A similar approach was also used in both (Scully and Nambiar 2002) and (Ricci et al. 2006) to validate a classical method and to superimpose skull radiographs, respectively.

2.4.2.2 Automatic skull-face overlay methods

We have found only two really interesting works to perform skull-face overlay in a fully automatic way. They are based on the use of machine learning algorithms (Mitchell 1997) from artificial intelligence, as artificial neural networks (Rumelhart and McClelland 1986) and EAs. The automation provided by these approaches represents an added value since they are typically faster than non-automatic methods. Moreover, they rely on quantitative measures and they can be easily reproduced. However, this sort of works often involve technical concepts that are usually unknown by most of the forensic anthropologists. Thus, a multidisciplinary research team is required. A brief description of the methods in this group is provided as follows:

- Nickerson et al. (1991) proposed a novel methodology to find the optimal fit be-

tween a 3D skull model and a 2D digital facial photograph. The most important novelty of this technique was the automatic calculation of the overlay of the skull surface mesh on the digital facial photograph. This mapping was achieved from the matching of four landmarks previously identified both in the face and the skull. The landmarks used in their work were: either the *glabella* or *nasion*, the two *ectocanthion* points, and an upper mandibular dentition point, if present, or the *subnasal* point. The mappings were developed from sets of similarity transformations and a perspective projection. The parameters of the transformations and the projection that overlay the 3D skull on the 2D photograph are optimized with three different methods: a heuristic, a classic nonlinear optimization, and a binary-coded GA, with the latter achieving the best results. Figure 2.5 depicts two skull-face overlays resulting from Nickerson's method.

- On the other hand, the method proposed by Ghosh and Sinha (2001) is an adaptation of their previous work for face recognition problems (Sinha 1998) and it was recently applied to an unusual identification case (Ghosh and Sinha 2005). It uses two neural networks to be applied to two different parts of the overlaying and allows to select fuzzy facial features to account for ambiguities due to soft tissue thickness. More in details, the system can implement an objective assessment of the symmetry between two nearly front 2D images, the cranial image and the facial image, that are the inputs as the source and the target images, respectively. The output is the mapped cranial image suitable for superimposition. Two neural networks need to be trained separately because each of them can correctly map only a part of the cranial image. Two limitations are pointed out by the authors: i) a part of the cranial image will not be properly mapped, and ii) a front view image is needed. Moreover, this method is not fully applicable because of two reasons. First, its long computation time is an important drawback. Second, the need of separately applying two different networks is a relevant flaw. Each network must deal with the upper skull contour and the front view cranial features, respectively. The superimposition found by the first network can be disrupted by that one achieved by the second network.

2.4.3 Decision making

Once the skull-face overlay is achieved, the decision making stage can be tackled. The straightforward approach would involve measuring the distances between every pair of landmarks in the face and in the skull. Nevertheless, this is not advisable because errors

Figure 2.5: Skull-face overlays resulting from Nickerson's method

are prone to be accumulated during the process of calibrating the size of the images. Instead, studies based on proportions among landmarks are preferred. Geometric figures like triangles or squares are good choices. It is also important to consider as many landmarks as possible, as well as different proportions among them (George 1993).

Although the methods described in the following are usually called in the literature as computer-aided CS, we prefer to refer to them as decision making methods since we think the authors fail on specifying the right CS stage where their works are included. Indeed, the proposed automatic techniques mainly focus on the decision making strategy as they are actually decision support systems assisting the anthropologist to take the final identification decision[4]. These algorithms are applied on the digitalized images stored on the computer, after the determination of the orientation and size of the skull by "routine" skull-face overlay techniques.

Tao (1986) developed the first procedure in which a computer was used for the decision making stage. That decision support system aimed to replace the previously used methods based on range estimation and subjective judgment. The system provided an identification conclusion by using distances between landmarks from the superimposed images. Later, Lan and Cai proposed the use of 52 different superimposition identification indexes for that aim in the TLGA-213 system (Lan 1990), Lan and Cai (1988, 1993). Those indexes were based on anthropometrical measures of Chinese adults, male and females, and were used together with proportion and distances be-

[4]We should remark that, although the reviewed systems are labeled as automatic in the sense that they are able to provide an identification decision without the intervention of the forensic expert, the supervision and final validation of the latter is always required as in any computer-aided medical diagnosis system (Berner 2007).

tween superimposed landmarks lines to automatically compute the final identification decision.

Pesce Delfino et al. (1986, 1993) applied *k*-th-order polynomial functions and Fourier harmonic analysis to assess the fit between the outline of the skull and the face. Ten cases including positive and negative identifications were investigated. The polynomial function was used to smooth the curve representing the investigated profile. The square root of the mean square error was taken to calculate the distance between polynomial function curves obtained for the skull and the face profile. The Fourier analysis considered the profile as an irregular periodic function whose sinusoidal contributors are found. Low-order harmonics (the first three or four) represented the basic profile shape and the high order harmonics corresponded to details. The sum of the amplitude differences of the sinusoidal contributors between profiles of the skull and the face represented the second independent parameter for numerical comparison. A Janus procedure (so called by the authors because of the double-headed Latin god Janus, the bi-front) was used to evaluate the symmetry differences between the two profiles. This procedure takes into account the relationship between the total arc and the chord length and the area they delimit in the two faced profiles. All these parameters are calculated by a computer software package called Shape Analytic Morphometry. However, this method would be only applicable when lateral or oblique photographs are available. Furthermore, their contribution requires manual repositioning of the skull for the correct superimposition.

Bajnóczky and Királyfalvi (1995) used the difference between the coordinate values of the pair of anatomical and/or anthropometrical points in both skull and face for judging the match between the skull and facial image obtained by the superimposition technique. Eight to twelve pairs of points were recorded and expressed as pixel units. Then, the final matrix, containing coordinates of measured points and calculated values, was established by computer-aided processing. Lacking the appropriate information, their model assumed that all data in that matrix were independent and followed a normal distribution with the same variance. A part of that variance was σ^2, which was the square of the measurement error and was itself assumed to be the same for all the data. The model of the authors was based on assumptions that:

The components of the error term are independent and distributed according to $N(0,2\,\sigma^2)$. (2.1)

The authors used a presupposed value of σ as part of the model assumptions. Under the assumption that the null hypothesis (Equation 2.1) is valid, it was statistically

tested using two values for σ. Authors claimed that when a given case is evaluated it is crucial to know what value can be considered as measurement error. One skull and two face photographs (frontal and lateral views) were used to test the method. They noted that their method is suitable for filtering out false positive identifications. Although the results obtained from this method are objective and easily interpreted for lay people, the anatomical and anthropometrical consistency between the skull and the face should be assessed by forensic examiners who are well versed in the anatomy of the skull and face. The authors concluded that their method should be used only in combination with classic video superimposition and could be regarded as an independent check.

In Yoshino et al.'s skull identification system (Yoshino et al. 1997) the distance between the landmarks and the thickness of the soft tissue of the anthropometrical points are semi-automatically measured on the monitor for the assessment of the anatomical consistency between the digitalized skull and face. The consistency is based on 13 criteria they previously defined using 52 skulls (Yoshino et al. 1995a). The software includes polynomial functions and Fourier harmonic analysis for evaluating the match of the outline such as the forehead and mandibular line in both digitized images. To extract the outline, gradient and threshold operations are used. Five case studies were carried out. However, they noted that these analysis could not always be applied because of the difficulties in extracting the facial contour from small and poor facial photographs offered from the victim's family.

The skull-face overlay in (Ricci et al. 2006) was guided by different crosses that were manually marked by the human operator in both the face and the skull radiograph photographs. Once that stage was performed, the algorithm calculated the distance of each cross moved and the respective mean in pixels. The algorithm considered a 7-pixel distance a negligible move. The mean value of the total distance in crosses moved represented the index of similarity between the given face and skull: the smaller the index value, the greater the similarity. The algorithm suggested an identification decision based on that index of similarity. The authors claim a 100% of correct identification over 196 cross-comparisons and report that the minimal number of needed landmarks is 4.

2.5 Related works

Nearly all the methods described in the previous section use anthropological landmarks to compute and/or to assess the fit between the skull and the face, but we found only one paper that addresses their automatic extraction in the skull (Parzianello et al. 1996).

The authors proposed a method based on simple image processing algorithms for the detection of craniometric points in video-based skull images. Their method works on 2D digitalized images of undamaged skulls and assumes they are in frontal view. The authors claimed that their method produces good results and it is potentially useful for the CS process. Nevertheless, we did not find any paper describing a system using the automatically extracted landmarks.

The literature on facial feature extraction is huge. Douglas (2004) reviews a number of image processing algorithms for the automatic extraction of landmarks in photograms and cephalograms. Interesting algorithms combining artificial intelligence techniques have been successfully developed and applied. However, they are out of the scope of this survey as well, as they are related to studies on craniofacial surgery or on face recognition and not to forensic skull identification.

Readers interested in 3D cranial landmark categorization can refer to (Brown et al. 2004). The accurate placement of anatomical features for CS is nowadays a real need (Stephan et al. 2009). However, to the best of our knowledge, no method for their automatic localization is found in the literature.

The area of 3D face processing (Zhen and Huang 2004; Zhao and Chellapa 2005) could also seem to have some relation with CS, specifically the face modeling topic. 3D face processing methods deal with the very complex task of properly turning a 3D object (the subject face) into a 2D image. Obtaining a skull 3D model is feasible –as well as very useful to improve the identification process– due to the availability of the physical object in the forensic anthropology lab. Nevertheless, the existing powerful methods in 3D face modeling, such as (Shan et al. 2001), are not applied since CS deals with the identification of deceased people. Hence, it is usually difficult for the anthropologist to get significant data in real conditions to apply the latter techniques. The availability of photographs and videos of the sample of candidates is low. This is one of the reasons why the currently established fundamentals of the forensic technique are based either on a 2D skull photo-2D face photo or on a 3D skull model-2D face photo comparison. The use of 3D face models is not considered by forensic anthropologists nowadays. Nevertheless, it could become an interesting area in the future when the massive use of video and imaging devices the world is experiencing will solve the problem of the lack of subject data.

Besides, recent literature has considerably developed the potential of another technique related to CS: craniofacial reconstruction preferably referred to as facial approximation (Vanezis et al. 2000; Claes et al. 2006; Wilkinson 2010). The 3D facial image may be reconstructed by either building muscle and soft tissue using clay, or by means of computer graphics. Data concerning the reliability of these methods for

forensic anthropology and the lack of relationship between facial approximation and resemblance rating have been reported (Stephan and Arthur 2006). An interesting review of current systems for computer-aided forensic facial reconstruction can be found in (Wilkinson 2005).

2.6 Discussion and recommendations for future research

In this section, we summarize a number of solved and unsolved problems in CS as well as possibilities for forensic applications by identifying some trends in the field. We also provide a list of recommendations for future research. Finally we discuss the need for public forensic data repositories and we present a web site we have created for this purpose.

2.6.1 Solved and unsolved problems

To date, no fully automatic method is used in practical applications despite the high number of cases examined (Ubelaker 2000) and the large amount of time the forensic experts need to spend in performing such examination. The need of a sophisticated procedure or an expensive hardware configuration to implement a digitalized 3D cranial image reconstruction has been stated to be the reason why computer-aided automatic CS methods did not gain much popularity by the late nineties (Ghosh and Sinha 2001). Nevertheless, the acquisition of a 3D model of the skull should not be a hinder nowadays. Indeed, such model could be reconstructed either by the scanner's software when the rotary device is available or by range image registration algorithms (see Section 3.2.1 of Chapter 3).

Nowadays, the limitations pointed out by some researchers, like the poor quality of the antemortem photographs (Ubelaker et al. 1992; Nickerson et al. 1991) or the curved surface of the monitor (Shahrom et al. 1996), which were claimed to influence a correct superimposition, should neither be a problem. We have to stress that these statements were valid when the equipments were either very expensive or not very accurate.

We believe that most of the claimed difficulties in finding an accurate magnification and orientation of the skull can be currently overcome by computer-aided automatic CS methods. Meanwhile, other reasons adduced for a low reliability in such methods are definitively solved presently. In particular, the high computation time spent by methods proposed more than a decade ago (for example, Nickerson et al.

(1991) required several days to achieve an automatic CS) is not a problem anymore.

Plenty of research has also focused on supporting the anthropologist in the decision making stage (Pesce Delfino et al. 1986; Yoshino et al. 1995a; Ricci et al. 2006) as well as on the validity of "routine" superimposition methods (Bajnóczky and Királyfalvi 1995; Scully and Nambiar 2002). Meanwhile, Jayaprakash et al. (2001) affirmed that visual assessment is more effective than metrical studies. Indeed, the method they propose, called "craniofacial morphoanalysis", is based on the visual evaluation of a number of attributes. This is the reason why this method is not included in the computer-aided approaches described in this survey.

2.6.2 Trends

Video superimposition has been preferred to photographic superimposition since the former is simpler and quicker (Jayaprakash et al. 2001). Video superimposition overcomes the protracted time involved with photographic superimposition, where many photographs of the skull had to be taken in varying orientations (Nickerson et al. 1991). Moreover, the fade and wipe facility in video superimposition allows the expert to analyze the congruence in every sector of the superimposed images, thereby rendering this method more popular (Jayaprakash et al. 2001). However, it has been indicated that CS based on the use of photographs is better than using video in terms of resolution of details (Yoshino et al. 1995a). Furthermore, video superimposition is still quite subjective, relying on the skill and dexterity of the operator (Nickerson et al. 1991).

Recent papers confirm that some authors think the most advanced method is based on computer-aided CS through the use of the imaging tools provided by Adobe Photoshop™and Corel Draw™software packages (Al-Amad et al. 2006; Bilge et al. 2003; Ross 2004). We agree with these authors in that working with digital images is definitively simpler and cheaper than with photographic or video superimposition equipments. However, we should note that the methods they use are not automatic as they manually resize, shift and rotate the images by trial and error. Thus, they deal with a very time consuming and error affected process. It is worth to remind that the forensic anthropologists of the Physical Anthropology lab at the University of Granada employed several hours to manually superimpose the skull and the face shown in Figure 2.6 following a computer-aided procedure similar to the one used those proposals.

There seems to be an increasing interest in facial reconstruction or approximation. Besides the advantages and disadvantages described in Wilkinson's review (Wilkinson 2005) and the undoubted attractiveness of these techniques, we believe

Figure 2.6: Manual CS

that they still need extensive research before being fully accepted in forensic investigations. Indeed, researchers involved in facial approximation think that CS may be preferred to reconstruction in cases where some clues can limit the identity to a few candidates (Turner et al. 2005).

2.6.3 Recommendations

It would be worthwhile to investigate how all the manual steps of the routine methods described in Section 2.4, from the skull modeling to the decision making, can be automated.

Automatic localization of anthropological landmarks on both 3D models of the skull and 2D images of the face are few examples of useful potential applications of image processing techniques to forensic sciences. Computer graphics techniques can provide accurate and automatic registration methods for 3D model building and for overlaying of 3D models on 2D images, which are a real need.

The use of 3D models of skulls should be preferred to their 2D representation (like photographs (Ghosh and Sinha 2001) or radiographs (Ricci et al. 2006)) due to the inherent problems of representing a 3D object with a 2D image.

The development of automatic methods tackling the skull-face overlay stage, the most tedious task of the whole process, is far away from its possibilities since only two proposals perform this complex process in an automatic way. Furthermore, as it has been commented on in Section 2.4.2.2, they have significant drawbacks that make them not applicable to real-world identification cases. The automatization of the skull-face overlay stage is the main contribution of this dissertation. Novel approaches in this direction are presented in Chapters 3 and 4.

Besides, we can explain the underlying uncertainty involved in the CS process. The correspondence between facial and cranial anthropometric landmarks is not always symmetrical and perpendicular: some landmarks are located in a higher position in the face of the alive person than in the skull, and some others have not a directly related landmark in the other set.

The identification decision is to be expressed according several confidence levels ("absolute matching", "absolute mismatching", "relative matching", "relative mismatching", and "lack of information"). Hence, we again find the uncertainty and partial truth involved in the identification process. In conclusion, fuzzy set theory (Klir and Yuan 1996) could be an interesting tool to be applied.

In this sense, a proposal for the modelization of the inherent uncertainty in CS are presented in Chapter 5. In that chapter we study the different sources of uncertainty and we present a novel proposal that deals with the location uncertainty by means of fuzzy methods.

The distortions that may arise during the CS process could influence the reliability of the identification. It is advised to use central projections or to apply a mathematical model to eliminate the distortions (Eliášová and Krsek 2007).

In computer-aided diagnosis, the general agreement is that the focus should be on making useful computer-generated information available to physicians for decision support rather than trying to make a computer act like a diagnostician (Berner 2007). Following the same track, the final goal of computer-aided automatic craniofacial identification systems should be to provide the forensic anthropologists with identification decisions they will have to supervise and validate.

2.6.4 The craniofacial superimposition challenge

Science evolves thanks to the knowledge exchange and the chance to either improve existing approaches or propose new methods for the problems that are tackled. Therefore, it is essential to guarantee objective procedures to evaluate the performance of

those proposals.

Unlike other related research fields like face recognition or machine learning, it is not possible to compare the performance of the developed CS methods since there is not a common forensic dataset available comprised by 3D partial views of skulls, the corresponding reconstructed 3D model, photographs of the person the skull belongs to, landmarks, superimposition results detailing the used techniques together with the identification decision, and so on. This fact has already been mentioned by some experts on the area, such as Carl N. Stephan (2009a) in his sentence quoted in the Introduction section):

"*We think this is the main reason for finding few practical applications of computer-aided automatic methods. In our opinion, having forensic material available is a keystone for the advance of the CS research field.*"

Large, publicly available databases of known case studies should be collected. Those databases will encourage the development and testing of new methods. They will also allow the validation of new methods by applying them to solved cases and by comparing the results with the identification previously determined by forensic anthropologists.

Assuming this challenge, we have created a web repository[5] with the aim to provide forensic data to the research community and to join forces by the collaboration with other forensic labs.

As said, there are different issues in CS that can be tackled by means of advanced artificial intelligence approaches. EAs, fuzzy sets theory, and neural networks have demonstrated their suitability for tackling different CS tasks. Moreover, the application of these techniques to the CS problem has been presented in the survey developed in this chapter as an emerging trend. Thus, public CS datasets will be interesting for the artificial intelligence research community. Indeed, different authors have recently claimed that a multidisciplinary research team is a real need in forensic identification by CS nowadays (Ricci et al. 2006; Benazzi et al. 2009).

2.7 Concluding remarks

We have proposed a new general framework for computer-based CS, dividing the process into three stages: face enhancement and skull modeling, skull-face overlay, and decision making.

[5] http://www.softcomputing.es/socovifi/en/home.php

We have expanded the computer-aided CS category defined in previous reviews by distinguishing between non-automatic and automatic methods depending on the actual role the computer plays in the different stages of the process.

We have reviewed and categorized the existing contributions of computer-aided CS systems. We have classified them according to the CS stage that is tackled using a computer-aided method.

We have summarized a number of solved and unsolved problems in CS as well as opportunities for forensic applications by identifying some trends in the field. We have also provided a list of recommendations for future research. Finally, we have discussed the need for public forensic data repositories and we have presented a web site we have created for that purpose.

Chapter 3

Automatic Skull-face Overlay in Craniofacial Superimposition by Advanced Evolutionary Algorithms

We think too much and feel
too little.

Charlie Chaplin (1889-1977)

3.1 Introduction

As said in the previous chapters, there is a strong interest in designing automatic methods to support the forensic anthropologist in the CS process (Ubelaker 2000).

Following our methodological proposal (see Section 2.3 of Chapter 2), the whole CS process is composed of three stages (see Figure 3.1). The main tasks to be developed in each one of the stages of our CS proposal are the following:

The first stage involves the enhancement of 2D images (if it is necessary) by well-known image processing algorithms (Gonzalez and Woods 2002) and the obtaining of an accurate 3D model of the skull. Once we have a 3D model of the skull and one (or more) photograph(s) of the face of the missing person, two sets of craniometric and cephalometric landmarks are located (by the forensic experts) in the skull and the photograph, respectively.

Next, in the second stage (skull-face overlay), we use these two sets of landmarks to guide an IR process that aims to automatically superimpose both the skull and the face.

Finally, a decision making stage will assist the forensic expert to take the final identification decision.

Among the three stages, skull-face overlay is the most time consuming and tough task when a manual approach is followed. A sensible way to design an automatic skull-face overlay procedure is through the use of an IR technique to properly align the 3D model and the 2D image in a common coordinate frame.

In this chapter, we will propose a formulation of the skull-face overlay task as a numerical optimization problem, solving the underlying 3D-2D IR task following a parameter-based approach. We will design different real-coded EAs to tackle this prob-

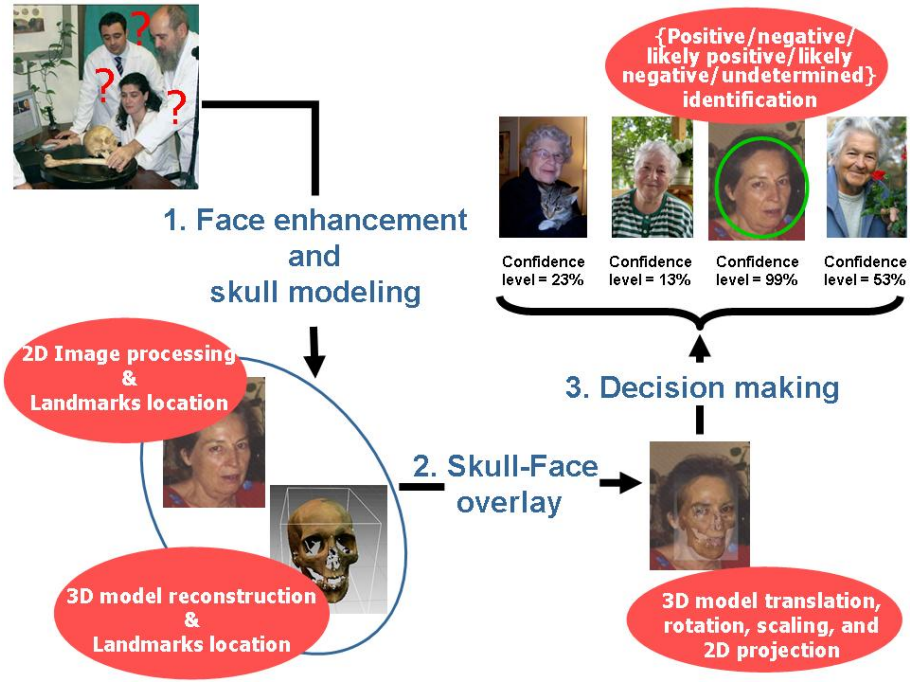

Figure 3.1: The three stages involved in our proposed framework for the 3D/2D computer-aided CS process

lem, comparing their performance with Nickerson et al.'s binary-coded GA (Nickerson et al. 1991), which shows several flaws making it unsuitable for the problem solving. Note that, we have used developments resulting from Santamaría et al. (2007a, 2007b, 2009) for the obtaining of a 3D model of the skulls in the tackled identification cases.

The structure of the chapter is as follows. In Section 3.2, we review Santamaría et al. works and the only two existing proposals on automatic skull-face overlay. In Section 3.3, the proposed problem formulation is detailed. Section 3.4 is devoted to describe the designed EAs and to explain their adaptation for solving the skull-face overlay problem. In Section 3.5, we will show the results obtained in the experiments developed on some real world cases, together with an analysis of the performance of the algorithms depending on the parameter values selected. Section 3.6 collects some conclusions.

3.2 Preliminaries

In the following sections we will analyze some preliminary works that have been important in the development of the evolutionary-based skull-face overlay method that will be presented in this chapter. On the one hand, Section 3.2.1 review the obtaining process of a 3D skull model. On the other hand, Section 3.2.2 is devoted to study the existing proposals of automatic computer-based skull-face overlay methods.

3.2.1 3D skull model reconstruction stage

As said, one of the main tasks of the first stage of the CS procedure is the acquisition of the 3D model of the skull. Recently, laser range scanners are being one of the most used devices for 3D image acquisition, mainly motivated by their inexpensive price and easy portability. These kinds of 3D scanners are able to capture 3D images of the surface of the object under study. Those images are also considered as $2\frac{1}{2}$-dimensional images because, roughly speaking, a range image is a conventional camera image, but every pixel stores a depth value rather than a color. Since a whole object cannot be completely scanned in a single image using a range scanner, multiple acquisitions from different views are needed to supply the information to construct the 3D model by a RIR (Dalley and Flynn 2001) algorithm, which is often used for the accurate integration of all the images. The latter procedure is known as 3D model reconstruction (Ikeuchi and Sato 2001) and its output is a 3D model of the scanned object, in our case a human skull.

When a 3D model reconstruction is needed, one critical consideration is the presence or absence of a turn table (also named rotary table) (Figure 3.3, right), which is a positioning device that accurately controls the amount of rotation between consecutive acquisitions. Some range scanners are provided with a turn table device that is connected to the scanner and an appropriate software that permits the 3D reconstruction. Some anthropologists are skilled enough to deal with the set of 3D views and they supervise the procedure of commercial software packages like RapidForm^{TM}. Nevertheless, these software packages do not always provide the expected outcomes and the anthropologists even have to "stitch up manually" every couple of adjacent views. Moreover, there are scenarios where it is not even possible to use the rotary table. That is the case when the size of the object to be scanned is too big, such as an excavation, a building or a statue, for instance.

A 3D robust and accurate IR by EAs is a real need for the anthropologists. However, this is a really complex optimization task, with a strongly multimodal huge search space. Thus, exhaustive search methods are not useful. This complex landscape led

Santamaria et al. to propose different evolutionary methods (Santamaría et al. 2007a; Santamaría et al. 2007b; Santamaría et al. 2009) achieving really good results in the automatic alignment of skull range images.

The 3D reconstruction procedure they proposed carries out several pair-wise alignments (registrations) of adjacent views, known as scene and model, in order to obtain the final (reconstructed) 3D model of the physical object. Every pair-wise RIR method tries to find the Euclidean motion that brings the *scene* view $I_s = \{p_i\}_1^{N_{I_s}}$ into the best possible alignment with the *model* view $I_m = \{q_i\}_1^{N_{I_m}}$, with p_i and q_i being the characteristic points from every image. The authors considered an Euclidean motion based on a 3D rigid transformation (f) determined by seven real-coded parameters, that is: a rotation[1] $R = (\theta, Axis_x, Axis_y, Axis_z)$ and a translation $\vec{t} = (t_x, t_y, t_z)$, with θ and $\vec{Axis}$ being the angle and axis of rotation, respectively. Then, the transformed points of the *Scene* view are denoted by

$$f(p_i) = R(p_i - C_{I_s}) + C_{I_s} + t, \;\; f(I_s) = \{f(p_i)\}_1^{N_{I_s}} \tag{3.1}$$

where C_{I_s} is the center of mass of I_s. They defined the distance from a transformed I_s point $f(p_i)$ to the *Model* view I_m as the squared Euclidean distance to the closest point q_{cl} of I_m, $d_i^2 = \|f(p_i) - q_{cl}\|^2$.

Then, the RIR task can be formulated as an optimization problem searching for the Euclidean transformation f^* achieving the best overlapping of both images according to the considered *Similarity metric* F:

$$F(I_s, I_m; f) = d_i^2, \;\; \forall i \in \{1, \ldots, N_{I_s}\} \tag{3.2}$$

$$f^* = \arg\min_f \; F(I_s, I_m; f) \;\; s.t.: \; f^*(I_s) \cong I_m \tag{3.3}$$

A two step pair-wise RIR technique (Bernardini and Rushmeier 2002) was successfully applied. The method includes a pre-alignment stage, that uses a SS-based algorithm, and a refinement stage based on the classical ICP algorithm. The procedure is very robust, indeed it reconstructs the skull 3D model even if there is no turn table and the views are wrongly scanned.

On the other hand, the successful performance of any RIR method drastically depends on the amount of overlapping present in the couple of range images (likewise,

[1] The authors used quaternions instead of the three classical Euler matrices representation that suffers the problem of *gimbal lock* (Shoemake 1985).

on the number of views acquired). The authors considered those scanning cases with a minimum overlapping degree, close to the fifty percent of the physical surface,in order to ease the acquisition procedure to the forensic experts. Taking into account the said overlapping consideration, an objective function based on the minimization of the median squared error (MedSE) of the closest point distances d_i^2 is considered:

$$F(I_s, I_m; f) = MedSE(d_i^2) \tag{3.4}$$

where $MedSE()$ corresponds to the computation of the median d_i^2 value of the $N_{I_s}^{th}$ scene points. The authors used the GCP scheme (Yamany et al. 1999) to speed up the computation of the closest point q_{cl} of I_m.

An example of a 3D skull model from the Physical Anthropology lab, automatically reconstructed from several partial views by using the evolutionary-based methods proposed by Santamaria et al. (2007a, 2007b, 2009), is shown in Figure 3.2.

Figure 3.2: First row: two photographs of a skull in different poses. Second row (from left to right): three 3D partial views of the previous skull, 3D skull model obtained from the previous views, and 3D skull model including textures

3.2.2 Analysis of existing proposals on automatic skull-face overlay

As it was pointed out in Section 2.4.2.2 of Chapter 2, there are only two proposals performing CS in a fully automatic way, based on the use of neural networks (Ghosh and Sinha 2001) and GAs (Nickerson et al. 1991), respectively. However, as we will see in the following, they are not suitable for forensic experts.

On the one hand, the method proposed by Ghosh and Sinha (2001) consisted of two neural networks (NN) (Arbib 1995) to be applied to two different parts of the overlaying and allows the user to select fuzzy facial features to account for ambiguities due to soft tissue thickness. It provides an overlay between cranial and face 2D images. Significant limitations make the method not applicable to real-world identification cases: i) it needs frontal view images; ii) there is a part of the cranial image that is never properly mapped; iii) the overlaying found by the first NN could be disrupted by the second; and iv) it needs a long computation time.

On the other hand, Nickerson et al.'s method (Nickerson et al. 1991) used a binary-coded genetic algorithm (BCGA) to find the optimal parameters of the similarity and perspective transformation that overlays the 3D skull model on the face photograph. More in details, this method included the following tasks:

- 2D digitalization of an antemortem facial photograph.
- 3D digitalization of the surface mesh of the skull.
- Application of digital filtering techniques to the 2D photo image and the 3D model to reduce or eliminate systematic error.
- Selection of four landmark points on the digital facial image and four equivalent non-coplanar landmarks on the skull surface mesh.
- Calculation of the near-optimal affine and perspective transformations required to map the skull surface mesh into two dimensions and onto the face image.
- Joint solid rendering of the digital facial photograph and transformed skull surface mesh for visual analysis.

A digital scanner and a laser range scanner were used for 2D and 3D digitizations, respectively. Well known image processing algorithms were considered for image enhancement. Rendering was done through computer graphics techniques, after polygonal texture mapping of the 2D image.

Three approaches were considered to solve the optimization task that automatically maps the skull surface mesh on the digital facial photograph: a heuristic technique, a classic numerical optimization method, and a BCGA. Results based on the GA outperformed the remainder.

The most important drawback of this technique is its lack of accuracy when dealing with real-world identification cases, as we will see in Section 3.5

3.3 Problem description

In Chapters 1 and 2 we presented the analogies between skull-face overlay and the IR problem. This section aims to supply an insight view into such relationship describing the geometric transformation involved in the CS problem.

3.3.1 Introduction

The final goal of the IR problem underlaying CS is to find a transformation that, when applied to the skull 3D model, can locate it exactly in the same pose it had when the available photograph of the missing person was taken. Along this process, we can easily differentiate two important moments (Figure 3.3). First, when the missing person was posing for the photograph. Second, when the skull found was scanned to obtain a skull 3D model that could be geometrically transformed in order to achieve the desired location. Hence, it is a really complex problem because we are trying to reproduce the scenario when the subject photograph was taken with an important number of unknowns coming from two different sources:

- The camera configuration. At the moment of the acquisition, there were different parameters that have an influence in the CS problem. Some of them are directly reflected on the photograph as the specific area of interest for the person taking it (highlighted in the example shown in the left side of Figure 3.3 using a dashed rectangle) or the lighting conditions. However, there are some other parameters that cannot be easily derived from the photograph as the distance from the camera to the missing person or the aperture of the camera that will determine what is finally projected into the photograph and what is outside it. Indeed, if a camera with a wide-angle lens was used it would be possible to acquire a wider piece of the scene while keeping the same distance to the object one wanted to photograph.

- The skull model. Once the first stage of the CS process is finished, a skull 3D model is available. This skull model will have a specific orientation, resolution and size given by the technical features of the scanner as well as by the skull modeling process (Figure 3.3, right). Notice that, the skull model size usually corresponds to the size of the real skull.

Figure 3.3: Photograph and skull model acquisitions

3.3.2 Geometric transformations for the image registration problem underlying skull-face overlay

This section aims to present the geometric transformations involved in the CS problem. A detailed description of projective geometry is out of the scope of this contribution, the interested reader is referred to (Foley 1995). The set of geometric transformations needed to accomplish the superimposition task follows:

- **Rotation** R**.** The first step to find the proper location of the skull will involve applying a rotation to orient the skull in the same pose of the photograph. In order to define a rotation, the direction of the rotation axis $\vec{d} = (d_x, d_y, d_z)$, the location of the rotation axis with respect to the center of coordinates $\vec{r} = (r_x, r_y, r_z)$, and the angle θ must be given. Once they are determined, the usual computer graphics procedure to apply this rotation is as follows:

  - Translate the skull to align the origin of coordinates with the rotation axis.
  - Rotate the skull so that the rotation axis coincides with one of the Cartesian axes.
  - Perform the rotation given by θ.
  - Use the inverse rotation matrices in reverse order in order to leave the rotation axis in its original orientation.
  - Apply the inverse translation matrix to leave the rotated skull in its original location.

This rotation process R is thus given by:

$$R = (A \cdot D_1 \cdot D_2 \cdot \Theta \cdot D_2^{-1} \cdot D_1^{-1} \cdot A^{-1}) \tag{3.5}$$

where:

$$A = \begin{bmatrix} 1 & 0 & 0 & 0 \\ 0 & 1 & 0 & 0 \\ 0 & 0 & 1 & 0 \\ -r_x & -r_y & -r_z & 1 \end{bmatrix} D_1 = \begin{bmatrix} 1 & 0 & 0 & 0 \\ 0 & d_z/\nu & d_y/\nu & 0 \\ 0 & -d_y/\nu & d_z/\nu & 0 \\ 0 & 0 & 0 & 1 \end{bmatrix} D_2 = \begin{bmatrix} \nu & 0 & d_x & 0 \\ 0 & 1 & 0 & 0 \\ -d_x & 0 & \nu & 0 \\ 0 & 0 & 0 & 1 \end{bmatrix}$$

$$\Theta = \begin{bmatrix} \cos\Theta & -\sin\Theta & 0 & 0 \\ \sin\Theta & \cos\Theta & 0 & 0 \\ 0 & 0 & 1 & 0 \\ 0 & 0 & 0 & 1 \end{bmatrix} \quad \nu = \sqrt{d_y^2 + d_z^2}$$

- **Scaling** S**.** The size of the skull model must be uniformly adapted according to the size of the missing person in the photograph. Hence, the coordinates of each point of the skull model will be resized considering a factor named s:

$$S = \begin{bmatrix} s & 0 & 0 & 0 \\ 0 & s & 0 & 0 \\ 0 & 0 & s & 0 \\ 0 & 0 & 0 & 1 \end{bmatrix}$$

- **Translation** T**.** The coordinates of the skull model are relative to the origin defined by the range scanner. Thus, it must be translated according to $T = (t_x, t_y, t_z)$ in order to be located in front of the camera and reproduce the conditions when the photograph of the missing person was taken. To do so, the following matrix is considered:

$$T = \begin{bmatrix} 1 & 0 & 0 & 0 \\ 0 & 1 & 0 & 0 \\ 0 & 0 & 1 & 0 \\ t_x & t_y & t_z & 1 \end{bmatrix}$$

- **Perspective projection** P**.** Cameras perform a perspective projection of the scene into the photograph in order to provide a more realistic perception of how far the object is from the viewer. In computer graphics, this effect is achieved defining a frustum[2] of a rectangular pyramid (Figure 3.4, left). There are thus two planes that are used to delimit what is visible in the scene and what is consequently represented in the computer. Those parts of the scene that are closer

[2] A frustum is the portion of a solid –normally a cone or a pyramid– which lies between two parallel planes cutting the solid.

to the camera than the near clipping plane (NCP) or farther than the far clipping plane (FCP) will not be considered for visualization purposes. They will be outside the field of view of the camera. This issue has also a direct effect on the geometric transformation of the skull we are describing.

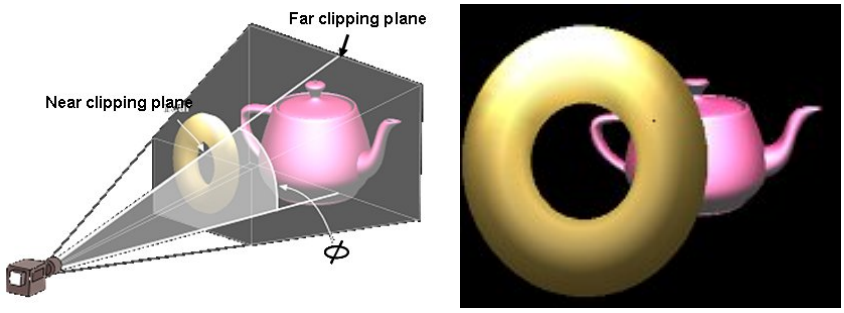

Figure 3.4: Camera configuration with angle of view ϕ (left) and the corresponding photograph (right)

Once the previous transformations are applied, the skull is located in front of the camera, with the proper orientation and size. Finally, we need to determine how far the camera is from the skull. If it is too close then the camera will capture just a projection of the skull without the rest of the elements that were captured in the photograph. This issue has a strong connection to the angle of view (ϕ) of the camera, which describes the angular extent of a given scene that is imaged by a camera. Figure 3.4 depicts this effect. Notice that, although the torus has a smaller size than the teapot in the real world (Figure 3.4, left), the former seems to be bigger than the latter in the picture acquired by the camera (Figure 3.4, right) because of the effect of the perspective when the object is too close to the camera. Once the camera is located in the proper position, all the rays connecting every 3D landmark of the skull with its corresponding 2D landmark in the photograph will converge in the center of projection. In addition, we should note that the torus is fully visible in the picture that has been acquired (Figure 3.4, right). However, if it had been placed slightly on the left then it would have been partially outside the defined frustum and there would be part of it missing in the picture.

The perspective transformation described is given by:

$$P = \begin{bmatrix} 1 & 0 & 0 & 0 \\ 0 & 1 & 0 & 0 \\ 0 & 0 & \tan(\phi/2) & \tan(\phi/2) \\ 0 & 0 & 0 & 1 \end{bmatrix}$$

3.3.3 3D Skull-2D face overlay problem statement

Given two sets of 2D facial and 3D cranial landmarks (F and C, respectively):

$$F = \begin{bmatrix} x_{f_1} & y_{f_1} & 1 & 1 \\ x_{f_2} & y_{f_2} & 1 & 1 \\ \vdots & \vdots & \vdots & \vdots \\ x_{f_N} & y_{f_N} & 1 & 1 \end{bmatrix} \quad C = \begin{bmatrix} x_{c_1} & y_{c_1} & z_{c_1} & 1 \\ x_{c_2} & y_{c_2} & z_{c_2} & 1 \\ \vdots & \vdots & \vdots & \vdots \\ x_{c_N} & y_{c_N} & z_{c_N} & 1 \end{bmatrix},$$

we aim to solve the following system of equations with twelve unknowns $(r_x, r_y, r_z, d_x, d_y, d_z, \theta, s, t_x, t_y, t_z, \phi)$ that represents the geometric transformation which maps every cranial landmark C_i in the skull 3D model onto its corresponding facial landmark F_i in the photograph:

$$F = C \cdot (A \cdot D_1 \cdot D_2 \cdot \theta \cdot D_2^{-1} \cdot D_1^{-1} \cdot A^{-1}) \cdot S \cdot T \cdot P \tag{3.6}$$

3.4 Design of real-coded evolutionary algorithms for skull-face overlay in craniofacial superimposition

EAs have been successfully applied to a variety of IR problems (see Section 1.3.5 in Chapter 1 and (Cordón et al. 2007; Santamaría et al. 2010)). As seen, skull-face overlay can be formulated as a numerical optimization problem with twelve unknowns in the framework of IR. Next, we propose four different EA designs in order to deal with this complex IR problem. Before going through them, we will firstly describe the common components to every method.

3.4.1 Common components to solve the skull-face overlay problem by means of evolutionary algorithms

In Section 3.3 we described the geometric transformation f for the IR problem underlying CS. This transformation f is determined fixing the described twelve unknowns. We consider a coding scheme representing these twelve unknowns in a vector of real numbers to be evolved by means of the real-coded EAs designed in this chapter. Hence, our individual will have the following form:

r_x	r_y	r_z	d_x	d_y	d_z	θ	s	t_x	t_y	t_z	ϕ

In order to adapt these twelve parameters through the use of evolutionary operators, their ranges must be defined. We have calculated them as follows:

$$\begin{array}{rcl} r_i & \in & [Centroid - radius,\ Centroid + radius], i \in \{x,y,z\} \\ d_i & \in & [-1,\ 1], i \in \{x,y,z\} \\ \theta & \in & [0^\circ,\ 360^\circ] \\ s & \in & [0.25,\ 2] \\ \phi & \in & [10^\circ,\ 150^\circ] \\ t_x & \in & [-length_{FB} - (C_x + radius),\ length_{FB} - (C_x - radius)] \\ t_y & \in & [-length_{FB} - (C_y + radius),\ length_{FB} - (C_y - radius)] \\ t_z & \in & [NCP - (C_z + radius),\ FCP - (C_z - radius)] \end{array}$$

where $radius = max(||Centroid - C_j||)$, with $Centroid$ being the centroid of the considered 3D landmarks, C_j being the j^{th} 3D cranial landmark, and $||\cdot||$ being the Euclidean distance between two 3D points; FCP and NCP are the Far and Near Clipping Planes, respectively; FB is the frustum Base; and

$$length_{FB} = \frac{(min_{FD} + FCP) * sin(\frac{\phi_{max}}{2})}{sin(90^o - (\frac{\phi_{max}}{2}))}$$

with FD being the Focal Distance, and

$$min_{FD} = \frac{1}{tan(\frac{\phi_{max}}{2})},$$

considering a 2×2 projection plane centered in the Z axis (see Section 3.3.2).

In preliminary experiments, we considered a higher scaling upper bound but we did not achieve better results. On the other hand, we should note that the field of view of a typical camera is $\phi = 45^\circ$. However, in professional ones, where even the lens can be changed, $\phi \in [5^\circ,\ 180^\circ]$.

To measure the quality of the registration transformation encoded in a specific individual a fitness function is needed. Therefore, given $C = \{C_1, C_2, ..., C_N\}$ and $F = \{F_1, F_2, ..., F_N\}$, two sets of 3D cranial and 2D facial landmarks respectively, we propose the minimization of the following fitness function for all the evolutionary approaches to the problem being considered:

$$fitness = \beta_1 \cdot ME + \widehat{w} \cdot \beta_2 \cdot MAX \tag{3.7}$$

where:

$$ME = \frac{\sum_{i=1}^{N} ||f(C_i) - F_i||}{N} \tag{3.8}$$

and

$$MAX = MAX_{i=1}^{N} ||f(C_i) - F_i||^2 \tag{3.9}$$

with $||\cdot||$ being the 2D Euclidean distance, N being the number of considered landmarks, and $f(C_i)$ being the positions of the transformed 3D landmarks once they have been spatially relocated and projected in the projection plane.

The scaling factor $\widehat{w}$ (used when $\beta_1 \neq 0$ and $\beta_2 \neq 0$) is obtained by averaging the proportion between ME and MAX (noted by w_{S_i}) for each individual S_i of the initial population (P_0):

$$\widehat{w} = \frac{\sum_{i=1}^{M} w_{S_i}}{M} \tag{3.10}$$

where $w_{S_i} = ME(S_i)/MAX(S_i)$ and M is the EA population size.

Finally, there is something important to be taken into account when trying to project 3D images into a 2D plane by means of the formulation introduced in Section 3.3. Due to the perspective projection (see Section 3.3.2), there are lots of values for the twelve unknowns (transformation parameters) which correspond to a non projectable solution. Depending on the transformation parameters values, the skull projection can be outside of the 2D image area. Hence, we are dealing with a strongly multimodal, constrained problem and, to solve these kinds of problem with EAs, two different approaches can be followed (Bäck et al. 1997; Eiben and Smith 2003; Goldberg 1989; Michalewicz 1996). On the one hand, we can restrict the search mechanism to avoid looking into the space of non projectable solutions. On the other hand, we can penalize non projectable solutions by means of the fitness function to avoid moving through the non projectable search space as much as possible. Since both solution spaces (projectable and non projectable) are quite interlaced in our CS solution space, we decided to implement the second approach by assigning a theoretical maximum value of penalization to the fitness of the individual when the solution is a non projectable one. Thanks to this, we allow the genetic material of these solutions to be considered for the generation of hopefully good quality projectable solutions.

3.4.2 Real-coded genetic algorithms

Since GAs (Goldberg 1989; Michalewicz 1996) are maybe the most representative EAs and the only existing proposal for our problem was based on them, we decided to start tackling skull-face overlay by using GAs. The natural coding considered, representing the twelve registration transformation parameters in a real-valued array, led us to use a RCGA (Herrera et al. 1998). RCGAs have become a very active area of research in the last decade achieving very good performance in many different applications and becoming a valid alternative to evolution strategies (Bäck 1996) and evolutionary programming (Schwefel 1995) for numerical optimization.

Thus, we designed a RCGA with the following features:

Initial population generation, as a consequence of the aforementioned problem of the non projectable solutions (see Section 3.4.1), a considerable proportion of the initial population could correspond to this kind of solutions. Due to the inability of evaluating non projectable solutions in terms of the proposed fitness function, we must avoid a convergence to the search space regions containing these solutions. This has to be done while keeping a useful diversity. With these aims, the initial population of the considered GA is generated as follows: new individuals are randomly created until at least the half of the population phenotypes correspond to projectable solutions.

Tournament selection method (Blickle 1997), in which t individuals ($t = 2$ is usually a common choice, the socalled binary tournament) are selected at random from the population with replacement and the best of them is inserted into the new population for further genetic processing. This procedure is repeated until the mating pool is filled.

Elitism, the individual with best (lowest) fitness value is kept unchanged in the next generation population.

Random mutation operator (Bäck et al. 1997), which randomly selects one of the genes of a parent and sets it equal to a uniform random number between the gene's lower and upper bounds.

Two crossover operators, thus involving two different designs of the RCGA:

1) the **blend crossover** (BLX-α) (Eshelman 1993) which uniformly picks new individuals with values that lie in $[x'_i, y'_i]$, an extended interval obtained from the two parents' gene values x_i and y_i for a particular variable i. The offspring O is sampled as follows:

$$o_i = x'_i + r \times (y'_i - x'_i); i = 1, ..., 12 \tag{3.11}$$

where $x'_i = x_i - \alpha \times (y_i - x_i)$; $y'_i = y + \alpha \times (y_i - x_i)$; and r is a uniform random number $\in [0,1]$, checking that x'_i and y'_i will lie between the variable's lower and upper bounds. In our case, two offsprings are generated by applying twice the operator on the two parents.

Although BLX-α was proposed more than fifteen years ago, it has become a standard in the area due to its good performance thanks to its ability to properly establish a good exploration-exploitation trade-off. In fact, Nomura and Shimohara (2001) have demonstrated theoretically that BLX-α has the ability to promote diversity in the population of an EA. They state that BLX-α spreads the distribution of the chromosomes when $\alpha > (\sqrt{3}-1)/2$ ($\simeq 0.366$), and reduces it otherwise. This property was verified through simulations.

From now on we will refer to this RCGA version as RCGA-BLX-α.

2) the **simulated binary crossover** (SBX) (Deb and Agrawal 1995) is another real-parameter recombination operator commonly used in the literature which has shown very good results. In SBX, offspring are created in proportion to the difference in parent solutions. The procedure of computing the offspring solutions $x_i^{(1,t+1)}$ and $x_i^{(2,t+1)}$ from parent solutions $x_i^{(1,t)}$ and $x_i^{(2,t)}$ is described as follows. First, a random number u between 0 and 1 is created. Thereafter, from a specified probability distribution function:

$$P(\beta) = \begin{cases} 0.5(\eta+1)\beta^n, & \text{if } \beta \leq 1; \\ 0.5(\eta+1)/\beta^{n+2}, & \text{otherwise,} \end{cases} \tag{3.12}$$

defined over a non-dimensionalized parameter $\beta = | (x_i^{(2,t+1)} - x_i^{(1,t+1)})/(x_i^{(2,t)} - x_i^{(1,t)}) |$, the ordinate β_q is found so that the area under the probability curve from 0 to β_q is equal to the chosen random number u:

$$\beta_q = \begin{cases} (2u)^{\frac{1}{\eta+1}}, & \text{if } u \leq 0.5; \\ (1/(2(1-u)))^{\frac{1}{\eta+1}}, & \text{otherwise,} \end{cases} \tag{3.13}$$

In the above expressions, the distribution index η is any non negative real number. A large value of η allows a large probability for creating near parent solutions while a small value of η allows distant points to be created as offspring solutions. After obtaining β_q from the above probability distribution, the descendent solutions are calculated as follows:

$$x_i^{(1,t+1)} = 0.5[(1+\beta_q)x_i^{(1,t)} + (1-\beta_q)x_i^{(2,t)}] \tag{3.14}$$

$$x_i^{(2,t+1)} = 0.5[(1+\beta_q)x_i^{(1,t)} + (1-\beta_q)x_i^{(2,t)}] \tag{3.15}$$

In the remainder of the chapter, this RCGA version will be noted RCGA-SBX.

3.4.3 Covariance matrix adaptation evolution strategy

As a second approach to solve the skull-face overlay problem, we took the CMA-ES algorithm, whose fundamentals and basic equations were already explained in Section 1.4.2 of Chapter 1.

To design this new method, some considerations have to be taken into account:

- Since we are dealing with a multimodal problem, we needed to adapt some parameter values to make CMA-ES become appropriate to solve it. As said, in (Hansen and Ostermeier 2001) the authors provide default values for all the set of parameters of the algorithm: $4+\lfloor 3\ln(n)\rfloor$ for λ (with n being the number of genes) and $\lambda/2$ for μ. In our problem, n=12, and thus λ=11 and μ=5. We used these values but an unacceptable low performance was achieved. However, in the same paper they recommend to enlarge λ, and choose μ accordingly, to make the strategy more robust or more explorative in case of multimodality. So, after several preliminary experimentations testing different parameter values, we established their values to $\lambda = 100$ and $\mu = 15$ (very typical values in (μ,λ)-ESs but not in the CMA-ES), which were the ones that provided better results.

- The other problem, as in the case of the GA approaches, refers to the non projectable solutions. For the already mentioned convergence problems, the initial solution, i.e., the one used to work out the initial distribution centre $<\overrightarrow{x}>_{\omega}^{(0)}$, is randomly generated until a set of transformation parameters corresponding to a projectable solution is obtained.

- In addition, the restart operator (Auger and Hansen 2005), which does not increase the population size, was determined to be used every 25000 evaluations to avoid the convergence of the algorithm to local minima.

The rest of the parameters are the default ones, reported in (Hansen and Ostermeier 1996). Notice that, in Section 3.5 we have changed the notation of parameter σ to θ in order to avoid confusing it with the standard deviation usual notation in the experimental results.

3.4.4 Binary-coded genetic algorithm

Finally, we considered Nickerson et al.'s approach (Nickerson et al. 1991) as a baseline to tackle the CS problem. This decision was due to the fact that it is the only automatic proposal in the literature dealing with a 3D model of the skull and a 2D face photograph. In this proposal, the authors only indicated the use of a BCGA, but they did not specified its components. Hence, in order to properly design the incomplete description we had to make several assumptions that were based on the date that contribution was published. In particular, we considered roulette-wheel selection, elitism, two point crossover and simple mutation operators (Goldberg 1989) for the proposed BCGA. We are aware of the fact that this evolutionary design is old fashioned and thus it is expected to achieve a very low performance. Nevertheless, we have preferred to keep it as a baseline for the performance of the remaining methods.

On the other hand, to make fairer the comparison between the designed algorithms, the same registration transformation and fitness function is considered, and the initial population of the BCGA is generated as in the case of the RCGA.

3.5 Experiments

Our experimental study will involve three real-world cases previously addressed by the staff of the Physical Anthropology lab at the University of Granada in collaboration with the Spanish scientific police. Those three identification cases were solved following a computer supported but manual approach for CS. We will consider the 2D photographs of the missing people and their corresponding 3D skull models acquired at the lab by using its Konica-Minolta© 3D Lasserscanner VI-910. In this section, we first show the parameter setting considered in the experiments. Next, we present the three cases of study (which involve four skull-face overlay problem instances), the obtained results, and their analysis. In addition, graphical representation of the skull-face overlay results are also shown for each case study.

3.5.1 Parameter setting

Regarding the experimental setup for the genetic approaches, we performed experiments with the following GA parameter values:

generations	=	600
population size	=	$\{100; 500; 1,000\}$
crossover probability	=	0.9
mutation probability	=	0.2
tournament size (for RCGA)	=	2
BLX-α parameter (for RCGA)	=	$\{0.1, 0.3, 0.5, 0.7, 0.9\}$
SBX η parameter (for RCGA)	=	$\{1, 2, 5, 10, 20\}$

As can be seen, three different population sizes are tested for the three GAs as well as five values for the crossover operator parameter (establishing different exploration-exploitation trade-offs) for each of the two RCGAs.

In the case of CMA-ES, the following values were considered for the different parameters:

evaluations	=	$\{55,200; 276,000; 552,000\}$
initial θ (mutation distribution variance)	=	$\{0.00001, 0.0001, 0.001\}$
	=	$\{, 0.01, 0.1, 0.3\}$
λ (population size, offspring number)	=	100
μ (number of parents/points for recombination)	=	15

Notice that, in order to perform a fair comparison, the number of evaluations for the CMA-ES are those corresponding to the number of evaluations needed to perform 600 generations of a GA with 100, 500 and 1,000 individuals, respectively, for the given mutation and crossover probabilities. Besides, six different values for the main CMA-ES parameter are also considered.

Regardless the specific parameter configuration for each proposed EA, there are some common considerations for all of them. Based on the values of the weighting coefficients (β_1, β_2), we can adjust the influence of the two error terms in the fitness function (Equation 3.7). In this experiment, we have considered three different choices, which in every case to be minimized: (1) $(\beta_1, \beta_2) = (1, 0)$: the resulting fitness function becomes the same that the original one proposed by Nickerson et al., i.e. the mean distance between the corresponding landmarks; (2) $(\beta_1, \beta_2) = (0, 1)$: it corresponds to the maximum distance between the corresponding landmarks; (3) $(\beta_1, \beta_2) = (0.5, 0.5)$: it becomes the average of the two former ones.

In order to avoid execution dependence, thirty different runs for each parameter

setting have been performed and different statistics are provided. We considered the ME (see Eq. 3.8) for the assessment of the final superimposition results.

Finally, all the methods are run on a PC with an AMD Athlon 64 X2 Dual (2 core 2.59GHz), 2 GB of RAM, and Linux CentOS.

3.5.2 Málaga case study

The facial photograph of this missing lady found in Málaga, Spain, was provided by the family and the final identification done by CS has been confirmed. We studied this real case with the consent of the relatives. The 3D model of the skull, represented in the left image of Figure 3.5, comprises 243,202 points (stored as x, y, z coordinates). The 2D image is a 290×371 RGB (red, green and blue) color image (see Figure 3.5, right). The forensic experts manually selected a set of six 3D landmarks on the skull 3D model and their counterpart 2D landmarks on the face present in the photo, both shown in the left and right images in Figure 3.5.

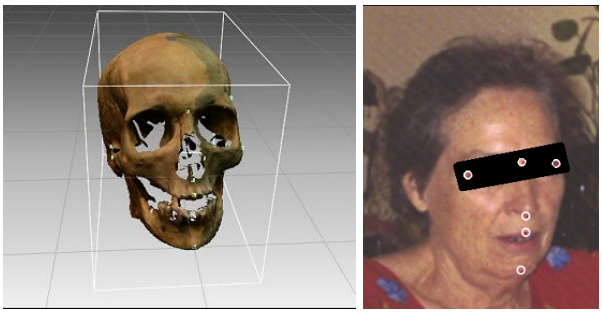

Figure 3.5: Málaga real-world case study: skull 3D model (left) and photograph of the missing person (right)

In order to avoid overloading the reader with the large number of experimental results obtained and to ease the following of this section, the tables here included will only report those outcomes corresponding to the population size which caused the best performance for each of the considered EAs. All the remaining results are collected in the tables shown in Appendix 3.A.

Table 3.1 shows the best results achieved by the implemented algorithms, BCGA, RCGA-BLX-α, RCGA-SBX; and CMA-ES, for the three given fitness function setups and for the different values of the parameters α, η and θ considered.

For each algorithm, the best (m), the worst (M), the mean (μ), and the

standard deviation (σ) values of the thirty runs are showed for the fitness, the ME, and the MAX measures. The best values for the minimum and mean results for each fitness function parameter combination are highlighted in boldface. Notice that, statistics of the fitness are only comparable between the same combination of (β_1, β_2) values while statistics of the ME and MAX are comparable all along the table[3].

From the reported results in Table 3.1 (and from those in corresponding tables in the Appendix 3.A, Tables 3.5 to 3.8) we can recognize how the fitness function $(\beta_1, \beta_2) = (1, 0)$ (that is to say, the ME) is the one which achieved the best and the most robust results in every case. Concerning the fitness $(\beta_1, \beta_2) = (0.5, 0.5)$ we can assert its better performance when compared to $(\beta_1, \beta_2) = (0, 1)$. The only exception is the BCGA case, where the performance of both functions is quite similar.

Looking carefully at the BCGA results, we can see that the best performance is achieved when considering a 1,000 individuals population. In addition, the poor robustness of the algorithm is clearly demonstrated. In spite of the the good quality of the best individual value reached, the results show high values for the means and standard deviations.

In the case of RCGA-BLX-α, 100 individuals and α values larger than 0.7 are the best configuration parameters. Anyway, it shows a low robustness (although higher than the BCGA), in view of the high means values.

Finally, the results obtained using RCGA-SBX and CMA-ES lead us to assert that they are clearly the best techniques for this identification case, with a very high robustness demonstrated by the fact that average values equal the minimum value in some cases. In the case of RCGA-SBX, the best performance is considered when using 1,000 individuals and small values of η, that is, the opposite exploration-exploitation trade-off than in RCGA-BLX-α. CMA-ES also performs better with the largest number of evaluations, 552,000, but with high values of θ. Although the best individual results (minima) reached by the RCGA-SBX are the best ones overall, CMA-ES achieved very similar values and is less sensitive to the parameter setting. In fact, this algorithm always obtains the same minimum for all the parameter configurations tested using the ME fitness.

Regarding to the visual results, the best overlays achieved are showed in Figure 3.6. The 2D facial landmarks are represented by an "o" while the projected 3D cranial landmarks by an "x". Though the best results are quite similar for all the algorithms, this is not the case of the worst results, i.e. the worst run of the best parameter

[3]This table structure will be the one followed for all the tables in this Section 3.5 and in the corresponding Appendix 3.A.

Table 3.1: Málaga case study: skull-face overlay results for the best performing population sizes

BCGA (1,000 individuals)													
β_1, β_2		*Fitness*				*ME*				*MAX*			
		m	M	μ	σ	m	M	μ	σ	m	M	μ	σ
1,0		0.017	0.250	0.156	0.075	**0.017**	0.250	**0.156**	0.075	0.039	0.415	0.268	0.118
0,1		0.094	0.372	0.298	0.073	0.075	0.272	0.220	0.052	0.094	0.372	0.298	0.073
0.5,0.5		0.023	0.265	0.163	0.083	0.025	0.267	0.163	0.085	0.029	0.366	0.229	0.113
RCGA-BLX-α (100 individuals)													
β_1, β_2	α	*Fitness*				*ME*				*MAX*			
		m	M	μ	σ	m	M	μ	σ	m	M	μ	σ
1,0	0.1	0.231	0.261	0.253	0.007	0.231	0.261	0.253	0.007	0.385	0.433	0.420	0.011
	0.3	0.233	0.262	0.254	0.007	0.233	0.262	0.254	0.007	0.387	0.434	0.422	0.011
	0.5	0.058	0.267	0.246	0.036	0.058	0.267	0.246	0.036	0.139	0.442	0.410	0.053
	0.7	0.020	0.237	0.080	0.074	**0.020**	0.237	**0.080**	0.074	0.030	0.376	0.129	0.116
	0.9	0.086	0.264	0.222	0.037	0.086	0.264	0.222	0.037	0.137	0.445	0.354	0.062
0,1	0.1	0.340	0.380	0.363	0.008	0.249	0.273	0.265	0.005	0.340	0.380	0.363	0.008
	0.3	0.341	0.375	0.362	0.007	0.250	0.274	0.265	0.004	0.341	0.375	0.362	0.007
	0.5	0.310	0.375	0.361	0.013	0.227	0.273	0.264	0.009	0.310	0.375	0.361	0.013
	0.7	0.332	0.377	0.363	0.010	0.243	0.275	0.264	0.007	0.332	0.377	0.363	0.010
	0.9	0.153	0.381	0.347	0.054	**0.105**	0.276	**0.246**	0.045	0.153	0.381	0.347	0.054
0.5,0.5	0.1	0.234	0.264	0.258	0.007	0.240	0.270	0.262	0.007	0.327	0.377	0.362	0.011
	0.3	0.246	0.266	0.259	0.006	0.250	0.271	0.264	0.006	0.343	0.372	0.362	0.008
	0.5	0.232	0.268	0.258	0.007	0.237	0.273	0.263	0.007	0.322	0.374	0.360	0.010
	0.7	0.022	0.269	0.163	0.100	**0.023**	0.273	**0.163**	0.101	0.030	0.375	0.230	0.139
	0.9	0.197	0.270	0.245	0.020	0.194	0.271	0.243	0.021	0.281	0.379	0.347	0.027
RCGA-SBX (1,000 individuals)													
β_1, β_2	η	*Fitness*				*ME*				*MAX*			
		m	M	μ	σ	m	M	μ	σ	m	M	μ	σ
1,0	1.0	0.016	0.020	0.018	0.001	**0.016**	0.020	**0.018**	0.001	0.036	0.056	0.051	0.004
	2.0	0.017	0.023	0.019	0.002	0.017	0.023	0.019	0.002	0.045	0.066	0.052	0.004
	5.0	0.016	0.044	0.024	0.006	**0.016**	0.044	0.024	0.006	0.031	0.155	0.055	0.021
	10.0	0.017	0.053	0.028	0.011	0.017	0.053	0.028	0.011	0.025	0.160	0.065	0.031
	20.0	0.017	0.062	0.034	0.012	0.017	0.062	0.034	0.012	0.034	0.183	0.080	0.037
0,1	1.0	0.021	0.032	0.024	0.002	0.020	0.028	**0.023**	0.002	0.021	0.032	0.024	0.002
	2.0	0.022	0.048	0.029	0.008	0.021	0.046	0.027	0.007	0.022	0.048	0.029	0.008
	5.0	0.022	0.086	0.042	0.016	0.021	0.065	0.038	0.014	0.022	0.086	0.042	0.016
	10.0	0.023	0.088	0.051	0.018	**0.019**	0.070	0.044	0.015	0.023	0.088	0.051	0.018
	20.0	0.028	0.242	0.072	0.059	0.026	0.182	0.060	0.043	0.028	0.242	0.072	0.059
0.5,0.5	1.0	0.017	0.028	0.019	0.002	**0.018**	0.029	**0.020**	0.002	0.023	0.038	0.025	0.003
	2.0	0.017	0.023	0.020	0.002	**0.018**	0.024	0.021	0.002	0.023	0.032	0.026	0.003
	5.0	0.017	0.048	0.026	0.009	**0.018**	0.056	0.027	0.010	0.023	0.058	0.034	0.011
	10.0	0.017	0.053	0.032	0.010	**0.018**	0.057	0.034	0.012	0.023	0.071	0.042	0.013
	20.0	0.019	0.086	0.041	0.018	0.021	0.087	0.041	0.016	0.024	0.120	0.059	0.029
CMA-ES (552,000 evaluations)													
β_1, β_2	θ	*Fitness*				*ME*				*MAX*			
		m	M	μ	σ	m	M	μ	σ	m	M	μ	σ
1,0	0.00001	0.017	0.043	0.021	0.009	**0.017**	0.043	0.021	0.009	0.045	0.133	0.062	0.028
	0.00010	0.017	0.043	0.019	0.007	**0.017**	0.043	0.019	0.007	0.051	0.132	0.057	0.020
	0.00100	0.017	0.044	0.021	0.009	**0.017**	0.044	0.021	0.009	0.051	0.140	0.063	0.028
	0.01000	0.017	0.043	0.019	0.008	**0.017**	0.043	0.019	0.008	0.051	0.134	0.059	0.025
	0.10000	0.017	0.018	0.017	0.000	**0.017**	0.018	**0.017**	0.000	0.051	0.053	0.051	0.000
	0.30000	0.017	0.019	0.017	0.001	**0.017**	0.019	**0.017**	0.001	0.049	0.054	0.052	0.001
0,1	0.00001	0.022	0.087	0.026	0.017	**0.021**	0.073	0.024	0.012	0.022	0.087	0.026	0.017
	0.00010	0.022	0.084	0.024	0.011	**0.021**	0.055	**0.022**	0.006	0.022	0.084	0.024	0.011
	0.00100	0.022	0.090	0.028	0.020	**0.021**	0.073	0.026	0.016	0.022	0.090	0.028	0.020
	0.01000	0.022	0.088	0.026	0.017	**0.021**	0.067	0.024	0.012	0.022	0.088	0.026	0.017
	0.10000	0.022	0.030	0.025	0.002	**0.021**	0.028	0.023	0.002	0.022	0.030	0.025	0.002
	0.30000	0.023	0.048	0.033	0.006	**0.021**	0.042	0.030	0.005	0.023	0.048	0.033	0.006
0.5,0.5	0.00001	0.017	0.059	0.020	0.011	**0.018**	0.051	0.020	0.008	0.023	0.092	0.028	0.018
	0.00010	0.017	0.059	0.022	0.013	**0.018**	0.052	0.022	0.010	0.023	0.092	0.030	0.021
	0.00100	0.017	0.059	0.019	0.008	**0.018**	0.052	0.019	0.006	0.023	0.092	0.025	0.013
	0.01000	0.017	0.059	0.019	0.008	**0.018**	0.052	0.020	0.006	0.023	0.092	0.027	0.014
	0.10000	0.017	0.019	0.018	0.000	**0.018**	0.019	**0.018**	0.000	0.023	0.025	0.024	0.001
	0.30000	0.018	0.025	0.019	0.002	**0.018**	0.027	0.020	0.002	0.023	0.033	0.026	0.003

configuration (see Figure 3.7). Notice that, in the case of BCGA and RCGA-BLX-α the skull has been downsized and it is located in the tip of the nose. Hence, results are only suitable for CMA-ES and RCGA-SBX.

Figure 3.6: Málaga case study. From left to right: the best superimposition results obtained by means of BCGA, RCGA-BLX-α, RCGA-SBX, and CMA-ES are shown

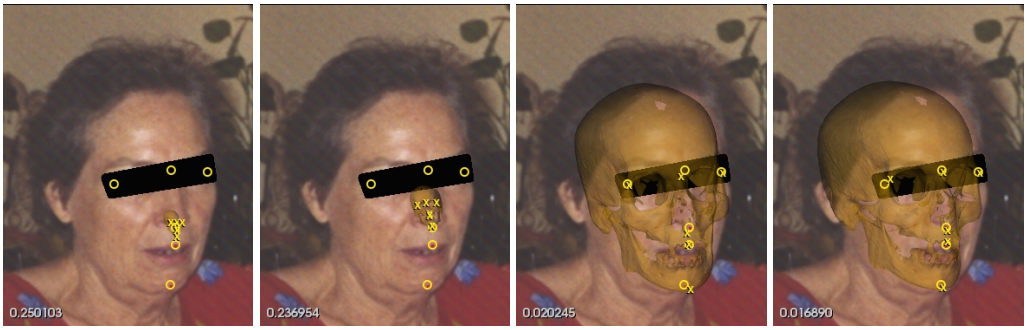

Figure 3.7: Málaga case study. From left to right: the worst superimposition results obtained with the best parameter configuration runs by means of BCGA, RCGA-BLX-α, RCGA-SBX, and CMA-ES are shown

3.5.3 Mallorca case study

The 3D model of the skull (199,609 points stored as x, y, z coordinates) has been acquired by the aforementioned 3D range scanner, and the considered 2D photograph (1,512 $\times$ 2,243 RGB image) has been provided by the family[4]. The forensic anthro-

[4]Due to legal issues, we are not allowed to publish images of this case. Nevertheless we will present and analyze numerical results.

pologists manually selected a set of six landmarks in both the skull and the photo.

The implemented algorithms have been applied to solve the skull-face overlay problem using the same experimental setup of the previous case. Table 3.2 shows the best results obtained with the three fitness function settings.

In general, the conclusions drawn are quite similar to those obtained in the first case study. Results from BCGA are very little robust, presenting high variability. CMA-ES and RCGA-SBX are again the best performing algorithms and, for this case, RCGA-BLX-α achieves a similar performance to them.

From the results reported in Table 3.2 and the corresponding ones in Appendix 3.A (Tables 3.9 to 3.12), it can be seen how, for all the configurations and algorithms, the fitness function weighting combination $(\beta_1, \beta_2) = (1, 0)$ is the one which produces the best and more robust results. Besides, $(\beta_1, \beta_2) = (0.5, 0.5)$ clearly performs better than $(\beta_1, \beta_2) = (0, 1)$. In every case, the best outcomes are obtained with the largest population size/evaluation number.

On the one hand, analyzing the BCGA results, the best results are achieved with 1,000 individuals. As was already mentioned, we can see the low robustness of the algorithm in spite of a few good quality best individual results achieved. On the other hand, the performance of the two RCGAs is similar regardless the crossover operator used. For both possibilities and for the CMA-ES algorithm the results are outstanding. They all reach the same value for the best individual results (minimum), with very low means and standard deviations of zero or close to zero. As in the previous case, CMA-ES shows to be robust with respect to different configuration parameters with an slightly better performance for small and medium values of θ. Concerning RCGA-BLX-α, the best results are achieved in this case with α=0.5. For RCGA-SBX, better results are again achieved with low values of η.

3.5.4 Cádiz case study

This third case study is again a real-world one happened in Cádiz, Spain. The skull 3D model (327,641 points stored as x, y, z coordinates) was acquired by the aforementioned 3D range scanner. Four photographs were provided by the family. They were acquired at different moments and in different poses and conditions. However, in this experiment we only used two of them because of their lateral pose, which makes the skull-face overlay simpler as it will be seen in Chapter 5 where the four photographs will be tackled.

Figure 3.8 depicts this data set. The forensic anthropologists manually selected

Table 3.2: Mallorca case study: skull-face overlay results for the best performing population sizes

BCGA (1,000 individuals)													
β_1, β_2		*Fitness*				*ME*				*MAX*			
		m	M	μ	σ	m	M	μ	σ	m	M	μ	σ
1,0		0.007	0.037	0.018	0.009	**0.007**	0.037	**0.018**	0.009	0.023	0.144	0.049	0.028
0,1		0.013	0.337	0.073	0.088	**0.013**	0.272	**0.060**	0.071	0.013	0.337	0.073	0.088
0.5,0.5		0.010	0.108	0.028	0.022	**0.010**	0.096	**0.027**	0.021	0.014	0.164	0.039	0.032
RCGA-BLX-α (1,000 individuals)													
β_1, β_2	α	*Fitness*				*ME*				*MAX*			
		m	M	μ	σ	m	M	μ	σ	m	M	μ	σ
1,0	0.1	0.029	0.081	0.063	0.011	0.029	0.081	0.063	0.011	0.058	0.195	0.131	0.031
	0.3	0.008	0.023	0.014	0.004	0.008	0.023	0.014	0.004	0.028	0.059	0.037	0.009
	0.5	0.007	0.009	0.008	0.001	**0.007**	0.009	**0.008**	0.001	0.026	0.030	0.029	0.001
	0.7	0.014	0.025	0.020	0.002	0.014	0.025	0.020	0.002	0.026	0.060	0.039	0.008
	0.9	0.060	0.141	0.099	0.022	0.060	0.141	0.099	0.022	0.090	0.339	0.199	0.063
0,1	0.1	0.120	0.342	0.308	0.057	0.098	0.287	0.255	0.051	0.120	0.342	0.308	0.057
	0.3	0.053	0.341	0.201	0.097	0.039	0.286	0.162	0.087	0.053	0.341	0.201	0.097
	0.5	0.014	0.021	0.018	0.001	**0.012**	0.017	**0.014**	0.001	0.014	0.021	0.018	0.001
	0.7	0.027	0.047	0.037	0.005	0.018	0.035	0.025	0.004	0.027	0.047	0.037	0.005
	0.9	0.099	0.260	0.196	0.042	0.080	0.186	0.138	0.028	0.099	0.260	0.196	0.042
0.5,0.5	0.1	0.053	0.099	0.077	0.012	0.049	0.087	0.071	0.009	0.070	0.160	0.117	0.025
	0.3	0.017	0.078	0.047	0.012	0.014	0.078	0.049	0.013	0.027	0.108	0.064	0.017
	0.5	0.010	0.013	0.012	0.001	**0.010**	0.013	**0.011**	0.001	0.015	0.019	0.017	0.001
	0.7	0.017	0.029	0.023	0.003	0.013	0.028	0.021	0.004	0.022	0.044	0.034	0.005
	0.9	0.069	0.161	0.124	0.023	0.065	0.155	0.117	0.024	0.102	0.250	0.181	0.033
RCGA-SBX (1,000 individuals)													
β_1, β_2	η	*Fitness*				*ME*				*MAX*			
		m	M	μ	σ	m	M	μ	σ	m	M	μ	σ
1,0	1.0	0.007	0.008	0.008	0.000	**0.007**	0.008	**0.008**	0.000	0.019	0.028	0.025	0.003
	2.0	0.007	0.012	0.008	0.001	**0.007**	0.012	**0.008**	0.001	0.020	0.030	0.025	0.003
	5.0	0.007	0.017	0.009	0.002	**0.007**	0.017	0.009	0.002	0.016	0.043	0.024	0.007
	10.0	0.008	0.057	0.015	0.012	0.008	0.057	0.015	0.012	0.020	0.171	0.044	0.041
	20.0	0.008	0.085	0.028	0.022	0.008	0.085	0.028	0.022	0.019	0.271	0.072	0.060
0,1	1.0	0.012	0.015	0.013	0.001	0.012	0.012	**0.012**	0.000	0.012	0.015	0.013	0.001
	2.0	0.012	0.023	0.014	0.002	0.012	0.019	0.013	0.001	0.012	0.023	0.014	0.002
	5.0	0.012	0.082	0.021	0.016	**0.011**	0.065	0.018	0.013	0.012	0.082	0.021	0.016
	10.0	0.013	0.091	0.038	0.022	0.012	0.079	0.033	0.019	0.013	0.091	0.038	0.022
	20.0	0.013	0.165	0.053	0.041	**0.011**	0.140	0.045	0.035	0.013	0.165	0.053	0.041
0.5,0.5	1.0	0.009	0.011	0.010	0.000	**0.009**	0.011	**0.010**	0.000	0.013	0.016	0.014	0.000
	2.0	0.010	0.014	0.010	0.001	0.010	0.014	**0.010**	0.001	0.013	0.020	0.015	0.001
	5.0	0.010	0.060	0.015	0.010	0.010	0.046	0.014	0.008	0.013	0.102	0.021	0.017
	10.0	0.010	0.073	0.017	0.012	**0.009**	0.076	0.017	0.013	0.013	0.097	0.022	0.016
	20.0	0.010	0.083	0.028	0.020	**0.009**	0.091	0.027	0.019	0.014	0.114	0.039	0.030
CMA-ES (552,000 evaluations)													
β_1, β_2	θ	*Fitness*				*ME*				*MAX*			
		m	M	μ	σ	m	M	μ	σ	m	M	μ	σ
1,0	0.00001	0.007	0.018	0.008	0.002	**0.007**	0.018	0.008	0.002	0.019	0.042	0.025	0.004
	0.00010	0.007	0.091	0.010	0.015	**0.007**	0.091	0.010	0.015	0.019	0.234	0.031	0.038
	0.00100	0.007	0.091	0.010	0.015	**0.007**	0.091	0.010	0.015	0.020	0.233	0.031	0.038
	0.01000	0.007	0.008	0.007	0.000	**0.007**	0.008	**0.007**	0.000	0.020	0.027	0.025	0.002
	0.10000	0.007	0.098	0.014	0.019	**0.007**	0.098	0.014	0.019	0.025	0.309	0.041	0.053
	0.30000	0.007	0.251	0.065	0.088	**0.007**	0.251	0.065	0.088	0.020	0.430	0.114	0.137
0,1	0.00001	0.012	0.012	0.012	0.000	**0.012**	0.012	**0.012**	0.000	0.012	0.012	0.012	0.000
	0.00010	0.012	0.012	0.012	0.000	**0.012**	0.012	**0.012**	0.000	0.012	0.012	0.012	0.000
	0.00100	0.012	0.012	0.012	0.000	**0.012**	0.012	**0.012**	0.000	0.012	0.012	0.012	0.000
	0.01000	0.012	0.012	0.012	0.000	**0.012**	0.012	**0.012**	0.000	0.012	0.012	0.012	0.000
	0.10000	0.012	0.310	0.065	0.080	**0.012**	0.230	0.047	0.056	0.012	0.310	0.065	0.080
	0.30000	0.012	0.357	0.195	0.131	**0.012**	0.276	0.140	0.095	0.012	0.357	0.195	0.131
0.5,0.5	0.00001	0.010	0.010	0.010	0.000	**0.009**	0.010	**0.009**	0.000	0.013	0.014	0.014	0.000
	0.00010	0.010	0.010	0.010	0.000	**0.009**	0.010	**0.009**	0.000	0.014	0.015	0.014	0.000
	0.00100	0.010	0.021	0.010	0.002	**0.009**	0.019	0.010	0.002	0.013	0.031	0.014	0.003
	0.01000	0.010	0.010	0.010	0.000	**0.009**	0.010	**0.009**	0.000	0.013	0.014	0.014	0.000
	0.10000	0.010	0.238	0.066	0.081	0.010	0.226	0.062	0.077	0.014	0.358	0.095	0.117
	0.30000	0.010	0.270	0.135	0.095	0.010	0.273	0.126	0.093	0.014	0.367	0.195	0.134

a large set of 3D landmarks on the skull. On the other hand, the 2D landmarks selected on the face photographs were eight and twelve, depending on the pose, as shown in Figure 3.8. Indeed not all the landmarks are visible in all the poses. Of course, only the corresponding 3D-2D landmarks are used for solving the two overlay problems.

Figure 3.8: Cádiz case study. From left to right: 3D model of the skull and two photographs of the missing person in different poses are shown

Tables 3.3 and 3.4 (as well as Tables 3.13 to 3.20 from Appendix 3.A) show the results of this case for the two different photographs provided, with the parameter configurations used in the previous two cases of study.

In view of this results, we can recognize that the best results were again obtained using the fitness settings $(\beta_1, \beta_2) = (1,0)$, followed by $(\beta_1, \beta_2) = (0.5, 0.5)$ and $(\beta_1 \beta_2) = (0,1)$ in descending order of performance. In every case but for RCGA-BLX-α, the best performance is obtained with the largest population size/evaluations number.

Besides, CMA-ES and RCGA-SBX are again the best choices for both poses. Their behavior is really robust: some means get equal to the best individual values and many standard deviations vanish or are close to zero. As in the remaining cases, CMA-ES behaves properly for all the different parameter values. For RCGA-SBX, the best results are again obtained using small values of η. The setting α=0.7 is the best one for RCGA-BLX-α

When dealing with pose 1, the worst values for the best individual results correspond to RCGA-BLX-α, which is not able to reach the same minima as the remaining algorithms. Furthermore, it shows a lack of robustness. The BCGA is able to achieve similar best individual values to CMA-ES and RCGA-SBX. Nevertheless, means and standard deviations relative to BCGA are very high, even a little bit worse than RCGA-BLX-α.

Table 3.3: Cádiz case study, pose 1: skull-face overlay results for the best performing population sizes

BCGA (1,000 individuals)													
β_1, β_2		*Fitness*				*ME*				*MAX*			
		m	M	μ	σ	m	M	μ	σ	m	M	μ	σ
1,0		0.017	0.128	0.072	0.036	**0.017**	0.128	**0.072**	0.036	0.035	0.341	0.194	0.099
0,1		0.037	0.231	0.132	0.063	**0.024**	0.164	**0.094**	0.044	0.037	0.231	0.132	0.063
0.5,0.5		0.023	0.145	0.091	0.044	**0.022**	0.140	**0.086**	0.042	0.030	0.202	0.129	0.062
RCGA-BLX-α (100 individuals)													
β_1, β_2	α	*Fitness*				*ME*				*MAX*			
		m	M	μ	σ	m	M	μ	σ	m	M	μ	σ
1,0	0.1	0.111	0.130	0.124	0.005	0.111	0.130	0.124	0.005	0.304	0.348	0.332	0.012
	0.3	0.065	0.131	0.119	0.014	0.065	0.131	0.119	0.014	0.153	0.347	0.319	0.040
	0.5	0.036	0.122	0.075	0.028	0.036	0.122	0.075	0.028	0.078	0.331	0.204	0.079
	0.7	0.022	0.094	0.053	0.022	**0.022**	0.094	**0.053**	0.022	0.039	0.259	0.137	0.070
	0.9	0.051	0.121	0.100	0.015	0.051	0.121	0.100	0.015	0.077	0.331	0.247	0.050
0,1	0.1	0.204	0.228	0.217	0.006	0.147	0.166	0.157	0.004	0.204	0.228	0.217	0.006
	0.3	0.185	0.226	0.216	0.008	0.136	0.163	0.155	0.005	0.185	0.226	0.216	0.008
	0.5	0.068	0.226	0.205	0.037	0.043	0.162	0.145	0.027	0.068	0.226	0.205	0.037
	0.7	0.034	0.225	0.176	0.055	**0.025**	0.165	**0.124**	0.040	0.034	0.225	0.176	0.055
	0.9	0.121	0.225	0.186	0.024	0.094	0.158	0.132	0.017	0.121	0.225	0.186	0.024
0.5,0.5	0.1	0.148	0.169	0.161	0.005	0.138	0.158	0.151	0.005	0.199	0.227	0.216	0.006
	0.3	0.093	0.169	0.158	0.015	0.089	0.157	0.147	0.014	0.121	0.225	0.211	0.021
	0.5	0.024	0.169	0.120	0.057	0.023	0.158	0.111	0.052	0.031	0.226	0.161	0.077
	0.7	0.026	0.156	0.076	0.043	**0.022**	0.144	**0.063**	0.039	0.035	0.217	0.111	0.062
	0.9	0.092	0.147	0.127	0.016	0.065	0.136	0.105	0.019	0.123	0.249	0.188	0.029
RCGA-SBX (1,000 individuals)													
β_1, β_2	η	*Fitness*				*ME*				*MAX*			
		m	M	μ	σ	m	M	μ	σ	m	M	μ	σ
1,0	1.0	0.015	0.020	0.015	0.001	**0.015**	0.020	**0.015**	0.001	0.035	0.044	0.040	0.002
	2.0	0.015	0.032	0.016	0.003	**0.015**	0.032	0.016	0.003	0.038	0.086	0.042	0.008
	5.0	0.015	0.037	0.018	0.005	**0.015**	0.037	0.018	0.005	0.034	0.113	0.043	0.017
	10.0	0.015	0.037	0.023	0.007	**0.015**	0.037	0.023	0.007	0.034	0.160	0.059	0.031
	20.0	0.016	0.040	0.026	0.007	0.016	0.040	0.026	0.007	0.034	0.123	0.068	0.028
0,1	1.0	0.028	0.053	0.031	0.006	0.022	0.041	0.026	0.007	0.028	0.053	0.031	0.006
	2.0	0.028	0.044	0.030	0.004	0.022	0.041	**0.024**	0.005	0.028	0.044	0.030	0.004
	5.0	0.028	0.059	0.036	0.009	0.021	0.051	0.030	0.009	0.028	0.059	0.036	0.009
	10.0	0.029	0.066	0.043	0.012	**0.020**	0.054	0.035	0.011	0.029	0.066	0.043	0.012
	20.0	0.031	0.181	0.052	0.034	0.023	0.133	0.041	0.025	0.031	0.181	0.052	0.034
0.5,0.5	1.0	0.021	0.035	0.021	0.003	**0.016**	0.039	**0.017**	0.004	0.031	0.040	0.032	0.002
	2.0	0.021	0.036	0.023	0.005	**0.016**	0.039	0.019	0.007	0.030	0.043	0.033	0.004
	5.0	0.021	0.040	0.026	0.007	**0.016**	0.041	0.025	0.009	0.029	0.049	0.035	0.006
	10.0	0.021	0.048	0.029	0.008	0.017	0.050	0.028	0.009	0.029	0.058	0.038	0.009
	20.0	0.021	0.058	0.031	0.010	0.017	0.054	0.030	0.010	0.029	0.077	0.040	0.011
CMA-ES (552,000 evaluations)													
β_1, β_2	θ	*Fitness*				*ME*				*MAX*			
		m	M	μ	σ	m	M	μ	σ	m	M	μ	σ
1,0	0.00001	0.015	0.032	0.016	0.003	**0.015**	0.032	0.016	0.003	0.040	0.086	0.042	0.008
	0.00010	0.015	0.015	0.015	0.000	**0.015**	0.015	**0.015**	0.000	0.040	0.041	0.040	0.000
	0.00100	0.015	0.032	0.016	0.004	**0.015**	0.032	0.016	0.004	0.040	0.085	0.043	0.011
	0.01000	0.015	0.032	0.017	0.006	**0.015**	0.032	0.017	0.006	0.040	0.086	0.046	0.016
	0.10000	0.015	0.015	0.015	0.000	**0.015**	0.015	**0.015**	0.000	0.040	0.041	0.040	0.000
	0.30000	0.015	0.079	0.023	0.018	**0.015**	0.079	0.023	0.018	0.034	0.219	0.055	0.039
0,1	0.00001	0.028	0.058	0.030	0.006	**0.022**	0.044	0.025	0.005	0.028	0.058	0.030	0.006
	0.00010	0.028	0.058	0.034	0.009	**0.022**	0.044	0.029	0.008	0.028	0.058	0.034	0.009
	0.00100	0.028	0.059	0.032	0.008	**0.022**	0.045	0.027	0.008	0.028	0.059	0.032	0.008
	0.01000	0.028	0.058	0.032	0.007	**0.022**	0.044	0.027	0.007	0.028	0.058	0.032	0.007
	0.10000	0.028	0.029	0.028	0.000	**0.022**	0.024	**0.023**	0.001	0.028	0.029	0.028	0.000
	0.30000	0.028	0.128	0.046	0.028	**0.022**	0.083	0.034	0.018	0.028	0.128	0.046	0.028
0.5,0.5	0.00001	0.021	0.045	0.025	0.008	**0.016**	0.044	0.023	0.010	0.031	0.058	0.035	0.006
	0.00010	0.021	0.045	0.024	0.007	**0.016**	0.044	0.020	0.009	0.031	0.058	0.034	0.006
	0.00100	0.021	0.047	0.024	0.008	**0.016**	0.046	0.021	0.010	0.031	0.060	0.034	0.008
	0.01000	0.021	0.036	0.023	0.005	**0.016**	0.039	0.019	0.008	0.031	0.042	0.033	0.003
	0.10000	0.021	0.022	0.021	0.000	**0.016**	0.017	**0.016**	0.000	0.031	0.033	0.031	0.000
	0.30000	0.021	0.103	0.033	0.023	**0.016**	0.095	0.028	0.022	0.031	0.137	0.047	0.031

Table 3.4: Cádiz case study, pose 2: skull-face overlay results for the best performing population sizes

BCGA (1,000 individuals)													
β_1, β_2		*Fitness*				*ME*				*MAX*			
		m	M	μ	σ	m	M	μ	σ	m	M	μ	σ
1,0		0.039	0.157	0.092	0.034	**0.039**	0.157	**0.092**	0.034	0.107	0.324	0.187	0.063
0,1		0.096	0.279	0.189	0.063	**0.060**	0.197	**0.133**	0.044	0.096	0.279	0.189	0.063
0.5,0.5		0.066	0.190	0.128	0.039	**0.052**	0.183	**0.122**	0.039	0.092	0.262	0.179	0.053
RCGA-BLX-α (100 individuals)													
β_1, β_2	α	*Fitness*				*ME*				*MAX*			
		m	M	μ	σ	m	M	μ	σ	m	M	μ	σ
1,0	0.1	0.145	0.188	0.172	0.011	0.145	0.188	0.172	0.011	0.295	0.401	0.364	0.027
	0.3	0.060	0.187	0.159	0.035	0.060	0.187	0.159	0.035	0.123	0.399	0.335	0.074
	0.5	0.036	0.063	0.052	0.009	**0.036**	0.063	**0.052**	0.009	0.106	0.149	0.128	0.013
	0.7	0.038	0.094	0.052	0.017	0.038	0.094	**0.052**	0.017	0.114	0.220	0.143	0.019
	0.9	0.095	0.164	0.131	0.019	0.095	0.164	0.131	0.019	0.177	0.387	0.278	0.053
0,1	0.1	0.251	0.289	0.279	0.008	0.176	0.210	0.201	0.007	0.251	0.289	0.279	0.008
	0.3	0.249	0.292	0.278	0.009	0.169	0.210	0.198	0.008	0.249	0.292	0.278	0.009
	0.5	0.129	0.292	0.245	0.052	0.065	0.205	0.168	0.044	0.129	0.292	0.245	0.052
	0.7	0.099	0.261	0.133	0.052	**0.060**	0.185	**0.085**	0.037	0.099	0.261	0.133	0.052
	0.9	0.137	0.276	0.230	0.037	0.085	0.194	0.159	0.028	0.137	0.276	0.230	0.037
0.5,0.5	0.1	0.171	0.206	0.196	0.008	0.168	0.202	0.192	0.008	0.239	0.288	0.274	0.011
	0.3	0.130	0.209	0.196	0.016	0.115	0.204	0.190	0.018	0.197	0.290	0.273	0.021
	0.5	0.062	0.205	0.143	0.058	**0.044**	0.199	0.134	0.063	0.106	0.284	0.207	0.072
	0.7	0.063	0.161	0.083	0.026	0.045	0.150	**0.069**	0.028	0.107	0.235	0.131	0.034
	0.9	0.098	0.183	0.153	0.023	0.081	0.176	0.141	0.024	0.152	0.276	0.221	0.032
RCGA-SBX (1,000 individuals)													
β_1, β_2	η	*Fitness*				*ME*				*MAX*			
		m	M	μ	σ	m	M	μ	σ	m	M	μ	σ
1,0	1.0	0.036	0.037	0.036	0.000	**0.036**	0.037	**0.036**	0.000	0.141	0.146	0.144	0.001
	2.0	0.036	0.037	0.036	0.000	**0.036**	0.037	**0.036**	0.000	0.141	0.145	0.144	0.001
	5.0	0.036	0.057	0.040	0.007	**0.036**	0.057	0.040	0.007	0.112	0.156	0.141	0.010
	10.0	0.036	0.061	0.046	0.009	**0.036**	0.061	0.046	0.009	0.107	0.236	0.140	0.025
	20.0	0.036	0.068	0.051	0.009	**0.036**	0.068	0.051	0.009	0.113	0.196	0.145	0.021
0,1	1.0	0.090	0.105	0.094	0.005	0.062	0.079	**0.068**	0.003	0.090	0.105	0.094	0.005
	2.0	0.089	0.105	0.095	0.006	0.061	0.073	**0.068**	0.003	0.089	0.105	0.095	0.006
	5.0	0.090	0.108	0.099	0.006	**0.059**	0.075	**0.068**	0.004	0.090	0.108	0.099	0.006
	10.0	0.090	0.118	0.102	0.006	0.061	0.096	0.070	0.007	0.090	0.118	0.102	0.006
	20.0	0.094	0.192	0.109	0.017	0.060	0.130	0.073	0.013	0.094	0.192	0.109	0.017
0.5,0.5	1.0	0.062	0.067	0.063	0.002	0.043	0.061	**0.046**	0.005	0.091	0.109	0.105	0.004
	2.0	0.062	0.067	0.063	0.002	**0.042**	0.062	0.047	0.007	0.091	0.111	0.105	0.006
	5.0	0.062	0.078	0.065	0.003	**0.042**	0.073	0.049	0.008	0.092	0.110	0.107	0.004
	10.0	0.062	0.075	0.067	0.003	0.043	0.069	0.055	0.008	0.093	0.111	0.106	0.005
	20.0	0.063	0.084	0.068	0.004	0.043	0.079	0.056	0.009	0.098	0.118	0.106	0.004
CMA-ES (552,000 evaluations)													
β_1, β_2	θ	*Fitness*				*ME*				*MAX*			
		m	M	μ	σ	m	M	μ	σ	m	M	μ	σ
1,0	0.00001	0.036	0.036	0.036	0.000	**0.036**	0.036	**0.036**	0.000	0.144	0.145	0.145	0.000
	0.00010	0.036	0.061	0.037	0.005	**0.036**	0.061	0.037	0.005	0.144	0.169	0.145	0.004
	0.00100	0.036	0.036	0.036	0.000	0.036	**0.036**	**0.036**	0.000	0.144	0.145	0.145	0.000
	0.01000	0.036	0.062	0.037	0.005	**0.036**	0.062	0.037	0.005	0.144	0.179	0.146	0.006
	0.10000	0.036	0.036	0.036	0.000	**0.036**	0.036	**0.036**	0.000	0.144	0.145	0.145	0.000
	0.30000	0.036	0.092	0.038	0.010	**0.036**	0.092	0.038	0.010	0.132	0.194	0.146	0.009
0,1	0.00001	0.089	0.108	0.098	0.007	**0.063**	0.074	0.068	0.004	0.089	0.108	0.098	0.007
	0.00010	0.089	0.108	0.100	0.007	**0.063**	0.074	0.068	0.004	0.089	0.108	0.100	0.007
	0.00100	0.089	0.108	0.097	0.006	**0.063**	0.074	**0.066**	0.003	0.089	0.108	0.097	0.006
	0.01000	0.089	0.108	0.098	0.007	**0.063**	0.074	0.068	0.004	0.089	0.108	0.098	0.007
	0.10000	0.089	0.100	0.091	0.003	0.065	0.071	0.069	0.001	0.089	0.100	0.091	0.003
	0.30000	0.089	0.176	0.098	0.021	**0.063**	0.124	0.070	0.011	0.089	0.176	0.098	0.021
0.5,0.5	0.00010	0.062	0.078	0.064	0.005	0.044	0.073	0.050	0.010	0.092	0.110	0.105	0.005
	0.00100	0.062	0.077	0.064	0.004	**0.042**	0.073	0.049	0.008	0.092	0.110	0.105	0.004
	0.01000	0.062	0.067	0.063	0.002	0.044	0.062	0.049	0.007	0.092	0.107	0.103	0.006
	0.10000	0.062	0.062	0.062	0.000	0.044	0.044	**0.044**	0.000	0.106	0.107	0.106	0.000
	0.30000	0.062	0.077	0.063	0.003	0.043	0.065	0.047	0.007	0.091	0.117	0.105	0.006

The case of pose 2 is the opposite. The worst results are associated to BCGA. Indeed, it achieves the worst minima and the least robust behavior. Meanwhile, RCGA-BLX-α is able to reach the same or similar best minima as CMA-ES and RCGA-SBX. However, its means and standard deviations are quite high.

Figures 3.9 and 3.10 show, respectively, the best and the corresponding worst superimpositions obtained by the implemented EAs for the first pose of the third case study. Figures 3.11 and 3.12 are associated to the second pose.

Figure 3.9: Cádiz case study, pose 1. From left to right: the best superimposition results obtained by BCGA, RCGA-BLX-α, RCGA-SBX, and CMA-ES are shown

Figure 3.10: Cádiz case study, pose 1. From left to right: the worst superimposition results obtained by BCGA, RCGA-BLX-α, RCGA-SBX, and CMA-ES are shown

Focusing on the first pose, we can see the good superimpositions achieved by the RCGA-SBX and the CMA-ES methods. Results from the other two algorithms are not good enough since the skull is too big, even bigger than the hair contour in the BCGA superimposition (see the left-most image in Figure 3.9). When checking the

Figure 3.11: Cádiz case study, pose 2. From left to right: the best superimposition results obtained by BCGA, RCGA-BLX-α, RCGA-SBX, and CMA-ES are shown

Figure 3.12: Cádiz case study, Pose 2. From left to right: worst superimposition results obtained by BCGA, RCGA-BLX-α, RCGA-SBX, and CMA-ES are shown

worst superimpositions obtained for the best parameter combination runs (Figure 3.10), we recognize how results from the first two algorithms (BCGA and RCGA-BLX-α) are absolutely unsuitable. The skull is again downsized around the nose, as it happened in the first case of study. However, those worst superimpositions corresponding to the other two EAs are acceptable. Notice that, they are as good as the best superimposition achieved by the BCGA in the case of RCGA-SBX, and even better than that achieved by RCGA-BLX-α in the case of CMA-ES.

Concerning the second pose of this case, we should remind that twelve landmarks were selected by the anthropologists, which is a higher number of landmarks than those in all the previous cases. However, the resulting skull-face overlay is not good at all whatever the EA used (in fact, all the best overlay results are almost the same, see Figure 3.11). Only some parts of the face are well fit, but the global overlay is not valid at all. We will deal with this case study in Chapter 5.

3.6 Concluding remarks

In this chapter we have developed a methodological evolutionary-based framework for automatically solving the skull-face overlay problem. In particular, the proposed methodology deals with a 3D model of the skull and a 2D photograph of the face

We have proposed and validated the use of real-coded EAs for the skull-face overlay stage of the process which involves the alignment/registration of the 3D skull model with the 2D face photograph of the missing person. The proposed methods are fast (they take between 30 and 40 seconds), robust and fully automatic, and therefore very useful for solving one of the most tedious activities performed by the forensic anthropologists (requiring several hours per case). In addition, our method supposed a systematic approach to solve the overlay problem and, in spite it still needs some improvements, it could be used now as a tool for automatically obtaining a good quality superimposition to be manually refined by the forensic expert in a quick way.

We have presented and discussed superimposition results obtained on four skull-face overlay problem instances related to three real-world identification cases. A large number of experiments to analyze the influence of the parameter values has been performed. Our good results show a large improvement of our methods with respect to our implementation of the original BCGA proposed by Nickerson et al. (Nickerson et al. 1991), that did not successfully work on our data. Results from RCGA-BLX-α seem not to be suitable mainly due to their high variability. RCGA-SBX and especially CMA-ES have a good performance, achieving high quality solutions in most of the cases and showing a high robustness. Only results corresponding to Cádiz case study, pose 2, show a bad performance of the evolutionary-based methods. In order to improve those skull-face overlay results that are far away from being a good overlay (see Figure 3.11), Chapter 5 will present a new proposal that uses fuzzy sets. In addition, to improve the robustness and the convergence time of the current evolutionary-based skull-face overlay method we will propose a new evolutionary design in Chapter 4.

3.A Experimental results

Table 3.5: Málaga case study: skull-face overlay results for the BCGA algorithm

β_1, β_2	pop size	*Fitness*				*ME*				*MAX*			
		m	M	μ	σ	m	M	μ	σ	m	M	μ	σ
1,0	100	0.156	0.268	0.241	0.026	0.156	0.268	0.241	0.026	0.289	0.446	0.404	0.035
	500	0.021	0.262	0.171	0.074	0.021	0.262	0.171	0.074	0.044	0.434	0.289	0.122
0,1	100	0.244	0.420	0.359	0.037	0.188	0.284	0.262	0.024	0.244	0.420	0.359	0.037
	500	0.025	0.373	0.289	0.097	0.021	0.272	0.214	0.069	0.025	0.373	0.289	0.097
0.5,0.5	100	0.039	0.282	0.246	0.049	0.044	0.278	0.250	0.049	0.050	0.410	0.344	0.071
	500	0.020	0.269	0.203	0.080	0.021	0.273	0.206	0.082	0.028	0.374	0.283	0.111

Table 3.6: Málaga case study: skull-face overlay results for the RCGA-BLX-α algorithm

β_1, β_2	pop size	α	*Fitness*				*ME*				*MAX*			
			m	M	μ	σ	m	M	μ	σ	m	M	μ	σ
1,0	500	0.1	0.221	0.257	0.250	0.009	0.221	0.257	0.250	0.009	0.336	0.426	0.412	0.022
		0.3	0.138	0.259	0.246	0.025	0.138	0.259	0.246	0.025	0.251	0.429	0.409	0.038
		0.5	0.065	0.259	0.242	0.037	0.065	0.259	0.242	0.037	0.125	0.430	0.400	0.059
		0.7	0.035	0.242	0.165	0.060	0.035	0.242	0.165	0.060	0.078	0.399	0.273	0.097
		0.9	0.179	0.255	0.228	0.021	0.179	0.255	0.228	0.021	0.241	0.537	0.374	0.051
	1.000	0.1	0.238	0.257	0.252	0.004	0.238	0.257	0.252	0.004	0.383	0.425	0.416	0.009
		0.3	0.068	0.258	0.227	0.055	0.068	0.258	0.227	0.055	0.137	0.427	0.375	0.091
		0.5	0.108	0.256	0.223	0.045	0.108	0.256	0.223	0.045	0.120	0.425	0.366	0.081
		0.7	0.115	0.242	0.197	0.037	0.115	0.242	0.197	0.037	0.192	0.412	0.324	0.062
		0.9	0.110	0.246	0.208	0.038	0.110	0.246	0.208	0.038	0.146	0.410	0.338	0.068
0,1	500	0.1	0.331	0.368	0.362	0.007	0.238	0.269	0.265	0.005	0.331	0.368	0.362	0.007
		0.3	0.244	0.368	0.360	0.022	0.174	0.269	0.263	0.017	0.244	0.368	0.360	0.022
		0.5	0.234	0.370	0.352	0.036	0.118	0.270	0.255	0.034	0.234	0.370	0.352	0.036
		0.7	0.334	0.376	0.366	0.011	0.231	0.274	0.265	0.012	0.334	0.376	0.366	0.011
		0.9	0.314	0.379	0.359	0.014	0.217	0.276	0.256	0.013	0.314	0.379	0.359	0.014
	1.000	0.1	0.358	0.366	0.363	0.002	0.260	0.268	0.265	0.002	0.358	0.366	0.363	0.002
		0.3	0.361	0.367	0.364	0.002	0.264	0.268	0.266	0.001	0.361	0.367	0.364	0.002
		0.5	0.211	0.368	0.357	0.031	0.149	0.269	0.259	0.027	0.211	0.368	0.357	0.031
		0.7	0.265	0.372	0.361	0.023	0.187	0.271	0.261	0.021	0.265	0.372	0.361	0.023
		0.9	0.280	0.371	0.346	0.025	0.172	0.269	0.243	0.027	0.280	0.371	0.346	0.025
0.5,0.5	500	0.1	0.233	0.263	0.258	0.005	0.239	0.267	0.262	0.005	0.324	0.368	0.361	0.008
		0.3	0.219	0.264	0.257	0.009	0.195	0.269	0.259	0.016	0.347	0.369	0.362	0.005
		0.5	0.200	0.265	0.256	0.015	0.202	0.269	0.259	0.016	0.279	0.369	0.357	0.021
		0.7	0.217	0.262	0.244	0.013	0.201	0.267	0.242	0.019	0.315	0.379	0.349	0.016
		0.9	0.108	0.269	0.233	0.042	0.099	0.272	0.230	0.044	0.164	0.380	0.332	0.055
	1.000	0.1	0.233	0.262	0.255	0.008	0.231	0.266	0.258	0.010	0.330	0.367	0.359	0.009
		0.3	0.124	0.262	0.249	0.031	0.109	0.265	0.250	0.035	0.197	0.367	0.349	0.039
		0.5	0.105	0.264	0.250	0.035	0.105	0.269	0.253	0.037	0.148	0.368	0.349	0.047
		0.7	0.125	0.265	0.228	0.042	0.125	0.267	0.227	0.043	0.175	0.371	0.321	0.058
		0.9	0.127	0.268	0.230	0.037	0.123	0.270	0.227	0.039	0.186	0.380	0.330	0.052

Table 3.7: Málaga case study: skull-face overlay results for the RCGA-SBX algorithm

β_1, β_2	pop size	η	*Fitness*				*ME*				*MAX*			
			m	M	μ	σ	m	M	μ	σ	m	M	μ	σ
1,0	100	1.0	0.017	0.059	0.029	0.010	0.017	0.059	0.029	0.010	0.028	0.129	0.063	0.026
		2.0	0.018	0.072	0.039	0.014	0.018	0.072	0.039	0.014	0.037	0.173	0.088	0.038
		5.0	0.021	0.093	0.049	0.020	0.021	0.093	0.049	0.020	0.039	0.218	0.110	0.048
		10.0	0.028	0.233	0.096	0.063	0.028	0.233	0.096	0.063	0.067	0.390	0.188	0.097
		20.0	0.037	0.265	0.188	0.084	0.037	0.265	0.188	0.084	0.090	0.442	0.326	0.122
	500	1.0	0.017	0.023	0.019	0.002	0.017	0.023	0.019	0.002	0.028	0.057	0.051	0.006
		2.0	0.017	0.037	0.020	0.004	0.017	0.037	0.020	0.004	0.031	0.068	0.050	0.009
		5.0	0.017	0.197	0.038	0.032	0.017	0.197	0.038	0.032	0.032	0.541	0.085	0.094
		10.0	0.017	0.061	0.036	0.011	0.017	0.061	0.036	0.011	0.035	0.160	0.085	0.038
		20.0	0.019	0.157	0.057	0.035	0.019	0.157	0.057	0.035	0.039	0.293	0.127	0.068
0,1	100	1.0	0.025	0.092	0.056	0.019	0.022	0.078	0.048	0.016	0.025	0.092	0.056	0.019
		2.0	0.032	0.184	0.066	0.033	0.028	0.154	0.056	0.026	0.032	0.184	0.066	0.033
		5.0	0.049	0.310	0.109	0.076	0.042	0.229	0.089	0.055	0.049	0.310	0.109	0.076
		10.0	0.052	0.389	0.237	0.121	0.045	0.283	0.177	0.085	0.052	0.389	0.237	0.121
		20.0	0.240	0.392	0.343	0.044	0.183	0.288	0.251	0.029	0.240	0.392	0.343	0.044
	500	1.0	0.022	0.058	0.029	0.008	0.021	0.055	0.027	0.007	0.022	0.058	0.029	0.008
		2.0	0.022	0.094	0.036	0.014	0.019	0.077	0.032	0.011	0.022	0.094	0.036	0.014
		5.0	0.024	0.078	0.046	0.014	0.023	0.069	0.040	0.013	0.024	0.078	0.046	0.014
		10.0	0.036	0.188	0.062	0.030	0.031	0.138	0.053	0.023	0.036	0.188	0.062	0.030
		20.0	0.027	0.376	0.176	0.124	0.025	0.274	0.132	0.088	0.027	0.376	0.176	0.124
0.5,0.5	100	1.0	0.019	0.072	0.033	0.011	0.020	0.073	0.034	0.011	0.025	0.099	0.044	0.017
		2.0	0.022	0.093	0.048	0.017	0.021	0.098	0.050	0.018	0.031	0.124	0.065	0.024
		5.0	0.024	0.275	0.076	0.058	0.027	0.277	0.076	0.059	0.031	0.385	0.107	0.081
		10.0	0.024	0.263	0.120	0.078	0.025	0.266	0.119	0.078	0.032	0.366	0.172	0.110
		20.0	0.024	0.267	0.204	0.084	0.023	0.270	0.205	0.087	0.034	0.378	0.287	0.115
	500	1.0	0.017	0.030	0.020	0.003	0.018	0.032	0.021	0.004	0.023	0.039	0.026	0.004
		2.0	0.017	0.053	0.024	0.008	0.018	0.060	0.026	0.009	0.023	0.064	0.031	0.009
		5.0	0.017	0.082	0.034	0.013	0.018	0.090	0.036	0.014	0.023	0.104	0.045	0.016
		10.0	0.018	0.093	0.040	0.018	0.020	0.085	0.041	0.016	0.023	0.141	0.055	0.028
		20.0	0.020	0.239	0.057	0.043	0.021	0.238	0.055	0.041	0.026	0.337	0.083	0.065

Table 3.8: Málaga case study: skull-face overlay results for the CMA-ES algorithm

β_1, β_2	evaluations	θ	*Fitness*				*ME*				*MAX*			
			m	M	μ	σ	m	M	μ	σ	m	M	μ	σ
1,0	55.200	0.00001	0.017	0.151	0.058	0.045	0.017	0.151	0.058	0.045	0.043	0.238	0.109	0.062
		0.00010	0.017	0.175	0.044	0.036	0.017	0.175	0.044	0.036	0.039	0.239	0.089	0.051
		0.00100	0.017	0.175	0.051	0.046	0.017	0.175	0.051	0.046	0.038	0.494	0.115	0.099
		0.01000	0.017	0.168	0.057	0.046	0.017	0.168	0.057	0.046	0.051	0.276	0.108	0.067
		0.10000	0.017	0.117	0.050	0.035	0.017	0.117	0.050	0.035	0.049	0.215	0.093	0.052
		0.30000	0.017	0.906	0.157	0.220	0.017	0.906	0.157	0.220	0.046	1.258	0.269	0.334
	276.000	0.00001	0.017	0.031	0.018	0.003	0.017	0.031	0.018	0.003	0.045	0.052	0.051	0.001
		0.00010	0.017	0.043	0.021	0.009	0.017	0.043	0.021	0.009	0.039	0.137	0.061	0.028
		0.00100	0.017	0.044	0.019	0.008	0.017	0.044	0.019	0.008	0.051	0.142	0.060	0.027
		0.01000	0.017	0.043	0.018	0.005	0.017	0.043	0.018	0.005	0.031	0.134	0.053	0.016
		0.10000	0.017	0.018	0.017	0.000	0.017	0.018	0.017	0.000	0.050	0.055	0.051	0.001
		0.30000	0.017	0.096	0.024	0.020	0.017	0.096	0.024	0.020	0.049	0.190	0.064	0.035
0,1	55.200	0.00001	0.022	0.355	0.109	0.072	0.019	0.251	0.076	0.050	0.022	0.355	0.109	0.072
		0.00010	0.022	0.340	0.118	0.076	0.020	0.243	0.085	0.053	0.022	0.340	0.118	0.076
		0.00100	0.022	0.304	0.102	0.073	0.020	0.154	0.072	0.045	0.022	0.304	0.102	0.073
		0.01000	0.022	0.283	0.120	0.082	0.019	0.191	0.083	0.055	0.022	0.283	0.120	0.082
		0.10000	0.022	0.296	0.088	0.069	0.019	0.186	0.065	0.047	0.022	0.296	0.088	0.069
		0.30000	0.022	1.258	0.248	0.331	0.020	0.906	0.168	0.224	0.022	1.258	0.248	0.331
	276.000	0.00001	0.022	0.087	0.028	0.017	0.020	0.067	0.025	0.012	0.022	0.087	0.028	0.017
		0.00010	0.022	0.090	0.029	0.020	0.021	0.076	0.026	0.016	0.022	0.090	0.029	0.020
		0.00100	0.022	0.088	0.029	0.020	0.020	0.064	0.025	0.012	0.022	0.088	0.029	0.020
		0.01000	0.022	0.089	0.026	0.017	0.020	0.069	0.023	0.011	0.022	0.089	0.026	0.017
		0.10000	0.022	0.034	0.025	0.004	0.020	0.031	0.023	0.003	0.022	0.034	0.025	0.004
		0.30000	0.023	0.194	0.057	0.051	0.021	0.129	0.044	0.032	0.023	0.194	0.057	0.051
0.5,0.5	55.200	0.00001	0.017	0.492	0.075	0.090	0.018	0.483	0.071	0.088	0.023	0.693	0.110	0.128
		0.00010	0.017	0.235	0.077	0.051	0.018	0.222	0.071	0.048	0.023	0.344	0.115	0.078
		0.00100	0.017	0.149	0.072	0.043	0.018	0.131	0.068	0.041	0.023	0.233	0.104	0.064
		0.01000	0.017	0.163	0.074	0.044	0.018	0.154	0.068	0.041	0.023	0.238	0.111	0.066
		0.10000	0.017	0.191	0.055	0.049	0.018	0.159	0.051	0.042	0.023	0.309	0.081	0.079
		0.30000	0.017	0.908	0.182	0.224	0.018	0.906	0.167	0.212	0.023	1.258	0.271	0.327
	276.000	0.00001	0.017	0.059	0.027	0.018	0.018	0.052	0.026	0.014	0.023	0.092	0.039	0.030
		0.00010	0.017	0.059	0.019	0.008	0.018	0.052	0.019	0.006	0.023	0.092	0.026	0.013
		0.00100	0.017	0.059	0.020	0.011	0.018	0.052	0.020	0.008	0.023	0.092	0.028	0.017
		0.01000	0.017	0.059	0.023	0.013	0.018	0.052	0.022	0.011	0.023	0.093	0.032	0.022
		0.10000	0.017	0.020	0.018	0.001	0.018	0.021	0.019	0.001	0.023	0.027	0.024	0.001
		0.30000	0.017	0.086	0.025	0.015	0.018	0.084	0.025	0.015	0.023	0.122	0.033	0.022

Table 3.9: Mallorca case study: skull-face overlay results for the BCGA algorithm

β_1, β_2	pop size	*Fitness*				*ME*				*MAX*			
		m	M	μ	σ	m	M	μ	σ	m	M	μ	σ
1,0	100	0.021	0.268	0.092	0.080	0.021	0.268	0.092	0.080	0.046	0.392	0.160	0.099
	500	0.009	0.190	0.029	0.036	0.009	0.190	0.029	0.036	0.019	0.258	0.059	0.051
0,1	100	0.041	0.373	0.293	0.097	0.036	0.289	0.236	0.077	0.041	0.373	0.293	0.097
	500	0.017	0.344	0.102	0.100	0.013	0.275	0.083	0.081	0.017	0.344	0.102	0.100
0.5,0.5	100	0.027	0.271	0.176	0.081	0.028	0.284	0.181	0.088	0.036	0.360	0.237	0.103
	500	0.011	0.114	0.039	0.027	0.011	0.122	0.039	0.027	0.013	0.147	0.055	0.038

Table 3.10: Mallorca case study: skull-face overlay results for the RCGA-BLX-α algorithm

β_1, β_2	pop size	α	*Fitness*				*ME*				*MAX*			
			m	M	μ	σ	m	M	μ	σ	m	M	μ	σ
1,0	100	0.1	0.023	0.133	0.072	0.021	0.023	0.133	0.072	0.021	0.051	0.273	0.168	0.058
		0.3	0.008	0.089	0.038	0.024	0.008	0.089	0.038	0.024	0.027	0.224	0.092	0.054
		0.5	0.007	0.016	0.010	0.003	0.007	0.016	0.010	0.003	0.020	0.048	0.030	0.007
		0.7	0.011	0.028	0.018	0.004	0.011	0.028	0.018	0.004	0.018	0.064	0.039	0.013
		0.9	0.029	0.111	0.052	0.017	0.029	0.111	0.052	0.017	0.050	0.212	0.104	0.041
	500	0.1	0.034	0.090	0.065	0.014	0.034	0.090	0.065	0.014	0.074	0.235	0.143	0.038
		0.3	0.008	0.058	0.019	0.012	0.008	0.058	0.019	0.012	0.028	0.147	0.050	0.028
		0.5	0.007	0.011	0.008	0.001	0.007	0.011	0.008	0.001	0.023	0.029	0.029	0.001
		0.7	0.015	0.028	0.021	0.003	0.015	0.028	0.021	0.003	0.021	0.069	0.040	0.011
		0.9	0.013	0.147	0.085	0.028	0.013	0.147	0.085	0.028	0.032	0.350	0.163	0.069
0,1	100	0.1	0.170	0.348	0.320	0.045	0.135	0.288	0.264	0.038	0.170	0.348	0.320	0.045
		0.3	0.061	0.343	0.231	0.100	0.054	0.284	0.187	0.084	0.061	0.343	0.231	0.100
		0.5	0.013	0.076	0.033	0.021	0.012	0.068	0.028	0.018	0.013	0.076	0.033	0.021
		0.7	0.019	0.043	0.030	0.006	0.013	0.031	0.021	0.005	0.019	0.043	0.030	0.006
		0.9	0.053	0.249	0.166	0.049	0.026	0.191	0.119	0.037	0.053	0.249	0.166	0.049
	500	0.1	0.167	0.346	0.316	0.041	0.129	0.287	0.261	0.036	0.167	0.346	0.316	0.041
		0.3	0.067	0.345	0.210	0.093	0.057	0.286	0.169	0.083	0.067	0.345	0.210	0.093
		0.5	0.013	0.053	0.019	0.007	0.012	0.045	0.015	0.006	0.013	0.053	0.019	0.007
		0.7	0.022	0.056	0.038	0.006	0.015	0.037	0.027	0.006	0.022	0.056	0.038	0.006
		0.9	0.112	0.274	0.217	0.044	0.057	0.217	0.152	0.033	0.112	0.274	0.217	0.044
0.5,0.5	100	0.1	0.043	0.190	0.123	0.034	0.047	0.202	0.120	0.038	0.056	0.259	0.178	0.047
		0.3	0.012	0.152	0.073	0.036	0.012	0.153	0.071	0.037	0.016	0.223	0.104	0.051
		0.5	0.010	0.022	0.014	0.003	0.010	0.020	0.014	0.003	0.014	0.033	0.020	0.005
		0.7	0.013	0.032	0.021	0.005	0.013	0.031	0.020	0.005	0.019	0.046	0.031	0.007
		0.9	0.028	0.161	0.074	0.033	0.025	0.155	0.069	0.031	0.043	0.258	0.111	0.052
	500	0.1	0.066	0.110	0.089	0.013	0.062	0.108	0.081	0.011	0.099	0.183	0.136	0.023
		0.3	0.011	0.082	0.049	0.017	0.010	0.089	0.049	0.018	0.016	0.110	0.067	0.023
		0.5	0.010	0.014	0.012	0.001	0.010	0.014	0.011	0.001	0.014	0.019	0.017	0.001
		0.7	0.016	0.032	0.024	0.003	0.016	0.028	0.023	0.003	0.023	0.054	0.036	0.006
		0.9	0.086	0.161	0.123	0.022	0.083	0.169	0.118	0.023	0.116	0.231	0.179	0.032

Table 3.11: Mallorca case study: skull-face overlay results for the RCGA-SBX algorithm

β_1, β_2	pop size	η	*Fitness*				*ME*				*MAX*			
			m	M	μ	σ	m	M	μ	σ	m	M	μ	σ
1,0	100	1.0	0.008	0.062	0.024	0.017	0.008	0.062	0.024	0.017	0.016	0.197	0.062	0.050
		2.0	0.008	0.089	0.032	0.024	0.008	0.089	0.032	0.024	0.020	0.322	0.091	0.072
		5.0	0.010	0.135	0.056	0.034	0.010	0.135	0.056	0.034	0.026	0.493	0.167	0.117
		10.0	0.010	0.133	0.071	0.035	0.010	0.133	0.071	0.035	0.027	0.396	0.179	0.099
		20.0	0.011	0.105	0.066	0.028	0.011	0.105	0.066	0.028	0.021	0.343	0.159	0.073
	500	1.0	0.007	0.014	0.008	0.001	0.007	0.014	0.008	0.001	0.017	0.040	0.026	0.004
		2.0	0.007	0.013	0.009	0.002	0.007	0.013	0.009	0.002	0.018	0.033	0.026	0.004
		5.0	0.008	0.052	0.013	0.010	0.008	0.052	0.013	0.010	0.016	0.174	0.036	0.029
		10.0	0.008	0.076	0.019	0.015	0.008	0.076	0.019	0.015	0.015	0.162	0.045	0.032
		20.0	0.008	0.105	0.029	0.023	0.008	0.105	0.029	0.023	0.019	0.260	0.071	0.056
0,1	100	1.0	0.012	0.131	0.042	0.028	0.012	0.094	0.035	0.022	0.012	0.131	0.042	0.028
		2.0	0.013	0.263	0.074	0.057	0.011	0.229	0.060	0.049	0.013	0.263	0.074	0.057
		5.0	0.027	0.318	0.123	0.077	0.023	0.281	0.101	0.066	0.027	0.318	0.123	0.077
		10.0	0.021	0.360	0.190	0.089	0.017	0.289	0.154	0.075	0.021	0.360	0.190	0.089
		20.0	0.051	0.359	0.223	0.104	0.045	0.289	0.180	0.085	0.051	0.359	0.223	0.104
	500	1.0	0.012	0.028	0.014	0.003	0.012	0.025	0.013	0.002	0.012	0.028	0.014	0.003
		2.0	0.012	0.035	0.019	0.007	0.011	0.030	0.016	0.006	0.012	0.035	0.019	0.007
		5.0	0.013	0.113	0.045	0.032	0.012	0.099	0.038	0.025	0.013	0.113	0.045	0.032
		10.0	0.013	0.164	0.063	0.048	0.012	0.125	0.052	0.038	0.013	0.164	0.063	0.048
		20.0	0.013	0.209	0.089	0.054	0.013	0.164	0.072	0.043	0.013	0.209	0.089	0.054
0.5,0.5	100	1.0	0.010	0.075	0.022	0.015	0.010	0.070	0.022	0.015	0.012	0.110	0.031	0.022
		2.0	0.011	0.093	0.039	0.023	0.011	0.105	0.039	0.022	0.014	0.142	0.056	0.034
		5.0	0.012	0.135	0.049	0.031	0.012	0.143	0.049	0.031	0.016	0.206	0.069	0.044
		10.0	0.012	0.223	0.082	0.050	0.012	0.227	0.078	0.047	0.016	0.336	0.120	0.075
		20.0	0.021	0.270	0.125	0.083	0.020	0.286	0.122	0.088	0.029	0.364	0.178	0.112
	500	1.0	0.009	0.013	0.010	0.001	0.009	0.013	0.010	0.001	0.013	0.018	0.014	0.001
		2.0	0.010	0.015	0.011	0.001	0.009	0.014	0.011	0.001	0.013	0.022	0.015	0.002
		5.0	0.010	0.066	0.020	0.016	0.010	0.073	0.021	0.017	0.014	0.083	0.028	0.020
		10.0	0.010	0.118	0.032	0.026	0.010	0.096	0.031	0.022	0.013	0.200	0.045	0.043
		20.0	0.010	0.144	0.047	0.036	0.010	0.123	0.046	0.035	0.014	0.229	0.064	0.052

Table 3.12: Mallorca case study: skull-face overlay results for the CMA-ES algorithm

β_1, β_2	evaluations	θ	*Fitness*				*ME*				*MAX*			
			m	M	μ	σ	m	M	μ	σ	m	M	μ	σ
1,0	55.200	0.00001	0.007	0.265	0.080	0.084	0.007	0.265	0.080	0.084	0.025	0.394	0.147	0.129
		0.00010	0.007	0.273	0.095	0.105	0.007	0.273	0.095	0.105	0.023	0.413	0.156	0.150
		0.00100	0.007	0.275	0.097	0.088	0.007	0.275	0.097	0.088	0.022	0.482	0.174	0.142
		0.01000	0.007	0.276	0.111	0.109	0.007	0.276	0.111	0.109	0.020	0.516	0.182	0.161
		0.10000	0.007	0.269	0.173	0.101	0.007	0.269	0.173	0.101	0.026	0.434	0.267	0.142
		0.30000	0.007	0.712	0.277	0.135	0.007	0.712	0.277	0.135	0.026	0.870	0.416	0.183
	276.000	0.00001	0.007	0.091	0.010	0.015	0.007	0.091	0.010	0.015	0.019	0.233	0.031	0.038
		0.00010	0.007	0.008	0.008	0.000	0.007	0.008	0.008	0.000	0.019	0.027	0.024	0.003
		0.00100	0.007	0.030	0.008	0.004	0.007	0.030	0.008	0.004	0.019	0.128	0.028	0.019
		0.01000	0.007	0.101	0.014	0.023	0.007	0.101	0.014	0.023	0.016	0.257	0.040	0.059
		0.10000	0.007	0.146	0.025	0.035	0.007	0.146	0.025	0.035	0.020	0.284	0.055	0.061
		0.30000	0.007	0.261	0.121	0.106	0.007	0.261	0.121	0.106	0.019	0.422	0.194	0.154
0,1	55.200	0.00001	0.012	0.353	0.153	0.116	0.012	0.277	0.116	0.089	0.012	0.353	0.153	0.116
		0.00010	0.012	0.360	0.124	0.112	0.012	0.284	0.091	0.084	0.012	0.360	0.124	0.112
		0.00100	0.012	0.359	0.158	0.128	0.012	0.284	0.122	0.101	0.012	0.359	0.158	0.128
		0.01000	0.012	0.361	0.152	0.111	0.012	0.283	0.111	0.085	0.012	0.361	0.152	0.111
		0.10000	0.012	0.362	0.304	0.095	0.012	0.288	0.234	0.077	0.012	0.362	0.304	0.095
		0.30000	0.012	0.870	0.415	0.185	0.012	0.712	0.299	0.131	0.012	0.870	0.415	0.185
	276.000	0.00001	0.012	0.166	0.020	0.030	0.011	0.122	0.017	0.021	0.012	0.166	0.020	0.030
		0.00010	0.012	0.012	0.012	0.000	0.011	0.012	0.012	0.000	0.012	0.012	0.012	0.000
		0.00100	0.012	0.030	0.013	0.003	0.012	0.024	0.012	0.002	0.012	0.030	0.013	0.003
		0.01000	0.012	0.012	0.012	0.000	0.012	0.012	0.012	0.000	0.012	0.012	0.012	0.000
		0.10000	0.012	0.324	0.118	0.100	0.012	0.245	0.083	0.074	0.012	0.324	0.118	0.100
		0.30000	0.012	0.358	0.273	0.097	0.012	0.280	0.197	0.079	0.012	0.358	0.273	0.097
0.5,0.5	55.200	0.00001	0.010	0.261	0.096	0.090	0.009	0.261	0.092	0.089	0.014	0.354	0.135	0.123
		0.00010	0.010	0.269	0.106	0.092	0.009	0.276	0.103	0.092	0.014	0.355	0.148	0.125
		0.00100	0.010	0.272	0.109	0.086	0.009	0.282	0.104	0.085	0.013	0.355	0.155	0.119
		0.01000	0.010	0.268	0.139	0.102	0.009	0.278	0.137	0.102	0.014	0.365	0.191	0.138
		0.10000	0.049	0.278	0.243	0.048	0.047	0.287	0.238	0.055	0.069	0.402	0.335	0.060
		0.30000	0.053	0.676	0.285	0.133	0.037	0.712	0.280	0.133	0.093	0.870	0.393	0.185
	276.000	0.00001	0.010	0.117	0.017	0.027	0.009	0.110	0.016	0.025	0.014	0.170	0.024	0.040
		0.00010	0.010	0.010	0.010	0.000	0.009	0.010	0.009	0.000	0.014	0.014	0.014	0.000
		0.00100	0.010	0.010	0.010	0.000	0.009	0.010	0.009	0.000	0.013	0.014	0.014	0.000
		0.01000	0.010	0.086	0.012	0.014	0.009	0.088	0.012	0.014	0.014	0.113	0.017	0.018
		0.10000	0.010	0.250	0.082	0.082	0.009	0.254	0.078	0.078	0.014	0.333	0.117	0.117
		0.30000	0.010	0.284	0.146	0.102	0.010	0.293	0.142	0.102	0.014	0.389	0.203	0.139

Table 3.13: Cádiz case study, pose 1: skull-face overlay results for the BCGA algorithm

β_1, β_2	pop size	*Fitness*				*ME*				*MAX*			
		m	M	μ	σ	m	M	μ	σ	m	M	μ	σ
1,0	100	0.085	0.137	0.122	0.013	0.085	0.137	0.122	0.013	0.229	0.361	0.324	0.034
	500	0.030	0.129	0.101	0.025	0.030	0.129	0.101	0.025	0.062	0.344	0.271	0.065
0,1	100	0.036	0.244	0.213	0.040	0.029	0.171	0.151	0.028	0.036	0.244	0.213	0.040
	500	0.061	0.229	0.189	0.036	0.051	0.161	0.133	0.024	0.061	0.229	0.189	0.036
0.5,0.5	100	0.038	0.175	0.159	0.025	0.037	0.168	0.153	0.024	0.050	0.240	0.216	0.034
	500	0.035	0.159	0.125	0.034	0.035	0.152	0.118	0.034	0.045	0.217	0.174	0.045

Table 3.14: Cádiz case study, pose 1: skull-face overlay results for the RCGA-BLX-α algorithm

β_1, β_2	pop size	α	*Fitness*				*ME*				*MAX*			
			m	M	μ	σ	m	M	μ	σ	m	M	μ	σ
1,0	500	0.1	0.106	0.125	0.120	0.004	0.106	0.125	0.120	0.004	0.288	0.336	0.323	0.010
		0.3	0.079	0.122	0.112	0.011	0.079	0.122	0.112	0.011	0.158	0.330	0.300	0.041
		0.5	0.027	0.079	0.054	0.011	0.027	0.079	0.054	0.011	0.051	0.225	0.144	0.039
		0.7	0.040	0.110	0.076	0.019	0.040	0.110	0.076	0.019	0.100	0.297	0.195	0.061
		0.9	0.071	0.119	0.102	0.012	0.071	0.119	0.102	0.012	0.113	0.308	0.251	0.051
	1.000	0.1	0.075	0.124	0.118	0.010	0.075	0.124	0.118	0.010	0.192	0.335	0.315	0.030
		0.3	0.040	0.121	0.103	0.023	0.040	0.121	0.103	0.023	0.113	0.328	0.272	0.072
		0.5	0.038	0.086	0.063	0.012	0.038	0.086	0.063	0.012	0.069	0.240	0.164	0.044
		0.7	0.038	0.112	0.074	0.016	0.038	0.112	0.074	0.016	0.094	0.307	0.191	0.053
		0.9	0.067	0.118	0.102	0.014	0.067	0.118	0.102	0.014	0.138	0.321	0.257	0.049
0,1	500	0.1	0.191	0.223	0.214	0.005	0.129	0.162	0.156	0.006	0.191	0.223	0.214	0.005
		0.3	0.195	0.223	0.215	0.006	0.139	0.159	0.154	0.004	0.195	0.223	0.215	0.006
		0.5	0.135	0.225	0.205	0.026	0.093	0.159	0.144	0.018	0.135	0.225	0.205	0.026
		0.7	0.133	0.228	0.208	0.023	0.095	0.168	0.146	0.017	0.133	0.228	0.208	0.023
		0.9	0.082	0.217	0.186	0.033	0.046	0.153	0.128	0.028	0.082	0.217	0.186	0.033
	1.000	0.1	0.169	0.219	0.212	0.011	0.117	0.165	0.155	0.010	0.169	0.219	0.212	0.011
		0.3	0.058	0.223	0.203	0.034	0.036	0.160	0.146	0.024	0.058	0.223	0.203	0.034
		0.5	0.080	0.224	0.188	0.042	0.052	0.160	0.130	0.033	0.080	0.224	0.188	0.042
		0.7	0.129	0.227	0.197	0.027	0.095	0.161	0.139	0.019	0.129	0.227	0.197	0.027
		0.9	0.100	0.217	0.180	0.030	0.071	0.154	0.124	0.023	0.100	0.217	0.180	0.030
0.5,0.5	500	0.1	0.142	0.166	0.160	0.006	0.129	0.155	0.149	0.006	0.190	0.224	0.215	0.007
		0.3	0.072	0.166	0.150	0.023	0.070	0.156	0.137	0.025	0.093	0.223	0.204	0.028
		0.5	0.036	0.164	0.127	0.037	0.036	0.153	0.113	0.038	0.046	0.239	0.177	0.049
		0.7	0.062	0.166	0.125	0.029	0.048	0.150	0.109	0.029	0.094	0.264	0.176	0.041
		0.9	0.070	0.157	0.124	0.027	0.052	0.146	0.110	0.027	0.092	0.231	0.175	0.038
	1.000	0.1	0.091	0.164	0.154	0.018	0.081	0.153	0.143	0.019	0.128	0.220	0.207	0.023
		0.3	0.050	0.166	0.134	0.035	0.047	0.155	0.121	0.037	0.065	0.222	0.184	0.044
		0.5	0.069	0.161	0.119	0.032	0.055	0.150	0.103	0.032	0.095	0.232	0.167	0.044
		0.7	0.064	0.159	0.130	0.023	0.045	0.147	0.113	0.025	0.104	0.246	0.182	0.031
		0.9	0.065	0.149	0.118	0.023	0.059	0.136	0.100	0.023	0.088	0.242	0.168	0.038

Table 3.15: Cádiz case study, pose 1: skull-face overlay results for the RCGA-SBX algorithm

β_1, β_2	pop size	η	*Fitness*				*ME*				*MAX*			
			m	M	μ	σ	m	M	μ	σ	m	M	μ	σ
1,0	100	1.0	0.015	0.044	0.029	0.010	0.015	0.044	0.029	0.010	0.036	0.110	0.065	0.023
		2.0	0.015	0.047	0.029	0.012	0.015	0.047	0.029	0.012	0.034	0.147	0.065	0.028
		5.0	0.015	0.048	0.033	0.009	0.015	0.048	0.033	0.009	0.036	0.181	0.080	0.032
		10.0	0.022	0.089	0.038	0.014	0.022	0.089	0.038	0.014	0.037	0.244	0.092	0.047
		20.0	0.025	0.126	0.082	0.028	0.025	0.126	0.082	0.028	0.038	0.333	0.225	0.077
	500	1.0	0.015	0.033	0.017	0.005	0.015	0.033	0.017	0.005	0.034	0.087	0.044	0.015
		2.0	0.015	0.033	0.017	0.005	0.015	0.033	0.017	0.005	0.034	0.092	0.048	0.018
		5.0	0.015	0.038	0.022	0.008	0.015	0.038	0.022	0.008	0.034	0.196	0.054	0.033
		10.0	0.015	0.040	0.023	0.007	0.015	0.040	0.023	0.007	0.034	0.105	0.058	0.023
		20.0	0.015	0.040	0.026	0.008	0.015	0.040	0.026	0.008	0.034	0.113	0.066	0.026
0,1	100	1.0	0.029	0.060	0.047	0.010	0.021	0.048	0.037	0.008	0.029	0.060	0.047	0.010
		2.0	0.032	0.069	0.048	0.010	0.021	0.053	0.039	0.008	0.032	0.069	0.048	0.010
		5.0	0.034	0.217	0.079	0.057	0.022	0.156	0.059	0.040	0.034	0.217	0.079	0.057
		10.0	0.034	0.232	0.118	0.068	0.022	0.163	0.086	0.048	0.034	0.232	0.118	0.068
		20.0	0.038	0.240	0.172	0.054	0.032	0.173	0.123	0.038	0.038	0.240	0.172	0.054
	500	1.0	0.028	0.045	0.033	0.006	0.022	0.041	0.028	0.008	0.028	0.045	0.033	0.006
		2.0	0.028	0.051	0.034	0.008	0.021	0.046	0.027	0.007	0.028	0.051	0.034	0.008
		5.0	0.029	0.067	0.041	0.011	0.021	0.057	0.034	0.010	0.029	0.067	0.041	0.011
		10.0	0.028	0.199	0.052	0.031	0.021	0.152	0.041	0.024	0.028	0.199	0.052	0.031
		20.0	0.029	0.210	0.080	0.055	0.021	0.155	0.061	0.040	0.029	0.210	0.080	0.055
0.5,0.5	100	1.0	0.021	0.058	0.038	0.009	0.017	0.058	0.037	0.009	0.031	0.073	0.048	0.011
		2.0	0.021	0.072	0.041	0.012	0.017	0.063	0.040	0.010	0.030	0.107	0.053	0.017
		5.0	0.022	0.053	0.040	0.008	0.020	0.052	0.039	0.008	0.030	0.074	0.052	0.012
		10.0	0.027	0.169	0.065	0.045	0.022	0.158	0.061	0.042	0.039	0.225	0.088	0.061
		20.0	0.028	0.171	0.111	0.048	0.025	0.161	0.102	0.045	0.038	0.227	0.150	0.064
	500	1.0	0.021	0.035	0.022	0.003	0.016	0.038	0.018	0.005	0.029	0.040	0.032	0.002
		2.0	0.021	0.040	0.024	0.005	0.016	0.041	0.020	0.007	0.029	0.048	0.034	0.005
		5.0	0.021	0.042	0.028	0.007	0.016	0.042	0.027	0.009	0.029	0.053	0.037	0.007
		10.0	0.021	0.051	0.029	0.007	0.018	0.050	0.027	0.008	0.029	0.065	0.037	0.008
		20.0	0.023	0.081	0.043	0.016	0.021	0.067	0.040	0.012	0.030	0.125	0.058	0.026

Table 3.16: Cádiz case study, pose 1: skull-face overlay results for the CMA-ES algorithm

β_1, β_2	evaluations	θ	*Fitness*				*ME*				*MAX*			
			m	M	μ	σ	m	M	μ	σ	m	M	μ	σ
1,0	55.200	0.00001	0.015	0.077	0.034	0.021	0.015	0.077	0.034	0.021	0.040	0.174	0.077	0.044
		0.00010	0.015	0.064	0.026	0.016	0.015	0.064	0.026	0.016	0.040	0.183	0.065	0.042
		0.00100	0.015	0.067	0.027	0.017	0.015	0.067	0.027	0.017	0.040	0.177	0.065	0.037
		0.01000	0.015	0.064	0.028	0.019	0.015	0.064	0.028	0.019	0.040	0.156	0.062	0.034
		0.10000	0.015	0.104	0.035	0.024	0.015	0.104	0.035	0.024	0.038	0.273	0.083	0.058
		0.30000	0.015	1.018	0.140	0.207	0.015	1.018	0.140	0.207	0.040	1.141	0.226	0.246
	276.000	0.00001	0.015	0.042	0.018	0.009	0.015	0.042	0.018	0.009	0.040	0.086	0.046	0.014
		0.00010	0.015	0.032	0.015	0.003	0.015	0.032	0.015	0.003	0.039	0.085	0.042	0.008
		0.00100	0.015	0.015	0.015	0.000	0.015	0.015	0.015	0.000	0.040	0.041	0.040	0.000
		0.01000	0.015	0.043	0.017	0.007	0.015	0.043	0.017	0.007	0.040	0.087	0.043	0.011
		0.10000	0.015	0.034	0.016	0.003	0.015	0.034	0.016	0.003	0.040	0.085	0.042	0.008
		0.30000	0.015	0.076	0.036	0.024	0.015	0.076	0.036	0.024	0.040	0.209	0.084	0.052
0,1	55.200	0.00001	0.028	0.137	0.059	0.038	0.021	0.092	0.043	0.024	0.028	0.137	0.059	0.038
		0.00010	0.028	0.118	0.055	0.030	0.022	0.070	0.039	0.016	0.028	0.118	0.055	0.030
		0.00100	0.028	0.119	0.055	0.032	0.022	0.072	0.038	0.017	0.028	0.119	0.055	0.032
		0.01000	0.028	0.254	0.071	0.047	0.022	0.175	0.050	0.030	0.028	0.254	0.071	0.047
		0.10000	0.028	0.146	0.087	0.037	0.023	0.104	0.058	0.024	0.028	0.146	0.087	0.037
		0.30000	0.028	1.141	0.209	0.237	0.024	1.018	0.147	0.198	0.028	1.141	0.209	0.237
	276.000	0.00001	0.028	0.060	0.032	0.010	0.022	0.046	0.026	0.008	0.028	0.060	0.032	0.010
		0.00010	0.028	0.059	0.034	0.012	0.022	0.045	0.027	0.008	0.028	0.059	0.034	0.012
		0.00100	0.028	0.060	0.034	0.010	0.022	0.046	0.029	0.009	0.028	0.060	0.034	0.010
		0.01000	0.028	0.061	0.034	0.010	0.022	0.046	0.028	0.008	0.028	0.061	0.034	0.010
		0.10000	0.028	0.074	0.031	0.009	0.022	0.053	0.025	0.007	0.028	0.074	0.031	0.009
		0.30000	0.028	0.137	0.070	0.037	0.022	0.089	0.047	0.022	0.028	0.137	0.070	0.037
0.5,0.5	55.200	0.00001	0.021	0.085	0.041	0.023	0.016	0.078	0.035	0.020	0.031	0.140	0.058	0.034
		0.00010	0.021	0.082	0.051	0.022	0.016	0.079	0.045	0.019	0.031	0.123	0.071	0.032
		0.00100	0.021	0.084	0.048	0.023	0.016	0.079	0.042	0.029	0.031	0.126	0.066	0.033
		0.01000	0.021	0.086	0.045	0.024	0.016	0.079	0.039	0.021	0.031	0.133	0.062	0.034
		0.10000	0.021	0.093	0.048	0.027	0.016	0.087	0.040	0.024	0.031	0.135	0.069	0.039
		0.30000	0.021	0.970	0.141	0.201	0.016	1.018	0.131	0.204	0.031	1.141	0.187	0.245
	276.000	0.00001	0.021	0.047	0.024	0.008	0.016	0.046	0.020	0.009	0.031	0.060	0.034	0.008
		0.00010	0.021	0.038	0.023	0.005	0.016	0.040	0.019	0.008	0.031	0.044	0.033	0.003
		0.00100	0.021	0.046	0.023	0.007	0.016	0.044	0.020	0.009	0.031	0.058	0.034	0.007
		0.01000	0.021	0.048	0.024	0.008	0.016	0.046	0.020	0.009	0.031	0.061	0.034	0.009
		0.10000	0.021	0.061	0.022	0.007	0.016	0.054	0.018	0.007	0.031	0.084	0.033	0.010
		0.30000	0.021	0.110	0.052	0.031	0.016	0.091	0.043	0.025	0.031	0.170	0.076	0.046

Table 3.17: Cádiz case study, pose 2: skull-face overlay results for the BCGA algorithm

β_1, β_2	pop size	*Fitness*				*ME*				*MAX*			
		m	M	μ	σ	m	M	μ	σ	m	M	μ	σ
1,0	100	0.077	0.193	0.166	0.030	0.077	0.193	0.166	0.030	0.129	0.414	0.351	0.067
	500	0.043	0.180	0.123	0.041	0.043	0.180	0.123	0.041	0.120	0.374	0.259	0.077
0,1	100	0.148	0.300	0.269	0.041	0.102	0.215	0.190	0.030	0.148	0.300	0.269	0.041
	500	0.094	0.283	0.201	0.071	0.066	0.198	0.141	0.051	0.094	0.283	0.201	0.071
0.5,0.5	100	0.101	0.214	0.196	0.026	0.090	0.209	0.191	0.027	0.153	0.298	0.274	0.035
	500	0.066	0.190	0.128	0.039	0.052	0.183	0.122	0.039	0.092	0.262	0.179	0.053

Table 3.18: Cádiz case study, pose 2: skull-face overlay results for the RCGA-BLX-α algorithm

β_1, β_2	pop size	α	*Fitness*				*ME*				*MAX*			
			m	M	μ	σ	m	M	μ	σ	m	M	μ	σ
1,0	500	0.1	0.092	0.177	0.148	0.021	0.092	0.177	0.148	0.021	0.172	0.376	0.311	0.053
		0.3	0.055	0.158	0.078	0.025	0.055	0.158	0.078	0.025	0.104	0.364	0.165	0.059
		0.5	0.052	0.058	0.055	0.001	0.052	0.058	0.055	0.001	0.106	0.136	0.124	0.006
		0.7	0.046	0.094	0.058	0.010	0.046	0.094	0.058	0.010	0.111	0.216	0.143	0.028
		0.9	0.088	0.166	0.136	0.020	0.088	0.166	0.136	0.020	0.187	0.396	0.273	0.060
	1.000	0.1	0.071	0.176	0.136	0.028	0.071	0.176	0.136	0.028	0.139	0.381	0.292	0.071
		0.3	0.051	0.114	0.072	0.017	0.051	0.114	0.072	0.017	0.107	0.249	0.146	0.037
		0.5	0.054	0.058	0.057	0.001	0.054	0.058	0.057	0.001	0.113	0.134	0.122	0.005
		0.7	0.047	0.074	0.058	0.007	0.047	0.074	0.058	0.007	0.104	0.190	0.134	0.021
		0.9	0.091	0.158	0.133	0.019	0.091	0.158	0.133	0.019	0.149	0.380	0.275	0.063
0,1	500	0.1	0.255	0.287	0.281	0.007	0.183	0.211	0.204	0.006	0.255	0.287	0.281	0.007
		0.3	0.111	0.287	0.271	0.035	0.057	0.211	0.193	0.029	0.111	0.287	0.271	0.035
		0.5	0.155	0.280	0.242	0.042	0.067	0.197	0.165	0.039	0.155	0.280	0.242	0.042
		0.7	0.119	0.285	0.228	0.036	0.079	0.201	0.156	0.029	0.119	0.285	0.228	0.036
		0.9	0.142	0.281	0.225	0.035	0.093	0.192	0.153	0.026	0.142	0.281	0.225	0.035
	1.000	0.1	0.182	0.287	0.271	0.027	0.132	0.211	0.197	0.022	0.182	0.287	0.271	0.027
		0.3	0.182	0.284	0.258	0.034	0.104	0.207	0.180	0.030	0.182	0.284	0.258	0.034
		0.5	0.128	0.280	0.237	0.051	0.056	0.196	0.162	0.043	0.128	0.280	0.237	0.051
		0.7	0.170	0.281	0.236	0.034	0.112	0.202	0.161	0.025	0.170	0.281	0.236	0.034
		0.9	0.160	0.269	0.221	0.031	0.101	0.190	0.147	0.030	0.160	0.269	0.221	0.031
0.5,0.5	500	0.1	0.179	0.202	0.197	0.006	0.174	0.197	0.191	0.006	0.249	0.283	0.274	0.008
		0.3	0.137	0.204	0.197	0.013	0.128	0.198	0.191	0.013	0.196	0.285	0.275	0.016
		0.5	0.062	0.197	0.106	0.042	0.043	0.191	0.094	0.045	0.106	0.274	0.160	0.052
		0.7	0.065	0.132	0.091	0.021	0.050	0.129	0.082	0.023	0.102	0.192	0.136	0.028
		0.9	0.092	0.189	0.148	0.025	0.073	0.185	0.131	0.027	0.128	0.299	0.225	0.040
	1.000	0.1	0.134	0.203	0.192	0.014	0.132	0.197	0.186	0.013	0.182	0.282	0.268	0.020
		0.3	0.073	0.204	0.164	0.046	0.049	0.197	0.154	0.050	0.116	0.286	0.233	0.056
		0.5	0.069	0.188	0.115	0.033	0.055	0.182	0.105	0.035	0.109	0.261	0.169	0.042
		0.7	0.067	0.160	0.098	0.026	0.053	0.147	0.085	0.024	0.108	0.269	0.148	0.040
		0.9	0.072	0.189	0.145	0.025	0.059	0.181	0.132	0.024	0.115	0.281	0.213	0.039

Table 3.19: Cádiz case study, pose 2: skull-face overlay results for the RCGA-SBX algorithm

β_1, β_2	pop size	η	*Fitness*				*ME*				*MAX*			
			m	M	μ	σ	m	M	μ	σ	m	M	μ	σ
1,0	100	1.0	0.036	0.062	0.048	0.010	0.036	0.062	0.048	0.010	0.111	0.291	0.153	0.032
		2.0	0.036	0.096	0.052	0.015	0.036	0.096	0.052	0.015	0.120	0.230	0.156	0.028
		5.0	0.037	0.086	0.056	0.014	0.037	0.086	0.056	0.014	0.118	0.213	0.155	0.024
		10.0	0.039	0.142	0.063	0.022	0.039	0.142	0.063	0.022	0.119	0.313	0.158	0.040
		20.0	0.037	0.184	0.118	0.049	0.037	0.184	0.118	0.049	0.116	0.395	0.264	0.098
	500	1.0	0.036	0.038	0.036	0.000	0.036	0.038	0.036	0.000	0.131	0.145	0.143	0.002
		2.0	0.036	0.060	0.040	0.008	0.036	0.060	0.040	0.008	0.103	0.246	0.144	0.021
		5.0	0.036	0.067	0.043	0.008	0.036	0.067	0.043	0.008	0.116	0.198	0.143	0.014
		10.0	0.036	0.065	0.049	0.009	0.036	0.065	0.049	0.009	0.109	0.199	0.147	0.020
		20.0	0.036	0.102	0.053	0.013	0.036	0.102	0.053	0.013	0.100	0.202	0.135	0.022
0,1	100	1.0	0.090	0.122	0.103	0.007	0.059	0.101	0.072	0.009	0.090	0.122	0.103	0.007
		2.0	0.091	0.212	0.109	0.023	0.060	0.144	0.075	0.016	0.091	0.212	0.109	0.023
		5.0	0.094	0.304	0.124	0.042	0.059	0.216	0.086	0.032	0.094	0.304	0.124	0.042
		10.0	0.104	0.298	0.196	0.074	0.066	0.213	0.138	0.055	0.104	0.298	0.196	0.074
		20.0	0.103	0.299	0.231	0.066	0.071	0.217	0.163	0.047	0.103	0.299	0.231	0.066
	500	1.0	0.089	0.103	0.098	0.005	0.059	0.073	0.066	0.004	0.089	0.103	0.098	0.005
		2.0	0.089	0.108	0.099	0.006	0.060	0.076	0.067	0.005	0.089	0.108	0.099	0.006
		5.0	0.091	0.180	0.106	0.016	0.060	0.122	0.073	0.012	0.091	0.180	0.106	0.016
		10.0	0.091	0.126	0.106	0.008	0.058	0.102	0.070	0.009	0.091	0.126	0.106	0.008
		20.0	0.092	0.254	0.125	0.039	0.060	0.175	0.084	0.029	0.092	0.254	0.125	0.039
0.5,0.5	100	1.0	0.063	0.081	0.068	0.004	0.043	0.077	0.055	0.009	0.102	0.112	0.107	0.002
		2.0	0.062	0.135	0.071	0.013	0.043	0.121	0.061	0.016	0.092	0.198	0.109	0.018
		5.0	0.065	0.192	0.084	0.030	0.045	0.185	0.075	0.031	0.095	0.265	0.124	0.040
		10.0	0.063	0.216	0.111	0.049	0.044	0.211	0.103	0.049	0.097	0.298	0.159	0.066
		20.0	0.075	0.215	0.170	0.044	0.070	0.208	0.164	0.044	0.107	0.299	0.238	0.061
	500	1.0	0.061	0.068	0.063	0.002	0.042	0.059	0.046	0.005	0.104	0.111	0.108	0.002
		2.0	0.062	0.071	0.064	0.002	0.043	0.064	0.049	0.008	0.091	0.111	0.105	0.007
		5.0	0.062	0.086	0.069	0.006	0.043	0.085	0.059	0.011	0.091	0.122	0.106	0.007
		10.0	0.062	0.077	0.069	0.004	0.044	0.077	0.059	0.010	0.096	0.118	0.105	0.004
		20.0	0.062	0.163	0.074	0.020	0.043	0.157	0.064	0.022	0.093	0.227	0.114	0.026

Table 3.20: Cádiz case study, pose 2: skull-face overlay results for the CMA-ES algorithm

β_1, β_2	evaluations	θ	*Fitness*				*ME*				*MAX*			
			m	M	μ	σ	m	M	μ	σ	m	M	μ	σ
1,0	55.200	0.00001	0.036	0.105	0.056	0.024	0.036	0.105	0.056	0.024	0.121	0.242	0.158	0.028
		0.00010	0.036	0.110	0.059	0.026	0.036	0.110	0.059	0.026	0.111	0.286	0.153	0.033
		0.00100	0.036	0.109	0.061	0.028	0.036	0.109	0.061	0.028	0.127	0.220	0.159	0.023
		0.01000	0.036	0.118	0.055	0.026	0.036	0.118	0.055	0.026	0.113	0.234	0.153	0.029
		0.10000	0.036	0.134	0.068	0.032	0.036	0.134	0.068	0.032	0.138	0.262	0.172	0.038
		0.30000	0.036	0.676	0.163	0.167	0.036	0.676	0.163	0.167	0.128	0.929	0.296	0.224
	276.000	0.00001	0.036	0.061	0.037	0.005	0.036	0.061	0.037	0.005	0.144	0.169	0.146	0.005
		0.00010	0.036	0.061	0.037	0.005	0.036	0.061	0.037	0.005	0.143	0.172	0.146	0.005
		0.00100	0.036	0.062	0.038	0.007	0.036	0.062	0.038	0.007	0.144	0.181	0.147	0.008
		0.01000	0.036	0.061	0.037	0.005	0.036	0.061	0.037	0.005	0.144	0.174	0.146	0.005
		0.10000	0.036	0.036	0.036	0.000	0.036	0.036	0.036	0.000	0.144	0.145	0.145	0.000
		0.30000	0.036	0.124	0.053	0.029	0.036	0.124	0.053	0.029	0.111	0.297	0.158	0.042
0,1	55.200	0.00001	0.089	0.809	0.136	0.129	0.063	0.559	0.092	0.090	0.089	0.809	0.136	0.129
		0.00010	0.090	0.177	0.119	0.028	0.062	0.116	0.078	0.015	0.090	0.177	0.119	0.028
		0.00100	0.090	0.166	0.120	0.022	0.063	0.106	0.078	0.013	0.090	0.166	0.120	0.022
		0.01000	0.089	0.174	0.117	0.026	0.061	0.099	0.074	0.012	0.089	0.174	0.117	0.026
		0.10000	0.089	0.176	0.119	0.026	0.063	0.103	0.077	0.013	0.089	0.176	0.119	0.026
		0.30000	0.090	0.929	0.249	0.226	0.063	0.676	0.163	0.152	0.090	0.929	0.249	0.226
	276.000	0.00001	0.090	0.108	0.098	0.006	0.060	0.073	0.066	0.004	0.090	0.108	0.098	0.006
		0.00010	0.089	0.108	0.098	0.007	0.063	0.073	0.067	0.004	0.089	0.108	0.098	0.007
		0.00100	0.089	0.108	0.098	0.007	0.063	0.074	0.067	0.004	0.089	0.108	0.098	0.007
		0.01000	0.089	0.108	0.100	0.006	0.063	0.075	0.067	0.005	0.089	0.108	0.100	0.006
		0.10000	0.089	0.101	0.092	0.004	0.063	0.071	0.068	0.002	0.089	0.101	0.092	0.004
		0.30000	0.090	0.129	0.096	0.009	0.063	0.089	0.067	0.005	0.090	0.129	0.096	0.009
0.5,0.5	55.200	0.00001	0.062	0.116	0.078	0.018	0.042	0.107	0.064	0.019	0.092	0.184	0.123	0.026
		0.00010	0.062	0.123	0.084	0.022	0.042	0.118	0.069	0.025	0.092	0.184	0.130	0.028
		0.00100	0.062	0.132	0.080	0.019	0.044	0.117	0.066	0.021	0.092	0.197	0.127	0.025
		0.10000	0.062	0.135	0.074	0.018	0.044	0.131	0.061	0.020	0.092	0.185	0.117	0.022
		0.30000	0.062	0.687	0.168	0.176	0.042	0.676	0.150	0.171	0.092	0.929	0.247	0.242
		0.00001	0.062	0.077	0.063	0.003	0.044	0.071	0.048	0.007	0.091	0.110	0.105	0.004
	276.000	0.00010	0.062	0.067	0.063	0.002	0.044	0.061	0.047	0.006	0.092	0.110	0.105	0.005
		0.00100	0.062	0.077	0.065	0.005	0.044	0.072	0.051	0.010	0.092	0.109	0.106	0.004
		0.01000	0.062	0.067	0.063	0.002	0.044	0.061	0.046	0.005	0.092	0.107	0.106	0.003
		0.10000	0.062	0.067	0.062	0.001	0.044	0.055	0.044	0.002	0.105	0.107	0.106	0.000
		0.30000	0.062	0.123	0.069	0.016	0.043	0.121	0.054	0.019	0.091	0.180	0.112	0.020
		0.00001	0.062	0.067	0.064	0.002	0.044	0.062	0.051	0.008	0.091	0.107	0.102	0.007

Chapter 4

A Quick and Robust Evolutionary Approach for Skull-Face Overlay Based on Scatter Search

I like to be surrounded by
splendid things.

Freddie Mercury (1946-1991)

4.1 Introduction

This chapter takes a new step ahead in the development of this PhD dissertation by focusing again on the second stage of the CS process, the skull-face overlay. More in detail, we try to exploit the benefits of applying SS (Laguna and Martí 2003) to design a new automatic method to develop this task. Our intention is to provide a faster and more accurate algorithm than those in the literature and than our previous proposal. In particular, we aim to ensure a faster approach (in terms of convergence) than our previous proposal based on the use of CMA-ES (see Chapter 3).

To do so, our SS design relies on: i) the use of a population size several times lower than the one typically defined with GAs; ii) the generation of an initial population spread throughout the search space, in order to encourage diversification; iii) the initialization of the population based on the delimitation of the rotation angles using problem-specific information (domain knowledge), in order to reduce the search space, thus decreasing the convergence time and increasing the robustness; iv) the establishment of a systematic solution combination criterion to favor the search space intensification; and v) the use of local search to achieve a faster convergence to promising solutions.

The proposed method will be validated over six different real-world identification cases previously addressed by the staff of the Physical Anthropology lab at the University of Granada in collaboration with the Spanish scientific police, following a computer supported but manual approach for skull-face overlay. Three of those problem instances were already tackled in Chapter 3, thus allowing the reader to perform a direct comparison.

The structure of this chapter is as follows. Section 4.2 describes our proposal, which is tested in Section 4.3 over the said six different skull-face overlay problem

instances. Finally, Section 4.4 collects some conclusions.

4.2 A Scatter Search method for skull-face overlay

As said, we aim to develop a new skull-face overlay method that is competitive enough considering accuracy criteria when it is compared to our previous proposal based on the use of CMA-ES (see Chapter 3), but becomes more robust and faster in terms of convergence.

We have followed the formulation proposed in Section 3.3 of Chapter 3 in which the goal is to find a near-optimal geometric transformation that minimizes the distance among pairs of landmarks, that is, a numerical optimization problem. To do so, we will use SS, whose fundamentals were explained in Section 1.4.3 of Chapter 1.

The fact that the mechanisms within SS are not restricted to a single uniform design allows the exploration of strategic possibilities that may prove effective in a particular implementation. Of the five methods in the SS methodology, only four are strictly required. The Improvement Method is usually needed if high quality outcomes are desired but a SS procedure can be implemented without it. In the following subsections, we will briefly describe the specific design of each component of our SS-based skull-face overlay method outlined in Figure 4.2, where P denotes the initial set of solutions generated with the *Diversification Generation Method* (with *Psize* being the size of P), the reference set is noted as *RefSet* (with b being its size, usually significantly lower than *Psize*), and *Pool* is the set of trial solutions constructed with the *Combination* and *Improvement Methods* each iteration.

4.2.1 Coding scheme and objective function

As in the previous evolutionary-based proposals, the geometric transformation that maps every cranial landmark C_i in the skull 3D model onto its corresponding facial landmark F_i in the photograph is encoded in a vector as follows: $(r_x, r_y, r_z, d_x, d_y, d_z, \theta, s, t_x, t_y, t_z, \phi)$

To measure the quality of the registration transformation encoded in a specific individual an objective function is needed. In Chapter 3 we studied the behavior of three different fitness functions. When the ME (Equation 3.8) was considered, better results were achieved in all the real world cases studied. Hence, we have only considered the ME as the objective function for the proposed SS method.

$P \leftarrow \emptyset$

While ($|P| < PSize$) do

Obtain a new solution x generated by the **Diversification Generation Method**

Improve x with the **Improvement Method** generating a solution x'

If $x' \notin P$ Then $P \leftarrow P \cup \{x'\}$

Sort the solutions in P according to their objective function value (the best overall solution in P, that one with the lowest F value, is the first in such list). Add the first b solutions from P to $RefSet$

While (not reached the stop stopping condition) do

$NewElements \leftarrow$ True

$Pool \leftarrow \emptyset$

While ($NewElements$) and (not reached the stopping condition) do

Generate all the subsets of (pairs of) solutions $s_i = \{x_j, x_k\}$ ($\{x_j, x_k\} \in Subsets \mid x_j, x_k \in Refset \wedge j,k = \{1, \cdots, \mid RefSet \mid\} \wedge j \neq k$) with the **Subset Generation Method**

$NewElements \leftarrow$ False

While ($Subsets \neq \emptyset$) do

Select the next subset s_i ($i = \{1, \cdots, \frac{b \cdot (b-1)}{2}\}$) from $Subsets$ and delete it from $Subsets$

Apply the **Solution Combination Method** to the next pair of solutions $\{x_j, x_k\} \in s_i$ that were not previously combined in order to obtain a new solution x

If ($F(x) < F(x_j)$ OR $F(x) < F(x_k)$) Then

Apply the **Improvement Method** to the solution x to obtain the solution x'

Else $x' \leftarrow x$

Add x' to $Pool$

Apply the **Reference Set Update Method** selecting the best b solutions in $RefSet \cup Pool$

If ($RefSet$ has at least one new solution) Then $NewElements \leftarrow$ True

If (not reached the stop criterion) Then

Build a new set P using the **Diversification Generation Method**

Replace the worst $b-1$ solutions from $RefSet$ with the best $b-1$ solutions from P

Figure 4.1: Pseudocode of the SS-based skull-face overlay optimizer.

4.2.2 Diversification Generation Method and Advanced Heuristic Initialization Strategy

This method makes use of a controlled randomization based on frequency memory to generate an initial set P of $Psize$ diverse solutions (Laguna and Martí 2003). We carry out this by dividing the range of each variable (in our case, each one of the twelve geometric transformation parameters) into four sub-ranges of equal size. A solution will be constructed in two steps. First, a sub-range is randomly selected for each variable, where the probability of choosing a sub-range is inversely proportional to its frequency count. Initially, the frequency count for each variable subrange is set to one and the number of times a sub-range j has been chosen to generate a value for

variable i in a solution is accumulated in $frequency\_count(i, j)$. Then, as a second step, a value is randomly generated within the selected sub-range. Finally, the *Improvement Method* is applied on the *Psize* solutions generated and the best b of them compose the initial *RefSet*.

Using specific information derived from the characteristics of the problem has demonstrated to be an important aid tackling IR problems (Cordón et al. 2008). In skull-face overlay most of the photographs show a near-frontal pose of the missing person. We found profile pictures in just a few cases. Of course, we know that we will never tackle a photograph where the missing person is looking backwards. Hence, we propose an initialization of the population based on the delimitation of the rotation angles using information from the domain knowledge. In order to specify reduced values for the feasible ranges where the twelve parameters will take values, we first orient the skull 3D model towards the camera axis[1]. It is evident that we are only interested in those transformations providing a near front view of the skull, i.e. $\theta \in [-90^\circ, 90^\circ]$ (see Figure 4.2). The advantages of this approach are two-fold. On the one hand, we will only generate good quality solutions for the initial population. On the other hand, the search space dimension is reduced from 360° to 180°, thus decreasing the convergence time.

To do so, we calculate the centroid, Z, of four non-coplanar cranial landmarks, C_j ($j \in 1,\ldots,4$), in order to estimate the current skull orientation and to rotate properly the skull towards a front view. We also use the maximum distance, r, from Z to the farthest of the said four landmarks ($r = \| Z - C_j \|$, $j = \{1,\ldots,4\}$) for the proper estimation of the valid ranges of values of the twelve parameters, as follows:

$$
\begin{array}{lcl}
r_i & \in & [Z_i - r,\ Z_i + r], i \in \{x,y,z\} \\
d_x, d_y & \in & [-1,\ 1] \\
d_z & \in & [0,\ 1] \\
\theta & \in & [-90^\circ,\ 90^\circ] \\
s & \in & [0.25,\ 2] \\
\phi & \in & [10^\circ,\ 150^\circ] \\
t_x & \in & [-length_{FB} - (Z_x + r),\ length_{FB} - (Z_x - r)] \\
t_y & \in & [-length_{FB} - (Z_y + r),\ length_{FB} - (Z_y - r)] \\
t_z & \in & [NCP - (Z_z + r),\ FCP - (Z_z - r)]
\end{array}
$$

where FCP and NCP are the far and near clipping planes[2], respectively; $lengthFB$ is

[1] Notice that, we can not assume that the initial pose of the skull 3D model is frontal. It may vary depending on the 3D digitalization process

[2] The FCP and NCP concepts were introduced in Section 3.3.2 of Chapter 3.

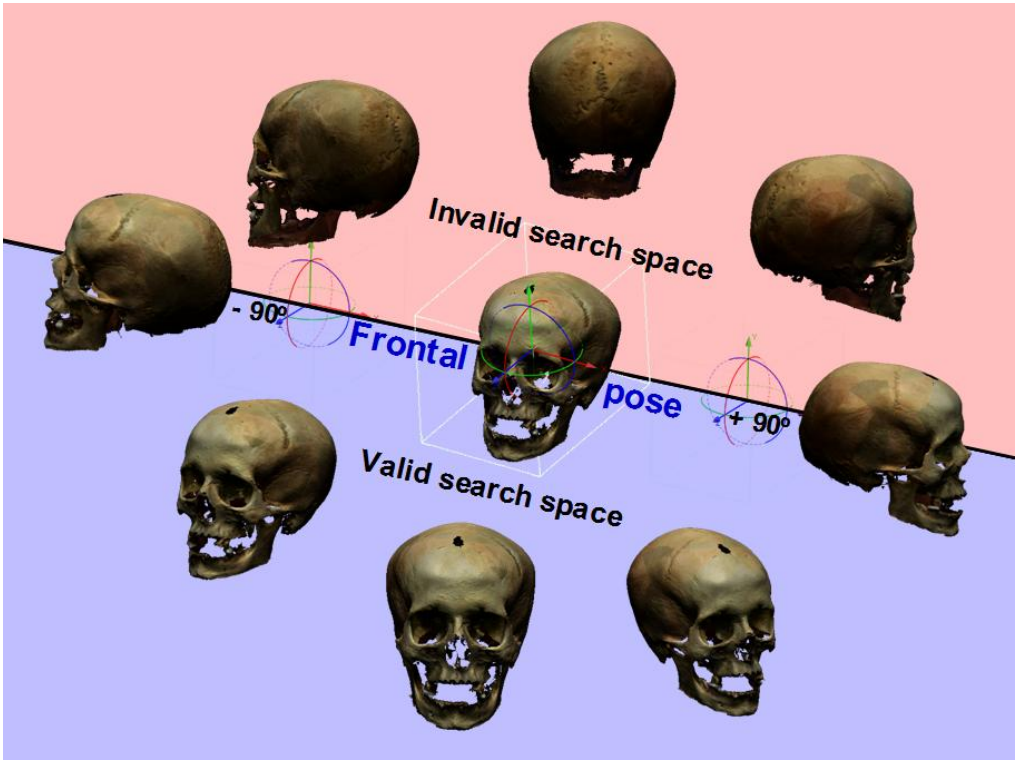

Figure 4.2: Search space constrained considering problem specific information.

the length of the frustum base; and

$$length_{FB} = 1 + FCP * tan(\frac{\phi_{max}}{2}).$$

In Section 4.3 we will experimentally demonstrate the benefits of applying this initialization procedure in terms of convergence speed and robustness.

4.2.3 Improvement Method

The considered Improvement Method is based on XLS, which is a crossover-based local search (LS) method that induces an LS on the neighborhood of the parents solutions involved in crossover (Lozano et al. 2004a; Noman and Iba 2005). Given a solution to be improved, called family father, L solutions are randomly selected in the current population for mating with the previous one to generate new trial solutions in the father's neighborhood by performing crossover operations. Finally, a selection operation is carried out for replacing the family father with the best solution of the L new solutions only if this one is better than the former. Hence, it can be called *best point neighborhood strategy* (Noman and Iba 2005). This procedure is repeated until the considered stop criterion is reached.

In this work we considered Parent-centric BLX-α crossover operator (Lozano et al. 2004a) (with $\alpha = 0.5$) to generate four neighboring solutions every LS iteration.

Parent-centric BLX-α (PBX-α) is described as follows:

Let us assume that $X = (x_1 \dots x_n)$ and $Y = (y_1 \dots y_n)$ $(x_i, y_i \in [a_i, b_i] \subset \mathbb{R}, i = 1 \dots n)$ are two real-coded chromosomes that have been selected to apply the crossover operator to them. PBX-α (randomly) generates one of these two possible offspring: $Z_1 = (z_1^1 \dots z_n^1)$ or $Z_2 = (z_1^2 \dots z_n^2)$, where

z_i^1 is a randomly (uniformly) chosen number from the interval $[l_i^1, u_i^1]$, with $l_i^1 = max\{a_i, x_i - I \cdot \alpha\}$ and $u_i^1 = min\{b_i, x_i + I \cdot \alpha\}$, and z_2 i is chosen from $[l_i^2, u_i^2]$, with $l_i^2 = max\{a_i, y_i - I \cdot \alpha\}$ and $u_i^2 = min\{b_i, y_i + I \cdot \alpha\}$, where $I = |x_i - y_i|$. This operator has the following features:

- It is a parent-centric crossover operator because it assigns more probability for creating offspring near parents than anywhere else in the search space.

- The degree of diversity induced by PBX-α may be easily adjusted by means of varying its associated α operator parameter. The greater the α value is, the higher the variance (diversity) introduced into the population.

- This operator assigns children solutions proportional to the spread of parent solutions. Thereby, it provides RCGAs using it with that use it the potential to exhibit self-adaptation.

4.2.3.1 Subset Generation Method

This method generates a collection of solution subsets (noted as *Subsets* in Figure 4.2) of the Reference Set as a basis for creating new combined solutions. In our implementation, the subsets are composed of all the possible pairs of solutions in *RefSet,* so $\frac{b\cdot(b-1)}{2}$ different subsets are generated at each iteration.

4.2.3.2 Solution Combination Method

It is based on the use of the BLX-α crossover operator (Eshelman 1993), commonly used in real-coded GAs. This combination mechanism obtains a trial solution, $x = (h_1,\ldots,h_k,\ldots,h_l)$ (with $l = 12$ being the number of parameters of the geometric transformation and h_k being a given value for such k^{th} variable) from the two parent solutions $x^1 = (c_1^1,\ldots,c_l^1)$ and $x^2 = (c_1^2,\ldots,c_l^2)$ composing a given subset s (see Figure 4.2). The offsprings are obtained by uniformly generating a random value for each variable h_k in the interval $[c_{min} - I\cdot\alpha\ ,\ c_{max} + I\cdot\alpha]$, with $c_{max} = \max(c_k^1, c_k^2)$, $c_{min} = \min(c_k^1, c_k^2)$, and $I = c_{max} - c_{min}$. Hence, the parameter α allows us to make this crossover as disruptive as desired. Such combination method was successfully incorporated to SS in (Herrera et al. 2006; Santamaría et al. 2007b; Santamaría et al. 2009).

In our real-world application, we think that applying the Improvement Method to every trial solution could excessively decrease the exploratory capabilities of the global search strategies of the SS. Indeed, as stated in (Krasnogor and Smith 2005), "*The majority of memetic algorithms in the literature* (in this case, SS) *apply local search to every individual in every generation of the evolutionary algorithm, our model makes it clear that this is not mandatory*". Hence, we have considered a particular selective application criteria for the Improvement Method. It is easy to implement and some members of our research group have recently obtained promising results tackling the IR problem using it in the first stage of the CS problem, 3D skull modeling (Santamaría et al. 2009). This criterion considers a deterministic scheme, in which the trial solution will be improved using the Improvement Method only if it is better than any of its parents. In the said contribution, it has been demonstrated that this strategy is more suitable than others based on random schemes.

4.2.3.3 Reference Set Update Method

A static strategy for updating the *RefSet* is carried out: first, the Pool set is built by solution combination of all the pairs of solutions being considered and next the RefSet is updated with the solutions of the Pool set according to a quality criterion.

4.3 Experiments

This section is devoted to develop an experimental study allowing us to validate the performance of the new SS-based skull-face overlay process proposed in this chapter. To do so, we first introduce the six different real-world skull-face overlay problems to be tackled, and then we show the parameter setting considered in the experiments. Next, we present the obtained results and their analysis, by developing a comparison with respect to the previously proposed CMA-ES-based method.

4.3.1 Case studies and experimental setup

Our experimental study will involve six different skull-face overlay problem instances, corresponding to four real-world cases previously addressed by the staff of the Physical Anthropology lab at the University of Granada in collaboration with the Spanish scientific police. Those four identification cases were solved following a computer-supported but manual approach for CS. Two of them, Cádiz and Mallorca case studies, have been already introduced in Sections 3.5.3 and 3.5.4 of Chapter 3. For the new cases we consider their 2D photographs (Figure 4.3) and their corresponding 3D skull models (Figure 4.4) acquired at the lab by using a Konica-Minolta© 3D Lasserscanner VI-910.

The first new case study is related with the skeletal remains of an old man found in the surroundings of Granada, Spain. Only one photograph, in a completely lateral pose, was provided by the family. The forensic experts identified seven 2D landmarks on it. We have named it “Granada”.

The second new case study also happened in Granada, Spain. Two photographs, acquired at different moments (Figure 4.3), were provided by the family. Hence, this case consists of two different skull-face overlay instances. The forensic anthropologists manually selected eight and fourteen 2D landmarks in the first and second photograph, respectively. This case case was named as “Portuguese” due to the nationality of the person that was later identified.

Figure 4.3: Face photographs of the missing people. From left to right. Granada case study and Portuguese case study, poses 1 and 2.

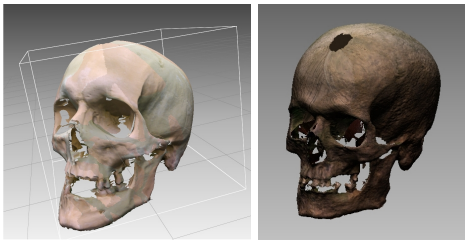

Figure 4.4: 3D skull models of Granada (left) and Portuguese (right) case studies.

Regarding the experimental setup, we will first study the performance of the proposed SS algorithm considering different settings. For that aim, we will start by analyzing its behavior when considering and not considering the advanced initialization approach proposed in Section 4.2.2, i.e., applying and not applying the restriction of the rotation angles. Then, we will compare its performance with that of the CMA-ES-based approach in terms of accuracy, robustness, and convergence speed. Different experiments were done considering several values for the number of evaluations (30,000, 60,000, 100,000, 150,000, and 300,000) in order to compare the convergence speed.

For the SS, the initial diverse set P comprises $Psize = 30$ solutions and the $RefSet$ is composed of the $b = 12$ best ones of them. BLX-α is applied with $\alpha = 1$ (Lozano et al. 2004b), while the *Improvement Method* is selectively applied during 40 iterations each time.

In the case of CMA-ES, the same values used in Section 3.5.1 of Chapter 3 were taken. In addition, we use the value 0.1 for the initial θ due to its better performance reported in Section 3.5 of the same Chapter.

In order to avoid execution dependence, thirty different runs for each parameter setting have been performed and different statistics (best result, worst result, mean, and standard deviation over the thirty runs) are provided. All the methods are run on a PC with an AMD Athlon 64 X2 Dual (2 core 2.59GHz), 2 GB of RAM, and Linux CentOS. We considered the ME for the assessment of the final superimposition results. Besides, some graphical representations of the obtained overlays are also shown in order to allow for a visual assessment.

4.3.2 Scatter search-based method results analysis

As it has been mentioned before, we will study the performance of the proposed SS algorithm by comparing its behavior applying and not applying the restriction of the rotation angles, i.e., considering and not considering the advanced initialization strategy, respectively. Tables 4.1 to 4.6 show the corresponding results for each of the six different skull-face overlay cases. For each algorithm (SS and CMA-ES), the best (Min.), the worst (Max.), the mean (Mean), and the standard deviation (St.Dev.) values for the fitness function (see Equation 3.8 in Chapter 3) after thirty runs are shown. The best minimum and mean results in each table are highlighted in bold.

Table 4.1: Cádiz case study, pose 1. Comparison between CMA-ES and SS results.

Case	Algorithm	Initialization	Evals (thousands)	Min.	Max.	Mean	St.Dev.
1, pose 1	SS	No	30	0.021	0.133	0.095	0.036
1, pose 1	SS	No	60	0.019	0.123	0.052	0.031
1, pose 1	SS	No	100	0.018	0.097	0.033	0.013
1, pose 1	SS	No	150	0.018	0.037	0.030	0.005
1, pose 1	SS	No	300	0.018	0.037	0.028	0.006
1, pose 1	SS	Yes	30	**0.015**	0.126	0.063	0.041
1, pose 1	SS	Yes	60	0.015	0.110	0.037	0.023
1, pose 1	SS	Yes	100	0.015	0.043	0.027	0.011
1, pose 1	SS	Yes	150	0.015	0.043	0.027	0.011
1, pose 1	SS	Yes	300	0.015	0.043	0.024	0.010
1, pose 1	CMA-ES	No	30	**0.015**	0.121	0.069	0.035
1, pose 1	CMA-ES	No	60	0.015	0.120	0.067	0.032
1, pose 1	CMA-ES	No	100	0.015	0.057	0.027	0.012
1, pose 1	CMA-ES	No	150	0.015	0.040	0.023	0.009
1, pose 1	CMA-ES	No	300	0.015	0.036	**0.020**	0.007
1, pose 1	CMA-ES	Yes	30	0.035	0.114	0.069	0.025
1, pose 1	CMA-ES	Yes	60	0.035	0.114	0.069	0.023
1, pose 1	CMA-ES	Yes	100	0.035	0.098	0.049	0.016
1, pose 1	CMA-ES	Yes	150	0.035	0.082	0.046	0.014
1, pose 1	CMA-ES	Yes	300	0.035	0.044	0.038	0.002

Table 4.2: Cádiz case study, pose 2. Comparison between CMA-ES and SS results.

Case	Algorithm	Initialization	Evals (thousands)	Min.	Max.	Mean	St.Dev.
1, pose 2	SS	No	30	**0.022**	0.157	0.032	0.024
1, pose 2	SS	No	60	0.022	0.038	0.024	0.003
1, pose 2	SS	No	100	0.022	0.027	0.023	0.001
1, pose 2	SS	No	150	0.022	0.027	0.023	0.001
1, pose 2	SS	No	300	0.022	0.027	0.023	0.001
1, pose 2	SS	Yes	30	**0.022**	0.060	0.025	0.008
1, pose 2	SS	Yes	60	0.022	0.033	**0.022**	0.002
1, pose 2	SS	Yes	100	0.022	0.024	0.022	0.000
1, pose 2	SS	Yes	150	0.022	0.023	0.022	0.000
1, pose 2	SS	Yes	300	0.022	0.023	0.022	0.000
1, pose 2	CMA-ES	No	30	**0.022**	0.171	0.071	0.060
1, pose 2	CMA-ES	No	60	0.022	0.171	0.069	0.058
1, pose 2	CMA-ES	No	100	0.022	0.039	0.024	0.004
1, pose 2	CMA-ES	No	150	0.022	0.053	0.024	0.006
1, pose 2	CMA-ES	No	300	0.022	0.046	**0.022**	0.004
1, pose 2	CMA-ES	Yes	30	0.064	0.165	0.104	0.038
1, pose 2	CMA-ES	Yes	60	0.063	0.161	0.089	0.031
1, pose 2	CMA-ES	Yes	100	0.063	0.143	0.070	0.018
1, pose 2	CMA-ES	Yes	150	0.063	0.098	0.065	0.006
1, pose 2	CMA-ES	Yes	300	0.063	0.064	0.063	0.000

In view of the results shown in the two top blocks of the tables, we can observe how, in most of the cases, the best minimum result obtained by the algorithm is the same regardless whether the initialization strategy is considered or not. Only in one of the problem instances, the first pose of Cádiz case study, the minimum value finally achieved by considering the initialization strategy is better than that obtained without using it (0.015 vs. 0.018, see Table 4.1). Besides, the derivation of this result requires only developing 30,000 evaluations in comparison with the 100,000 evaluations performed by the latter SS variant (i.e., the SS variant including the "intelligent" initialization is more than three times faster). In the remaining five instances, the use of the advanced initialization strategy has no influence (neither positive nor negative) over the quality of the best minimum result.

Nevertheless, the fact that the initialization allows the algorithm to become more robust can be easily checked in view of the mean and standard deviation values of the thirty runs performed and collected in the six tables of results. Notice that, the SS variant with initialization outperforms the variant not considering it in terms of mean results in all the problem instances considered. This performance advantage is also supported by the fact that it also achieves lower standard deviation values in all the cases but one (case study Cádiz-pose 1, see Table 4.1). Nevertheless, we should

Table 4.3: Granada case study. Comparison between CMA-ES and SS results.

Case	Algorithm	Initialization	Evals (thousands)	Min.	Max.	Mean	St.Dev.
2	SS	No	30	**0.018**	0.167	0.033	0.026
2	SS	No	60	0.018	0.056	0.028	0.008
2	SS	No	100	0.018	0.054	0.028	0.007
2	SS	No	150	0.018	0.049	0.027	0.007
2	SS	No	300	0.018	0.043	0.026	0.006
2	SS	Yes	30	**0.018**	0.170	0.030	0.026
2	SS	Yes	60	0.018	0.034	0.024	0.004
2	SS	Yes	100	0.018	0.034	0.024	0.004
2	SS	Yes	150	0.018	0.034	0.023	0.004
2	SS	Yes	300	0.018	0.034	0.023	0.004
2	CMA-ES	No	30	**0.018**	0.198	0.110	0.070
2	CMA-ES	No	60	0.018	0.218	0.121	0.065
2	CMA-ES	No	100	0.018	0.083	0.026	0.014
2	CMA-ES	No	150	0.018	0.027	0.023	0.004
2	CMA-ES	No	300	0.018	0.027	**0.020**	0.004
2	CMA-ES	Yes	30	0.103	0.193	0.168	0.022
2	CMA-ES	Yes	60	0.090	0.186	0.145	0.021
2	CMA-ES	Yes	100	0.072	0.178	0.123	0.030
2	CMA-ES	Yes	150	0.070	0.162	0.109	0.022
2	CMA-ES	Yes	300	0.068	0.125	0.088	0.017

note that this single standard deviation loss is justified by an important reduction in the mean value.

Furthermore, the SS variant considering the initialization strategy has also shown to converge more quickly than its counterpart which does not make use of this component. We should highlight that the best mean value achieved for the latter SS variant after 300,000 evaluations is always outperformed by the initialization-based SS taking a significantly lower number (and thus a shorter run time). This value is reduced to 100,000 evaluations in two instances (Cádiz-pose 1 and Portuguese-pose 1 cases), 60,000 evaluations in another two instances (Cádiz-pose 2 and case Granada cases), and even to 30,000 evaluations in the other two instances (Portuguese-pose 2 and Mallorca cases).

In view of these results, we can assert that the inclusion of the initialization strategy performing a restriction on the rotation angles in the SS method implies a more robust behavior and a faster convergence.

Table 4.4: Portuguese case study, pose 1. Comparison between CMA-ES and SS results.

Case	Algorithm	Initialization	Evals (thousands)	Min.	Max.	Mean	St.Dev.
3, pose 1	SS	No	30	**0.042**	0.057	0.046	0.004
3, pose 1	SS	No	60	0.042	0.057	0.046	0.004
3, pose 1	SS	No	100	0.042	0.057	0.046	0.004
3, pose 1	SS	No	150	0.042	0.057	**0.045**	0.004
3, pose 1	SS	No	300	0.042	0.057	0.045	0.004
3, pose 1	SS	Yes	30	**0.042**	0.061	0.046	0.003
3, pose 1	SS	Yes	60	0.042	0.060	0.046	0.003
3, pose 1	SS	Yes	100	0.042	0.060	**0.045**	0.003
3, pose 1	SS	Yes	150	0.042	0.060	0.045	0.003
3, pose 1	SS	Yes	300	0.042	0.060	0.045	0.003
3, pose 1	CMA-ES	No	30	**0.042**	0.284	0.186	0.107
3, pose 1	CMA-ES	No	60	0.042	0.285	0.189	0.111
3, pose 1	CMA-ES	No	100	0.042	0.239	0.078	0.066
3, pose 1	CMA-ES	No	150	0.042	0.218	0.068	0.050
3, pose 1	CMA-ES	No	300	0.042	0.256	0.053	0.040
3, pose 1	CMA-ES	Yes	30	0.076	0.284	0.184	0.090
3, pose 1	CMA-ES	Yes	60	0.076	0.286	0.190	0.089
3, pose 1	CMA-ES	Yes	100	0.066	0.273	0.094	0.042
3, pose 1	CMA-ES	Yes	150	0.059	0.186	0.081	0.021
3, pose 1	CMA-ES	Yes	300	0.060	0.098	0.076	0.007

4.3.3 Comparison with respect to the state-of-the-art results

In this second experimental study we focus on comparing the performance of the proposed SS-based skull-face overlay method algorithm with respect to that achieved by the CMA-ES-based one. For this aim, we take into account the best configuration for CMA-ES and for SS. As it was demonstrated in Section 4.3.2, SS works better when the initialization strategy based on the rotation angles restriction is considered. Hence, in order to develop a fair comparison, we have incorporated that novel component to the CMA-ES-based skull-face overlay method proposed in Chapter 3. We have thus studied the behavior of CMA-ES algorithm with and without this initialization. Nevertheless, on the contrary to the SS case, this mechanism to reduce the search space did not manage to improve CMA-ES results, as can be seen in the two bottom blocks of Tables 4.1 to 4.6. Indeed, the algorithm's performance gets worse once we included the delimitation of the rotation angles. It seems that, although the advanced initialization induces an appropriate intensification-diversification trade-off within the SS design, that is not the case for CMA-ES which shows a less flexible structure.

Tables 4.1 to 4.6 show CMA-ES and SS results for the six cases of study. Due

Table 4.5: Portuguese case study, pose 2. Comparison between CMA-ES and SS results.

Case	Algorithm	Initialization	Evals (thousands)	Min.	Max.	Mean	St.Dev.
3, pose 2	SS	No	30	**0.058**	0.069	0.063	0.003
3, pose 2	SS	No	60	0.058	0.068	0.062	0.003
3, pose 2	SS	No	100	0.058	0.068	0.062	0.003
3, pose 2	SS	No	150	0.058	0.068	0.062	0.003
3, pose 2	SS	No	300	0.058	0.068	0.062	0.003
3, pose 2	SS	Yes	30	**0.058**	0.069	**0.059**	0.002
3, pose 2	SS	Yes	60	0.058	0.064	0.059	0.001
3, pose 2	SS	Yes	100	0.058	0.063	0.059	0.001
3, pose 2	SS	Yes	150	0.058	0.063	0.059	0.001
3, pose 2	SS	Yes	300	0.058	0.063	0.059	0.001
3, pose 2	CMA-ES	No	30	**0.058**	0.331	0.256	0.101
3, pose 2	CMA-ES	No	60	0.058	0.330	0.243	0.118
3, pose 2	CMA-ES	No	100	0.058	0.318	0.101	0.079
3, pose 2	CMA-ES	No	150	0.058	0.302	0.105	0.067
3, pose 2	CMA-ES	No	300	0.058	0.149	0.070	0.026
3, pose 2	CMA-ES	Yes	30	0.161	0.331	0.290	0.053
3, pose 2	CMA-ES	Yes	60	0.156	0.331	0.293	0.062
3, pose 2	CMA-ES	Yes	100	0.141	0.328	0.214	0.062
3, pose 2	CMA-ES	Yes	150	0.142	0.323	0.219	0.066
3, pose 2	CMA-ES	Yes	300	0.141	0.299	0.177	0.038

to the reasons cited in the paragraph before, we directly compare CMA-ES without initialization against SS with initialization.

On one hand, the best minimum values achieved by both algorithms are exactly the same for five of the six cases considered. They are only significantly different in Mallorca case study, where SS clearly outperforms CMA-ES (0.010 vs. 0.029, see Table 4.3).

On the other hand, if we focus on the mean values of the thirty runs, SS improves CMA-ES results, for all the tested number of evaluations, in three cases: Portuguese-poses 1 and 2, and Mallorca (see Tables 4.4, 4.5, and 4.6). In the other three cases (Cádiz-poses 1 and 2, and Granada) SS improves all CMA-ES results excepting for the case of 300,000 evaluations. This results lead us to assert that SS converges more quickly than CMA-ES, despite the fact that when the number of evaluations is high (from 300,000 evaluations), there are some cases where CMA-ES finally achieves a slightly better mean accuracy than SS. Besides, we should notice the low standard deviation values obtained by SS, which are an additional proof of its robustness.

Finally, to allow for a visual inspection of the obtained overlays, Figures 4.5,

Table 4.6: Mallorca case study. Comparison between CMA-ES and SS results.

Case	Algorithm	Initialization	Evals (thousands)	Min.	Max.	Mean	St.Dev.
4	SS	No	30	**0.010**	0.043	0.019	0.008
4	SS	No	60	0.010	0.042	0.019	0.008
4	SS	No	100	0.010	0.042	0.019	0.008
4	SS	No	150	0.010	0.042	0.019	0.008
4	SS	No	300	0.010	0.042	0.019	0.008
4	SS	Yes	30	**0.010**	0.031	0.017	0.006
4	SS	Yes	60	0.010	0.029	0.017	0.006
4	SS	Yes	100	0.010	0.029	0.017	0.005
4	SS	Yes	150	0.010	0.029	0.017	0.005
4	SS	Yes	300	0.010	0.029	**0.016**	0.005
4	CMA-ES	No	30	0.063	0.284	0.261	0.051
4	CMA-ES	No	60	0.032	0.285	0.233	0.081
4	CMA-ES	No	100	0.029	0.275	0.105	0.087
4	CMA-ES	No	150	0.029	0.271	0.102	0.083
4	CMA-ES	No	300	0.029	0.251	0.069	0.055
4	CMA-ES	Yes	30	0.264	0.287	0.283	0.004
4	CMA-ES	Yes	60	0.265	0.287	0.283	0.005
4	CMA-ES	Yes	100	0.142	0.284	0.244	0.045
4	CMA-ES	Yes	150	0.139	0.283	0.231	0.044
4	CMA-ES	Yes	300	0.137	0.280	0.204	0.045

4.6, and 4.7 graphically represent the best skull-face overlay results obtained by the two algorithms in the thirty runs performed. The corresponding worst results are shown in Figures 4.8, 4.9, and 4.10. These overlays correspond to the best configuration of CMA-ES and SS, after 300,000 evaluations. Notice that, visual results of Mallorca case study are not shown since we are not allowed to publish them due to legal reasons.

In all the cases, the best overlays are almost the same. In contrast, the worst overlays obtained by SS are usually better than those provided by CMA-ES. The CMA-ES result is only better for Cádiz-pose 1 case. On the contrary, the SS results are slightly better in SS for Cádiz-pose 2 and Portuguese-pose 1 cases, as well as much better for Portuguese-pose 2 case. In the remaining instance (Granada case), both results could be considered as showing a similar low quality.

4.4 Concluding remarks

In this chapter, we have introduced the use of a novel metaheuristic framework, SS, as a new 3D-2D IR optimizer for the skull-face overlay task in forensic identification by CS. Having in mind the interesting properties and the recent successful outcomes

Figure 4.5: Best skull-face overlay results for Cádiz-poses 1 and 2 cases. For both cases, the first image corresponds to the CMA-ES result and the second to the SS one.

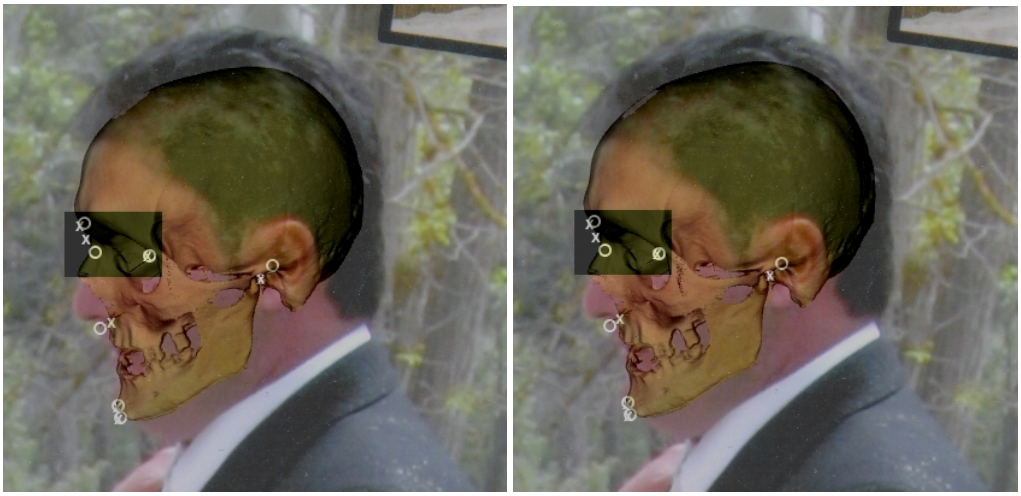

Figure 4.6: Best skull-face overlay results for Granada case. The first image corresponds to the CMA-ES result and the second to the SS one.

achieved by the former technique in other global optimization problems (Laguna and Martí 2003), our starting point was focused on the suitable design of the SS components and the way they were assembled, in order to achieve faster and more robust solutions to the skull-face overlay problem.

We have proposed a method to properly initialize the algorithm and to restrict the parameter ranges using problem-specific information (domain knowledge). That "intelligent" initialization is based on the orientation of the skull to a frontal pose and

Figure 4.7: Best skull-face overlay results for Portuguese-poses 1 and 2 cases. For both cases, the first image corresponds to the CMA-ES result and the second to the SS one.

Figure 4.8: Worst skull-face overlay results for Cádiz-poses 1 and 2 cases. For both cases, the first image corresponds to the CMA-ES result and the second to the SS one.

the corresponding limitation of the rotation angles, which results in a significant reduction of the solution space, thus easing the problem solving.

We have presented and discussed skull-face overlay results obtained on six real-world identification cases. A sound experimental study to compare the robustness and convergence speed regarding the use of the proposed initialization has been performed. We have demonstrated the benefits (faster convergence and higher robustness) of including this advanced strategy in the proposed SS algorithm. Indeed, the run time needed for SS to achieve the best skull-face overlay showed goes from 10 to 20 seconds (depending on the size of the image and the number of landmarks used) while in the case of CMA-ES goes from 30 to 40 seconds.

Besides, we have shown how it does not properly cooperate with the existing CMA-ES design to solve the problem. The main experimentation dealt with a comparison between the proposed SS and our previous CMA-ES-based skull-face overlay

Figure 4.9: Worst skull-face overlay results for Granada case. The first image corresponds to the CMA-ES result and the second to the SS one.

Figure 4.10: Worst skull-face overlay results for Portuguese-poses 1 and 2 cases. For both cases, the first image corresponds to the CMA-ES result and the second to the SS one.

procedure. Despite both algorithms have a really good behavior, achieving similar minima, our new proposal has been shown to converge faster than CMA-ES and to behave more robustly in view of the mean values obtained in the thirty runs developed.

However, as it shown in Cádiz case study, pose 2, the evolutionary-based method needs improvements. To do so, Chapter 5 will present a new proposal that uses fuzzy set theory for that aim.

Chapter 5

Modeling the Skull-Face Overlay Uncertainty Using Fuzzy Logic

As far as the laws of mathematics refer to reality,
they are not certain; and as far as they are certain,
they do not refer to reality.

Albert Einstein (1879-1955)

5.1 Introduction

The whole CS process is influenced by uncertainty. In particular, skull-face overlay is affected by two different sources of uncertainty of different nature. On the one hand, there is uncertainty inherently associated with the two different kinds of objects involved in the skull-face overlay process, i.e. a skull and a face. On the other hand, there is also uncertainty associated with the proposed 3D-2D overlay that tries to superimpose a 3D model over a 2D image.

In this chapter we will try to overcome most of the limitations associated with the different sources of uncertainty, namely: the difficult task of invariantly locating anthropometric landmarks, the precise location of cephalometric landmarks in digital photographs with a poor quality, and the inability to locate a large set of (non coplanar) landmarks due to occlusions. With that aim, two different approaches to handle the imprecision in landmark location will be proposed: weighted and fuzzy set theory-based. Specifically, fuzzy sets have largely demonstrated their capability to deal with vagueness and imprecise information (Klir and Yuan 1996).

The structure of the chapter is as follows. First we will study the two said sources of uncertainty in detail (Sections 5.2 and 5.3). Section 5.4 will be devoted to study the influence of coplanar set of landmarks in a synthetic 3D skull model-2D skull photograph overlay case. Then, we will introduce our proposal to deal with the different sources of uncertainty (see Section 5.5). In Section 5.6, we will test our proposals over four different skull-face overlay problem instances. Finally, we will present some concluding remarks in Section 5.7.

5.2 Uncertainty inherently associated with the objects under study

We have identified two inherent sources of uncertainty regarding the objects under study (a skull and a face) and their relationship. On the one hand, the *landmark location uncertainty* is related to the extremely difficult task of locating the points in an invariable place, since the definition of any anthropometric landmark is imprecise as it has been shown in Chapter 1, Section 1.2.2. For example, the Ectocanthion is the point at the outer commissure of the palpebral fissure just medial to the malar tubercle to which the lateral palpebral ligaments are attached. Indeed, every forensic anthropologist is prone to locate the landmarks in a slightly different position (Richtsmeier et al. 1995), regardless the means used to represent the involved objects (skull and face), i.e. 3D model, 2D photo, video-shot, ... Figure 5.1 shows some examples of this situation.

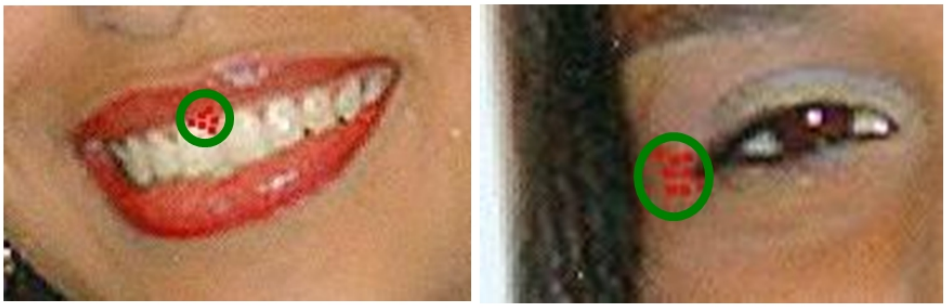

Figure 5.1: Examples of precise landmark location (each red spot) by different forensic anthropologists. Labiale superius (left) and right ectocanthion (right) landmarks.

On the other hand, the *landmark matching uncertainty* refers to the imprecision involved in the matching of two sets of landmarks corresponding to two different objects: a face and a skull. As shown in Figure 5.2, there is a clear partial matching situation. The correspondence between facial and cranial anthropometric landmarks is not always symmetrical and perpendicular, some landmarks are located in a higher position in the alive person face than in the skull, and some others have not got a directly related landmark in the other set (Iscan 1993). Besides, the facial soft tissue depth varies for each cephalometric landmark and also for every person group (regarding age, race, and sex). Many works have been done in order to study distances between each pair of anthropometric landmarks for different groups of study. The interested reader is referred to Stephan et al. (2008a, 2008b) for a deep review. In addition, in the case of skull-face overlay, considerations of how these distances are affected by the pose of the face in

the image have to be taken into account.

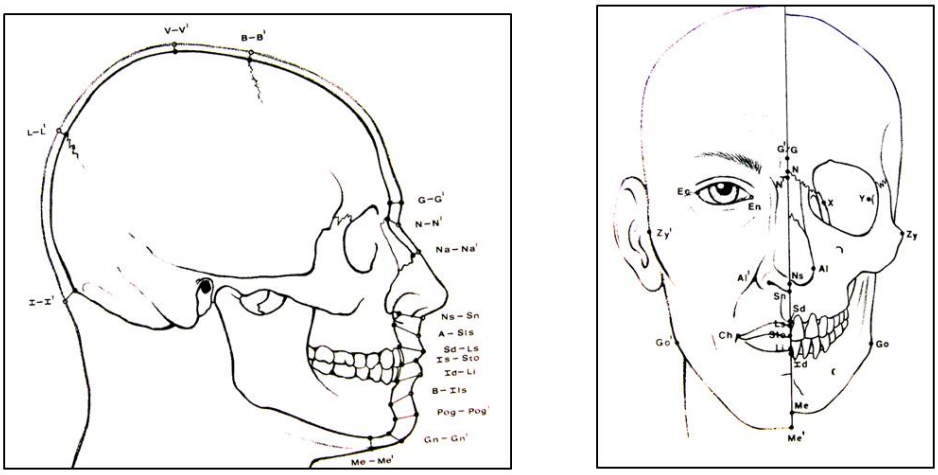

Figure 5.2: Correspondences between facial and craniometric landmarks: lateral (left) and frontal (right) views.

5.3 Uncertainty associated with the 3D skull model-2D face photo overlay process

The uncertainty associated with the 3D skull model-2D face photo overlay is inherent to our proposed approach, where we try to overlay a 3D model and a 2D image. As done in Section 5.2, we can also distinguish between landmark matching and landmark location uncertainty. However, the nature of these two sources of uncertainty is different in the current case.

On the one hand, the landmark location uncertainty refers to the difficulty of locating landmarks with the accuracy required for this application, i.e., the automatic overlay of a 3D skull model and a 2D face photo. The ambiguity may arise from reasons like variation in shade distribution depending on light condition during photographing, unsuitable camera focusing, poor image quality, face pose in the photograph, partial or whole landmark occlusion, etc. Of course, the location uncertainty may affect any of the landmarks involved in the skull-face overlay process, regardless if they belong to the face photograph or the skull model. Nevertheless, it has a stronger influence on the cephalometric (i.e., facial) ones because of the typical high resolution of the 3D

skull models carrying the craniometric landmarks. In addition, 3D models do not suffer from occlusions originated by the projection as 2D photographs do. Forensic experts are prone to only locate those landmarks which can be unquestionably identified in the 3D skull model and, especially, in the photograph. Due to different reasons as the pose of the missing person, the quality of the image, or partial occlusions of landmark regions, it can be difficult for the anthropologists to do so for many of the existing cephalometric landmarks. Therefore, forensic experts are usually only able to locate a reduced set of all the available cephalometric landmarks.

On the other hand, the matching uncertainty refers to the influence of a small number of landmarks with a unsuitable spatial distribution in the 3D-2D overlay results. As a consequence of the fact described in the previous paragraph, the landmark set usually handled by the forensic experts is coplanar or near-coplanar. In fact, we already noticed how the resulting skull-face overlay degenerates to undesirable solutions when these kinds of landmark sets are considered (see the skull-face overlay results over Cádiz-pose 2 case study in Chapters 3 and 4). Furthermore, those case studies where the pose of the face in the photograph is frontal or near-frontal are preferred by the forensic experts because they normally show a higher number of landmarks as well as the symmetries of the face can be easily perceived. This situation causes 3D skull-2D face overlay to be more affected by this coplanarity problem (as we will show in Section 5.4).

This landmark coplanarity makes the equation system (objective function of the IR procedure) become undetermined (or near-undetermined), i.e. there is uncertainty (there is not enough information or it is imprecise) regarding which of the possible solutions is the best. It is not possible to numerically distinguish among the different resulting (after a search process) sets of projection parameters which originate different skull-face overlay results.

Looking through the CV field, we can clearly relate the skull-face overlay process (and in general every kind of 3D-2D overlay) to another well known process called camera calibration (CC) (Hartley and Zisserman 2004). The aim of CC is to study the relationship between 3D world coordinates and their corresponding 2D image coordinates that have been acquired by a camera. Reviewing the main CC approaches existing in the specialized literature, we found that they normally carry out a process composed of two different stages:

- Determination of the *intrinsic parameters*, the center of focus and focal length of the camera.
- Determination of the *extrinsic parameters*, the rigid transformation (rotation and

translation) that links the camera coordinate system to the world coordinate system. That means finding the pose of the camera that properly superimposes scene and photo.

These intrinsic/extrinsic CC parameters are commonly derived from 3D-2D landmark correspondences (the strong similarity with the skull-face overlay problem can thus be recognized). There is a broad number of CV works tackling the data/landmark collection problem in CC (Salvi et al. 2002). In particular, Tsai (Tsai 1986) faced the CC problem when coplanar landmarks are used, i.e. the 3D landmarks lie on the same plane.

The number of correspondences n that are necessary to solve the CC problem in a general framework is studied as follows. In general, when the internal parameters are known, $n = 3$ leads to four possible solutions. When either $n = 4$ or $n = 5$, there are at least two solutions in general configurations. However, when the landmarks are coplanar and there are not triplets of collinear landmarks then the solution is unique for $n \geq 4$. Finally, in the case of having coplanar landmarks with triplets of collinear ones, the solution is unique for $n \geq 6$.

Nevertheless, in our case, we have to face the undesired situation that all the internal parameters are unknown because the camera used to acquire the photograph of the missing person is usually unknown. Hence, they must be also estimated during the optimization procedure. Thus, the previous assertions about the number of 3D-2D correspondences cannot be considered and having a large landmark set becomes a real need.

The next section will be devoted to study the influence of coplanar landmarks in a synthetic 3D skull model-2D skull photograph overlay case.

5.4 Coplanarity study in skull-face overlay

This preliminary study aims to analyze the behavior of an EA tackling a synthetic 3D skull model-2D skull photograph overlay problem when coplanar landmarks are considered. This synthetic experiment, not directly related with craniofacial identification, aims to show the negative effects of having a coplanar set of landmarks in our framework. In addition, it also shows how the coplanarity problem can be solved by increasing the size of the landmark sets.

Unlike the usual skull-face overlay procedure, the current synthetic case does not consider face and skull as two different objects to deal with during the overlay

process. As a first approach to the coplanarity problem, we have preferred to simplify skull-face overlay by considering the same object. The reason is that, proceeding in this way, the 3D-2D overlay problem is not influenced by the inherent uncertainty existing when considering two different objects (see Section 5.2). In particular, the case study is based on two different poses of a real human skull provided by the Physical Anthropology lab at the University of Granada (Spain). A rotated (lateral) and a frontal pose photographs of the skull are considered. Regarding the craniometric landmark set, we simulated the procedure followed by the forensic experts and marked seven landmarks on the skull 3D model surface. Although a set of theoretically coplanar landmarks is unfeasible in our skull 3D model, we selected a near-coplanar set of craniometric landmarks. In a real skull-face overlay case, cephalometric landmarks are identified as relevant facial features in the 2D photograph. In this synthetic study, cephalometric landmarks directly correspond to the projected craniometric landmarks onto the image (skull photo) plane. Figure 5.3 depicts the synthetic case and the two considered poses of the skull model, showing also the selected near-coplanar landmarks.

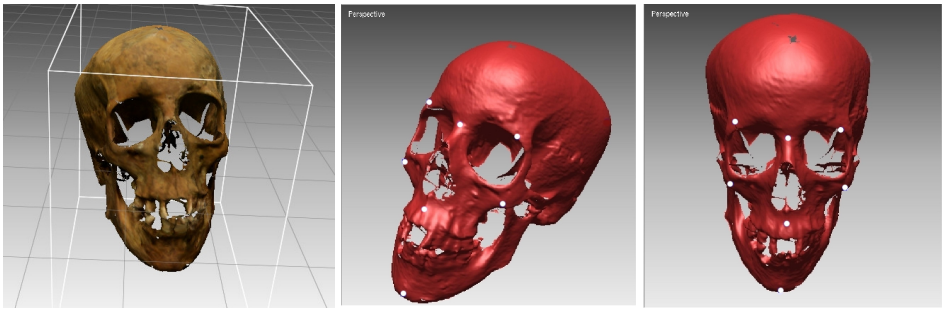

Figure 5.3: From left to right. 3D model of the skull and lateral and frontal poses of the synthetic human skull case. The 2D landmarks are highlighted in every photo using white circles.

Thirty different runs of the SS-based method proposed in Chapter 4 were performed for each of the two skull 3D-2D overlay problem instances, i.e.: a) overlay of the 3D skull model and the 2D lateral pose photo, and b) overlay of the 3D skull model and the 2D frontal pose photo.

Focusing on the lateral pose, Figure 5.4 shows the good performance of SS when dealing with the seven selected landmarks. In the best overlay result, it is not possible to visually differentiate the projected 3D model and the 2D image.

Nevertheless, the behavior of the algorithm when dealing with the frontal pose

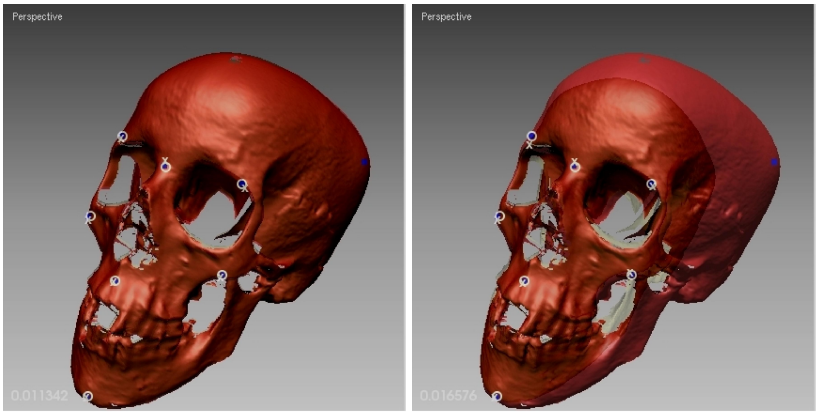

Figure 5.4: Best and worst superimposition results in the lateral pose. White crosses and circles are used to highlight 3D and 2D landmarks, respectively.

and the same seven landmarks is rather different (see the top row of Figure 5.5). The near-coplanar landmark situation leads to different low quality local minima as it is shown in the best and worst overlay results. However, adding a new landmark that lies on a different plane easily solves the previous undesirable situation (see the bottom row of Figure 5.5). Besides, notice that, the worst result is quite similar to the best one. Therefore, the robustness of the method is also demonstrated.

Taking into account that lateral and frontal poses share the same set of near-coplanar craniometric landmarks, this simple case study leads us to the following conclusion. The undesirable behavior of the 3D skull-2D face overlay optimization procedure is mainly due to: i) the definition of a coplanar or near-coplanar set of craniometric landmarks; and ii) the parallelism between the plane containing the craniometric landmarks and the camera image plane.

Therefore, a more robust alternative for solving this particular class of skull-face overlay optimization scenarios must be studied. We must also keep in mind that the real scenarios will become even more complex due to the uncertainty associated with consideration of two different objects, which has been ignored in the current preliminary experiment. The next section will introduce a proposal to deal with this problem which will also become a proper approach to handle some of the other uncertainty sources present in CS.

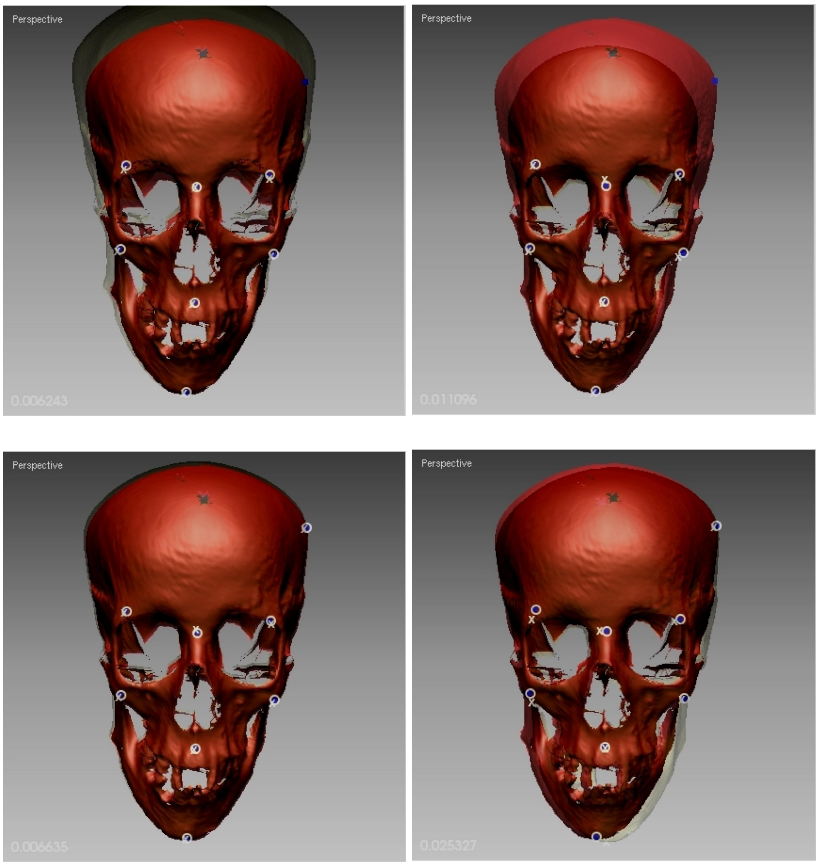

Figure 5.5: From left to right. The top row shows the best and the worst superimposition results of the frontal pose considering seven landmarks. The bottom row corresponds to the case of eight landmarks.

5.5 An imprecise approach to jointly tackle landmark location and coplanarity in automatic skull-face overlay

The most appropriate way to handle the latter source of uncertainty is to increase the number of landmarks. Nevertheless, this is not an easy task in a real environment like ours, as already mentioned. To overcome this problem, we propose a novel framework to allow the *imprecise location of landmarks*. By locating landmarks in a imprecise way, forensic experts will be able to locate a larger landmark set with the proper level

of confidence (using imprecise regions of different sizes). In contrast, following the classical precise approach, they would only be able to mark those landmarks whose position they can determine accurately. Hence, this approach presents an important advantage. The bigger the set of landmarks, the more complete the information available to guide the automatic search of the best transformation which properly superimpose the skull on the photograph. As already explained, those additional landmarks are essential to face the coplanarity problem.

At the same time, the use of *imprecise landmarks* in this work aims to handle the location uncertainty in the photograph of the missing person (see Figure 5.6). According to that problem, each forensic anthropologist could place each landmark in different positions in the 2D image. Hence, the higher the uncertainty related to a landmark, the broader the region where the forensic experts will locate the landmark.

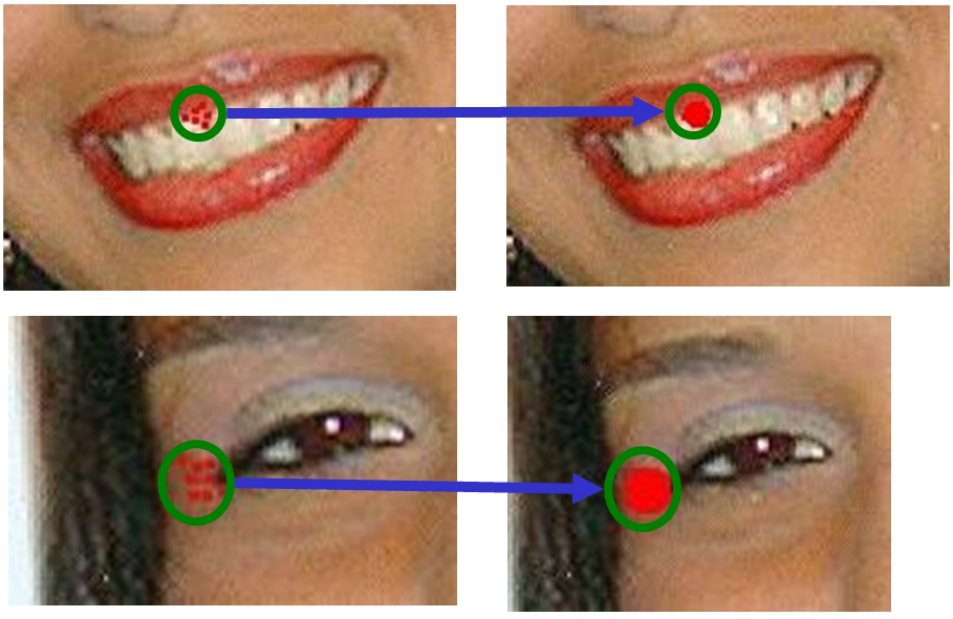

Figure 5.6: Examples of precise landmark location (on the left) and imprecise ones (on the right).

In summary, using an imprecise location of landmarks we are tackling the two sources of uncertainty associated with the 3D skull model-2D face photo overlay process (see Section 5.3 and the landmark location uncertainty associated with the two objects under study 5.2). Nevertheless, the landmark matching uncertainty associated

with the latter has not been tackled in this dissertation and will be left for future works.

The imprecise landmarks location approach is implemented through two alternative models of imprecise landmarks: weighted and fuzzy ones. The next two subsections are devoted to introduce them.

5.5.1 Weighted landmarks

Based on the work by Sinha (1998), we consider modeling the cephalometric landmarks as rectangular zones, instead of directly using crisp locations as usual. We will refer to these rectangular zones as weighted landmarks because they contribute to the optimization process depending on their size[1]. Every weighted landmark is given by a rectangular array of pixels defined by diagonally opposite corners (x_1, y_1) and (x_2, y_2) (say $x_2 > x_1$ and $y_2 > y_1$). Hence, the bigger the rectangle, the higher the uncertainty associated to the landmark (see Figure 5.7).

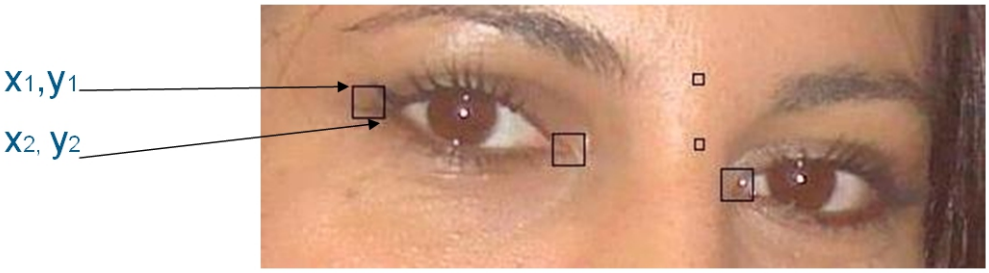

Figure 5.7: Example of weighted landmarks.

Sinha (1998) introduced the latter concepts to provide more robustness and tolerance to a NN designed to match 2D facial images. Ghosh and Sinha (2001) adapted the original proposal to tackle 2D CS (see Section 2.4.2.2 in Chapter 2). In these works, crisp points were substituted by rectangles to avoid human error due to image ambiguity. Each rectangular landmark was then temporarily "defuzzied" by taking the centroid as a crisp target feature. Those crisp features were used to learn the preliminary weights of the NN. Then, there was a later stage where the rectangle landmarks were adapted (reduced) by means of the NN responses. Limitations of Ghosh and Sinha approach has been already pointed out in Chapter 3, Section 3.2.2.

[1] Despite Sinha named them as fuzzy landmarks, we found that terminology incorrect since they are not based on fuzzy set theory at all.

In contrast to Sinha's work, which used these rectangular zones to train a NN, we will model this source of uncertainty to guide our evolutionary-based skull-face overlay procedure. In our case, this is done with the aim of avoiding local minima by prioritizing some landmarks (more precisely located) rather than others (imprecisely located). Notice that, proceeding in that way we establish an order of importance between the different landmarks selected by the forensic expert. While those showing a lower uncertainty have a higher influence to guide the search, those others less precisely located are also considered, although to a lower degree. Therefore, we have modified the previous definition of the objective function (see Chapter 3, Section 3.4.1) as follows:

$$Weighted_{ME_1} = \frac{\sum_{i=1}^{N} \sqrt{[u_i(x'_{ci} - x_{fi})]^2 + [v_i(y'_{ci} - y_{fi})]^2}}{N} \tag{5.1}$$

where x'_{ci} and y'_{ci} are respectively the coordinates of the transformed 3D craniometric landmark C_i in the projection plane, x_{fi} and y_{fi} are coordinates of the centroid of the weighted landmark of every 2D cephalometric landmark, and N is the number of considered landmarks. The terms u_i, v_i are used to represent the uncertainty around each landmark. Their value depends on the size of the rectangular zone, such that,

$$u_i = \frac{1}{1+|x_2 - x_1|} \quad v_i = \frac{1}{1+|y_2 - y_1|}$$

where (x_1, y_1) and (x_2, y_2) are diagonally opposite corners (Sinha 1998).

In this formulation, $(x_2 - x_1)$ and $(y_2 - y_1)$ are, respectively, measures of X and Y axis uncertainty. According to it, when the rectangle defining the weighted landmark is bigger (i.e., it shows a lower value of u_i and/or v_i), the corresponding weight in the fitness function (i.e., the landmark influence to guide the search) will be lower. Thus, the more imprecise the location of a landmark, the less important this landmark will be.

Alternatively, we propose a new formulation where, instead of providing weighting factors to the localization of each component of the Euclidean distance (Equation 5.1), we weight each component of the distance as follows:

$$Weighted_{ME_2} = \frac{\sum_{i=1}^{N} \sqrt{u_i(x'_{ci} - x_{fi})^2 + v_i(y'_{ci} - y_{fi})^2}}{N} \tag{5.2}$$

Notice that, $Weighted_{ME_2}$ is an alternative way to model the existing location uncertainty that strengthen it (note that the component square distance is multiplied

by u_i/v_i here while by u_i^2/v_i^2 in Equation 5.1. Both fitness functions will be tested in Section 5.6.

5.5.2 Fuzzy landmarks

In the weighted landmarks approach introduced in the previous section, we tackled the imprecise landmark location considering the cephalometric landmarks as rectangular zones of different size, instead of using crisp locations, taking inspiration from (Sinha 1998). However, we think that is a too simple way to represent the underlying uncertainty since all the possible crisp points in the rectangle are equally likely to be the actual location, which is not so realistic.

In addition, in that first approach we calculated the Euclidean distances between craniometric and cephalometric landmarks by using the centroid of the rectangle associated with the latter ones. Thus, once the centroids of the imprecise cephalometric landmarks were considered, the problem of computing distances between a set of imprecise landmarks and a set of crisp ones became the problem of measuring a set of Euclidean distances between different pairs of crisp landmarks.

In summary, that was just a first approach to model the location uncertainty, which did not take into account the inherent uncertainty involved when we are measuring distances between fuzzy and crisp points. In this subsection we will introduce a new imprecise landmark approach improving the previous one. It is based on allowing the forensic experts to locate the cephalometric landmarks using ellipses and on considering fuzzy sets to model the uncertainty related to them. Besides, we will also consider fuzzy distances to model the distance between each pair of craniometric and cephalometric landmarks.

To ease the comprehension of our formulation to the reader, we will first review some required basic concepts from fuzzy sets theory (Klir and Yuan 1996) as follows:

α-cuts definitions: For each $\alpha \in (0,1]$ the α-level set $\widetilde{A}_\alpha$ of a fuzzy set $\widetilde{A}$, $\mu_{\widetilde{A}} :\rightarrow [0,1]$, is $\widetilde{A}_\alpha = \{x \in X; \mu_{\widetilde{A}(x)} \geq \alpha\}$. Hence, the core $\widetilde{A}_1 = \{x \in X; \mu_{\widetilde{A}(x)} = 1\}$ of a fuzzy set is the subset of X whose elements have membership equal to 1. The support $\widetilde{A}_0$ is defined as the closure of the union of all its level sets, that is:

$$\widetilde{A}_0 = \overline{\bigcup_{\alpha \in (0,1]} \widetilde{A}_\alpha}$$

Distance between a point and a set of points: Given a point x of $\mathbb{R}^n$ and a nonempty

subset A of $\mathbb{R}^n$ we can define a distance $d : \mathbb{R}^n \times \mathbb{P}(\mathbb{R}^n) \to \mathbb{R}^+$ by:

$$d(x,A) = inf\{||x-a||; a \in A\}$$

for a certain norm $||.||$ on $\mathbb{R}^n$. Thus, $d(x,A) \geq 0$ and $d(x,A) = 0 \Rightarrow x \in A$.

Distance between a point and a fuzzy set of points: Now we can define the distance between a point x of $\mathbb{R}^n$ an a fuzzy set of points $A : \mathbb{R}^n \to [0,1]$ by:

$$d^*(x,\widetilde{A}) = \int_0^1 d(x,\widetilde{A}_\alpha) d\alpha$$

Lemma 5.5.1. *The distance from the point x to the fuzzy set $\widetilde{A}$ is lesser or equal than the distance to the core of $\widetilde{A}$ and greater or equal than the distance to the support of $\widetilde{A}_0$. That is,*

$$d(x,\widetilde{A}_1) \leq d^*(x,\widetilde{A}) \leq d(x,\widetilde{A}_0)$$

The proof is straight forward.

In case that we have a discrete fuzzy set of points $\widetilde{A} = x_1/\alpha_1 + \cdots + x_m/\alpha_m$, the distance can be expressed by:

$$d^*(x,\widetilde{A}) = \frac{\sum_{i=1}^{m} d(x,\widetilde{A}_{\alpha_i}) \cdot \alpha_i}{\sum_{i=1}^{m} \alpha_i}$$

Following the idea of metric spaces in (Diamond and Kloeden 2000) we will define a fuzzy landmark as a fuzzy convex set of points having a nonempty core and a bounded support. That is, all its α-levels are nonempty bounded, and convex sets.

In our case, since we are dealing with 2D photographs with an $x \times y$ resolution, we can define the fuzzy landmarks as 2D masks represented as a matrix m with $m_x \times m_y$ points (i.e., a discrete fuzzy sets of pixels). Each fuzzy landmark will have a different size depending on the imprecision on its localization but at least one pixel (i.e. crisp point related to a matrix cell) will have membership with degree one.

These masks are easily built starting from two triangular fuzzy sets $\widetilde{V}$ and $\widetilde{H}$ modeling the approximate vertical and horizontal position of the ellipse representing the location of the landmark, thus becoming two-dimensional fuzzy sets. Each triangular fuzzy set $\widetilde{A}$ is defined by its center c and its offsets l, r as follows:

$$\widetilde{A}(x) = \begin{cases} 1 - \frac{|x-c|}{c-l}, & \text{if } l \leq x \leq c \\ 1 - \frac{|x-c|}{r-c}, & \text{if } c < x \leq r \\ 0, & \text{otherwise} \end{cases}$$

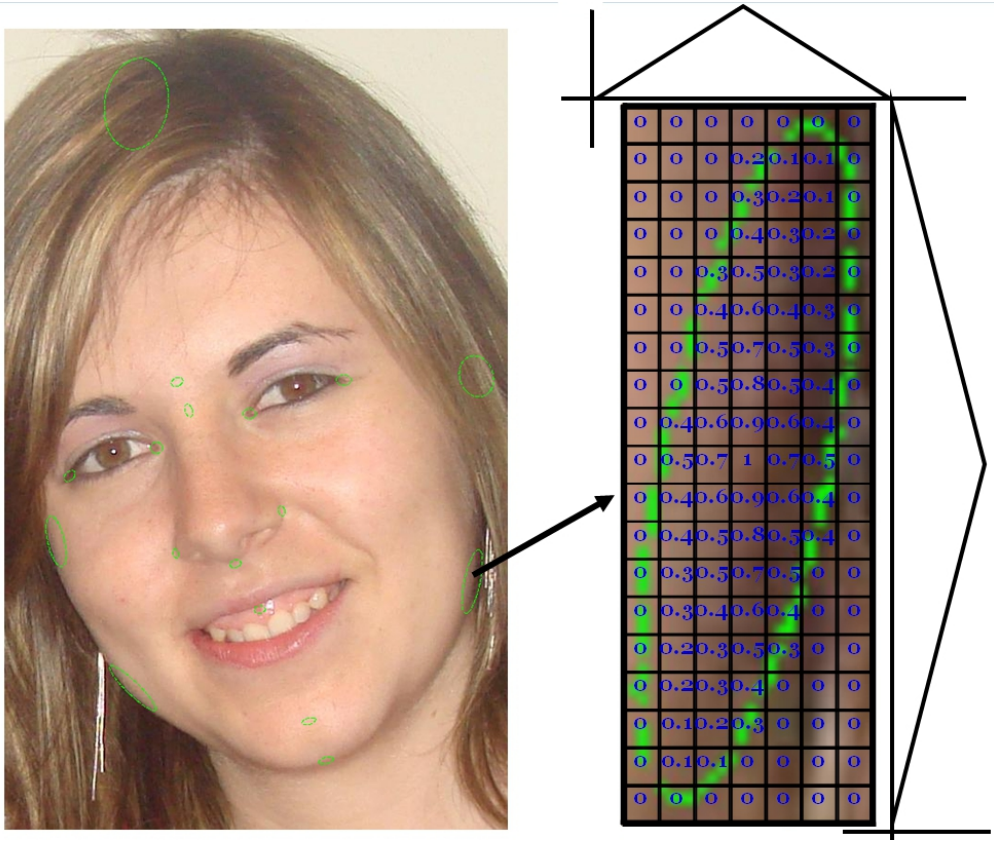

Figure 5.8: Example of fuzzy location of cephalometric landmarks (on the left) and representation of an imprecise landmark using fuzzy sets (on the right).

and the membership functions of the fuzzy landmarks are calculated using the product t-norm by:

$$\mu_{\widetilde{F}}(i,j) = \mu_{\widetilde{V}}(i) \cdot \mu_{\widetilde{H}}(j)$$

An example of these fuzzy cephalometric landmarks is given in Figure 5.8, where the corresponding membership values of the pixels of one of those landmarks is depicted on the right.

Now we can calculate the distance between a point (which will be the pixel constituting the projection of a 3D craniometric landmark on the 2D face photo) and a fuzzy landmark (the discrete fuzzy set of pixels representing the imprecise position of the cephalometric landmark), as depicted in Figure 5.9. Note that the implemented dis-

tance between a point and a fuzzy set of points is quite similar to that defined in (Dubois and Prade 1983). In fact, it was already used in other image processing applications in (Bloch 1999).

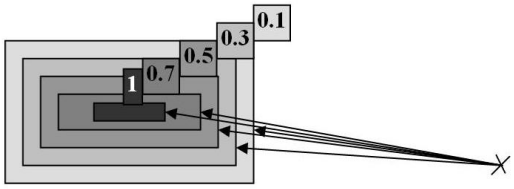

Figure 5.9: Distance between a crisp point and a fuzzy point

If we denote as $d_i = d(x, \widetilde{F}_{\alpha_i})$ the distance from point x to the α-level set $\widetilde{F}_{\alpha_i}$, then the distance from the point to the fuzzy landmark $\widetilde{F}$, can be expressed by:

$$d^*(x, \widetilde{F}) = \frac{\sum_{i=1}^{m} d_i \cdot \alpha_i}{\sum_{i=1}^{m} \alpha_i}$$

In the example of Figure 5.9, taking $\{\alpha_1 = 0.1, \alpha_2 = 0.3, \alpha_3 = 0.5, \alpha_4 = 0.7, \alpha_5 = 1\}$ and assuming $\{d_1 = 4.5, d_2 = 5.4, d_3 = 6.3, d_4 = 7.3, d_5 = 9\}$, we calculate the distance as:

$$d^*(x, \widetilde{F}) = \frac{d_1 \cdot \alpha_1 + \cdots + d_5 \cdot \alpha_5}{\alpha_1 + \cdots + \alpha_5} = \frac{19.33}{2.6} = 7.43$$

Therefore, we have modified the previous definition of our evolutionary-based skull-face overlay techniques' fitness function as follows:

$$\textit{fuzzy ME} = \frac{\sum_{i=1}^{N} d^*(f(cl^i), \widetilde{F}^i)}{N} \tag{5.3}$$

where N is the number of considered landmarks; cl^i corresponds to every 3D craniometric landmark; f is the function which defines the geometric 3D-2D transformation; $f(cl^i)$ represents the position of the transformed skull 3D landmark cl^i in the projection plane, that is to say, a crisp point; $\widetilde{F}^i$ represents the fuzzy set points of each 2D cephalometric landmark; and, finally, $d^*(f(C_i), \widetilde{F}^i)$ is the distance between a point and a fuzzy set of points.

5.6 Experiments

The experiments developed in this section are devoted to study the performance of the proposed approaches to model the imprecise location of cephalometric landmarks within our skull-face overlay method in comparison with the classical crisp location method (see Chapters 3 and 4). Section 5.6.1 presents the considered experimental design. Sections 5.6.2 and 5.6.3 describe the analysis of the overlay results on four different skull-face overlay problem instances from two real-world cases.

5.6.1 Experimental design

For all the experiments we used SS with the same set of parameters used in Chapter 4, guided by the corresponding objective functions, Equations 5.1 and 5.2 for weighted landmarks, and Equation 5.3 for fuzzy landmarks. Thirty independent runs were performed for each case.

Two different types of landmark sets were provided by the forensic experts for each available subject photograph in each case study. The first type is the one classically used in the manual overlay process, i.e., that considered in the previous chapters of this dissertation. It is composed of crisp landmarks, those the forensic anthropologists can place in a unquestionable single pixel. The second one is a set of imprecise landmarks, that is to say, a region for each landmark where the precise location of the landmark is to be contained. As said, in this second set, the forensic expert could place more landmarks than in the other, due to the possibility of drawing bigger (in size) square- or ellipse-shaped areas of different sizes associated with weighted regions or fuzzy sets of points.

We compare the results of the SS-based skull-face overlay method using a crisp set of landmarks with those reached by using imprecise locations of cephalometric landmarks (weighted and fuzzy landmarks). In order to perform a significant and fair comparison between the crisp and the imprecise approaches, we considered the following experimental design concerning the number of landmarks: two different sets of each kind of imprecise landmarks (weighted and fuzzy) are used, one with the same size (and, of course, the same specific landmarks) as the crisp set and another also including the additional landmarks identified thanks to the use of the imprecise location approach.

Finally, we should note that the numerical results are not significant because of the different objective functions to be minimized (as well as because of the different

number of landmarks considered). Besides, the ME is not necessarily in correspondence with the visual overlay results. Due to the latter two reasons, we adopted an alternative, specifically designed scheme to evaluate the performance of every skull-face overlay approach. First, the forensic experts approximately extracted the head boundary of the missing person in the photograph (they did so for all the cases of study). Next, we obtained a binary image of both the head boundary and the projected skull. Then, the XOR logic operator was applied considering both images. Finally, the error was computed as a percentage of the head boundary that is not covered by the area of the projected skull. Figure 5.10 shows two examples of the application of this evaluation procedure, which has been called "area deviation error".

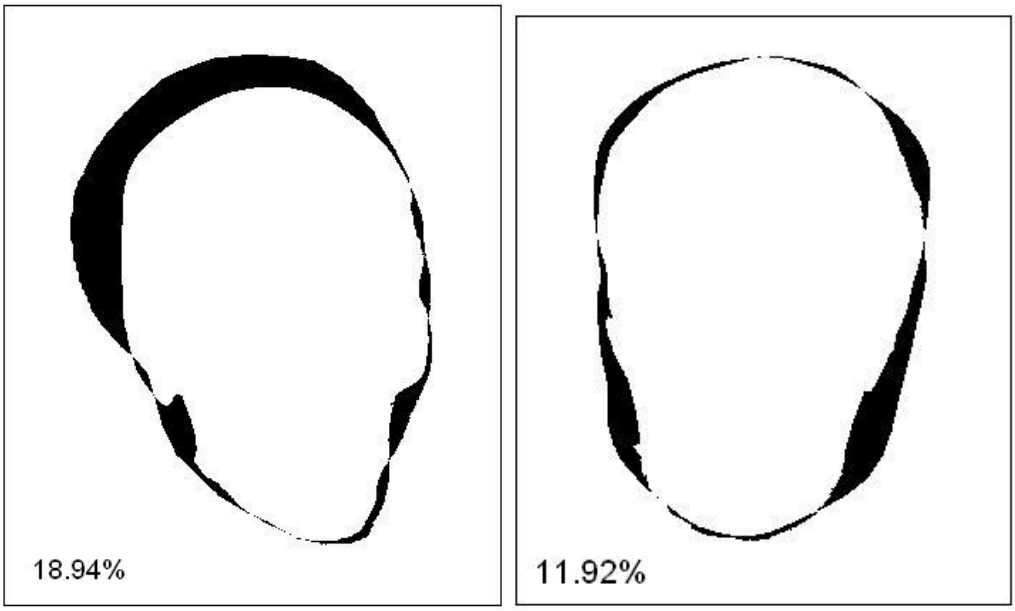

Figure 5.10: Example of XOR binary images. Their corresponding area deviation error is shown on the bottom left corner of the images.

In our opinion, this is definitely a more appropriate error estimator for the skull-face overlay problem, since is more in concordance with the visual results achieved than the ME. Even so, it fails at measuring how inner parts of the skull (set of teeth, eye cavity, and so on) fit to the corresponding ones in the face. In addition, it is based on an imprecise head boundary extraction, since it is done using the provided photographs

of the faces of the missing people, where in most of the cases there is hair occluding some parts of the head boundary. However, regardless the latter drawbacks, it can successfully provide us with a fair numerical index to compare the obtained skull-face overlays in an objective way.

5.6.2 Cádiz case study

The first real-world case of study, Cádiz, was already introduced in Chapter 3, Section 3.5.4. As it was mentioned there, four photographs were provided by the family but only two of them have been addressed until this moment. This is due to the fact that they were the most appropriate poses for the manual overlay developed by the forensic experts. We have incorporated the remaining two photographs (Figure 5.11) to the current experimental study, corresponding to Cádiz case study, poses 3 and 4. In addition, pose 2 has also been considered. These three images have been selected for this experiment because of the frontal or near-frontal pose of the face and/or because of the coplanarity of the corresponding craniometric set of landmarks.

The forensic experts were able to locate 12, 9, and 11 landmarks following a crisp (precise) approach and, 15, 14, and 16 using imprecise landmarks for poses 2, 3 and 4, respectively. These additional landmarks will play an essential role in order to tackle the coplanarity problem, as we will see in the following. Indeed, their corresponding craniometric pairs (see Chapter 1) lay on a plane that is not parallel to the camera image plane. A clear example is the landmark on the top of the head, named vertex (see Section 1.2.2), which is never used by the forensics because it is normally occluded by hair (and thus they are not able to precisely locate it) although it is very useful for the automatic overlay process since it lays in a complete different plane.

5.6.2.1 Pose 2

On the one hand, Table 5.1 presents the ME values for the obtained skull-face overlays in this first case, distinguishing between crisp, weighted, and fuzzy locations. We should remind that results are not fully comparable since the overlay processes using weighted and fuzzy landmarks do not minimize the ME but a different function (see Equations 5.1, 5.2, and 5.3). According to these results, the three approaches behave quite similarly for the case of the set of twelve landmarks (not significant differences were observed). As it was expected, ME values are higher when more landmarks are taken into account (imprecise location) since we are minimizing distances among a bigger number of corresponding landmarks but calculating the ME over the same smaller

Figure 5.11: Cádiz case study. From left to right: photographs of the missing person corresponding to poses 2, 3, and 4. The top row pictures show the used crisp landmarks sets, composed of 12, 9, and 11 crisp landmarks, respectively. The bottom row pictures show the used imprecise landmarks sets, composed of 15, 14, and 16 landmarks, respectively.

set of landmarks. We should also highlight the strong robustness of the method as the standard deviations are always null or almost 0.

On the other hand, regarding visual results, Figures 5.12 and 5.13 present respectively the best and worst skull-face overlay results corresponding to the crisp, the weighted, and the fuzzy approaches to allow for a visual comparison. The fact that the overlays achieved are much more precise when using a larger number of landmarks can be clearly identified in Figure 5.12. This is mainly due to the new landmark positions that lie in a different plane, solving the coplanarity problem of the previous landmark set. Among the imprecise location approaches, the fuzzy one achieves the best overlay. Finally, notice again how the robust skull-face overlay method derives the same results for both the best and the worst superimpositions.

Table 5.1: Cádiz case study, pose 2. Skull-face overlay results.

Landmark set	Fitness	*ME*			
		m	M	μ	σ
twelve crisp l.	Eq. 3.8	0.0220	0.0222	0.0220	0.0000
twelve weighted l.	Eq. 5.1	0.0220	0.0222	0.0220	0.0000
twelve weighted l.	Eq. 5.2	0.0222	0.0225	0.0224	0.0000
twelve fuzzy l.	Eq. 5.3	0.0217	0.0219	0.0218	0.0000
fifteen weighted l. (ME over twelve)	Eq. 5.1	0.0251	0.0258	0.0254	0.0001
fifteen weighted l. (ME over twelve)	Eq. 5.2	0.0250	0.0252	0.0251	0.0000
fifteen fuzzy l. (ME over twelve)	Eq. 5.3	0.0269	0.0274	0.0271	0.0001

These conclusions regarding the skull-face overlay results are also supported by the area deviation error, presented in Table 5.2. The best results were achieved following an imprecise location approach with the larger number of landmarks (15), using fuzzy landmarks (18.94%) or weighted ones (similar performance whatever the fitness function used, 23.82% with Eq. 5.1 and 23.95% with Eq. 5.2). They both clearly outperform the results achieved using a crisp set of landmarks (53.85%). Notice that, considering the same number of landmarks, even of an imprecise nature, is not enough to derive good performance due to the coplanarity problem.

Table 5.2: Area deviation error of the best skull-face overlay estimations of every approach for Cádiz case study, pose 2.

Approach	Number of landmarks	Area deviation error
Crisp	12	53.85%
Weighted (Eq. 5.1)	12	54.97%
Weighted (Eq. 5.2)	12	55.28%
Fuzzy	12	54.84%
Weighted (Eq. 5.1)	15	23.82%
Weighted (Eq. 5.2)	15	23.95%
Fuzzy	15	**18.94**%

Figure 5.12: Cádiz case study, pose 2. Best skull-face overlay results. On the first row, from left to right, results using 12 crisp, 12 weighted (Equations 5.1 and 5.2), and 12 fuzzy landmarks. On the second row, from left to right, results using 15 weighted (Equations 5.1 and 5.2) and 15 fuzzy landmarks.

5.6.2.2 Pose 3

According to the numerical results shown in Table 5.3, the three approaches behave again in a similar way than in the pose 2 case study. The same conclusions can be drawn according to the method robustness and the ME values differences between the small and the large landmark sets.

Nevertheless, the skull-face overlay results (see Figures 5.14 and 5.15) show again the best performance achieved when an imprecise location approach is followed. By using a larger number of fuzzy landmarks, the obtained overlays are more accurate. One more time, the reason seems to be the coplanarity of the crisp set of landmarks. Table 5.4 shows the area deviation errors for all the approaches, and with fuzzy one achieving the best performance (27.97%) one more time.

Figure 5.13: Cádiz case study, pose 2. Worst skull-face overlay results. On the first row, from left to right, results using 12 crisp, 12 weighted (Equations 5.1 and 5.2), and 12 fuzzy landmarks. On the second row, from left to right, results using 15 weighted (Equations 5.1 and 5.2) and 15 fuzzy landmarks.

5.6.2.3 Pose

As in the previous cases, ME values in Table 5.5 are higher when more landmarks are taken into account (imprecise location) for the already given reasons. The skull-face overlay graphical results (see Figures 5.16 and 5.17) and the area deviation errors (see Table 5.6) clearly show that the latter ME error is drawing a wrong scenario, as expected. The bad performance using a coplanar set of landmarks is easily identified (area deviation errors from 32.97% to 42.84%). These values are clearly outperformed when an imprecise location approach is followed (area deviation errors from 21.27% to 28.11%). Finally, the robustness of the method is again recognized although in this case there is a worst result different than the best one in the weighted approach when considering the small landmark set.

Table 5.3: Cádiz case study, pose 3. Skull-face overlay results.

Landmark set	Fitness	*ME*			
		m	M	μ	σ
nine crisp l.	Eq. 3.8	0.0083	0.0084	0.0083	0.0000
nine weighted l.	Eq. 5.1	0.0083	0.0088	0.0084	0.0000
nine weighted l.	Eq. 5.2	0.0083	0.0084	0.0083	0.0000
nine fuzzy l.	Eq. 5.3	0.0084	0.0085	0.0084	0.0000
fourteen weighted l. (*ME* over nine)	Eq. 5.1	0.0094	0.0095	0.0094	0.0000
fourteen weighted l. (*ME* over nine)	Eq. 5.2	0.0092	0.0093	0.0093	0.0000
fourteen fuzzy l. (*ME* over nine)	Eq. 5.3	0.0100	0.0102	0.0101	0.0000

Table 5.4: Area deviation error of the best skull-face overlay estimations of every approach for Cádiz case study, pose 3.

Approach	Number of landmarks	Area deviation error
Approach	Number of landmarks	Area deviation error
Crisp	9	50.28%
Weighted (Eq. 5.1)	9	49.84%
Weighted (Eq. 5.2)	9	49.49%
Fuzzy	9	51.60%
Weighted (Eq. 5.1)	14	34.34%
Weighted (Eq. 5.2)	14	33.60%
Fuzzy	14	**27.97**%

5.6.3 Morocco case study

The second real-world case considered is called "Morocco" because of the origin of the subject. In this case, there is a single available photograph corresponding to that one in the alleged passport. Notice that, passport photographs usually include an undulating watermark that makes the accurate location of cephalometric landmarks even more difficult. Therefore, the use of fuzzy landmarks can help the forensic expert in the recognition of a higher number of facial reference points in this low quality photograph. In particular, the selection of non coplanar landmarks is thus eased. In this case of study,

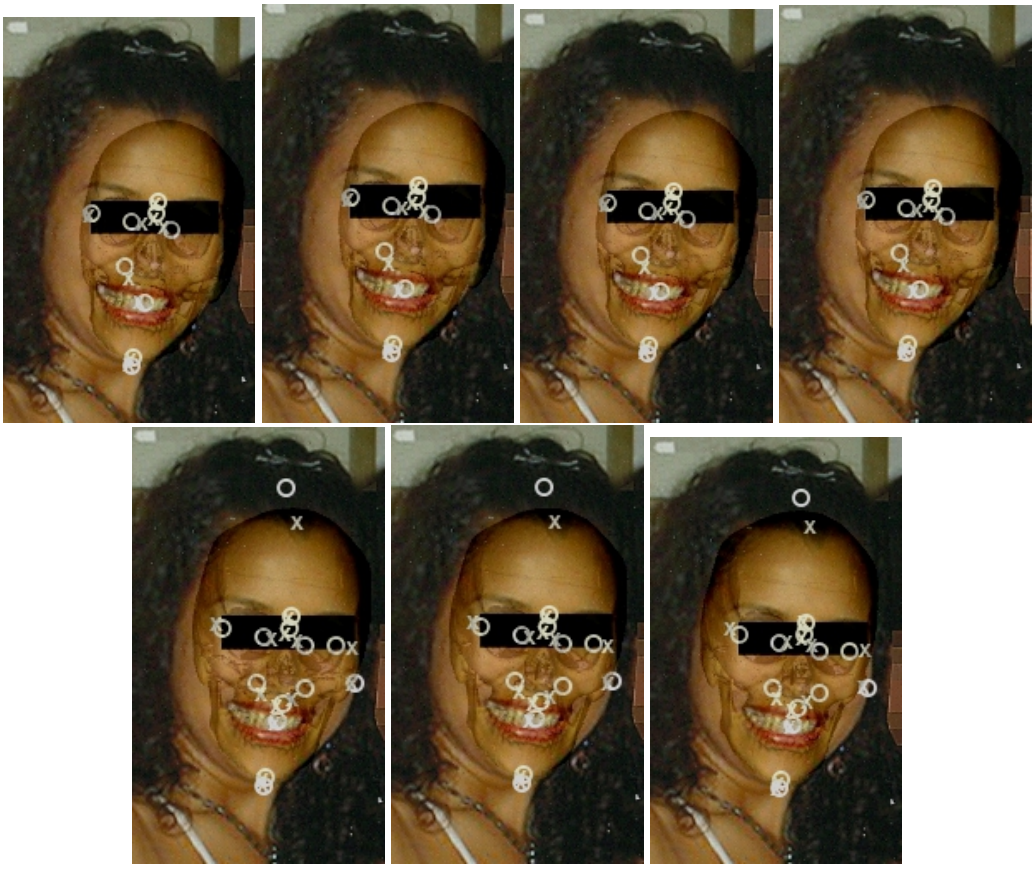

Figure 5.14: Cádiz case study, pose 3. Best skull-face overlay results. On the first row, from left to right, results using 9 crisp, 9 weighted (Equations 5.1 and 5.2), and 9 fuzzy landmarks. On the second row, from left to right, results using 14 weighted (Equations 5.1 and 5.2) and 14 fuzzy landmarks.

the forensic experts identified 6 and 16 cephalometric landmarks following a crisp and a imprecise approach, respectively (see Figure 5.18).

Table 5.7 collects the ME values for the obtained skull-face overlays, distinguishing between crisp and imprecise locations. The large difference among the results achieved using a smaller or a larger set of landmarks is due to the big difference between the number of landmarks of each set (more than the double). As in all the other

Figure 5.15: Cádiz case study, pose 3. Worst skull-face overlay results. On the first row, from left to right, results using 9 crisp, 9 weighted (Equations 5.1 and 5.2), and 9 fuzzy landmarks. On the second row, from left to right, results using 14 weighted (Equations 5.1 and 5.2) and 14 fuzzy landmarks.

case studies, there is not a correspondence between these numerical results (ME) and the visual representation of the skull-face overlay (see Figures 5.19 and 5.20). The same high robustness observed in the previous experiments is found again. Finally, results in Table 5.8 demonstrate, once again, the best performance of the imprecise location approach (and specifically of the fuzzy one) in comparison with the precise one, achieving much more better area deviation errors (11.92% against 32.63%).

Table 5.5: Cádiz case study, pose 4. Skull-face overlay results.

Landmark set	Fitness	*ME*			
		m	M	μ	σ
eleven crisp l.	Eq. 3.8	0.0096	0.0097	0.0096	0.0000
eleven weighted l.	Eq. 5.1	0.0096	0.0141	0.0098	0.0008
eleven weighted l.	Eq. 5.2	0.0111	0.0114	0.0112	0.0001
eleven fuzzy l.	Eq. 5.3	0.0092	0.0094	0.0092	0.0000
sixteen weighted l. (ME over eleven)	Eq. 5.1	0.0126	0.0128	0.0127	0.0000
sixteen weighted l. (ME over eleven)	Eq. 5.2	0.0121	0.0128	0.0125	0.0001
sixteen fuzzy l. (ME over eleven)	Eq. 5.3	0.0133	0.0134	0.0133	0.0000

Table 5.6: Area deviation error of the best skull-face overlay estimations of every approach for Cádiz case study, pose 4.

Approach	Number of landmarks	Area deviation error
Crisp	11	42.84%
Weighted (Eq. 5.1)	11	42.67%
Weighted (Eq. 5.2)	11	32.97%
Fuzzy	11	41.54%
Weighted (Eq. 5.1)	16	27.88%
Weighted (Eq. 5.2)	16	28.11%
Fuzzy	16	**21.27**%

5.7 Concluding remarks

In this chapter we have identified and studied the sources of uncertainty related with the skull-face overlay process and procedure. We have distinguished between the uncertainty associated with the objects under study and that inherent to the overlay process. In addition, we have studied how the coplanarity of landmark sets affects the skull-face overlay process.

Two different approaches, weighted and fuzzy landmarks, have been proposed to jointly deal with the imprecise landmark location and the coplanarity problem. Sum-

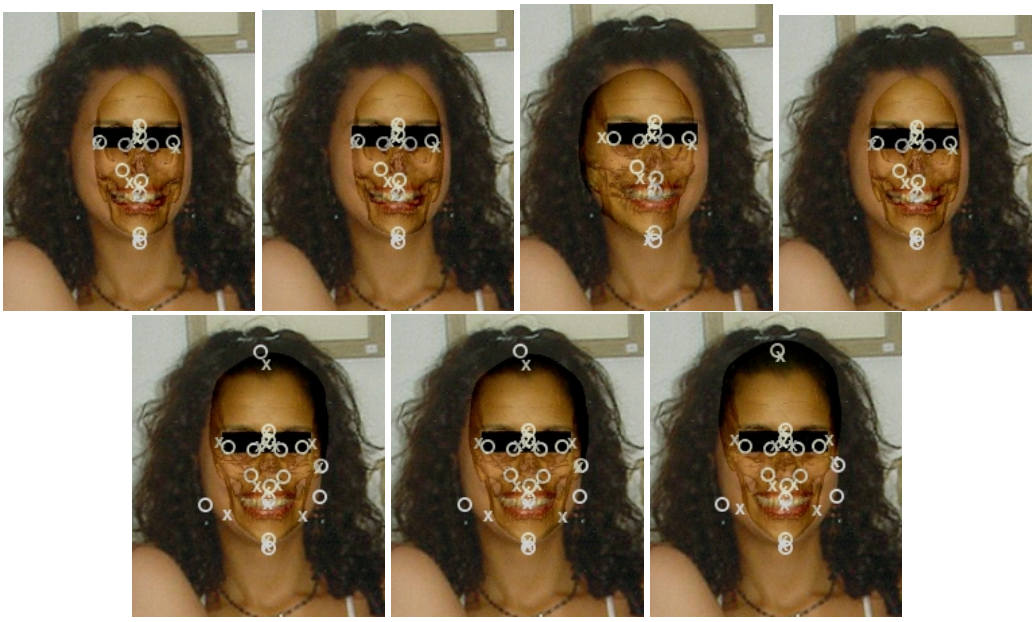

Figure 5.16: Cádiz case study, pose 4. Best skull-face overlay results. On the first row, from left to right, results using 11 crisp, 11 weighted (Equations 5.1 and 5.2), and 11 fuzzy landmarks. On the second row, from left to right, results using 16 weighted (Equations 5.1 and 5.2) and 16 fuzzy landmarks.

marizing the results, it is clear that a larger number of landmarks results in more accurate skull-face overlays. Hence, the imprecise location of landmarks is a promising approach to improve the performance of our evolutionary-based skull-face overlay method.

After looking at the two error measures used, and comparing them with the visual results achieved, we conclude that the area deviation error provides a more reliable error indicator. Using this error function as a reference measure, the fuzzy landmark approach clearly overcomes the weighted one as the best way to model the imprecise location of cephalometric landmarks.

Finally, despite the new proposed method based on the use of imprecise landmarks provides very accurate results and still behaves robustly, we should note it implies more computational operations with the consequent increment in the run time

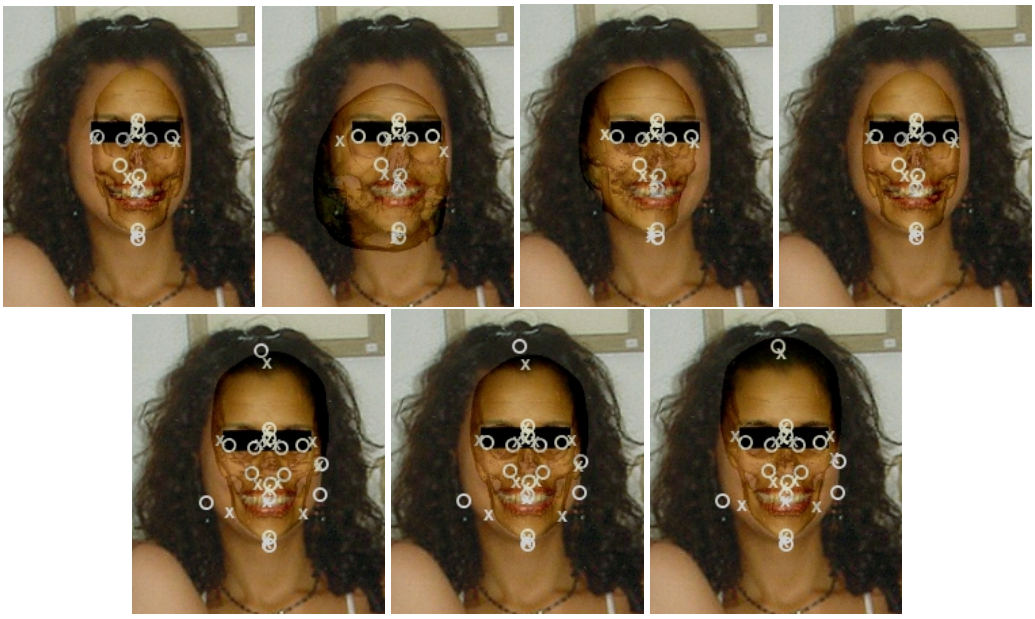

Figure 5.17: Cádiz case study, pose 4. Worst skull-face overlay results. On the first row, from left to right, results using 11 crisp, 11 weighted (Equations 5.1 and 5.2), and 11 fuzzy landmarks. On the second row, from left to right, results using 16 weighted (Equations 5.1 and 5.2) and 16 fuzzy landmarks.

Figure 5.18: Morocco case study: photograph of the missing person with two different sets of 6 crisp (left) and 16 fuzzy (right) landmarks.

Table 5.7: Morocco case study. Skull-face overlay results.

Landmark set	Fitness	*ME*			
		m	M	μ	σ
six l.	Eq. 3.8	0.0153	0.0154	0.0153	0.0000
six weighted l.	Eq. 5.1	0.0154	0.0155	0.0154	0.0000
six weighted l.	Eq. 5.2	0.0154	0.0155	0.0154	0.0000
six fuzzy l.	Eq. 5.3	0.0155	0.0158	0.0157	0.0000
sixteen weighted l. (*ME* over six)	Eq. 5.1	0.0221	0.0.0230	0.0224	0.0001
sixteen weighted l. (*ME* over six)	Eq. 5.2	0.0233	0.0236	0.0235	0.0000
sixteen fuzzy l. (*ME* over six)	Eq. 5.3	0.0214	0.0225	0.0219	0.0002

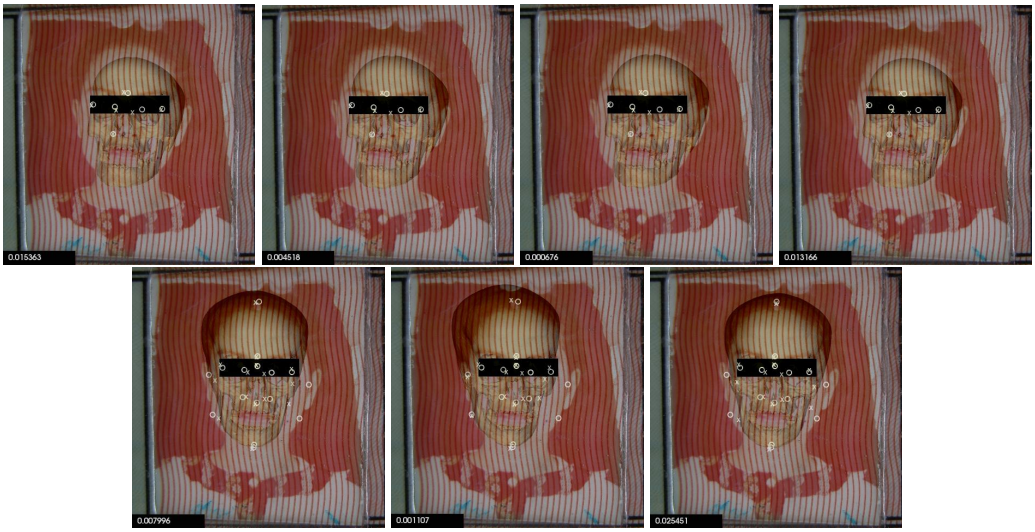

Figure 5.19: Morocco case study. Best skull-face overlay results. On the first row, from left to right, results using 6 crisp, 6 weighted (Equations 5.1 and 5.2), and 6 fuzzy landmarks. On the second row, from left to right, results using 16 weighted (Equations 5.1 and 5.2) and 16 fuzzy landmarks.

Figure 5.20: Morocco case study. Worst skull-face overlay results. On the first row, from left to right, results using 6 crisp, 6 weighted (Equations 5.1, and 5.2) and 6 fuzzy landmarks. On the second row, from left to right, results using 16 weighted (Equations 5.1 and 5.2) and 16 fuzzy landmarks.

Table 5.8: Area deviation error of the best skull-face overlay estimations of every approach for Morocco case study.

Approach	Number of landmarks	Area deviation error
Crisp	6	32.63%
Weighted (Eq. 5.1)	6	33.17%
Weighted (Eq. 5.2)	6	33.17%
Fuzzy	6	32.88%
Weighted (Eq. 5.1)	12	16.66%
Weighted (Eq. 5.2)	12	29.92%
Fuzzy	12	**11.92**%

required. From the 20 seconds per run using crisp landmarks, the SS-based skull-face overlay method increases its run time to 2-4 minutes when using fuzzy landmarks. However, it is still a significantly short time if we compare it with the usual time needed

by the forensic anthropologists to perform a manual superimposition, up to 24 hours in many cases.

Chapter 6

Global Validation of the Obtained Results in Real-World Identification Cases

The difference between what we do
and what we are capable of doing
would suffice to solve most of the world's problems.

Mahatma Gandhi (1869-1948)

6.1 Introduction

EAs are being increasingly applied to difficult real-world problems (Cagnoni et al. 2000; Arcuri and Yao 2008; Koza et al. 2008; Ugur 2008; Chiong 2009; Brainz 2010; Chiong et al. 2011) and they are becoming competitive to the work done by creative and inventive human beings day by day, as attested by the "*annual HUMIES awards for human-competitive results produced by genetic and evolutionary computation*" (HUMIES 2008).

The aim of this chapter is to evaluate the actual performance of the skull-face overlay methodology based on EAs and fuzzy sets theory introduced in this contribution. To do so, we will compare the overlays returned by our automatic method for the real-world forensic identification cases tackled through the current dissertation to the manual (in fact, computer assisted) skull-face overlays the forensic experts from the Physical Anthropology lab of the University of Granada, Spain, developed for the said cases. This comparison will rely on two different evaluation procedures: a visual assessment (Section 6.2) and a numerical assessment based on the area deviation error (Section 6.3).

Under both assessment procedures, all the available cases of study will be benchmarked. The five real-world cases tackled, some of them considering more than one photograph of the missing person, make up a test set composed of nine skull-face overlay problems.

The automatic skull-face overlays shown in this chapter have been obtained by the SS-based skull-face overlay method since, as shown in Chapter 4, it seems to be the most robust and faster approach. Besides, a fuzzy set of landmarks was provided for each case of study, solving the skull-face overlay process following an imprecise landmark location approach. As it has been shown in Chapter 5, this variant provides

the more accurate results.

The structure of this chapter is as follows. Section 6.2 is devoted to show and visually analyze manual and automatic skull-face overlay results. In Section 6.3, the area deviation errors corresponding to the same overlays are compared. Finally, some concluding remarks are presented in Section 6.4.

6.2 Visual assessment

In order to analyze the human-competitiveness of the skull-face overlays quality, we should first mention that, although comparing two graphical results is always a subjective issue, we benefit from having available an experienced forensic team to validate our results. Besides, any non expert reader can even directly perform his own visual comparison of the human and EA-based overlays when they are represented in two consecutive images.

6.2.1 Cádiz case study

The first case of study was firstly introduced in Chapter 3, where two of the four available photographs of the missing person were considered for experimentation. Later, in Chapter 5, we dealt with the remaining two. Below, the best skull-face overlay results obtained by our method over the four photographs are shown (see Figures 6.1, 6.2, 6.3 and 6.4). In each figure, the manual overlay achieved by the forensic experts is shown for comparison.

Figure 6.1 shows the graphical comparison between forensic experts' overlay and SS-based one for the first pose. Even a non expert reader can directly recognize the large similarity between the two superimpositions, which present a really close pose. In addition, it can be easily seen how ours achieves a better fit of the top part of the head (thanks to our better treatment of the perspective transformation) as well as on the right cheekbone. When we provided the forensic anthropologists with our overlay and asked them about this fact, they first recognized the defects of their overlay, which were due the limitations of the perspective transformations they can obtain when projecting the 3D skull into a 2D image with the commercial software package used (RapidForm^{TM}and Photoshop^{TM}). They mentioned how their main interest when performing the superimposition is always addressed to properly match the main landmarks in the frontal horizontal and vertical axis, and that small misalignments in other parts of the face could be allowed. As a final conclusion, they confirmed the high

Figure 6.1: Cádiz case study, pose 1. Best superimposition manually obtained by the forensic experts (left) and automatic one achieved by our automatic fuzzy-evolutionary method (right)

quality of our automatic overlay.

Figure 6.2 shows the same graphical comparison for the second pose. Trying to develop the identification by means of this photograph constitutes a particularly difficult situation for the forensic anthropologists. As described in Chapter 1 when introducing the basis of craniofacial identification the more frontal the pose of the person in the photograph, the more robust and easily applicable the technique. However, notice that, the pose of the young woman in the second available photograph for this case does not correspond to this assumption as it is very lateral. Thus, they had to deal with significant perspective deformations causing a lower confidence on the extracted landmarks (as already mentioned in Chapter 5, this is the case for which a highest number of facial landmarks were selected, 15). The left image in Figure 6.2 shows the overlay the forensic experts managed to get when they solved this case. As can be seen, although they were able to fit the frontal axis (see the proper alignment of the jaw and the eye caves), the skull is clearly downsized and the top and right parts of the face do not properly fit. This is again a consequence of the limitations of the considered software, even more noticeable in this pose than in the previous one. *That was the reason why the current photograph was finally ignored for the positive identification performed, that*

Figure 6.2: Cádiz case study, pose 2. Best superimposition manually obtained by the forensic experts (left) and automatic one achieved by our automatic fuzzy-evolutionary method (right)

was confirmed by only considering the previous picture. Nevertheless, the outstanding quality of the obtained fuzzy-evolutionary-based superimposition, depicted in the right side of Figure 6.2, can be clearly recognized. Not only the frontal axis but also the outer parts of the face (the forehead and the right cheek) are properly overlayed, thanks to the said better handling of the perspective projection provided by our automatic methodology. Actually, *the forensic experts were positively impressed by the quality of that superimposition*.

For the pose 3, manual and automatic results are quite similar in terms of the size and situation of the projected skull (see Figure 6.3). However, the orientation of the skull is a bit different, what makes the overlay achieved by the forensic fit better the right side of the face but in contrast fit worst the left side (notice how the SS-based overlay matches better the left cheekbone). Anyway, both overlays need some improvement regarding the perspective in order to be able to properly capture the top part of the head and the right part of the jaw.

Figure 6.3: Cádiz case study, pose 3. Best superimposition manually obtained by the forensic experts (left) and automatic one achieved by our automatic fuzzy-evolutionary method (right)

Finally, the last pose demonstrates the problems of the fuzzy-evolutionary-based skull-face overlay method when dealing with some frontal images like the current one. Automatic overlay results are specially bad in both sides of the face, since the projected skull is too narrow. We think that these problems can be solved once the matching uncertainty will be considered as it explained in Section 6.4. Nevertheless, the overlay achieved by the forensic experts also needs improvements showing how this is a difficult problem instance for them as well as due to the face pose. It fits the chin better than the automatic overlay, but it is not able to properly fit both sides of the jaw. In addition it has problems with the perspective again, fitting worse the skull covered by hair.

In summary, we can conclude the performance of our proposal in the four skull-face overlay problem instances associated with this case study can be considered as very satisfactory. Although two of the overlays could require some improvement, we have managed to derive comparable or even better superimpositions than those obtained by the forensic experts in three cases of the four.

Figure 6.4: Cádiz case study, pose 4. Best superimposition manually obtained by the forensic experts (left) and automatic one achieved by our automatic fuzzy-evolutionary method (right)

6.2.2 Málaga case study

The second case of study was introduced in Chapter 3, where we dealt with the only provided photograph of the missing person.

The left image in Figure 6.5 shows the final skull-face overlay used by the forensic experts, which allowed them to take a positive identification decision for that case in the past. The right image in the same figure depicts the best overlay obtained by our SS-based method. A direct inspection of both images allows us to recognize some problems on them. Even if the proper matching of the central axis of the face is good enough for the forensic anthropologists to support a positive identification decision, their overlay is not properly "matching" the right part of the face (notice how the right side of the skull does not properly reach the cheek and ear level) as well as the part of the skull covered by hair again. Besides, it seems that it slightly overfits the chin and the left cheekbone. Regarding the automatic overlay, it is true that it seems to be slightly excessively rotated to the left, but it would become definitively better than the forensic anthropologist' manual superimposition after a little manual refinement. That conclusion was confirmed by the forensic experts.

Figure 6.5: Málaga case study. Best superimposition manually obtained by the forensic experts (left) and automatic one achieved by our automatic fuzzy-evolutionary method (right)

6.2.3 Granada case study

The third case of study was introduced in Chapter 4, where we dealt with the only available photograph of the missing person. In this case study a set of crisp landmarks was enough to achieve a very good skull-face overlay, as can be seen in Figure 6.6.

It is clear that the manual and the automatic overlays are very similar with only a few differences on the back part of the head. They both are almost perfect since, as the forensic experts state, all parts of the projected skull perfectly fit. Regarding this minor difference in the back of the head, they are not able to choose which of the two overlays is the best.

6.2.4 Portuguese case study

The fourth case of study was also introduced in Chapter 4. Results over the two available images of the missing person are depicted in Figures 6.7 and 6.8.

Regarding the first pose (see Figure 6.7), the overlay achieved by the forensic

Figure 6.6: Granada case study, best superimposition manually obtained by the forensic experts (left) and automatic one achieved by our automatic fuzzy-evolutionary method (right)

experts is definitely better. It fits well the chin, the jaw, the cheekbones, and all the inner parts of the face. As in other cases, it still has problems with the perspective projection, since the top part of the head is not well fitted but again the good central part matching allows for a positive identification. On the other hand, the overlay achieved by our proposal needs important improvements. It is both over-rotated to the left side of the face and not properly scaled. It could affected by the poor quality of the image, with a very low resolution, 129 x 133 pixels.

Concerning the second photograph of the same case (see Figure 6.8), the overlay achieved by the forensic anthropologists has problems with the perspective projection one more time, what makes the projected skull fitting only the vertical and horizontal axis marked by the Ectocanthions and the Gnathion-Glabella cephalometric landmarks. In contrast, the automatic overlay is able to fit the top and back part of the head while it also properly fits the same vertical and horizontal axis. It only has

Figure 6.7: Portuguese case study, pose 1. Best superimposition manually obtained by the forensic experts (left) and automatic one achieved by our automatic fuzzy-evolutionary method (right)

Figure 6.8: Portuguese case study, pose 2. Best superimposition manually obtained by the forensic experts (left) and automatic one achieved by our automatic fuzzy-evolutionary method (right)

problems fitting the both sides of the jaw. Although the position of the projected skull regarding both cheekbones should be improved, it is better than the manual approach.

6.2.5 Morocco case study

The last case of study was tackled in Chapter 5 following an imprecise cephalometric landmark location approach because of the special characteristics (watermarks) of the image (we should remind that a passport photograph was only available).

The left image in Figure 6.9 shows the skull-face overlay achieved by the forensic team. It has problems with the size (too small) and the perspective projection. It does not fit neither the forehead nor both sides of the face. Finally, it is not able to fit the upper part of the head. In contrast, the fuzzy-evolutionary-based overlay properly deals with most of these problems and only fails fitting the jaw. The automatic overlay is definitively better than the manual one.

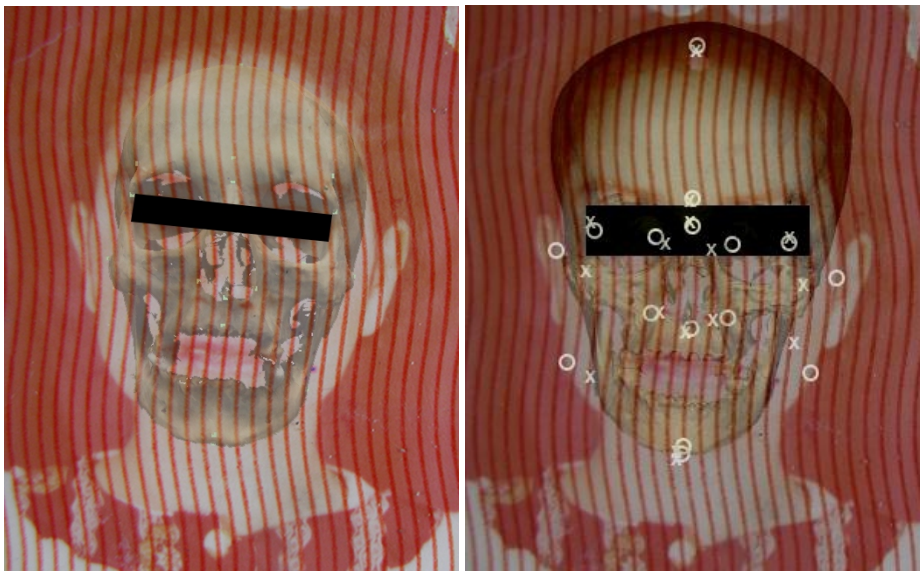

Figure 6.9: Morocco case study. Best superimposition manually obtained by the forensic experts (left) and automatic one achieved by our automatic fuzzy-evolutionary method (right)

6.3 Area deviation error assessment

In order to provide a more objective metric, we adopted the area deviation error, that was already introduced in Chapter 5. As it was mentioned there, this is the most reliable

error metric we could propose, being more in concordance with the visual results than ME. However, it fails measuring how inner parts of the skull (set of teeth, eye cavity, and so on) fit to the corresponding ones in the face. In addition, it is based on an imprecise head boundary extraction, since it is done using the provided photographs of the face of the missing people, where in most of the cases there is hair occluding some parts of the head boundary.

Table 6.1 shows the deviation error values for all the case studies considered, distinguishing between the overlays manually achieved by the forensic experts and those automatically obtained using our fuzzy-SS-based approach.

Table 6.1: Area deviation error of the best skull-face overlays manually obtained by the forensic experts and the automatic ones achieved by our automatic fuzzy-evolutionary method.

Case study	Area deviation error	
	Manual approach	Automatic approach
Cádiz, pose 1	32.64%	15.84%
Cádiz, pose 2	38.22%	18.95%
Cádiz, pose 3	31.58%	27.96%
Cádiz, pose 4	31.84%	21.26%
Málaga	34.70%	13.23%
Granada	13.81%	4.73%
Portuguese, pose 1	28.26%	21.79%
Portuguese, pose 2	37.54%	21.04%
Morocco	31.73%	11.96%

The first issue the results show up is the lower area deviation error of the automatic approach for all the cases of study. In most of the cases these errors are approximately the half of the corresponding manual ones. In addition, they are really small, most of them below 20%, and some of them are specially good like Morocco (11.96%) or Granada (4.73%). All these errors are closely related with the visual assessment shown in the previous Section.

However, as already explained, the area deviation error only provides a measure about the contour of the overlay, but it does not take into account the inner parts. This explains why all the forensics' overlays are worse regarding this metric, because they mainly focus on properly fitting the inner parts of the skull and they do not pay much attention to those parts that are not visible in the image (e.g., occluded by the hair). As said, they are not able to apply the adequate perspective to the projected skull because

of the limitations of the means.

6.4 Concluding Remarks

In this chapter we have made a comparison between the skull-face overlays provided by the forensic team of the Physical Anthropology Lab at the University of Granada and the best ones achieved by means of our SS-based approach combined with the use of fuzzy landmarks.

After a visual assessment we can conclude that the overlays achieved by our technique are competitive with the forensic ones and, in some cases, they are even better. Besides, if we consider the area deviation error, we can see how our automatic method properly manages to get a good overall alignment of the skull and the face objects.

Even so, it was recognized that some of the achieved SS-based overlays need small refinements regarding their orientation or size. Nevertheless, the short time required to generate them makes our fuzzy-evolutionary skull-face overlay method an outstanding automatic tool to provide the forensic experts with good quality preliminary approximations. High quality skull-face overlays can be obtained by the forensic anthropologist performing slight manual refinements, in a very simple and quick way.

Finally, we should also remark that some of the latter non optimal skull-face overlays achieved by our automatic method could be directly improved in case the evolutionary process would be updated to handle the other source of uncertainty, the matching uncertainty. Notice that, while the human experts are implicity considering the non perfect matching between craniometric and cephalometric landmarks, the automatic procedure does not do so. This issue is left for future improvements of the methodology.

Chapter 7

Final Comments

We must be the change we wish to see.

Mahatma Gandhi (1869-1948)

7.1 Concluding remarks

In this dissertation we have proposed different automatic methods based on soft computing techniques to solve the skull-face overlay problem in craniofacial superimposition. In particular, evolutionary algorithms and fuzzy sets have been applied in order to solve this complex and uncertain problem. The promising results achieved, confirmed by the forensic anthropologists of the Physical Anthropology lab at the University of Granada, have demonstrated the suitability of our proposal. They emphasized the accuracy of the resulting skull-face overlays as well as the short time needed to obtain them in an automatic fashion. In fact, the same team of forensic anthropologists recently used our method to solve a real-world identification case of a Portuguese man whose remains were found in the surroundings of the Alhambra for the Spanish Scientific Police.

In the following items, the results obtained in this dissertation as well as the fulfilment degree for each of the objectives set up at the beginning of the current work are analyzed:

- *Study the state of the art in forensic identification by craniofacial superimposition*. After a deep study of the craniofacial superimposition field, its fundamentals, and the main contributions in the topic, we can conclude that the technique has demonstrated being a really solid identification method. However, basic methodological criteria ensuring the reliability of the technique have not been established yet. Instead of following a uniform methodology, every expert tends to apply his own approach to the problem based on the available technology and on his deep knowledge on human craniofacial anatomy, soft tissues, and their relationships.

- *Propose a methodological framework for computer-based craniofacial superimposition*. With the aim of alleviating the absence of a uniform methodology, we have proposed a new general framework for computer-based craniofacial superimposition which divides the process into three stages: face enhancement and skull modeling, skull-face overlay, and decision making. Using this general framework we have reviewed and categorized the existing contributions of computer-aided craniofacial superimposition systems, classifying them according to the stage of the process which is addressed using a computer-aided method and clearly identifying the actual use of the computer in each stage.

  The work developed for the previous objectives has resulted in a paper describing our proposed methodological framework for computer-based craniofacial superimposition together with the complete review of the state of the art in the said technique. This contribution has been accepted for publication in the journal with the highest impact factor in the Computer Science area. Besides, issues related with the methodological framework as well as the application of soft computing techniques in its different stages have been published in a digital journal:

  - S. Damas, O. Cordón, O. Ibáñez, J. Santamaría, I. Alemán, MC. Botella, F. Navarro. Forensic identification by computer-aided craniofacial superimposition: A survey. ACM Journal on Computing (2010), to appear. Impact factor 2008: 9.920. Category: Computer Science, Theory & Methods. Order: $1/84$.
  - O. Cordón, S. Damas, R. del Coso, O. Ibáñez, C. Peña. Soft Computing Developments of the Applications of Fuzzy Logic and Evolutionary Algorithms Research. eNewsletter: Systems, Man and Cybernetics Society (2009). Vol. 19. Available on-line at $http://www.my-smc.org/main\_article1.html$.

- *Propose a mathematical formulation for the skull-face overlay problem*. We have formulated the skull-face overlay task as a numerical optimization problem, allowing us to solve the underlying 3D-2D IR task following a parameter-based approach. The registration transformation to be estimated includes a rotation, a scaling, a translation, and a projection. It was specified as a set of eight equations in twelve unknowns.

- *Propose an automatic method for skull-face overlay based on evolutionary algorithms*. We have proposed and validated the use of real-coded EAs for the skull-face overlay of a 3D skull model and the 2D face photograph of the missing person. In particular, two different designs of a real-coded GA, a CMA-ES,

and a SS method have been proposed. Among them, CMA-ES and SS have demonstrated the best performance, achieving high quality solutions in all the cases and showing a high robustness. Besides, SS attested a faster convergence than CMA-ES.

The mathematical formulation for the skull-face overlay problem and the proposal of different evolutionary algorithms that deal with it have allowed us to develop different contributions to international journals, book chapters, and international conferences:

- O. Ibáñez, L. Ballerini, O. Cordón, S. Damas, and J. Santamaría (2009). An experimental study on the applicability of evolutionary algorithms to craniofacial superimposition in forensic identification. Information Sciences 179, 3998–4028. Impact factor 2008: 3.095. Category: Computer Science, Information Systems. Order: $8/99$.
- O. Ibáñez, O. Cordón, S. Damas, and J. Santamaría (2009). Multimodal genetic algorithms for craniofacial superimposition. In R. Chiong (Ed.), Nature-Inspired Informatics for Intelligent Applications and Knowledge Discovery: Implications in Business, Science and Engineering, IGI Global, pp. $119-142$.
- J. Santamaría, O. Cordón, S. Damas, and O. Ibáñez (2009). 3D–2D image registration in medical forensic identification using covariance matrix adaptation evolution strategy. In 9th International Conference on Information Technology and Applications in Biomedicine, Larnaca, Cyprus.
- O. Ibáñez, O. Cordón, S. Damas, J. Santamaría. An advanced scatter search design for skull-face overlay in craniofacial superimposition. ECSC Research Report: AFE 2010-01, Mieres. Submitted to Applied Soft Computing. Feb 2010. Impact factor 2008: 1.909. Category: Computer Science, Artificial Intelligence. Order: $30/94$. Category: Computer Science, Interdisciplinary Applications. Order: $23/94$.

- *Study the sources of uncertainty present in skull-face overlay*. We have identified and studied the sources of uncertainty related with the skull-face overlay process and procedure. We have distinguished between the uncertainty associated with the objects under study and that inherent to the overlay process. In addition, we have studied how the coplanarity of cephalometric landmark sets affect the quality of skull-face overlay results.

- *Model the latter sources of uncertainty*. Two different approaches, weighted and fuzzy landmarks, have been proposed to jointly deal with the imprecise landmark location and the coplanarity problem. Between them, the fuzzy landmark approach clearly overcame the weighted one as the best way to model the imprecise location of cephalometric landmarks. The main advantage of this proposal is the larger number of landmarks the forensic anthropologists are able to locate following it. This results on more accurate skull-face overlays.

  We have developed several contributions describing the study of the sources of uncertainty, the two imprecise location approaches, and the coplanarity study. They have been published in national and international conferences from which we should highlight the 3DIM workshop, one of the most relevant international conferences in the computer vision field:

  - O. Ibáñez, O. Cordón, S. Damas, and J. Santamaría (2008). Craniofacial superimposition based on genetic algorithms and fuzzy location of cephalometric landmarks. In Hybrid artificial intelligence systems, Number 5271 in LNAI, pp. 599–607.
  - O. Ibáñez, O. Cordón, S. Damas, and J. Santamaría (2008). Superposición craneofacial basada en algoritmos genéticos y localización difusa de puntos de referencia cefalométricos. In Actas del XIV Congreso Español sobre Tecnologías y Lógica Fuzzy, Mieres, Spain, pp. 323–329.
  - O. Ibáñez, O. Cordón, S. Damas, and J. Santamaría (2009). A new approach to fuzzy location of cephalometric landmarks in craniofacial superimposition. In International Fuzzy Systems Association − European Society for Fuzzy Logic and Technologies (IFSA-EUSFLAT) World Congress, Lisbon, Portugal, pp. 195–200.
  - J. Santamaría, O. Cordón, S. Damas, and O. Ibáñez (2009). Tackling the coplanarity problem in 3D camera calibration by means of fuzzy landmarks: a performance study in forensic craniofacial superimposition. In 3D Image Modeling Workshop (3DIM), IEEE International Conference on Computer Vision, Kyoto, Japan, pp. 1686–1693.
  - O. Ibáñez, O. Cordón, S. Damas, and J. Santamaría (2010). Uso de marcadores difusos para solucionar el problema de la coplanaridad en la calibración de la cámara en 3D. Aplicación en identificación forense por superposición craneofacial. In Actas del XV Congreso Español sobre Tecnologías y Lógica Fuzzy, Huelva, Spain, pp. 501–506.

- *Analyze the performance of the proposed methods*. We have made a comparison between the skull-face overlays provided by the forensic team of the Physical Anthropology Lab at the University of Granada and those automatically achieved by means of our SS-based approach combined with the use of fuzzy landmarks. After a visual assessment we concluded that the overlays obtained by our approach are competitive with the forensic ones and, in some cases, they are even better. Anyway, comparing the time needed for our evolutionary-based techniques (between 10 and 40 seconds using precise landmarks and 2-4 minutes using imprecise ones) with that our forensic anthropologists needed to perform a manual skull-face overlay –several hours for each case– the evolutionary approaches are always much better, lower in several orders of magnitude. Due to the latter, apart from their already analyzed quality, new outlooks in forensic identification have emerged from the work developed in this dissertation. On the one hand, our proposal could be considered as a very fast initialization to provide a high quality skull-face overlay to be later slightly refined by the forensic scientist, in a very simple and quick way. On the other hand, the chance of comparing a skull 3D model with a large data base of missing people has arised, taking the same or less time than an anthropologist would need to perform a single skull-face overlay.

Finally, we would like to remark the contribution of the outcomes of the dissertation to the development of a patent, "Method and system for forensic identification by craniofacial superimposition", which was submitted to the Spanish National Agency last July 2009.

- Inventors: O. Cordón, S. Damas, O. Ibáñez, J. Santamaría, I. Alemán, M. Botella, Title: Method and system for forensic identification by craniofacial superimposition. Application number: P200901732/3. Priority country: Spain. Priority date: 2009-07-30. Entity owner: European Centre for Soft Computing and University of Granada.

7.2 Future works

Next, we will discuss some open research lines concerning the issues tackled in this dissertation. Besides, we consider some extensions of our proposals that will be developed as future works.

- *Increase the number of real-world cases considered*. We aim to tackle a higher number of real-world identification cases provided and solved by the Physical

Anthropology lab at the University of Granada. Our results will thus be validated through a more extensive study, once legal issues allow us to use a higher number of real-world identification cases.

- *Make a poll among different forensic anthropologists*. We will make an on-line poll among different forensic experts, asking them to locate the cephalometric landmarks over a set of photographs. We aim to study some aspects such as the variations in the locations of the same landmarks, how the location procedure is affected by the quality of the image, what landmarks are more difficult to locate, and how the pose of the face in the photograph influences the location procedure. That poll will be also helpful in order to define the most appropriate shapes and sizes for the fuzzy landmarks in several face photographs corresponding to real-world identification cases previously solved.

- *Achieve a ground-truth solution for skull-face overlay*. In order to obtain objective and fair comparisons between different skull-face overlay results there is a real need to get a ground-truth solution. Computerized tomographies of the head could be an interesting possibility to be explored for that aim.

- *Study of new fuzzy distance definitions*. We plan to study alternative fuzzy distances between a crisp point and a fuzzy set of points. Experiments using different fuzzy distances definitions (Bloch 1999) will lead us to choose the most appropriate one in order to improve the performance of our fuzzy-evolutionary-based approach.

- *Tackle the matching uncertainty*. We are planning to tackle the inherent matching uncertainty regarding each pair of cephalometric-craniometric landmarks. With the support of the forensic anthropologists of the Physical Anthropology lab of the University of Granada and starting from Stephan and Simpson works (2008a, 2008b), we aim to deal with this partial matching situation by using fuzzy sets and fuzzy distance measures.

- *Study the influence of the face pose over the matching uncertainty*. We plan to study the variation of the matching distance between all the cephalometric-craniometric correspondences with respect to changes in the pose of the face.

- *3D pose extraction from a 2D face photograph*. We aim to approximate the 3D orientation of the head from a 2D face photograph. This information will be very helpful to reduce the search space of the proposed evolutionary-based skull-face overlay procedure. It will also be useful to modify the uncertainty associated to the matching of corresponding landmarks

- *Tackle the decision making stage*. We aim to tackle the identification stage, i.e. the final decision making process, by using fuzzy logic, in order to assist the forensic expert in the final identification decision.

- *Study new problem formulations*. The study of new possibilities to formulate the geometric transformation associated with the skull-face overlay problem from a camera calibration point of view seems to be a promising future line of research. In particular, we would like to find a way to include the internal camera parameters in the model in order they can also be automatically computed by the evolutionary method. That can be useful to tackle old identification cases where the available photographs have been taken with outdated cameras.

References

I find television very educating.
Every time somebody turns on the set,
I go into the other room and read a book.

Groucho Marx (1890-1977)

References

Al-Amad, S., M. McCullough, J. Graham, J. Clement, and A. Hill (2006). Craniofacial identification by computer-mediated superimposition. *J. Forensic Odontostomal 24*, 47–52.

Albert, A. M., K. Ricanek Jr., and E. Patterson (2007). A review of the literature on the aging adult skull and face: Implications for forensic science research and applications. *Forensic Science International 172*, 1–9.

Alemán, I., M. C. Botella, and L. Ruíz (1997). Determinación del sexo en el esqueleto postcraneal. Estudio de una población mediterránea actual (in Spanish). *Archivo Español de Morfología 2*, 69–79.

Allen, P. K., A. Troccoli, B. Smith, S. Murray, I. Stamos, and M. Leordeanu (2003). New methods for digital modeling of historic sites. *IEEE Computer Graphics and Applications 23*(6), 32–41.

Arbib, M. (1995). *The Handbook of Brain Theory and Neural Networks*. MIT Press.

Arcuri, A. and X. Yao (2008). Search based software testing of object-oriented containers. *Information Sciences 178*(15), 3075–3095.

Arun, K. S., T. S. Huang, and S. D. Blostein (1987). Least-squares fitting of two 3-D points sets. *IEEE Transactions on Pattern Analysis and Machine Intelligence 9*(5), 698–700.

Arya, K., P. Gupta, P. Kalra, and P. Mitra (2007). Image registration using robust m-estimators. *Pattern Recognition Letters 28*(15), 1957–1968.

Audette, M. A., F. P. Ferrie, and T. M. Peters (2000). An algorithmic overview of surface registration techniques for medical imaging. *Medical Image Analysis 4*(3), 201–217.

Auger, A. and N. Hansen (2005). A restart CMA evolution strategy with increasing population size. In *Proceedings of the IEEE Congress on Evolutionary Computation CEC 2005*, pp. 1769–1776.

Aulsebrook, W. A. Iscan, M. Y., J. H. Slabbert, and P. Becker (1995, October). Superimposition and reconstruction in forensic facial identification: a survey. *Forensic Science International 75*(2-3), 101–120.

Austin-Smith, D. and W. R. Maples (1994, March). The reliability of skull/photograph superimposition in individual identification. *Journal of Forensic Sciences 39*(2), 446–455.

Bäck, T. (1996). *Evolutionary Algorithms in Theory and Practice: Evolution Strategies, Evolutionary Programming, Genetic Algorithms*. Oxford University Press.

Bäck, T., D. B. Fogel, and Z. Michalewicz (Eds.) (1997). *Handbook of Evolutionary Computation*. IOP Publishing Ltd and Oxford University Press.

Bajnóczky, I. and L. Királyfalvi (1995). A new approach to computer-aided comparison of skull and photograph. *International Journal of Legal Medicine 108*, 157–161.

Ballerini, L., O. Cordón, S. Damas, and J. Santamaría (2009). Automatic 3D modeling of skulls by scatter search and heuristic features. In E. Avineri, M. Koepen, K. Dahal, Y. Sunitiyoso, and R. Roy (Eds.), *Applications of Soft Computing. Updating the State of the Art*, pp. 149–158. Springer.

Barnea, D. I. and H. F. Silverman (1972). A class of algorithms for fast digital image registration. *IEEE Transactions on Computers 21*, 179–186.

Benazzi, S., M. Fantini, F. De Crescenzio, G. Mallegni, F. Mallegni, F. Persiani, and G. Gruppioni (2009). The face of the poet Dante Alighieri reconstructed by virtual modelling and forensic anthropology techniques. *Journal of Archaeological Science 36*(2), 278–283.

Bernardini, F. and H. Rushmeier (2002). The 3D model acquisition pipeline. *Computer Graphics Forum 21*(2), 149–172.

Berner, E. S. (2007). *Clinical Decision Support Systems: Theory and Practice*. New York, USA: Springer.

Bertillon, A. (1896). *Signaletic Instructions: Including The Theory And Practice Of Anthropometrical Identification*. Werner.

Besl, P. J. and N. D. McKay (1992). A method for registration of 3-D shapes. *IEEE Transactions on Pattern Analysis and Machine Intelligence 14*, 239–256.

Bilge, Y., P. Kedici, Y. Alakoc, K. Ulkuer, and Y. Ilkyaz (2003). The identification of a dismembered human body: a multidisciplinary approach. *Forensic Science International 137*, 141–146.

Biwasaka, H., K. Saigusa, and Y. Aoki (2005). The applicability of holography in forensic identification: a fusion of the traditional optical technique and digital technique. *Journal of Forensic Sciences 50*(2), 393–399.

Blais, G. and M. Levine (1995). Registering multiview range data to create 3D computer objects. *IEEE Transactions on Pattern Analysis and Machine Intelligence 17*(8), 820–824.

Blickle, T. (1997). Tournament selection. In T. Bäck, D. B. Fogel, and Z. Michalewicz (Eds.), *Handbook of Evolutionary Computation*, pp. C2.3:1–C2.3:4. IOP Publishing Ltd and Oxford University Press.

Bloch, I. (1999). On fuzzy distances and their use in image processing under imprecision. *Pattern Recognition 32*, 1873–1895.

Brainz (2010). 15 Real-World Uses of Genetic Algorithms. `http://brainz.org/15-real-world-applications-genetic-algorithms/`, visited on May, 3, 2010.

Broca, P. (1875). Instructions craniologiques et craniométriques. *Mémoires de la Société d'Anthropologie de Paris*, 63–96.

Brocklebank, L. M. and C. J. Holmgren (1989, September). Development of equipment for the standardisation of skull photographs in personal identifications by photographic superimposition. *Journal of Forensic Sciences 34*(5), 1214–1221.

Bronkhorst, D. (2006). Truth and justice: A Guide to Truth Commissions and Transitional Justice. Amnesty International Dutch Section. 2nd edition.

Brown, L. G. (1992). A survey of image registration techniques. *ACM Computing Surveys 24*(4), 325–376.

Brown, R. E., T. P. Kelliher, P. H. Tu, W. D. Turner, M. A. Taister, and K. W. P. Miller (2004). A survey of tissue-depth landmarks for facial approximation. *Forensic Science Communications 6*(1), [online].

Brunnström, K. and A. Stoddart (1996). Genetic algorithms for free-form surface matching. In *International Conference of Pattern Recognition*, Vienna, Germany, pp. 689–693.

Burns, K. (2007). *Forensic Anthropology Training Manual*. Prentice-Hall.

Cagnoni, S., R. Poli, G. Smith, D. Corne, M. Oates, E. Hart, P. Lanzi, E. Willem, Y. Li, B. Paechter, and T. Fogarty (Eds.) (2000). *Real-world applications of evolutionary computing*. Lecture Notes in Computer Science. Springer.

Campbell, R. J. and P. J. Flynn (2001). A survey of free-form object representation and recognition techniques. *Computer Vision and Image Understanding 81*(2), 166–210.

Campos, V., F. Laguna, and R. Martí (2001). An experimental evaluation of a scatter search for the linear ordering problem. *Journal of Global Optimization 21*(4), 397–414.

Cattaneo, C. (2007, January). Forensic anthropology: development of a classical discipline in the new millennium. *Forensic Science International 165*(2-3), 185–193.

Chalermwat, P., T. El-Ghazawi, and J. LeMoigne (2001). 2-phase GA-based image registration on parallel clusters. *Future Generation Computer Systems 17*, 467–476.

Chandra Sekharan, P. (1993). Positioning the skull for superimposition. In M. Y. Iscan and R. Helmer (Eds.), *Forensic Analysis of the Skull*, pp. 105–118. Wiley.

Chao, C. and I. Stamos (2005, June 13-17). Semi-automatic range to range registration: a feature-based method. In *5th International Conference on 3-D Digital Imaging and Modeling*, Otawa, Canada, pp. 254–261.

Chiong, R. (Ed.) (2009). *Nature-Inspired Informatics for Intelligent Applications and Knowledge Discovery: Implications in Business, Science and Engineering*. IGI Global-Information Science Reference.

Chiong, R., T. Weise, and Z. Michalewicz (Eds.) (2011). *Variants of Evolutionary Algorithms for Real-World Applications*. Springer. In press.

Chow, C. K., H. T. Tsui, and T. Lee (2004). Surface registration using a dynamic genetic algorithm. *Pattern Recognition 37*, 105–117.

Chow, C. K., H. T. Tsui, T. Lee, and T. K. Lau (2001, October 9–13). Medical image registration and model construction using genetic algorithms. In *International Workshop on Medical Imaging and Augmented Reality (MIAR 2001)*, Shatin N.T. (Hong Kong), pp. 174–179. IAPR.

Claes, P., D. Vandermeulen, S. De Greef, G. Willems, and P. Suetens (2006, May). Craniofacial reconstruction using a combined statistical model of face shape and soft tissue depths: methodology and validation. *Forensic Science International 159S*, S147–S158.

Clement, J. G. and D. L. Ranson (1998). *Craniofacial Identification in Forensic Medicine*. New York, USA: Oxford University Press.

Cordón, O. and S. Damas (2006). Image Registration with Iterated Local Search. *Journal of Heuristics 12*, 73–94.

Cordón, O., S. Damas, R. Martí, and J. Santamaría (2008). Scatter search for the 3D point matching problem in image registration. *INFORMS Journal on Computing* (1), 55–68.

Cordón, O., S. Damas, and J. Santamaría (2006). A Fast and Accurate Approach for 3D Image Registration using the Scatter Search Evolutionary Algorithm. *Pattern Recognition Letters 27*(11), 1191–1200.

Cordón, O., S. Damas, and J. Santamaría (2006). Feature-based image registration by means of the CHC evolutionary algorithm. *Image and Vision Computing 24*(5), 525–533.

Cordón, O., S. Damas, and J. Santamaría (2007). A practical review on the applicability of different EAs to 3D feature-based registration. In S. Cagnoni, E. Lutton, and G. Olague (Eds.), *Genetic and Evolutionary Computation in Image Processing and Computer Vision*, pp. 241–263. EURASIP Book Series on SP&C.

Cordón, O., S. Damas, J. Santamaría, and R. Martí (2008). Scatter Search for the 3D Point Matching Problem in Image Registration. *INFORMS Journal on Computing 20*, 55–68.

Dalley, G. and P. Flynn (2001). Range image registration: A software platform and empirical evaluation. In *Third International Conference on 3-D Digital Imaging and Modeling (3DIM'01)*, pp. 246–253.

De Angelis, D., R. Sala, A. Cantatore, M. Grandi, and C. Cattaneo (2009, July). A new computer-assisted technique to aid personal identification. *International Journal of Legal Medicine 123*(4), 351–356.

De Castro, E. and C. Morandi (1987). Registration of translated and rotated images using finite fourier transforms. *IEEE Transactions on Pattern Analysis and Machine Intelligence 9*(4), 700–703.

Deb, K. and R. B. Agrawal (1995). Simulated binary crossover for continuous search space. *Complex Systems 9*, 115–148.

Diamond, P. and P. Kloeden (2000). Metric topology of fuzzy numbers and fuzzy analysis. In D. Dubois and H. Prade (Eds.), *Fundamentals of Fuzzy Sets*, The Handbooks of Fuzzy Sets, Chapter 11, pp. 583–637. Kluwer Academic.

Donsgsheng, C. and L. Yuwen (1993). Standards for skull-to-photo superposition. In M. Iscan and R. Helmer (Eds.), *Forensic Analysis of the Skull: Craniofacial*

Analysis, Reconstruction, and Identification, pp. 171–182. New York: Wiley Liss.

Dorion, R. B. (1983, July). Photographic superimposition. *Journal of Forensic Sciences 28*(3), 724–734.

Douglas, T. S. (2004). Image processing for craniofacial landmark identification and measurement: a review of photogrammetry and cephalometry. *Computerized Medical Imaging and Graphics 28*, 401–409.

Dubois, D. and H. Prade (1983). On distance between fuzzy points and their use for pausible reasoning. In *International Conference on Systems, Man and Cybernetics*, pp. 300–303.

Eiben, A. and J. Smith (2003). *Introduction to Evolutionary Computing*. Springer-Verlag.

El Hakim, S. F. and H. Ziemann (1984). A step-by-step strategy for gross-error detection. *Photogrammetric Engineering and Remote Sensing 50*(6), 713–718.

Eliášová, H. and P. Krsek (2007). Superimposition and projective transformation of 3D object. *Forensic Science International 167*, 146–153.

Enciso, R., A. Memon, and J. Mah (2003). Three-dimensional visualization of the craniofacial patient: volume segmentation, data integration and animation. *Orthodontics & Craniofacial Research 6*(s1), 66–71.

Eshelman, L. J. (1991). The CHC adaptive search algorithm: how to safe search when engaging in non traditional genetic recombination. In G. J. E. Rawlins (Ed.), *Foundations of Genetic Algorithms 1*, San Mateo, EEUU, pp. 265–283. Morgan Kaufmann.

Eshelman, L. J. (1993). Real-coded genetic algorithms and interval schemata. In L. D. Whitley (Ed.), *Foundations of Genetic Algorithms 2*, pp. 187–202. San Mateo: Morgan Kaufmann.

Eshelman, L. J. and J. D. Schaffer (1991). Preventing premature convergence by preventing incest. In R. Belew and L. B. Booker (Eds.), *4th International Conference on Genetic Algorithms*, San Mateo, EEUU, pp. 115–122. Morgan Kaufmann.

Fantini, M., F. De Crescenzio, F. Persiani, and S. Benazzi (2008, September). 3D restitution, restoration and prototyping of a medieval damaged skull. *Rapid Prototyping Journal 14*(5), 1–1.

Faugeras, O. (1996). *Three-Dimensional Computer Vision*. MIT Press.

Feldmar, J. and N. Ayache (1996). Rigid, affine and locally affine registration of free-form surfaces. *International Journal of Computer Vision 18*(2), 99–119.

Fenton, T. W., A. N. Heard, and N. J. Sauer (2008, January). Skull-photo superimposition and border deaths: identification through exclusion and the failure to exclude. *Journal of Forensic Sciences 53*(1), 34–40.

Fitzpatrick, J., J. Grefenstette, and D. Gucht (1984). Image registration by genetic search. In *In IEEE Southeast Conference*, Louisville, USA, pp. 460–464.

Fogel, D. (1991). *System Identification through Simulated Evolution: A Machine Learning Approach to Modeling*. Ginn Press.

Fogel, D. (2005). *Evolutionary Computation: Toward a New Philosophy of Machine Intelligence*. Wiley-IEEE Press.

Foley, J. D. (1995). *Computer Graphics: Principles and Practice*. Addison-Wesley.

Förstner, W. (1985). The Reliability of Block Triangulation. *Photogrammetric Engineering and Remote Sensing 51*(6), 1137–1149.

Galantucci, L., G. Percoco, C. Angelelli, G.and Lopez, F. Introna, C. Liuzzi, and A. De Donno (2006, April). Reverse engineering techniques applied to a human skull, for CAD 3D reconstruction and physical replication by rapid prototyping. *Journal of Medical Engineering & Technology 30*(2), 102–111.

George, R. M. (1993). Anatomical and artistic guidelines for forensic facial reconstruction. In M. Y. Iscan and R. Helmer (Eds.), *Forensic Analysis of the Skull*, pp. 215–227. Wiley.

Ghosh, A. and P. Sinha (2001, March). An economised craniofacial identification system. *Forensic Science International 117*(1-2), 109–119.

Ghosh, A. and P. Sinha (2005, March). An unusual case of cranial image recognition. *Forensic Science International 148*(2-3), 93–100.

Glaister, J. and J. Brash (1937). *Medico-Legal Aspects of the Ruxton Case*. Edinburgh, U.K.: E. & S. Livingstone.

Glover, F. (1977). Heuristic for integer programming using surrogate constraints. *Decision Sciences 8*, 156–166.

Glover, F. and G. A. Kochenberger (Eds.) (2003). *Handbook of Metaheuristics*. Kluwer Academic Publishers.

Glover, F., M. Laguna, and R. Martí (2003). Scatter search. In A. Ghosh and S. Tsutsui (Eds.), *Theory and Applications of Evolutionary Computation: Recent Trends*, pp. 519–537. Springer-Verlag.

Goldberg, D. E. (1989). *Genetic algorithms in search, optimization, and machine learning*. Reading, MA: Addison-Wesley.

Gonzalez, R. and R. Woods (2002). *Digital image processing* (2nd ed.). Upper Saddle River, New Jersey: Prentice Hall.

Gonzalez, R. C. and R. E. Woods (2008, May). *Digital Image Processing*. Addison-Wesley. 3rd edition.

González-Colmenares, G., M. Botella-López, G. Moreno-Rueda, and J. Fernández-Cardenete (2007, September). Age estimation by a dental method: A comparison of Lamedin's and Prince & Ubelaker's technique. *Journal of Forensic Sciences 52*(5), 1156–1160.

Goshtasby, A. A. (2005). *2-D and 3-D Image Registration for Medical, Remote Sensing, and Industrial Applications*. Wiley Interscience.

Hansen, N. (2005). Compilation of results on the CEC benchmark function set. Technical report, Institute of Computational Science, ETH Zurich, Switzerland. Available at `http://www.ntu.edu.sg/home/epnsugan/index_files/CEC-05/compareresults.pdf`.

Hansen, N. and A. Ostermeier (1996). Adapting arbitrary normal mutation distributions in evolution strategies: The covariance matrix adaptation. In *Proceedings of the 1996 IEEE International Conference on Evolutionary Computation*, Piscataway, New Jersey, pp. 312–317.

Hansen, N. and A. Ostermeier (2001). Completely derandomized self-adaptation in evolution strategies. *Evolutionary Computation 9*(2), 159–195.

Hartley, R. I. and A. Zisserman (2004). *Multiple View Geometry in Computer Vision* (Second ed.). Cambridge University Press.

He, R. and P. A. Narayana (2002). Global optimization of mutual information: application to three-dimensional retrospective registration of magnetic resonance images. *Computerized Medical Imaging and Graphics 26*, 277–292.

Helmer, R. (1986). Identifizierung der leichenuberreste das josef mengele (in German). *Archives Kriminology 177*, 130–144.

Herrera, F., M. Lozano, and D. Molina (2006). Continuous scatter search: an analysis of the integration of some combination methods and improvement strategies. *European Journal of Operational Research 169*(2), 450–476.

Herrera, F., M. Lozano, and J. L. Verdegay (1998). Tackling real-coded genetic algorithms: operators and tools for the behavioural analysis. *Artificial Intelligence Reviews 12*(4), 265–319.

Holland, J. H. (1975). *Adaptation in Natural and Artificial Systems*. MIT press.

Horn, B. K. P. (1987). Closed-form solution of absolute orientation using unit quaternions. *Journal of the Optical Society of America 4*, 629–642.

Huber, P. J. (1981). *Robust Statistics*. New York: John Wiley.

HUMIES (2008). Annual HUMIES awards for human-competitive results produced by genetic and evolutionary computation. `www.human-competitive.org`, visited on October, 9, 2008.

Ikeuchi, K. and D. Miyazaki (2008). *Digitally Archiving Cultural Objects*. Springer Verlag.

Ikeuchi, K. and Y. Sato (2001). *Modeling from reality*. Kluwer.

Indriati, E. (2009). Historical perspectives on forensic anthropology in Indonesia. In S. Blau and D. H. Ubelaker (Eds.), *Handbook of Forensic Anthropology and Archaeology*, pp. 115–125. California, USA: Left Coast Press.

Iscan, M. (1981a). Concepts in teaching forensic anthropology. *Medical Anthropol Newsletter 13*(1), 10–12.

Iscan, M. (1981b). Integral forensic anthropology. *Practicing Anthropol 3*(4), 21–30.

Iscan, M. Y. (1993). Introduction to techniques for photographic comparison. In M. Y. Iscan and R. Helmer (Eds.), *Forensic Analysis of the Skull*, pp. 57–90. Wiley.

Iscan, M. Y. (2005). Forensic anthropology of sex and body size. *Forensic Science International 147*, 107–112.

Jayaprakash, P. T., G. J. Srinivasan, and M. G. Amravaneswaran (2001). Craniofacial morphoanalysis: a new method for enhancing reliability while identifying skulls by photosuperimposition. *Forensic Science International 117*, 121–143.

Keen, P. G. W. (1978). *Decision Support Systems: An Organizational Perspective*. Reading, Massachusetts, USA: Addison-Wesley Pub. Co.

Klir, G. J. and B. Yuan (1996). *Fuzzy sets, fuzzy logic, and fuzzy systems: selected papers by Lotfi A. Zadeh*. World Scientific Publishing Co., Inc.

Koza, J. R. (1992). *Genetic Programming: On the Programming of Computers by Natural Selection*. MIT Press.

Koza, R., M. J. Streeter, and M. A. Keane (2008). Routine high-return human-competitive automated problem-solving by means of genetic programming. *Information Sciences 178*(23), 4434–4452.

Krasnogor, N. and J. Smith (2005). A tutorial for competent memetic algorithms: model, taxonomy and design issues. *IEEE Transactions on Evolutionary Computation 9*(5), 474– 488.

Krogman, W. M. and M. Y. Iscan (1986). *The human skeleton in forensic medicine*. Springfield, IL: Charles C. Thomas. 2nd edition.

Kumari, T. R. and P. Chandra Sekharan (1992). Remote control skull positioning device for superimposition studies. *Forensic Science International 54*, 127–133.

Laguna, M. and R. Martí (2003). *Scatter search: methodology and implementations in C*. Kluwer Academic Publishers.

Lan, Y. (1990). Research report on model TLGA-213 image superimposition identification system. In *Special Issue on Criminal Technology Supplement*, The Fifth Bureau of the National Public Security Department, pp. 13. Beijing, China.

Lan, Y. (1992). Development and current status of skull image superimposition methodology and instrumentation. *Forensic Science Review 4*(2), 126–136.

Lan, Y. and D. Cai (1985). Study on model TLGA-1 skull identification apparatus. In *Special Issue on Criminal Technology Supplement*, The Fifth Bureau of the National Public Security Department, pp. 23. Beijing, China, Germany.

Lan, Y. and D. Cai (1988). A new technology in skull identification. In R. Helmet (Ed.), *Advances in Skull Identification Via Video Superimposition*, pp. 3. Kiel, Germany.

Lan, Y. and D. Cai (1993). Technical advances in skull-to-photo superimposition. In M. Y. Iscan and R. Helmer (Eds.), *Forensic Analysis of the Skull*, pp. 119–129. New York, USA: Wiley.

Landa, M., M. Garamendi, M. Botella, and I. Alemán (2009). Application of the method of kvaal et al. to digital orthopantomograms. *International Journal of Legal Medicine 123*(2), 123–128.

Larrañaga, P. and J. Lozano (Eds.) (2002). *Estimation of Distribution Algorithms: a new tool for evolutionary computation*. Kluwer Academic Publishers.

Liu, Y. (2004). Improving ICP with easy implementation for free form surface matching. *Pattern Recognition 37*(2), 211–226.

Lomonosov, E., D. Chetverikov, and A. Ekart (2006). Pre-registration of arbitrarily oriented 3D surfaces using a genetic algorithm. *Pattern Recognition Letters 27*(11), 1201–1208.

Lozano, M., F. Herrera, N. Krasnogor, and D. Molina (2004a). Real-coded memetic algorithms with crossover hill-climbing. *Evolutionary Computation 12*(3), 273–302.

Lozano, M., F. Herrera, N. Krasnogor, and D. Molina (2004b). Real-coded memetic algorithms with crossover hill-climbing. *Evolutionary Computation 12*(3), 273–302.

Luenberger, D. G. (1997). *Optimization by Vector Space Methods*. New York, NY, USA: John Wiley & Sons, Inc.

Maat, G. J. R. (1989). The positioning and magnification of faces and skulls for photographic superimposition. *Forensic Science International 41*(3), 225–235.

Maes, F., D. Vandermeulen, and P. Suetens (1999). Comparative evaluation of multiresolution optimization strategies for image registration by maximization of mutual information. *Medical Image Analysis 3*(4), 373–386.

Maintz, J. B. and M. A. Viergever (1998). A survey of medical image registration. *Medical Image Analysis 2*(1), 1–36.

Mandava, V. R., J. M. Fitzpatrick, and D. R. Pickens (1989). Adaptive search space scaling in digital image registration. *IEEE Transactions on Medical Imaging 8*(3), 251–262.

Martin, R. and K. Saller (1966). *Lehrbuch der Anthropologie in Systematischer Darstellung (in German)*. Stuttgart, Germany: Gustav Fischer Verlag.

Matsopoulos, G. K., N. A. Mouravliansky, K. K. Delibasis, and K. S. Nikita (1999). Automatic retinal image registration scheme using global optimization techniques. *IEEE Transactions on Information Technology in Biomedicine 3*(1), 47–60.

Michalewicz, Z. (1996). *Genetic algorithms + data structures = evolution programs*. Springer-Verlag.

Mitchell, T. (1997). *Machine Learning*. McGraw Hill.

Moscato, P. (1989). On evolution, search, optimization, genetic algorithms and martial arts: Towards memetic algorithms. Report 826, Caltech Concurrent Computation Program, Pasadena, California.

Muratore, D. M., J. H. Russ, B. M. Dawant, and R. L. Jr. Galloway (2002). Three-Dimensional Image Registration of Phantom Vertebrae for Image-Guided Surgery: A Preliminary Study. *Computer Aided Surgery 7*, 342–352.

Nakasima, A., M. Terajima, N. Mori, Y. Hoshino, K. Tokumori, Y. Aoki, and S. Hashimoto (2005, March). Three-dimensional computer-generated head model reconstructed from cephalograms, facial photographs, and dental cast models. *American Journal of Orthodontics and Dentofacial Orthopedics 127*(3), 282–292.

Nickerson, B. A., P. A. Fitzhorn, S. K. Koch, and M. Charney (1991, March). A methodology for near-optimal computational superimposition of two-dimensional digital facial photographs and three-dimensional cranial surface meshes. *Journal of Forensic Sciences 36*(2), 480–500.

Noman, N. and H. Iba (2005). Enhancing Differential Evolution Performance with Local Search for High Dimensional Function Optimization. In *Genetic and Evolutionary Computation Conference (GECCO'05), ACM*, pp. 967–974.

Nomura, T. and K. Shimohara (2001). An analysis of two-parent recombinations for real-valued chromosomes in an infinite population. *Evolutionary Computation 9*(3), 283–308.

Parzianello, L. C., M. A. M. Da Silveira, S. S. Furuie, and F. A. B. Palhares (1996). Automatic detection of the craniometric points for craniofacial identification. In *Anais do IX SIBGRAPI'96*, pp. 189–196.

Pesce Delfino, V., M. Colonna, E. Vacca, F. Potente, and F. Introna Jr. (1986). Computer-aided skull/face superimposition. *American Journal of Forensic Medicine and Pathology 7*(3), 201–212.

Pesce Delfino, V., E. Vacca, F. Potente, T. Lettini, and M. Colonna (1993). Shape analytical morphometry in computer-aided skull identification via video superimposition. In M. Y. Iscan and R. Helmer (Eds.), *Forensic Analysis of the Skull*, pp. 131–159. Wiley.

Pickering, R. and D. Bachman (2009). *The Use of Forensic Anthropology*. New York, USA: CRC Press. 2nd edition.

Ranson, D. (2009). Legal aspects of identification. In S. Blau and D. H. Ubelaker (Eds.), *Handbook of Forensic Anthropology and Archaeology*. California, USA: Left Coast Press.

Rathburn, T. (1984). Personal identification. In T. Rathburn and J. Buikstra (Eds.), *Human Identification*, pp. 647–656. Springfield, USA: Charles C Thomas Publisher.

Ricci, A., G. L. Marella, and M. A. Apostol (2006, March). A new experimental approach to computer-aided face/skull identification in forensic anthropology.

Am J Forensic Med Pathol 27(1), 46–49.

Richtsmeier, J., C. Paik, P. Elfert, T. Cole, and F. Dahlman (1995). Precision, repeatability and validation of the localization of cranial landmarks using computed tomography scans. *The Cleft Palate-Craniofacial Journal 32*(3), 217–227.

Ross, A. H. (2004). Use of digital imaging in the identification of fragmentary human skeletal remains: A case from the Republic of Panama. *Forensic Science Communications 6*(4), [online].

Rouet, J. M., J. J. Jacq, and C. Roux (2000). Genetic algorithms for a robust 3-D MR-CT registration. *IEEE Transactions on Information Technology in Biomedicine 4*(2), 126–136.

Rumelhart, D. E. and D. McClelland (1986). *Parallel Distributed Processing: Explorations in the Microstructure of Cognition*. Cambridge, Mass.: MIT Press.

Rusinkiewicz, S. and M. Levoy (2001). Efficient variants of the ICP algorithm. In *Third International Conference on 3D Digital Imaging and Modeling (3DIM'01)*, Quebec, Canada, pp. 145–152.

Salvi, J., X. Armangué, and J. Batlle (2002). A comparative review of camera calibrating methods with accuracy evaluation. *Pattern Recognition 35*(7), 1617–1635.

Salvi, J., C. Matabosch, D. Fofi, and J. Forest (2007). A review of recent range image registration methods with accuracy evaluation. *Image and Vision Computing 25*(5), 578–596.

Santamaría, J., O. Cordón, and S. Damas (2010). A comparative study of state-of-the-art evolutionary image registration methods for 3D modeling. Technical Report AFE 2010-02, European Centre for Soft Computing, Mieres, Spain. Submitted.

Santamaría, J., O. Cordón, S. Damas, I. Alemán, and M. Botella (2007a). Evolutionary approaches for automatic 3D modeling of skulls in forensic identification. In *Applications of Evolutionary Computing*, Number 4448 in Lecture Notes in Computer Science, pp. 415–422. Berlin, Germany: Springer.

Santamaría, J., O. Cordón, S. Damas, I. Alemán, and M. Botella (2007b). A scatter search-based technique for pair-wise 3D range image registration in forensic anthropology. *Soft Computing 11*(9), 819–828.

Santamaría, J., O. Cordón, S. Damas, J. M. García-Torres, and A. Quirin (2009). Performance evaluation of memetic approaches in 3D reconstruction of forensic objects. *Soft Computing 13*(8-9), 883–904.

Schwefel, H. (1993). *Evolution and Optimum Seeking: The Sixth Generation*. New York, NY, USA: John Wiley & Sons, Inc.

Schwefel, H. (1995). *Evolution and Optimum Seeking*. Wiley, New York.

Scully, B. and P. Nambiar (2002). Determining the validity of Furue's method of craniofacial superimposition for identification. *Malaysian Journal of Computer Science 9*(1), 17–22.

Sen, N. K. (1962). Identification by superimposed photographs. *International Criminal Police Review 162*, 284–286.

Seta, S. and M. Yoshino (1993). A combined apparatus for photographic and video superimposition. In M. Y. Iscan and R. Helmer (Eds.), *Forensic Analysis of the Skull*, pp. 161–169. Wiley.

Shahrom, A. W., P. Vanezis, R. C. Chapman, A. Gonzales, C. Blenkinsop, and M. L. Rossi (1996). Techniques in facial identification: computer-aided facial reconstruction using a laser scanner and video superimposition. *International Journal of Legal Medicine 108*(4), 194–200.

Shan, Y., Z. Liu, and Z. Z. (2001). Model-based bundle adjustment with application to face modeling. In *IEEE International Conference on Computer Vision*, Volume 2, Vancouver, Canada, pp. 644–651.

Shoemake, K. (1985, July 22-26). Animating rotation with quaternion curves. In *ACM SIGGRAPH*, San Francisco, pp. 245–254.

Silva, L., O. R. P. Bellon, and K. L. Boyer (2005). *Robust range image registration using genetic algorithms and the surface interpetenetration measure*. World Scientific.

Simunic, K. and S. Loncaric (1998). A genetic search-based partial image matching. In *2nd IEEE International Conference on Intelligent Processing Systems (ICIPS'98)*, Gold Coast, Australia, pp. 119–122.

Singare, S., Q. Lian, W. P. Wang, J. Wang, Y. Liu, D. Li, and B. Lu (2009). Rapid prototyping assisted surgery planning and custom implant design. *Rapid Prototyping Journal 15*(1), 19–23.

Sinha, P. (1998, November). A symmetry perceiving adaptive neural network and facial image recognition. *Forensic Science International 98*(1-2), 67–89.

Stephan, C., A. Huang, and P. Davison (2009, March). Further evidence on the anatomical placement of the human eyeball for facial approximation and craniofacial superimposition. *Journal of Forensic Sciences 54*(2), 267–269.

Stephan, C. N. (2009a). Craniofacial identification: method background and overview. http://www.craniofacial.com.

Stephan, C. N. (2009b). Craniofacial identification: techniques of facial approximation and craniofacial superimposition. In S. Blau and D. H. Ubelaker (Eds.), *Handbook of Forensic Anthropology and Archaeology*, pp. 304–321. California, USA: Left Coast Press.

Stephan, C. N. and R. S. Arthur (2006, May). Assessing facial approximation accuracy: How do resemblance ratings of disparate faces compare to recognition tests? *Forensic Science International 159S*, S159–S163.

Stephan, C. N. and E. Simpson (2008a). Facial soft tissue depths in craniofacial identification (part i): An analytical review of the published adult data. *Journal of Forensic Sciences 53*(6), 1257–1272.

Stephan, C. N. and E. Simpson (2008b). Facial soft tissue depths in craniofacial identification (part ii): An analytical review of the published sub-adult data. *Journal of Forensic Sciences 53*(6), 1273–1279.

Stephan, C. N., R. G. Taylor, and J. A. Taylor (2008). Methods of facial approximation and skull-face superimposition, with special consideration of method development in Australia. In M. Oxenham (Ed.), *Forensic Approaches to Death, Disaster and Abuse*. Australia: Australian Academic Press.

Stratmann, H. (1998). Excuses for the truth. http://home.wxs.nl/˜loz/maneng.htm.

Suganthan, P., N. Hansen, J. Liang, K. Deb, Y. Chen, A. Auger, and S. Tiwari (2005). Problem definitions and evaluation criteria for the CEC 2005 special session on real parameter optimization. Technical report, Nanyang Technological University. Available at `http://www.ntu.edu.sg/home/epnsugan/index_files/CEC-05/Tech-Report-May-30-05.pdf`.

Svedlow, M., C. D. Mc-Gillem, and P. E. Anuta (1976). Experimental examination of similarity measures and preprocessing methods used for image registration. In *Symposium on Machine Processing of Remotely Sensed Data*, Volume 4(A), Indiana, EEUU, pp. 9–17.

Tao, C. (1986). Report on computer programming for model TLGA-1 skull identification. In *Special Issue on Criminal Technology Supplement*, The Fifth Bureau of the National Public Security Department, Beijing, China, pp. 41.

Taylor, J. and K. Brown (1998). Superimposition techniques. In J. Clement and D. Ranson (Eds.), *Craniofacial Identification in Forensic Medicine*, pp. 151–164. London: Arnold.

Tsai, R. (1986). An efficient and accurate camera calibration technique for 3D machine vision. In *Proceedings of IEEE Conference on Computer Vision and Pattern Recognition*, Volume 1, pp. 364–374.

Tsang, P. W. M. (1997). A genetic algorithm for aligning object shapes. *Image and Vision Computing 15*, 819–831.

Turner, W. D., R. E. B. Brown, T. P. Kelliher, P. H. Tu, M. A. Taister, and K. W. P. Miller (2005). A novel method of automated skull registration for forensic facial approximation. *Forensic Science International 154*, 149–158.

Ubelaker, D. H. (2000). A history of Smithsonian-FBI collaboration in forensic anthropology, especially in regard to facial imagery. *Forensic Science Communications 2*(4), [online].

Ubelaker, D. H., E. Bubniak, and G. O'Donnel (1992, May). Computer-assisted photographic superimposition. *Journal of Forensic Sciences 37*(3), 750–762.

Ugur, A. (2008). Path planning on a cuboid using genetic algorithms. *Information Sciences 178*(16), 3275–3287.

Urquiza, R., M. Botella, and M. Ciges (2005). Study of a temporal bone of homo heidelbergensis. *Acta Oto-Laryngologica 125*, 457–463.

Vanezis, P., M. Vanezis, G. McCombe, and T. Niblett (2000, December). Facial reconstruction using 3-D computer graphics. *Forensic Science International 108*, 81–95.

Viola, P. and W. M. Wells (1997). Alignment by maximization of mutual information. *International Journal of Computer Vision 24*, 137–154.

Webster, G. (1955). Photography as an aid in identification: the Plumbago Pit case. *Police Journal 28*, 185–191.

Welcker, H. (1867). Der schädel Dantes (in German). In K. Witte and G. Boehmer (Eds.), *Jahrbuch der deutschen Dantegesellschaft*, Volume 1, pp. 35–56. Liepzig: Brockhaus.

Wilkinson, C. (2005). Computerized forensic facial reconstruction: A review of current systems. *Forensic Science, Medicine, and Pathology 1*(3), 173–177.

Wilkinson, C. (2009, January). 13th meeting of International Association of Craniofacial Identification (IACI). *Forensic Science, Medicine, and Pathology 5*(1), 1.

Wilkinson, C. (2010). Facial reconstruction: anatomical art or artistic anatomy? *Journal of Anatomy 216*(2), 235–250.

Yamany, S. M., M. N. Ahmed, and A. A. Farag (1999). A new genetic-based technique for matching 3D curves and surfaces. *Pattern Recognition 32*, 1817–1820.

Yoshino, M., K. Imaizumi, S. Miyasaka, and S. Seta (1995a). Evaluation of anatomical consistency in craniofacial superimposition images. *Forensic Science International 74*, 125–134.

Yoshino, M., K. Imaizumi, S. Miyasaka, and S. Seta (1995b). Evaluation of anatomical consistency in craniofacial superimposition images. *Forensic Science International 74*, 125–134.

Yoshino, M., H. Matsuda, S. Kubota, K. Imaizumi, S. Miyasaka, and S. Seta (1997). Computer-assisted skull identification system using video superimposition. *Forensic Science International 90*, 231–244.

Yoshino, M. and S. Seta (2000). Skull-photo superimposition. In J. A. Siegel, G. C. Knupfer, and P. J. Saukko (Eds.), *Encyclopedia of Forensic Sciences*, Volume 2, pp. 807–815. Elsevier Science and Technology.

Yuen, S. Y., C. K. Fong, and H. S. Lam (2001). Guaranteeing the probability of success using repeated runs of genetic algorithm. *Image and Vision Computing 19*, 551–560.

Yuwen, L. and C. Dongsheng (1993). Technical advances in skull-to-photo superposition. In M. Iscan and R. Helmer (Eds.), *Forensic Analysis of the Skull: Craniofacial Analysis, Reconstruction, and Identification*, pp. 119–130. New York: Wiley Liss.

Zadeh, L. A. (1965). Fuzzy sets. *Information and Control 8*, 338–353.

Zhang, Z. (1994). Iterative point matching for registration of free-form curves and surfaces. *International Journal of Computer Vision 13*(2), 119–152.

Zhao, W. and R. Chellapa (Eds.) (2005). *Face Processing: Advanced Modeling and Methods*. Elsevier.

Zhen, W. and T. Huang (2004). *3D Face Processing: Modeling, Analysis and Synthesis*. Springer.

Zitová, B. and J. Flusser (2003). Image registration methods: a survey. *Image and Vision Computing 21*, 977–1000.

Acronyms

BCGA: Binary-Coded Genetic Algorithm

CAD: Computer-Aided Design

CC: Camera Calibration

CMA-ES: Covariance Matrix Adaption Evolutionary Strategy

CT: Computer Tomography

CV: Computer Vision

EAs: Evolutionary Algorithms

EC: Evolutionary Computation

EP: Evolutionary Programming

ES: Evolution Strategies

GAs: Genetic Algorithms

GCP: Grid Closest Point

ICP: Iterative Closest Point

ILS: Iterative Local Search

IR: Image Registration

LS: Local Search

LSq: Least Squares

MAs: Memetic Algorithms

MI: Mutual Information

MRIs: Magnetic Resonance Images

MSE: Mean Square Error

NN: Neural Network

PSO: Particle Swarm Optimization

RCGA: Real-Coded Genetic Algorithm

RIR: Range Image Registration

SC: Soft Computing

SPECT: Single-Photon Emission Computerized Tomography

SS: Scatter Search

SIM: Surface Interpenetration Measure

TS: Tabu Search